KERNFORSCHUNGSANLAGE JÜLICH GmbH
Projektleitung Energieforschung
International Energy Agency IEA

# Implementing Agreement for Co-Operation in the Development of Large Scale Wind Energy Conversion Systems

## 14th Meeting of Experts-Modelling of Atmospheric Turbulenc for Use in WECS Rotor Loading Calculations

Organised by:
Project Management for Energy Research (PLE) of the
Nuclear Research Establishment Jülich (KFA) on behalf of the
Federal Minister of Research and Technology,
the Fluid Mechanics Department
of the Technical University of Denmark

Jül - Spez - 368
August 1986
ISSN 0343-7639

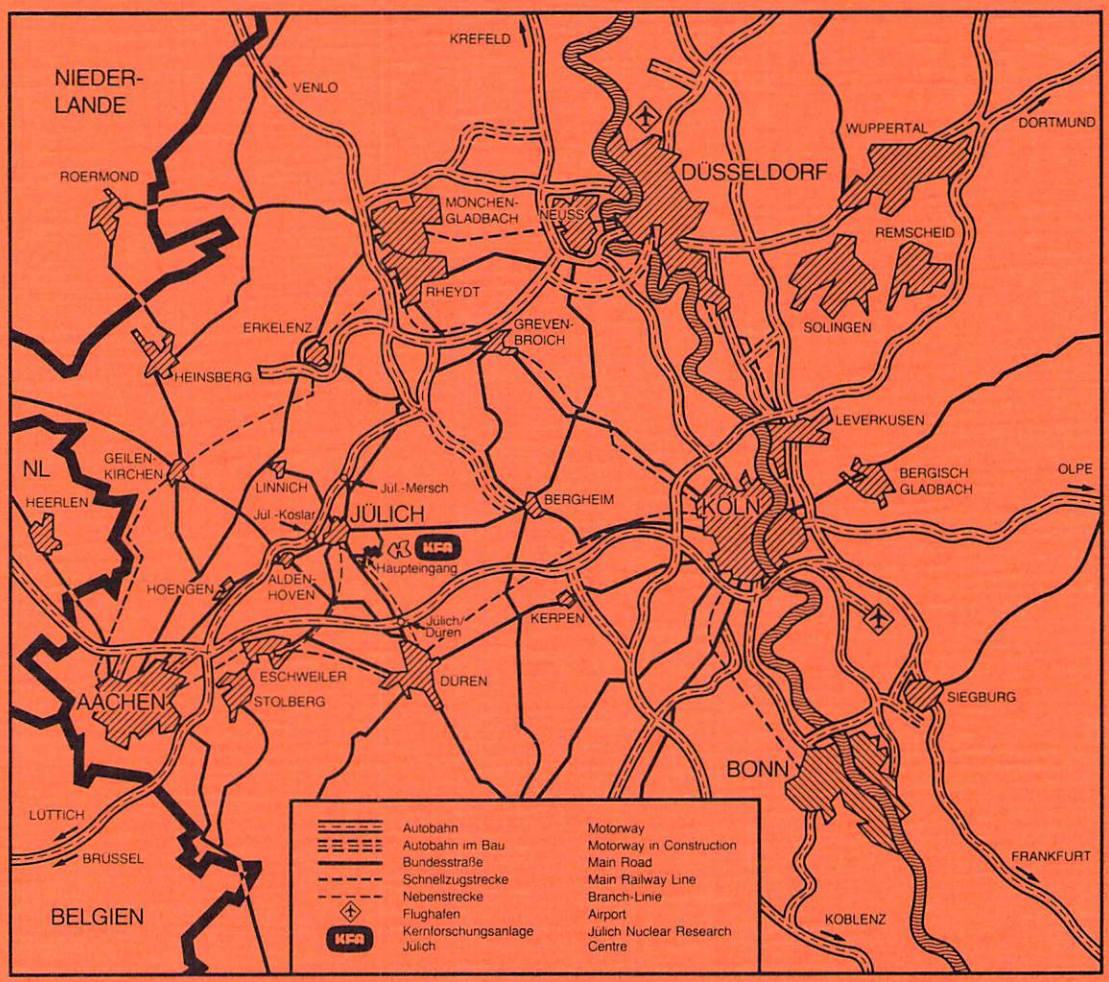


Als Manuskript gedruckt

**Spezielle Berichte der Kernforschungsanlage Jülich – Nr. 368**

Projektleitung Energieforschung Jül - Spez - 368

Zu beziehen durch: ZENTRALBIBLIOTHEK der Kernforschungsanlage Jülich GmbH

Postfach 1913 · D-5170 Jülich (Bundesrepublik Deutschland)

Telefon: 02461/610 · Telex 833556-0 kf d

# Implementing Agreement for Co-Operation in the Development of Large Scale Wind Energy Conversion Systems

## 14th Meeting of Experts-Modelling of Atmospheric Turbulenc for Use in WECS Rotor Loading Calculations

**Stockholm, December 4–5, 1985**

Organised by:
Project Management for Energy Research (PLE) of the
Nuclear Research Establishment Jülich (KFA) on behalf of the
Federal Minister of Research and Technology,
the Fluid Mechanics Department
of the Technical University of Denmark

Scientific Coordination:
Maribo Petersen (Techn. Univ. of Denmark)
Rolf Windheim (PLE-KFA Jülich)

CONTENTS

# MICROSCALE WIND CHARACTERISTICS

J. R. Connell

1. How microscale wind characteristics fit, topically and historically, into R&D and implementation of wind turbines.

2. Direct and indirect evidence of fluctuating response of wind turbines to wind: spectra, cross spectra, response or transfer functions, probability and conditional probability densities.

   2.1. Stresses and strains

   2.2. Power output

   2.3. Observed wind velocity of the rotating rotor coordinate system

   2.4. Aerodynamic forces

3. Current descriptions of rotationally sampled wind velocity. Measures of accuracy and improvement of the models over a reference model of disc-average Eulerian wind velocity fluctuations plus mean wind shear. HAWT and VAWT rotor cases.

   3.1. Measured, rotationally sampled wind velocity

      3.1.1. methods of measurement
      3.1.2. methods of analysis and synthesis
      3.1.3. quantitative, discriminating results (spectra, etc.)

   3.2. Theoretical wind velocity in the rotational coordinate systems.

      3.2.1. methods, principle
      3.2.2. quantitative results

   3.3. Stochastic simulations involving generation of random time series. Modification of the time series to have some statistical properties of real rotationally sampled wind velocities.

3.4. Other considerations relating to rotationally sampled wind for wind turbine rotors, benefits and limitations.

3.4.1. Eulerian-to-rotational frame of reference transfer functions
3.4.2. different mean and turbulence wind conditions.
3.4.2.1. static stability variation
3.4.2.2. complex terrain effects
3.4.2.3. other turbines and structures

3.4.3. modification of free stream turbulent wind characteristics
3.4.3.1. induction effects of rotor blades
3.4.3.2. wake effects of tower and nacelle
3.4.3.3. upwind-blade flow effects on downwind blades: same rotor (VAWT), other rotors (HAWT and VAWT)

4. Current research for improving descriptions of rotationally sampled wind velocity.

4.1. Specific objectives of improvements

4.1.1. fluid flow physics
4.1.2. methods of use or application

4.2. Methods of research and development of models

4.3. Approximate realistic schedules of contributors.

5. Summary and overview of current and projected research, development and application of wind models.

5.1. Current models

5.2. Active organizations and people

5.3. Specific improvements needed in wind models

5.4. Probable achievements in research and time tables of contributors

# Modelling of Atmospheric Turbulence for Use in WECS Rotor Loading Calculations.

B. Maribo Pedersen

Over the last decade the development of the calculational tools for prediction of the response of a WECS structure to a fluctuating wind field has progressed rapidly. Hence the need of having the correct input for these calculations has become increasingly important.

Statistical models of atmospheric turbulence have existed for a number of years based on measurements, the bulk of the data coming from anemometer measurements on meteorological towers.

Not many measurements have been made however, where the complete spatial and temporal structure of the wind field has been determined over an area of the order of the swept area of a large wind turbine, and with a sufficiently high resolution.

Rotationally sampled wind velocity measurements have been performed in a few places. The results have been extremely valuable, particularly when wind turbine rotor calculations are performed in a rotor-fixed frame of reference.

Models of the turbulent field in the time domain have been attempted. These discrete gust models however are rather crude, but may be adequate for extreme events.

Development of more refined time domain models is going on in several places, and the state of the art in this particular field should be an important part of the discussions at this meeting.

Finally it must be taken into account, that the degree of sophistication in the input model for the calculation of the response of the wind turbine structure must be compatible with the accuracy by which the remainder of the calculations can be performed.

As the final calculation normally is a calculation of the fatigue life of the structure, and as the fatigue properties of materials and structural elements are intrinsically rather inaccurate, the demands on a turbulence model may not be too stringent.

Some suggestions of questions or topics for discussion are listed below. Other suggestions are being put forward in the accompanying notes prepared by J.R. Connell and R.J. Templin.

- What are the most urgent needs for measurements to fill the gaps in the existing data bases.
- Which countries have measurement programmes going on.
- Do there exist simultaneous measurements of the turbulent flow field and the structural response of a wind turbine.
- What is the state of the art with respect to turbulence models in the frequency domain.
- What is the state of the art for models in the time domain.
- Is the modelling of all three components of the turbulent velocity equally important.
- What kind of turbulence model is currently used by designers of wind turbines.
- Would there be any difference in the type of model one would use in calculations for a horizontal axis machine and a vertical axis machine.
- Is there a need for closer international collaboration in this field.

# Modelling of Atmospheric Turbulence for Use in WECS Rotor Loading Calculations

R.C. Templin

- How many individuals or groups are now developing computer models of atmospheric turbulence suitable for loading calculations of large-scale WECS?
- How much is known about the importance of atmospheric turbulence on the loading and fatigue life of large or small WECS, relative to the cyclic loads arising from wind shear, yaw, etc?
- Blade cyclic loads are probably higher on VAWT's than on HAWT's. Does this mean that the effects of atmospheric turbulence are less important on VAWT's?
- What methods are available for computing unsteady rotor loads (and stresses) in response to atmospheric turbulence? If such methods exist, are they affordable to typical WECS designers?
- Statistical/probabilistic models of atmospheric turbulence have existed for many years and have been used for estimation of the spectra of loads, stresses and deflections of aircraft and large-scale civil engineering structures such as tall towers and long-span bridges. Has the wind energy community been able to adapt any of these earlier techniques to the problems of WECS design?

# Evaluation of Loads Measured at the Näsudden Turbine.

Hans Ganander

## Introduction.

An essential part of the evaluation of the two horisontal axis wind turbines Maglarp (3 MW) and Näsudden (2 MW) in Sweden is the analysis of loads and dynamics. The main purpose is to map loads at different wind conditions and modes of operation in order to :

- improve knowledge and the understanding of how the turbines work during different conditions
- verify the computational tools
- update specifications for future turbines
- carry out fatigue calculations

The presentation here is concentrated on the interaction between the variation in windspeed called turbulance and corresponding loads and their variations. From the designers point of view load variations consists of periodic as well as stocastic variations. The periodic part is due to gravity, tower influence and wind shear, while turbulence is the main factor causing the stocastic part of the variations. In this presentation loads and their variations evaluated from the Näsudden measurements are shown together with separation of these variations in the periodic and the stocastic parts.

Typical questions that the designer ask are :

- what are the relative portion between the periodic and stocastic parts of the load variation?
- what influence has the size and the type of turbine on that portions ?
- how much does different site locations influense the turbulence contribution to load variations ?
- what kind of calculating tools are suitable when studying loads caused by turbulance ?
- how accurate is knowledge about turbulance and its correlation in space and time ?

- what degree of accuracy in turbulance descibtion is needed ?

In the following preliminary evaluated results from the Näsudden turbine indicate one way of answering some of these questions.

Näsudden load evaluation.

On-line measurements ("measurement campaigns") have been carried out with a relatively high resolution and with a large number of sensors connected, including wind measurements and control signals in addition to strain gauges and accelerometers. Up to now we have evaluated 75 campaigns. They represent a wide variety of conditions. Figure 1 b and c below is an example of how results of the evaluation are illustrated. In this case the averages of the blade root moment both in rotational (edge) and wind direction (flap) are presented as function of the mean wind speed.

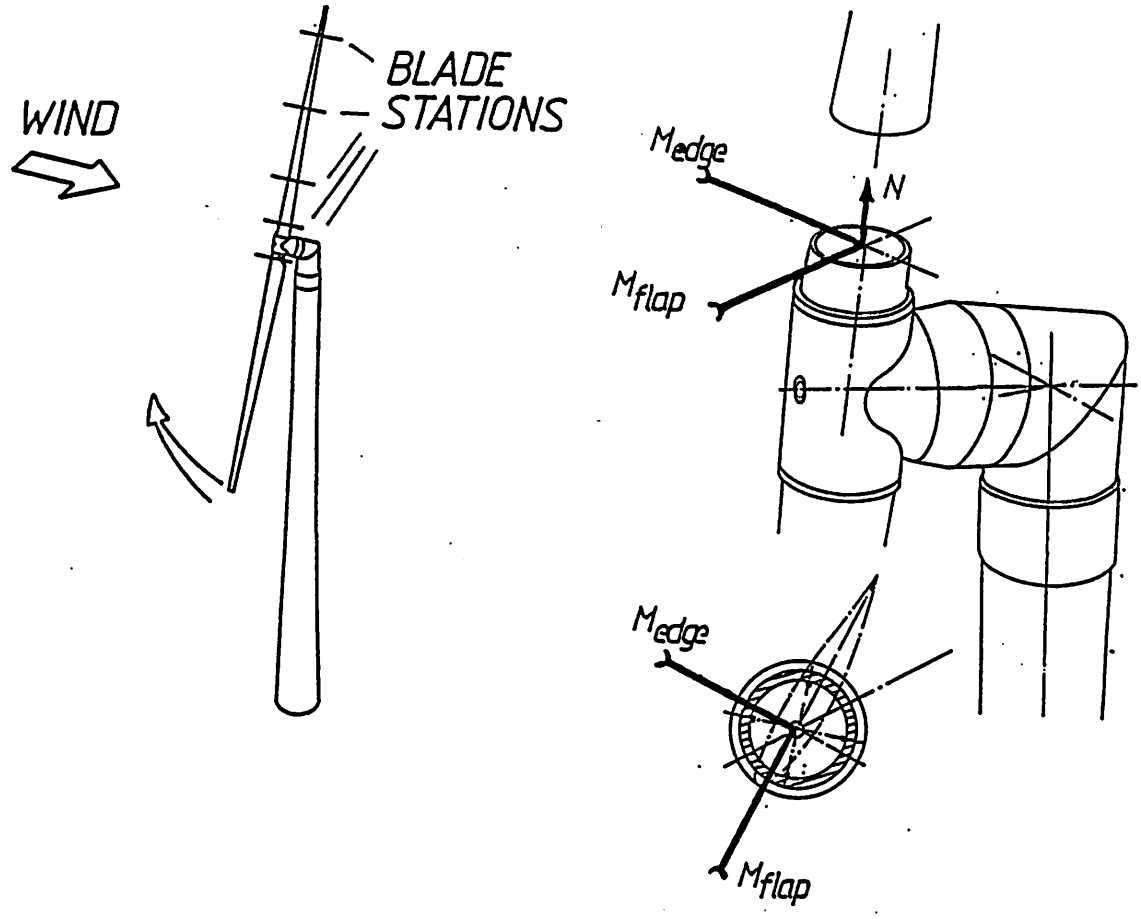


Definition of blade root moments

Fig 1 a

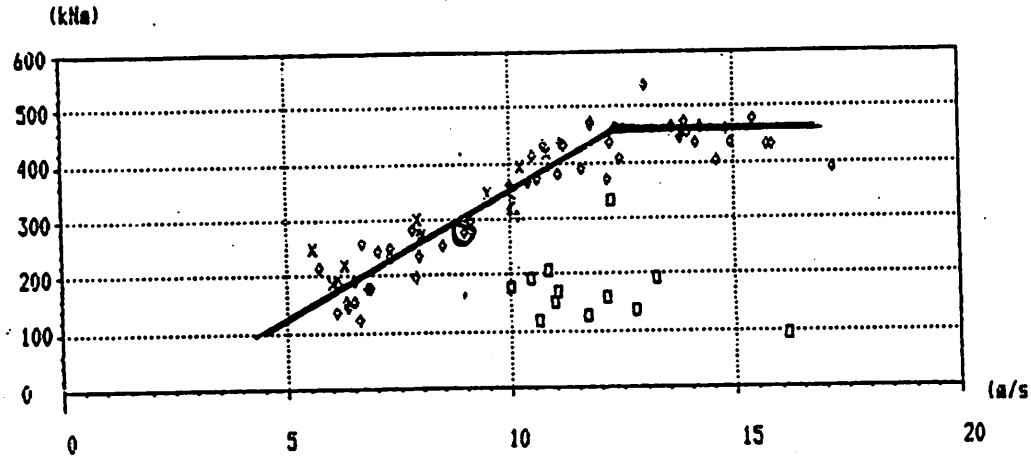


Average edgemoment as funcion of mean wind speed

Fig 1 b

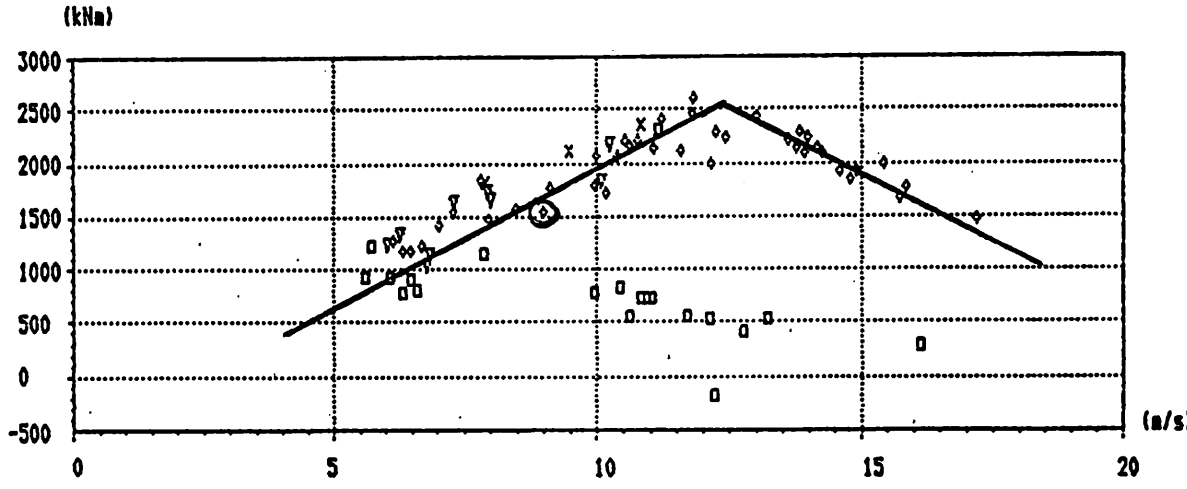


Average flapmoment as function of mean wind speed

Fig 1 c

When regarding only situations which represent normal operation ( ◊ in figures), the shape of the tendency lines are as expected. The average edgemoment, not including the wheight of the blade, shows the contribution from one blade to the driving torque of the primary shaft and corresponds to the power control as the wind increases. In the same manner the average flapmoment shows what happens to loads in wind direction.

In our evaluation tried to separate the periodic and stocastic parts of the load variation. This information is, as mentioned

before, of great value for the designer. The polar diagram in figure 2 below shows to the left evaluated flapmoment representing several revolutions. In the right part of the figure an evaluation of the mean curve with superimposed standard deviations (+/-) are shown.

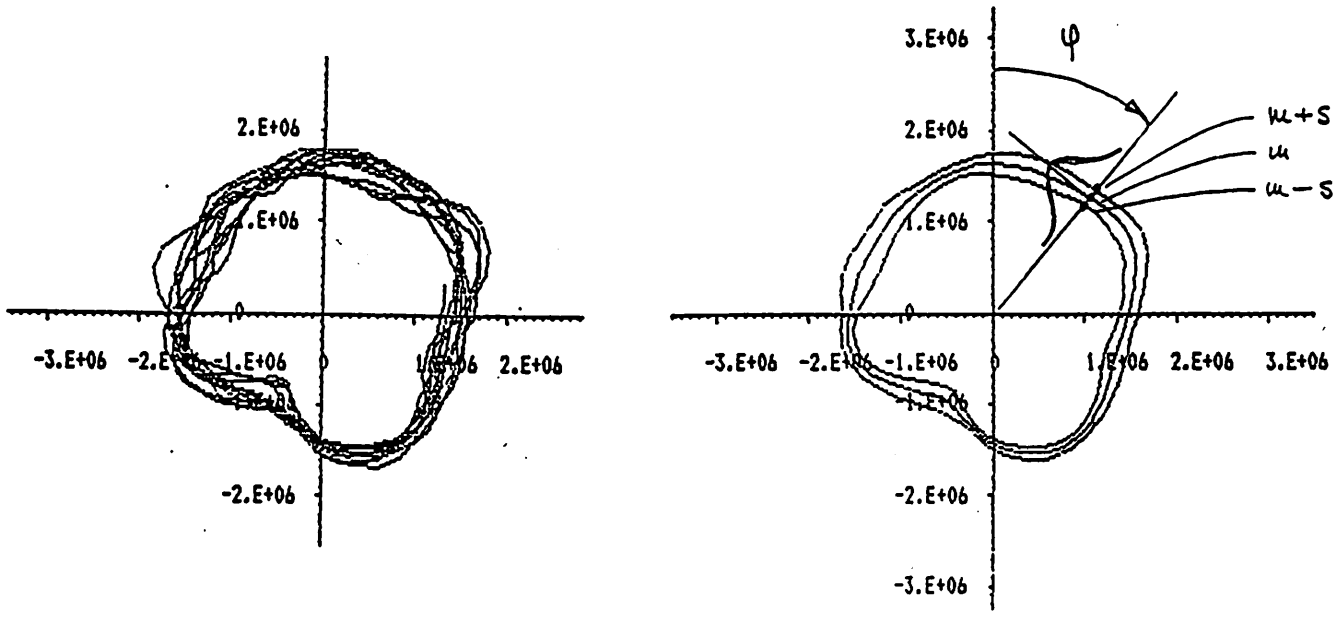


Flapmoment mean curve and standard deviation calculated from a polar diagram.

Fig 2.

Calculating the variance ($\sigma^2$cycl) of the cyclic mean curve gives an estimate of the periodic contribution to the load variation. Then comparing the cyclic mean curve with individual evaluated points makes it possible to calculate the variance "around" that mean curve. The value of that variance ($\sigma^2$stoc) could be interpreted as the stocastic part of the load variation.

As an exemple of the results of evaluated flapmoment from measured campaigns, figure 3 shows the two separated parts of the total variance. One of the preliminary result is that these two parts are almost alike. What the relation is for other parts of the blade remains to evaluate. Another result is the correspondence between the two load variances and wind parameters describing windshear ( $\Delta V$ ) and turbulence ( $\sigma_v$ ). This comparison indicates that the designers way of regaring the wind as composed of one periodic and one stocastic part has some confidence.

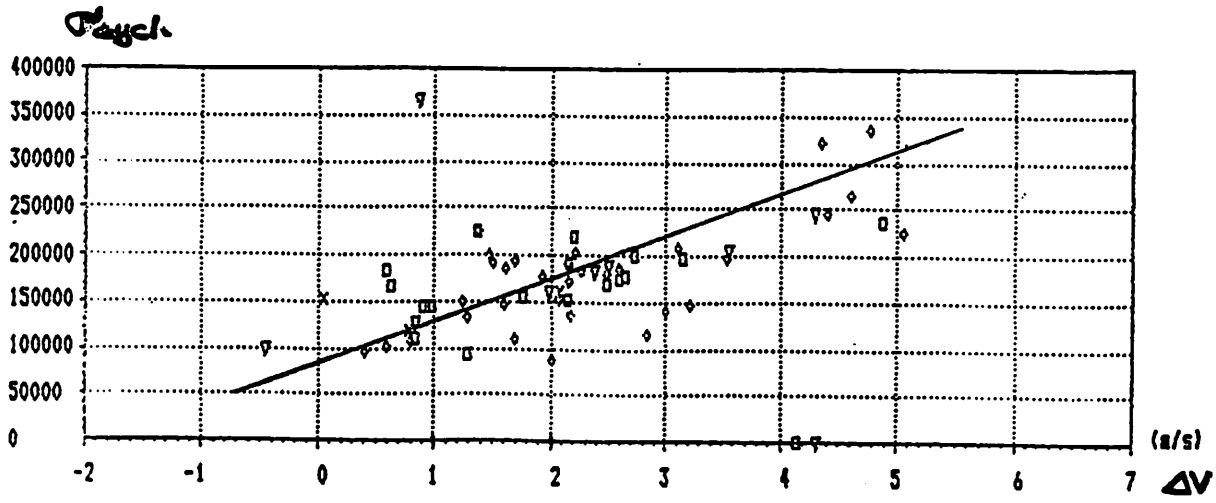


The cyclic standard deviation of the flapmoment as funcion of wind shear, defined as differens in wind speed over the rotorarea.

Fig 3 a.

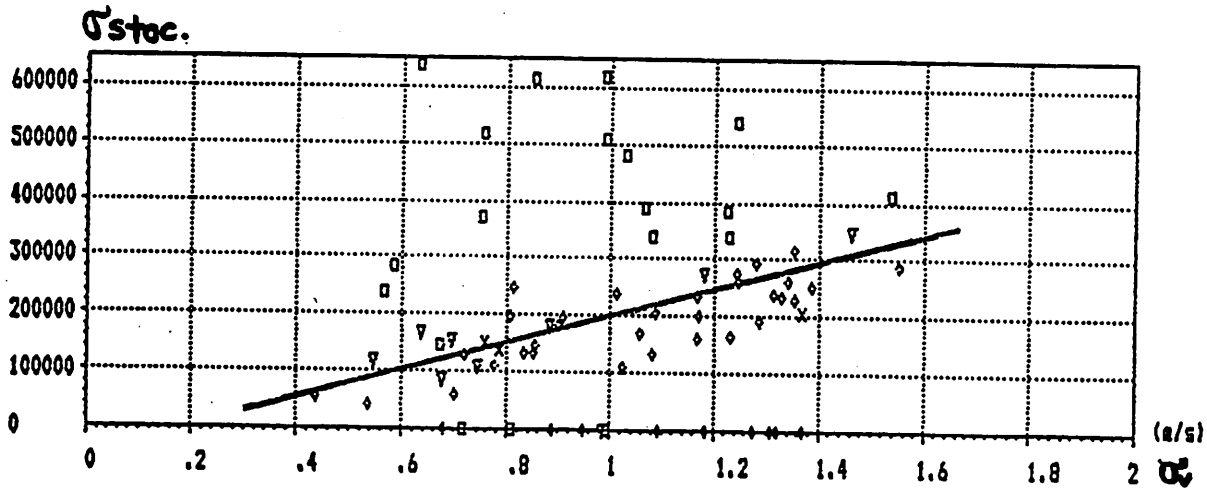


The stocastic standard deviation of the flapmoment as function of standard deviation of the wind speed.

Fig 3 b.

# THE PREDICTION OF TURBULENCE INDUCED LOADS ON A WIND TURBINE ROTOR

A D GARRAD

This note is intended as a brief record of the presentation made at the IEA expert meeting. It provides a commentary for the slides used by the author in his presentation.

The prediction of turbulence induced loads on a wind turbine rotor involves several stages: the characterisation of the turbulence input in the rotating field; a model of the aerodynamic behaviour of the rotor and a model of the dynamics of the structure. Each stage involves certain assumptions and approximations. The approach taken in this study has been very traditional in the sense that the modelling of each stage of the analysis has been performed using well tried and tested techniques, albeit in rather unfamiliar conditions. Thus the wind is modelled using the von Karman correlation function suitably transferred into the rotating frame. The aerodynamic model is based on strip theory and the structural dynamic behaviour is characterised by the natural modes and frequencies of the structure.

The total load experienced by a wind turbine is a mixture of both stochastic turbulence induced, loads and the deterministic, periodic, loads produced by tower shadow, wind shear etc. The latter features are therefore also included in the mathematical model.

The philosophy and purpose of the present model is outlined in slide 1. It will be noticed that the end product of the model is the prediction of fatigue life. Implementation of this last step is presently under way.

The capabilities of the computer model are listed in slide 2. The treatment is limited to horizontal axis machines, but otherwise all generally used designs may be analysed.

The structure of the program itself is shown schematically in slide 3. It should be noticed that using this arrangement the two types of load are calculated separately. This is an important point when comparisons are to be made between theory and experiment.

Slide 4 shows two important mathematical details of the analysis, both of which make the analysis rather more difficult to deal with than a simple uncoupled system. The main reason for the complexity is the fact that the aerodynamic damping matrix is full, which results in a degree of coupling between all the originally uncoupled modes. This characteristic, combined with the importance of correlation of the loads over the rotor disc, results in spectral densities of the generalised coordinates which are (n x n) matrices for a system with n natural modes.

The status of the code at the time of writing is shown in slide 5. At present the power spectrum and hence the variance of the loads, both stochastic and deterministic, as a function of radius and tower height can be computed for one-, two- and three-bladed machines. The code is developing very fast in the directions shown in slide 6. The major thrust of the development is being undertaken under the first two headings.

In slide 1 it was stated that one of the purposes of this model was to provide a code which could be validated at different stages and thus an attempt could be made to assess the accuracy of each separate step. Slide 7 attempts to consider each of these steps.

It is judged, based on experience with the Wind Energy Group - Department of Energy monitoring programme on Orkney, that the deterministic input, the modal dynamic approach and the resultant deterministic dynamic loads, are reasonably well understood, at least for fairly stiff machines.

The stochastic input - the wind turbulence - is that used as standard practice in wind loading calculations. It does, nevertheless, suffer from considerable simplifications. In so far as the model has been tested in its application to wind turbine technology it seems to have performed reasonably well. The transformation of the turbulent input into aerodynamic loads requires the development of a linear transfer function. Again there appears to be little alternative. This may well be a weak link.

The dynamic model can be used with some confidence and can be tested separately from the rest of the system.

Without any further assumptions or approximations the output spectra and time histories can be calculated which, in turn, may be presented in terms of their variance as sketched on slide 7.

The question now arises of how to interpret these results. To produce fatigue estimates further assumptions must be made about the material properties, the way in which the loads combine, the nature of the underlying probability distribution of the stochastic loads and the type of response that results, i.e. whether it is broad or narrow based. The group at Risø have tackled these problems and by making various, unavoidable, assumptions have produced fatigue estimates. Our code is shortly to be extended in the same way.

Finally, slide 8 gives a list of limitations to the method described here. The turbulence is assumed to be homogeneous, isotropic and stationary. In practice it is rarely any of these things. In particular the definition of stationarity is important when attempting validation. During the validation process it is necessary to separate the deterministic and stochastic signals by averaging over a certain time. For meteorological purposes 10 minutes is normally taken to be the minimum and 60 minutes a sensible period. For wind turbine applications experience has shown that the active elements of the system, i.e. power and yaw control may obscure the underlying patterns and thus preclude use of these long averaging periods. There are non-linearities at many points in the system and for the stochastic part of the analysis all of these must be linearised. One important approximation, which is shared by time series methods, is the treatment of blade stall. When stall occurs the characteristic signature of the loads will no longer be closely connected to the input turbulence; it will be dominated by the nature of the separated flow - a very non-linear process.

The use of spectral techniques demands that the basic differential equations of the system should be linear and have constant coefficients. The inclusion of a proper model of the tower will result in the presence of periodic coefficients. Thus only a simple tower model can be accommodated.

It has been shown that the method used here to predict wind turbine loads has a firm foundation and allows close examination of the assumptions made at each step of the process. Clearly there are weaknesses which should be appreciated when interpreting results. Nevertheless the method offers a fast and complete means of predicting the important loads that takes proper account of the turbulent input.

# PURPOSE

- Include all realistic load contributions

  Deterministic

  Stochastic

- Create economical model whose validity can be tested

- Provide aeroelastic model of *salient* features

- Interpret in terms of fatigue life

# CAPABILITIES

- Arbitrary aerofoil characteristics
- Arbitrary chord and twist
- Up to 10 rotor modes
- 1, 2 or 3 blades
- Teeter or rigid hub
- Accurate rotor dynamics and approximate tower dynamics

# PROGRAM STRUCTURE

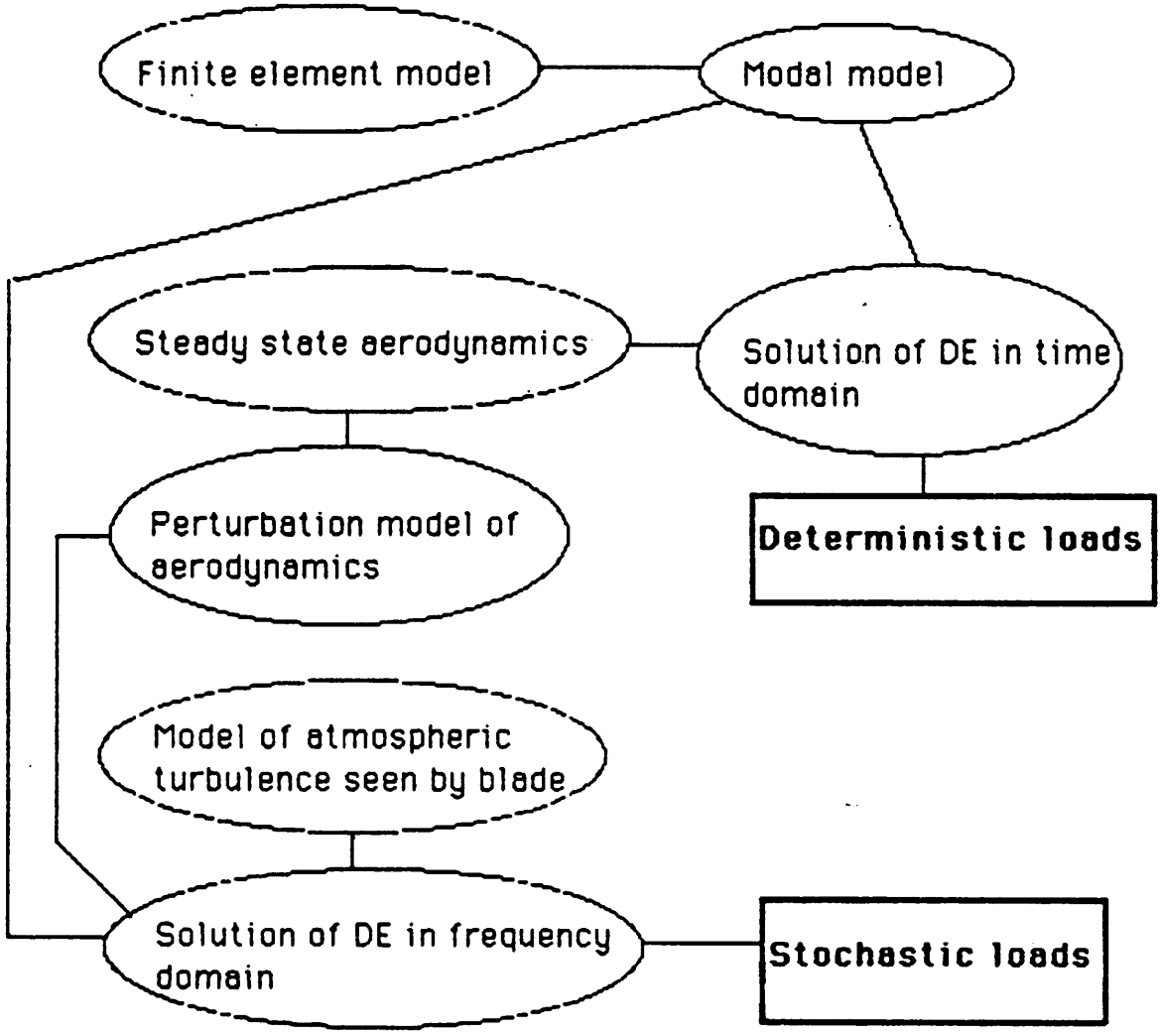

# MATHEMATICAL COMPLEXITIES

*Time domain*

- $[M]\ddot{\underline{q}} + [C_S + C_A]\dot{\underline{q}} + [K]\underline{q} = \underline{p}$

  *Structural and aerodynamic* — *Structural and centrifugal*

The damping matrix is full due to aerodynamic coupling beween modes.

*Frequency domain*

- $[S_{QQ}(w)] = [H][S_{PP}(w)][H]^{*T}$

$H = H(w)$

$[S_{PP}]$ and $[S_{QQ}]$ are matrices.

# PRESENT STATUS OF GARRAD HASSAN ANALYSIS

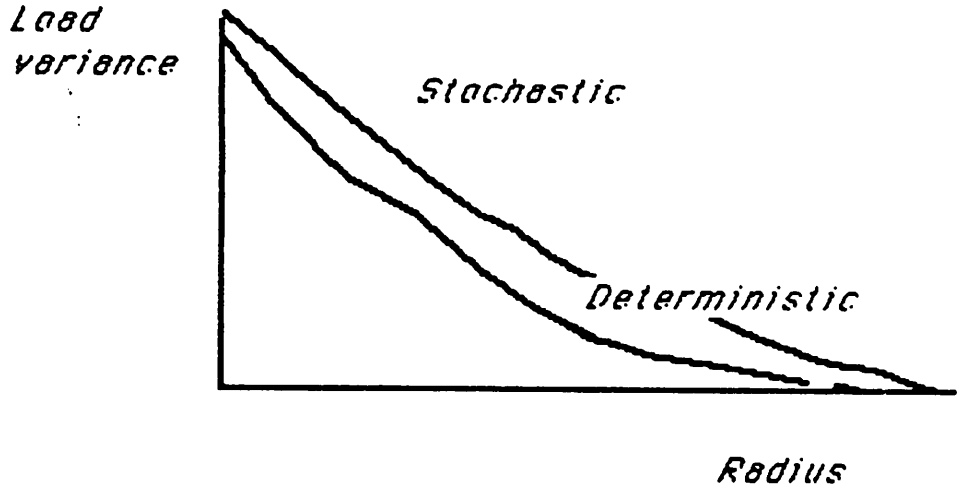


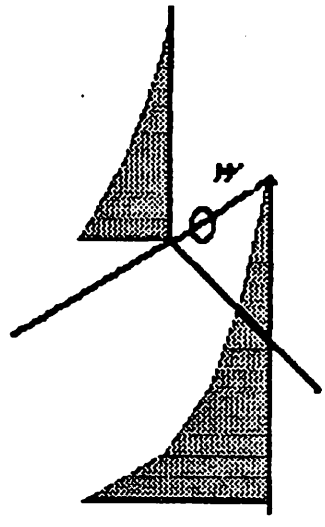


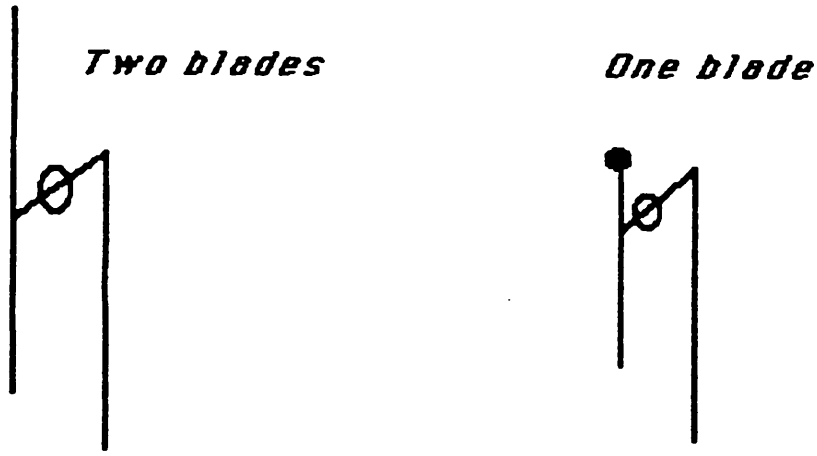

## DEVELOPMENTS

- Fatigue calculations

  *Raab*
  *Madsen Frandsen et al*

- Validation

- Unsteady aerodynamics

- Improve wind model

# Where do the problems lie?

**Deterministic** **Stochastic**

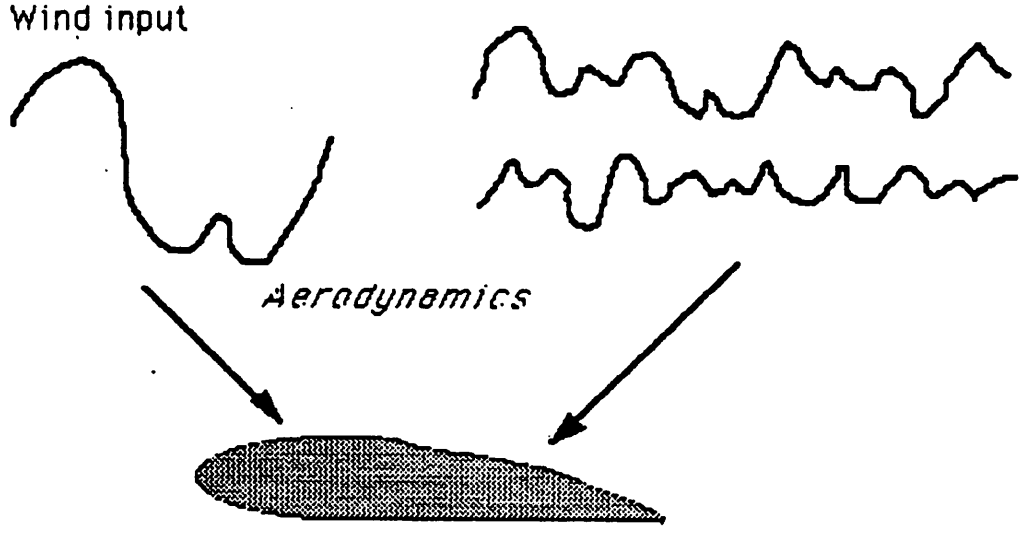


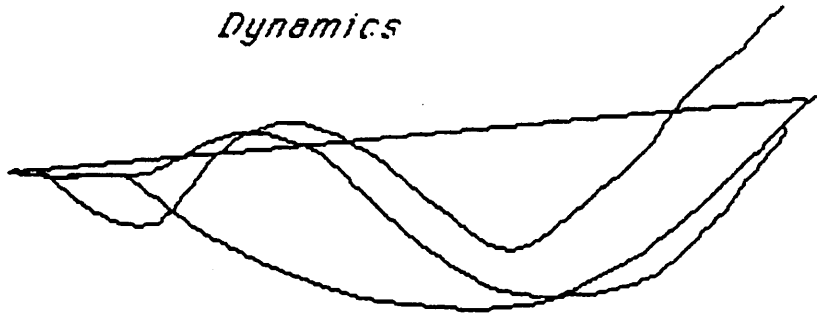


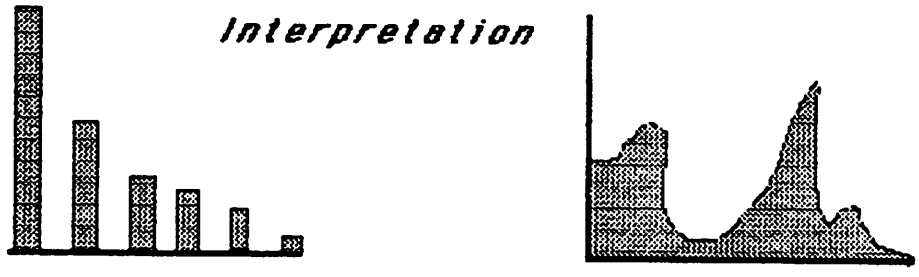


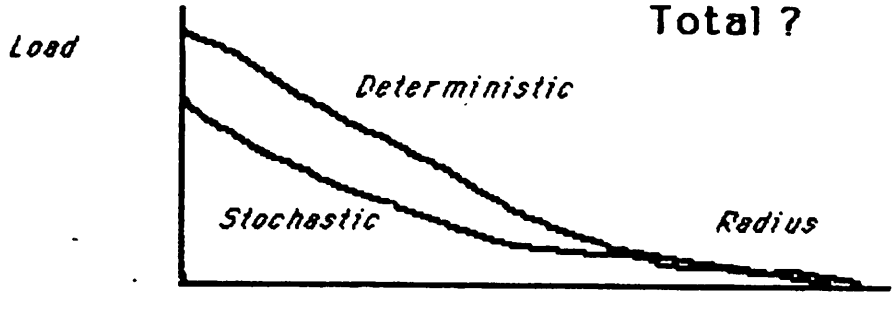

## GENERAL LIMITATIONS

- HI Turbulence
- Stationarity
- Linearity

  *Inability to cope with stalled blades*
  *transient stall*

- Periodic coefficients

  *No proper treatment of tower loads*

J.B. Dragt

Load fluctuations and response of rotor systems in turbulent wind fields.

A model has been developed at ECN to take both time and space dependence of incoming wind turbulence into account to determine the apparent wind speed fluctuations for a rotating wind turbine blade and the consequent load fluctuations. There are some recent publications on this work [1-3], which also give references to related work elsewhere.

The model emphasizes a frequency domain approach from the beginning. First it is shown from a simple physical picture how the frequency spectrum of the (most relevant) longitudinal wind speed fluctuations is transformed, when the fluctuations are observed from a point of a wind turbine blade, rotating at the relatively high frequency $f_o$ in a plane perpendicular to the mean wind speed. The transformation is sketched in fig. 1. The power of a fluctuating component at frequency f is attenuated, and this power is shifted by a kind of modulation mechanism to frequencies $f_o \pm f$, $2f_o \pm f$, etc. ("rotational modes"). The simple physical picture is described in ref. [1] and the mathematical details have been reported in [2,3]. An example of a computed wind velocity spectrum under realistic conditions is shown in fig. 2.

For these fluctuations both spectra and cross-spectra (for two different arbitrary blade elements) can be obtained. They are the basis for the computation of spectra of fluctuating loads. If the response is linear (no stall) such spectra can be calculated for a rigid rotor. Such spectra can be compared to experimental spectra. One such comparison has been made in ref. [1] for the 25 m HAWT of ECN. Some results are reproduced in fig. 3. The overall agreement is satisfying. At a closer look some discrepancies exist, however, which have been shown to be largely due to blade and drive train dynamic effects. This experimental model verification is still under further study.

It is important to include the blade dynamics and the aero-elastic effects in the analysis. This can be done in a rather general way, but a simple demonstration is given in ref. [2,3] for the case of blades which are attached to the hub by hinges, with or without own stiffness. The flapping motion of such a mechanism appears to work as a frequency filter for the loads, depending on physical blade parameters like mechanical, centrifugal and aerodynamic stiffness and aerodynamic damping.
A computed example is given in fig. 4.

Finally, it is possible to use these frequency spectra of loads to estimate fatigue damage rates. Several calculations have been made (using a Risø recipe) and reported in ref. [3]. To allow general conclusions, avoiding specification of constructional details, the damage rates have been normalized to the situation of a (hypothetical) turbulence which is fully coherent over the plance of the rotor. Results are dependent on the rotational modes that contribute to the damage rate of a particular component. An excerpt for a stiff rotor is given in table I.

References

[1] Dragt, J.B., The Spectra of Wind Speed Fluctuations Met by a Rotating Blade, and Resulting Load Fluctuations,
Proc. European Wind Energy Conf. 1984, Stephens & Ass., Bedford 1985, p. 453.

[2] Dragt, J.B., Load fluctuations and response of rotor systems in turbulent wind fields, paper at the WIND POWER '85 conference, San Francisco 1985, proceedings to be published.

[3] Dragt, J.B., Load fluctuations and response of rotor systems in turbulent wind fields, Extended version of the WIND POWER '85 conference paper, report ECN-172 (Oct. 1985).

Table I: Fatigue damage rates due to turbulence (25 m HAWT at 11 m/s), relative to the case of full coherence, for different sets of rotational modes, with an S/N-curve of slope -3.

| modes contributing | relative damage rate |
|---|---|
| 0 | 0.11 |
| 0+1 | 0.65 |
| 0+1+2 | 1.09 |
| 0+1+2+3 | 1.47 |
| 0+1+2+3+4 | 1.79 |
| 0 | 0.11 |
| 0+2 | 0.72 |
| 0+2+4 | 1.10 |

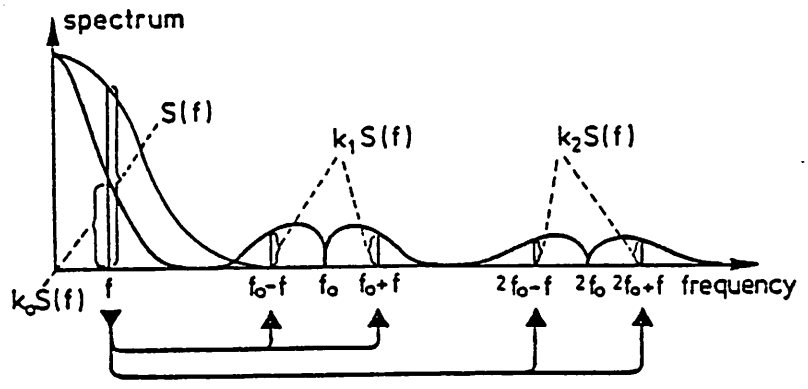


Fig. 1. Schematic diagram, showing the transformation of the power spectrum of wind speed fluctuations.
The transformation of the original spectrum (S(f)) of a stationary observer is due to the rotational sampling by an observer on a wind turbine blade element. As a result the original turbulence is attenuated and the power is shifted and concentrated around rotor rotational frequency $f_o$ and harmonics (i.e. 1P, 2P, ... peaks) - denoted as "rotational modes".

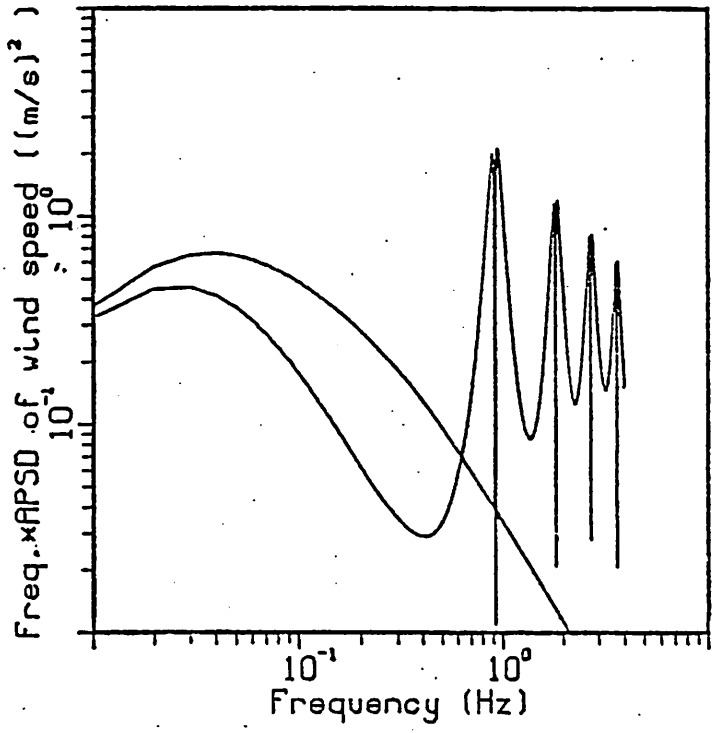


Fig. 2. Spectrum of longitudinal wind speed fluctuations, as seen from a rotating blade element ($\bar{U}$ = 11 m/s, r = 12.5 m, $f_o$ = 0.92 Hz i.e. 55 rpm), compared with the smooth stationary spectrum.

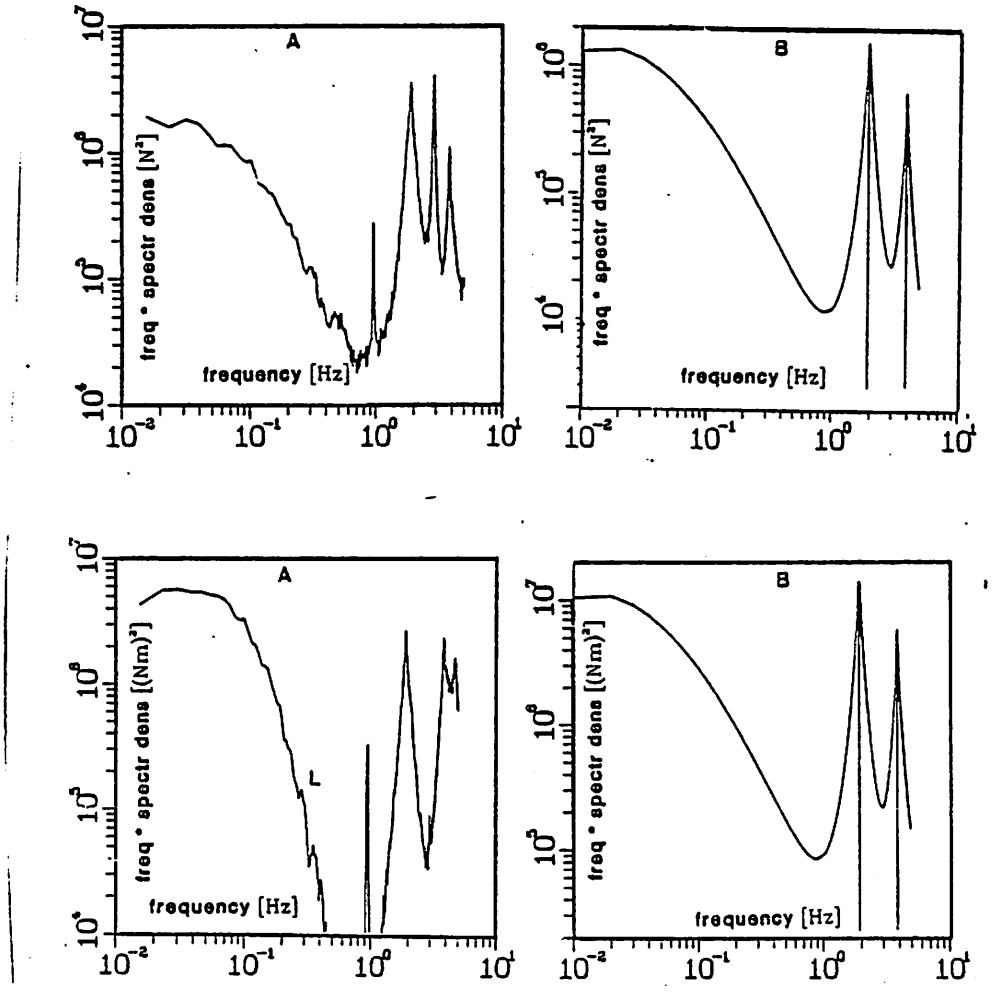


Fig. 3. Comparison of measured and calculated load spectra of 25 m HAWT:
- upper figures for the axial force of the rotor,
- lower figures for the shaft torque.
The model parameters for the incoming wind speed fluctuations were derived from simultaneous wind measurements with an anemometer array ahead of the rotor. This is the only normalization of data for this comparison.

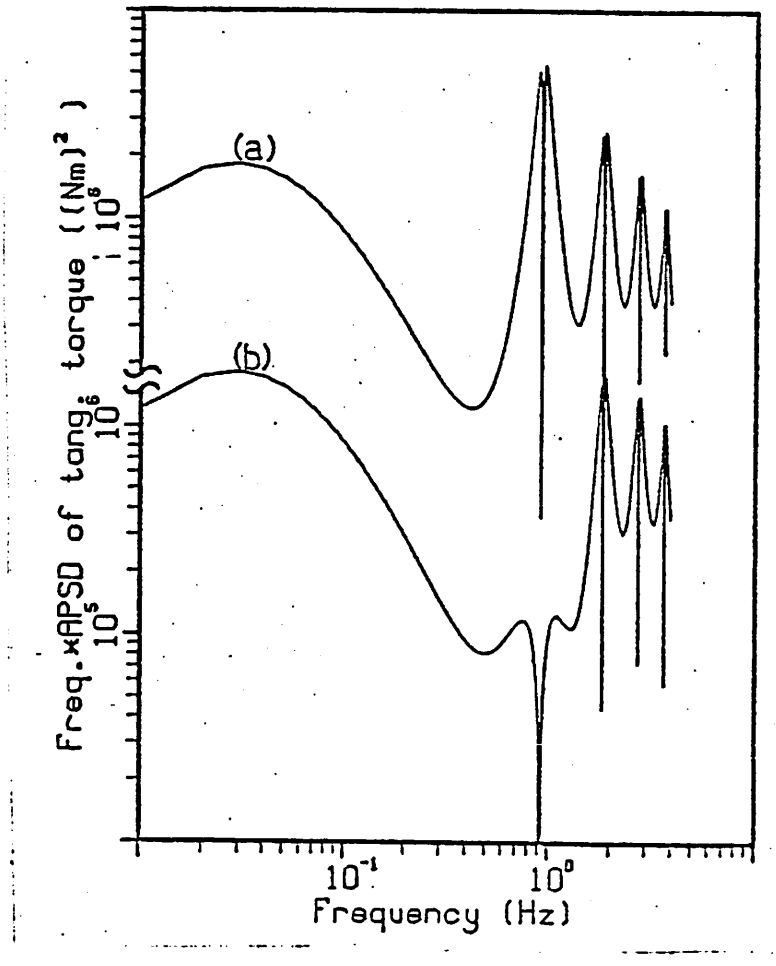


Fig. 4. Spectrum of edgewise moment fluctuations of a 25 m HAWT blade, (a) for rigid hub, (b) for freely hinged blade.

The calculation demonstrates that the flapping motion largely filters the 1P-component in the load spectrum away.

# TURBULENCE INDUCED ROTOR FATIGUE DAMAGE

D.C. Quarton

Synopsis The impact of wind turbulence upon the measured blade strain and fatigue damage of the WEG 20m wind turbine rotor is considered. A brief description of the theoretical method adopted by WEG for computation of turbulence induced response is given, and comparisons of prediction and measurement presented. The comparisons are discussed with reference to their discrepancies.

## 1. INTRODUCTION

It has become increasingly clear over recent years that a major problem in the design of wind turbines is the inability to predict accurately the fatigue life of the principal structural components. One reason for this is the lack of definitive data describing the fatigue properties of the commonly used materials and structural elements. However, a further, and somewhat more fundamental cause of the problem, has been the inadequacy of methods used in design for the calculation of component loads and stresses. Such inadequacy is associated in particular with the calculation of wind turbulence induced loads, the methods used for prediction of deterministic response being relatively well researched, and validated for most operational conditions.

The Wind Energy Group (WEG) is concerned to develop models for the prediction of structural response and fatigue lifetime, which may be used economically, and with confidence of their accuracy, during design. The procedure adopted has been to consider the problem firstly from basics, in terms of the steady aerodynamic loads on the wind turbine structure, building up the realism and complexity of the theoretical models in step with their validation by means of measured data. Such measured data, obtained from the Orkney 20m turbine, MS1, by means of the Burgar Hill monitoring system (1), has therefore been invaluable for this process of model development.

Previous reports of the analysis of MS1 monitored data, (2, 3, 4), have been concerned chiefly with the deterministic response of the machine. The main subject of this paper is the impact of wind turbulence upon rotor fatigue damage. Following the presentation of measured data indicating the damaging influence of turbulence, the principal features of a theoretical model for the calculation of turbulence induced structural response will be described. Finally, predicted and measured responses are compared in terms of spectra. The analysis of measured data discussed in the paper is typical of that carried out at WEG as part of the MS1 Monitoring Project.

## 2. STRAIN DATA COLLECTION AND PROCESSING

The strain data considered in this paper has been measured during steady, rigid hub, operation of the MS1, by means of strain gauges mounted at 33% radius on blade B. The data was collected at a sampling frequency of 125 Hz for a campaign duration of 240 secs. Further data describing the meteorological conditions during the campaign was also recorded, and this is summarised in Table 1. It is clear that the hub height windspeed, turbulence intensity and yaw offset were approximately constant throughout the campaign.

### 2.1 Fatigue Damage Assessment

The strain data of particular interest when studying the effects of wind turbulence, is that measured in the flapwise direction, the edgewise strain being dominated by the gravity induced cyclic response at 1P. A 20 sec. sample of the flapwise strain time history recorded at the 33% radius location is shown in Figure 1. The time history shows clearly the stochastic nature of the strain response. By means of the fatigue damage assessment program, FATIMAS, the cycle distribution for the whole 240 sec. strain time history may be computed using rainflow techniques. The results of such a calculation are presented as a histogram in Figure 2, giving the percentage of the total number of cycles within a specified stress mean and range bin.

The calculation may then be taken a stage further to obtain the equivalent fatigue damage distribution presented in Figure 3. Here the histogram gives the percentage of total damage accumulated in the 240 sec. time history, associated with each stress mean and range.

The cycle and damage distributions display an important characteristic in that a high proportion of the total damage is associated with a relatively low number of large range stress cycles. In fact, it is only the upper 5.5% of cycles which cause 61% of the total damage during the campaign. This clearly indicates the extremely damaging effect of wind turbulence.

The analysis may be extended. The underlying deterministic strain response during the campaign, excited by cyclic pertubations of the incident wind velocity due to such as wind shear, yaw and tower shadow, may be extracted from the total measured signal by means of azimuth binning. This procedure has been described in some detail in (4) and consists essentially of dividing the rotor disk into a number of azimuthal bins, and binning the measured data such that the strain at a particular blade azimuth is stored in the bin which spans that azimuth. The mean strain in each bin then gives the underlying deterministic response. This has been carried out for the data discussed above, and the deterministic signal is presented in Figure 4. The fatigue damage associated with this deterministic strain during the 240 sec. campaign has been calculated at $0.025 \times 10^{-6}$ and is to be compared with the damage accumulated by the total strain at $0.18 \times 10^{-6}$. Assuming continuous operation under these meteorological conditions, failure of the blade according to the deterministic strain would occur after approximately 300 years, whereas according to the total measured strain, failure would occur after 43 years. Although this comparison may not be wholly meaningful in practice, it nevertheless gives a clear indication of the critical impact of turbulence upon blade fatigue lifetime.

## 3. PREDICTION OF TURBULENCE INDUCED RESPONSE

The frequency domain approach to the prediction of turbulence induced wind turbine dynamic response has been described in detail by Madsen et al (5), and Garrad and Hassan (6).

Longitudinal turbulence is assumed to be described by the von Karman correlation function which, by means of Taylor's Frozen Turbulence hypothesis, can be used to relate windspeed fluctuations at two points separated in time and space. Adjustment of the model to a frame of reference rotating with the blades, has the effect of transferring turbulent energy from low frequencies to higher ones associated with the rotational frequency and its harmonics.

### 3.1 Blade Surface Pressure Spectrum

Pressure data collected from the MS1 turbine rotor has allowed the validation of an analytical model of turbulent response. The transducer was mounted at 7.0 metres radius on the high pressure side of the blade at the 17% chord position. After only a short operational life the transducer failed, but fortunately sufficient data had been collected by this time for comparison purposes.

The pressure at a discrete point on the blade is a function of the square of the incident wind velocity and also the local pressure coefficient. The latter is in turn a function of the angle of attack. Given the high ratio of

blade rotational velocity to longitudinal wind velocity all these factors can be approximated as linear functions of the longitudinal wind velocity. Thus the spectrum of turbulent pressure can be obtained by applying an appropriate factor to the turbulent wind spectrum.

Figure 5 shows the hub level wind spectrum (solid line) calculated from a ten minute campaign of data. Superimposed on this plot is the von Karman spectrum of hub level wind turbulence with the turbulence length chosen to produce a 'good fit' to the monitored spectrum. The final curve on this figure is a prediction of wind turbulence as sampled on a rotating blade at 7.0 metres radius. The turbulence parameters for this case were unchanged from the stationary hub level condition.

These spectra show clearly the transfer of energy to the blade rotation frequency and the higher harmonics.

Figure 6 shows the pressure spectrum (solid line) calculated from data monitored during the same campaign. Superimposed on this plot is the prediction of turbulent pressure. These two curves agree closely in all regions except at the blade rotation frequency, and its harmonics. This discrepancy is as expected since the spectrum of monitored pressure contains both deterministic and turbulent components.

Figure 7 presents the turbulent energy levels associated with each harminic peak in the form of standard deviation. In this case the deterministic energy, identified by binning, has been subtracted from the monitored data to allow direct comparison of the turbulent components. Given the complex physical nature of the problem, these results exhibit remarkably good agreement.

## 3.2 Bending Moment Spectrum

The dynamic behaviour of the rotor is assumed to be described in terms of its natural modes, and the turbulent forcing of the modes is calculated by means of double integrals involving modeshapes, local aerodynamic influence functions and the rotating frame cross correlation function referred to above. These forcing terms are then developed in the frequency domain by means of 'fast Fourier transforms' to give the matrix of modal force spectral densities, $[S_{pp}]$. The response to turbulent forcing is subsequently computed by application of $[S_{pp}]$ to a transfer function representation of the rotor aerodynamics and dynamics, [H], where

$$[H] = \left[([K]-w^2\,[M]) + iw([C_s]+[C_a])\right]^{-1}$$

and the modal response matrix is given by,

$$[S_{QQ}] = [H]^* \,[S_{pp}]\,[H]^T$$

Here, [M], $[C_s]$, $[C_a]$ and [K] are the modal mass, structural damping, aerodynamic damping and modal stiffness matrices, and w is the frequency of response. It should be noted that the aerodynamic damping matrix is generally full due to coupling between rotor modes. Having evaluated $[S_{QQ}]$, the calculation of spectral density of real blade deflections and hence bending moments is relatively straightforward.

In order to validate the method, equivalent measured data is required. This is not however straightforward. Direct spectral analysis of measured strain

or bending moment time histories such as that discussed above, will result in the spectrum containing not only turbulent response but also that due to deterministic excitation. The solution is therefore to firstly azimuth bin the measured time history to obtain the deterministic response, subtract this from the total signal leaving the purely turbulent response, and perform the spectral analysis on this data for comparison with prediction. Although this process seems rather involved, it nevertheless offers the best method for step by step validation of the theory.

The campaign data considered in section 2.1, has been analysed in this way. The measured strain time history was, however, firstly transformed into out-of-plane bending moment, the deterministic response then extracted, and the turbulent spectrum computed as shown in Figure 8. The spectrum exhibits turbulent bending moment response at the rotational frequency and its harmonics up to 8P, and also at the rigid body drive train, tower fore-aft and first two blade flapwise modal frequencies. It should be noted that the spectral density is plotted on a logarithmic scale, and hence the response at frequencies above 8 Hz is approximately two orders of magnitude less than the dominant responses at frequencies close to 1P and 4P.

For prediction of the out-of-plane bending moment spectrum to compare with the measured data in Figure 8, only the first two blades modes have been included in the dynamic model. The predicted spectrum is shown in Figure 9.

A comparison of predicted and measured linear spectral density is given in Figure 10. It is apparent that prediction and measurement are in close agreement although discrepancies do exist in terms of an underprediction of the responses at 1P and 2P, and the non- prediction, due to the neglect from the theoretical model, of the rigid body drive train and tower fore-aft responses. Such discrepancies should not, however, be over-emphasised, the degree of predictive accuracy exhibited by the results of Figure 10 is very encouraging given the complex nature of the problem.

## 4. CONCLUDING REMARKS

It is now well known that wind turbulence has a critical impact upon the fatigue lifetime of wind turbine structural components. This has been demonstrated by means of a simple damage analysis of typical strain data recorded during an experimental campaign.

The procedure for prediction of turbulence induced response has been described, and comparison of prediction with typical measured data demonstrated. The agreement obtained to date is particularly pleasing, and encourages further effort towards a comprehensive validation of the predictive method.

A further step to be taken in the near future is the development of methods for combining predicted deterministic and stochastic components of blade load, This step is particularly important since it is the combination of the two components which is required as a realistic input to fatigue damage calculations during design.

## ACKNOWLEDGEMENTS

The authors acknowledge the support of the UK Department of Energy and the directors of WEG for their financial support and their permission to publish this paper. (WEG is the Wind Energy Group, a consortium of Taylor Woodrow Construction Ltd., British Aerospace plc., and GEC Energy Systems Ltd.).

REFERENCES

(1) HASSAN, U., HENSON, R.C. & PARRY, E.T. Design of a micromputer based data acquisition and processing system for the Burgar Hill, Orkney, wind turbines. 4th International Symposium on Wind Energy Systems, Stockholm, Sweden, September, 1982, 2, pp 137-152.

(2) GARRAD, A.D., HASSAN, U. & LINDLEY, D. Monitoring results and design validation of the Orkney 20m wind turbine generator. 6th British Wind Energy Association Conference, Reading, UK, March 1984, pp 76-84.

(3) GARRAD, A.D., QUARTON, D.C. & LINDLEY, D. Performance and operational data from the Orkney 20m diameter WTG. European Wind Energy Conference, Hamburg, W. Germany, October 1984, pp 170-176.

(4) WARREN, J.G., QUARTON, D.C. & LINDLEY, D. An evaluation of the measured dynamic response of the Orkney 20m Diameter WTG. 7th British Wind Energy Association Conference, Oxford, UK, March 1985, pp 259-268.

(5) MADSEN, P.H., FRANDSEN, S., HOLLEY, W.E. & HANSEN, J. Dynamic analysis of wind turbine rotors for lifetime prediction. Report, RISO Nat. Lab., 102-43-51, 1983.

(6) GARRAD, A.D. & HASSAN, U. Turbulence induced loads on a wind turbine rotor. 5th British Wind Energy Association Conference, Reading, UK, March 1983.

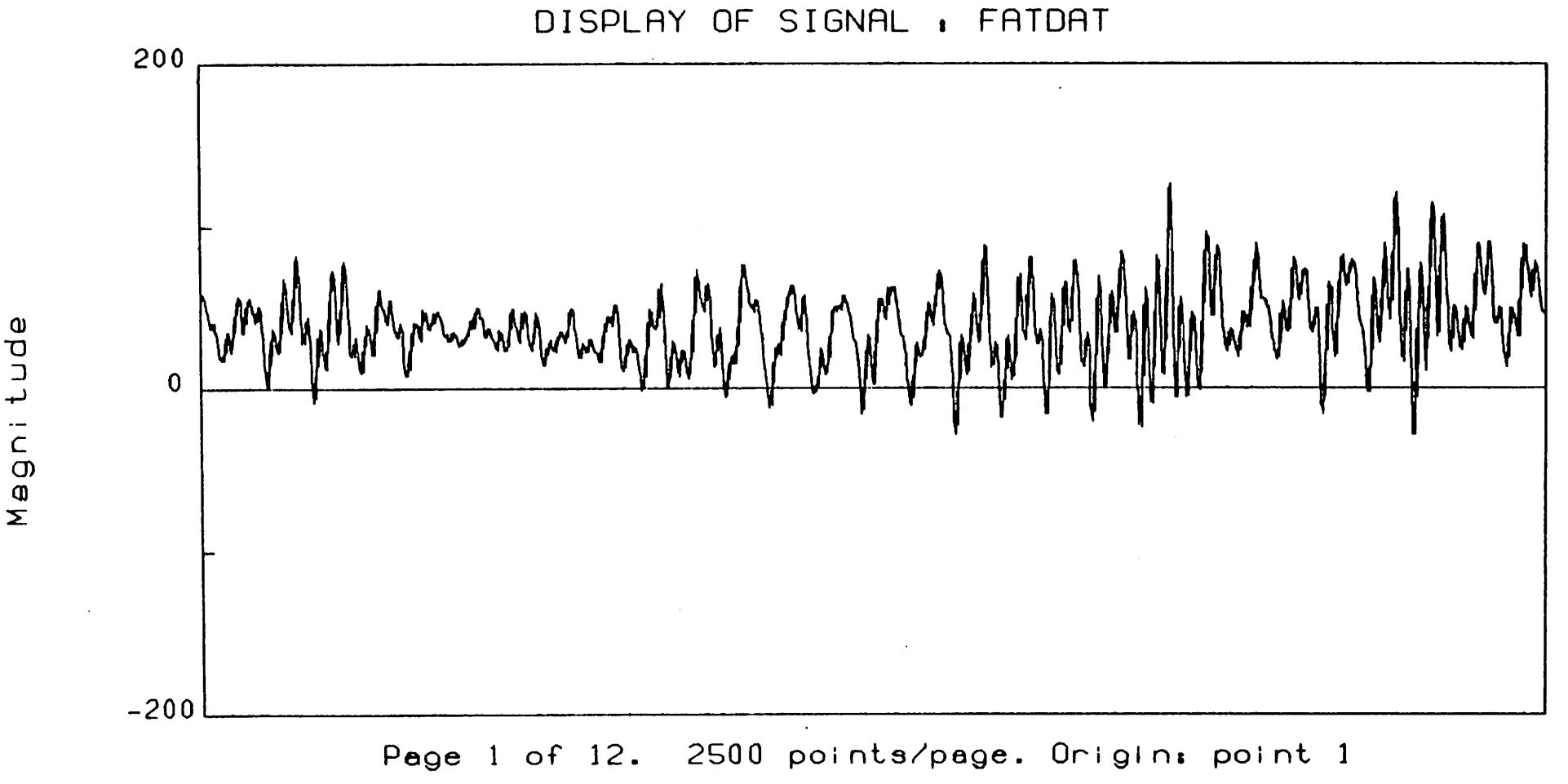


Figure 1 Flapwise Strain at 3.28 m on Blade B (20 secs.)

FATIMAS V2.3

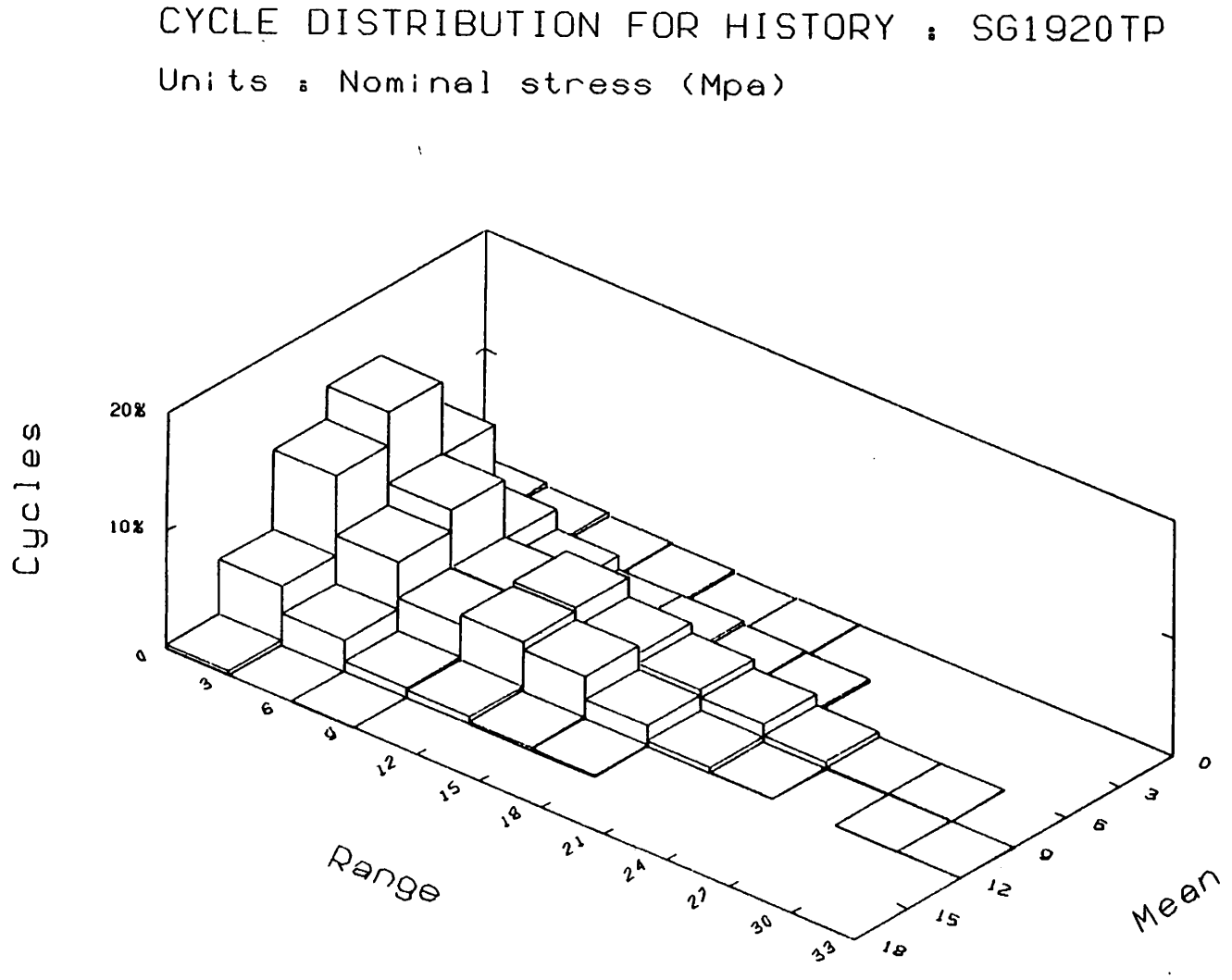


Figure 2 Cycle Distribution for Flapwise Strain at 3.28 m

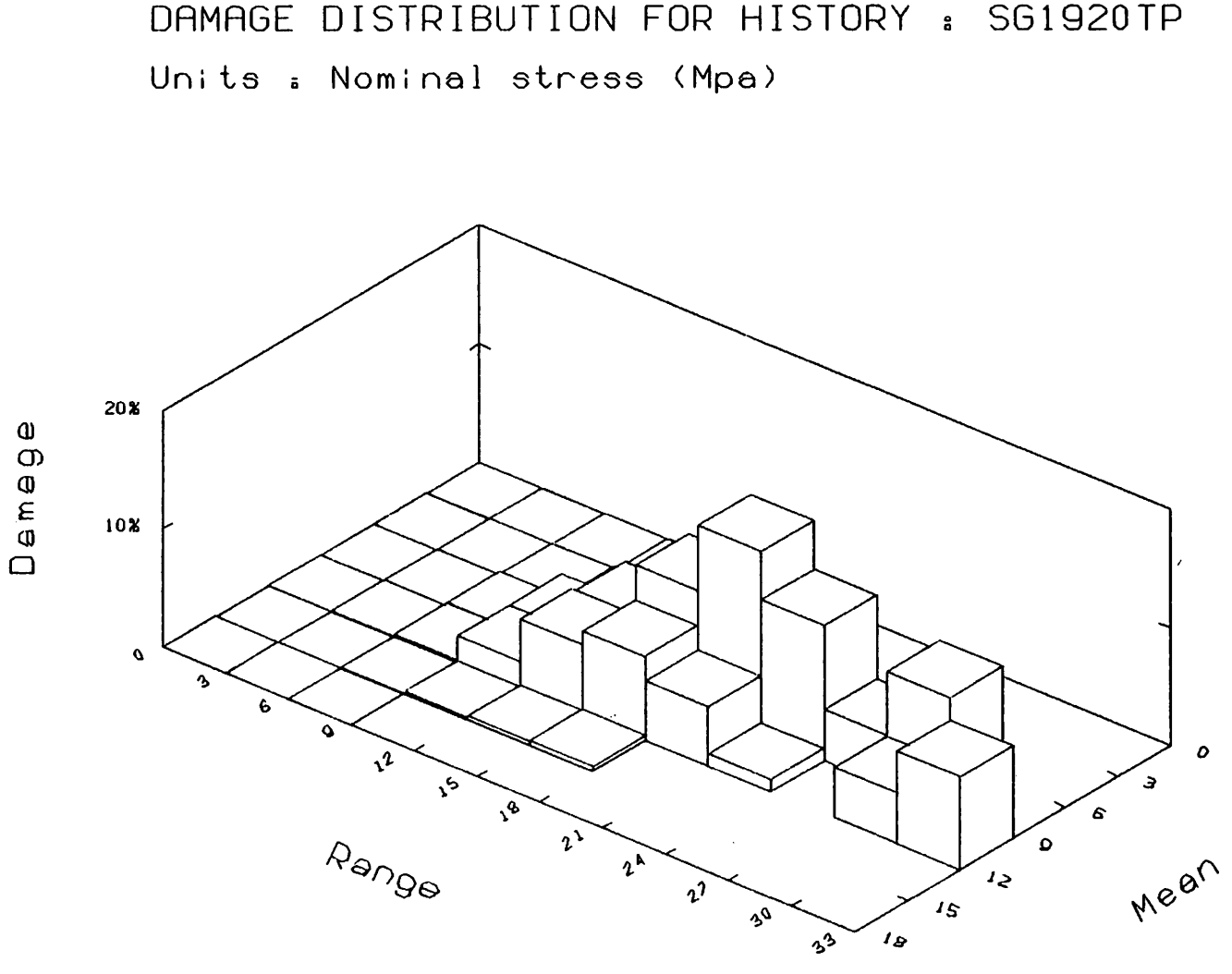


Figure 3 Damage Distribution for Flapwise Strain at 3.28 m

FATIMAS V2.3

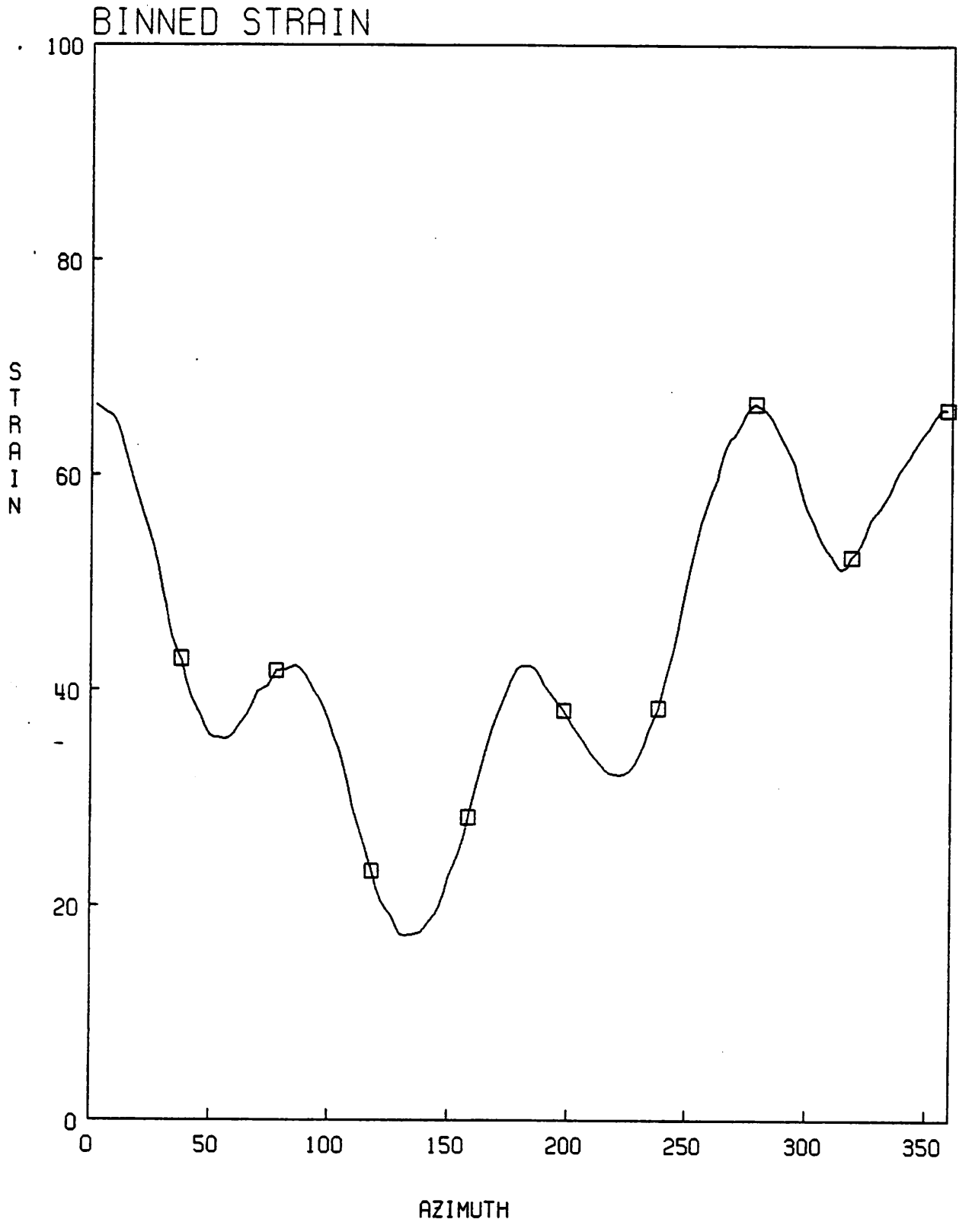


Figure 4 Azimuth Binned Flapwise Strain

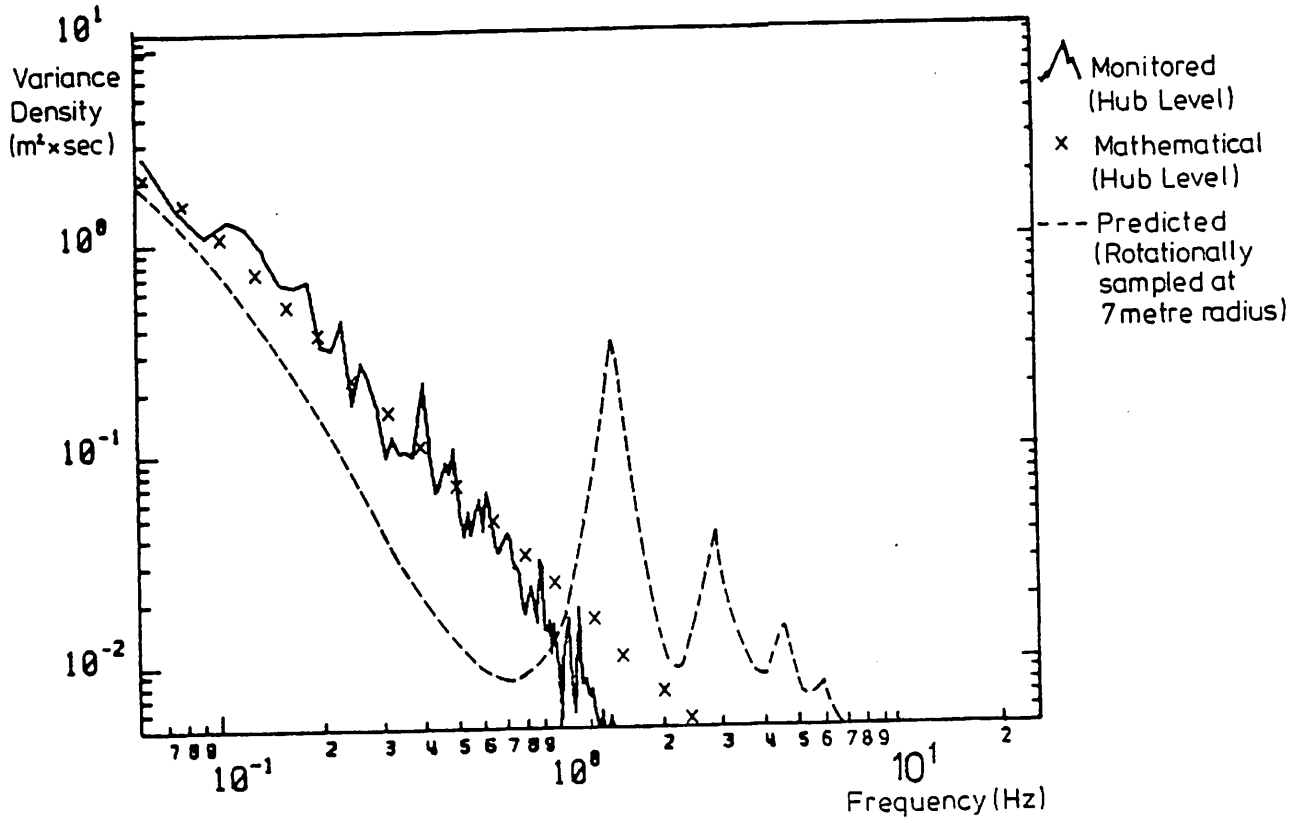


Figure.5. Wind Velocity Spectra

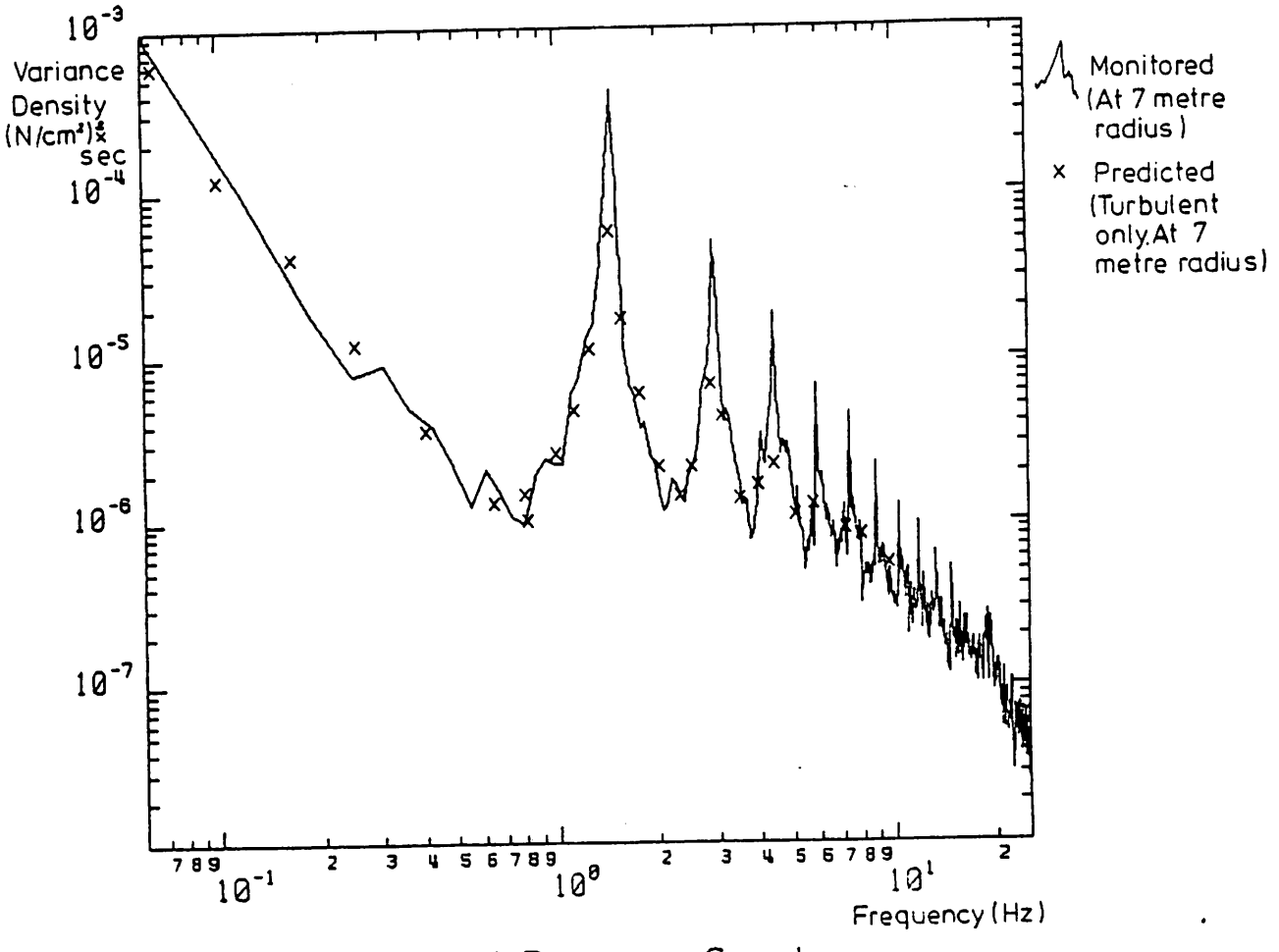


Figure.6. Pressure Spectra

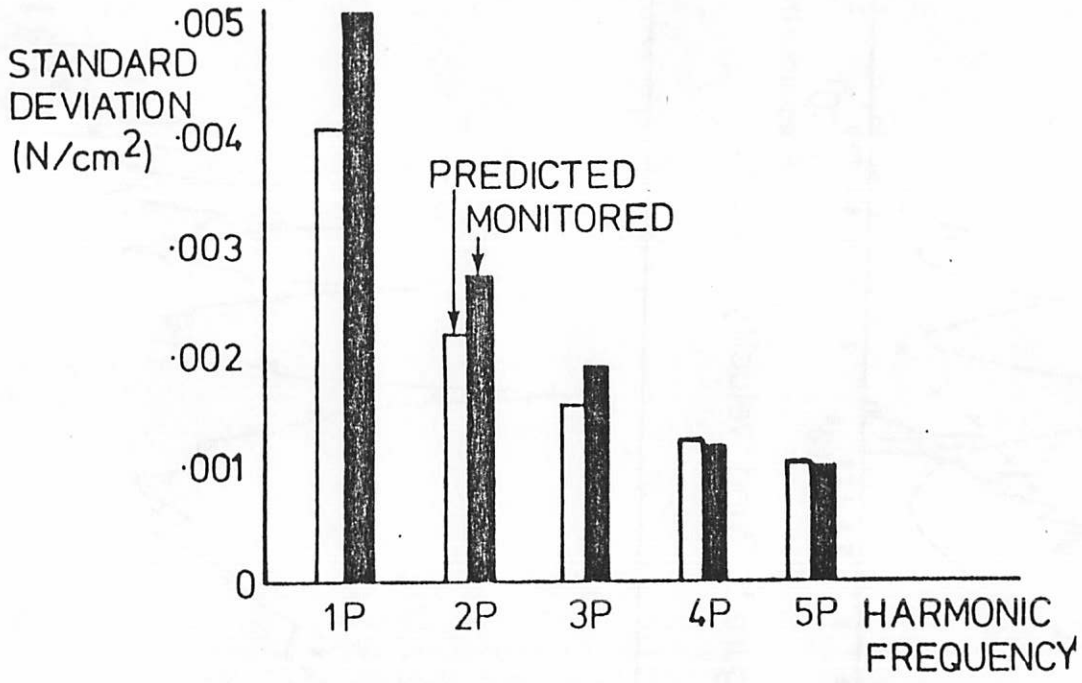


FIGURE 7 TURBULENT PRESSURE
AT 7m RADIUS

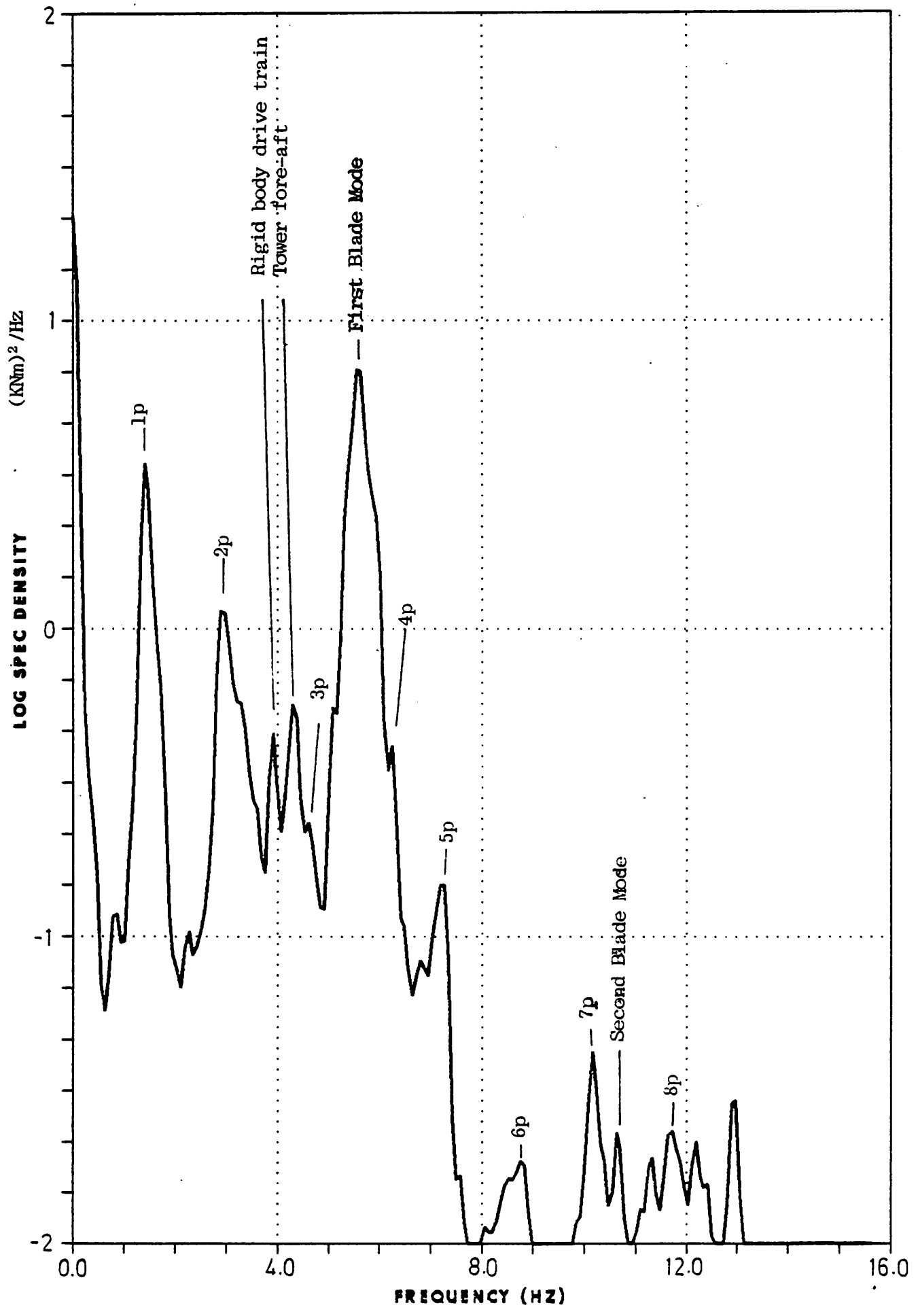


Figure 8 Turbulent Bending Moment - Measured at 3.28 m

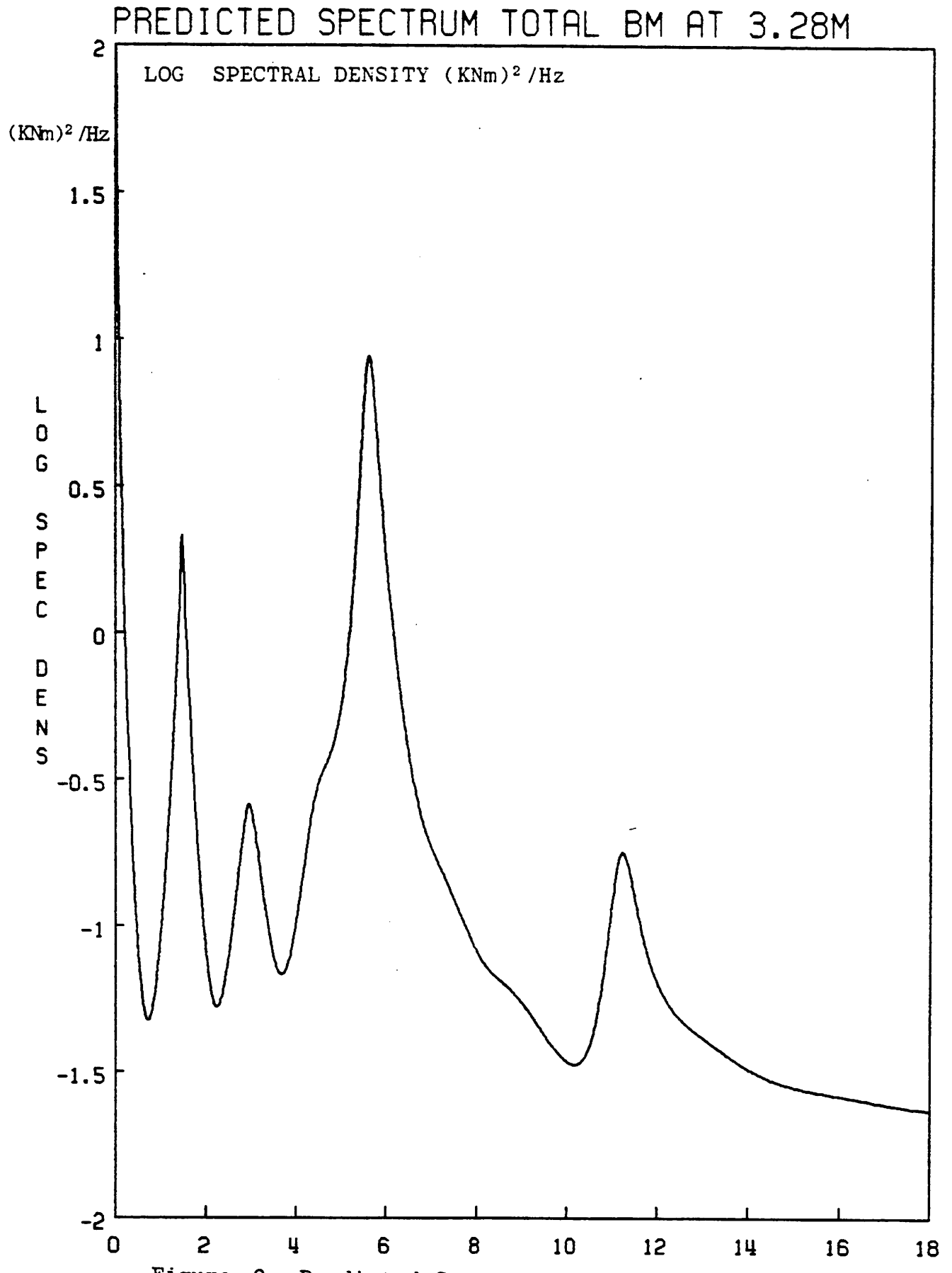


Figure 9 Predicted Spectrum of Total Bending Moment

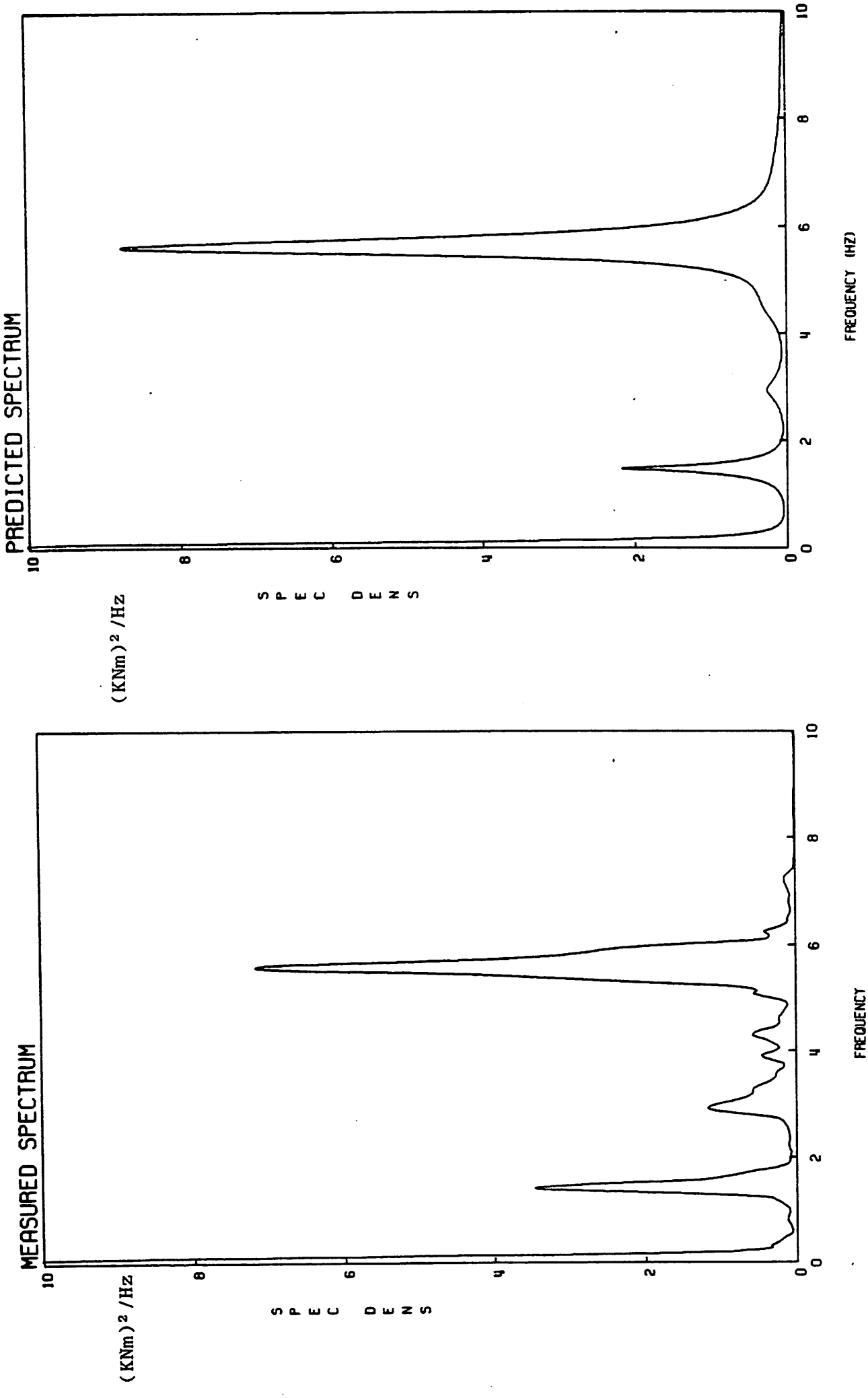


Figure 10 Measured and Predicted Bending Moment Spectra - Linear Scales

| 60 sec. period | Mean Windspeed (m/s) | Windspeed Standard Deviation (m/s) | Turbulence Intensity (%) | Mean Yaw (deg.) |
|---|---|---|---|---|
| 1 | 13.39 | 0.98 | 7.3 | -4.3 |
| 2 | 12.79 | 0.95 | 7.4 | -3.5 |
| 3 | 12.89 | 0.91 | 7.1 | -4.0 |
| 4 | 13.01 | 0.94 | 7.2 | -3.6 |

Table 1 Meteorological Conditions During Campaign - Initiated at 21:07:59 on 12.7.86

# DESCRIPTION OF A DISCRETE GUST TURBULENCE MODEL

OLE FABIAN

KURT S. HANSEN

B. MARIBO PEDERSEN

Description of a discrete gust turbulence model.

1. What is described in the following are the results of using a discrete gust model for determination of the distribution of the longitudinal component of the turbulent velocity across the plane of a wind turbine rotor.

   The model has been used as input for a direct simulation, structural dynamics code for calculation of the structural response of the components of a horizontal axis wind turbine.

   It has been the intention to develop a model which incorporates some of the general features of the eddy structure in the lower part of the atmospheric boundary layer.

   The model is an ad-hoc model in which the statistical descriptors of the model wind field can be matched to those of the real wind field by adjusting a number of free parameters.

   The model has been tested on the NIBE-B wind turbine, and a number of corresponding measurement results and calculated results of various quantities are shown on the accompanying figures.

2. The wind field in which the wind turbine blades rotate is created as a linear superposition on the stationary wind field, deformed by wind shear and tower shadow, of a number of discrete 3-d gusts, randomly distributed over the rotor disk area.

   The centerline velocity of the basic gust varies in time as shown on fig. 1, and the spatial extent of the gust, i.e. the axially symmetric distribution of the velocity in a plane perpendicular to the direction of the wind, is illustrated on fig. 2.

   A gust is classified according to the maximum centerline velocity $\hat{u}_i$, where $\hat{u}_i$ is determined by

$$\frac{\hat{u}_i}{\bar{V}} = a \times b^i \quad , \quad i = 1,..,N$$

Where N is the number of gust classes and $\bar{V}$ is the mean wind speed.

The duration of each single gust $\hat{P}_i$ in class i is a random variable, normally distributed with mean value $\hat{T}_i$ and standard deviation $\sigma(\hat{P}_i)$. $\hat{T}_i$ is determined by

$$\hat{T}_i = c \times d^i \; ; \; i = 1,..,N$$

also we define

$$\frac{\sigma(\hat{P}_i)}{\hat{T}} = \alpha$$

Gust of all classes i, and for each class with different durations $\hat{P}_i$, are distributed randomly over a reference area $A_i$, which is defined on fig 3.
$R_{imax}$ is determined by

$$R_{imax} = \frac{1}{4} \times \bar{V} \times \hat{T}_i (1+3\alpha)$$

hence the reference area for different classes is different.

The area-density of gusts in class i is $\gamma_i$, so that the number of gust of class i present at any time in the reference area is

$$S_i = \gamma_i \times A_i$$

The total number gusts of the all classes present at any time is $\Sigma S_i$, and these gusts are distributed at random over the reference areas, i. e. the coordinates for the centerline of a gust are determined by

$$\Theta_{ij} = 2\pi\beta \quad ; \quad \beta \in [0;1]$$
$$\hat{R}_{ij} = R_{iref}\sqrt{\eta}; \quad \eta \in [0;1]$$

where $\beta$ and $\eta$ are uniformly distributed random variables or

$$x_{ij} = \hat{R}_{ij}\cos\theta_{ij}$$
$$y_{ij} = \hat{R}_{ij}\sin\theta_{ij}$$

The resulting velocity at any point within the rotor disk is the sum of all gust velocities added to the stationary velocity at that point.

When a gust has died away, another gust of the same class is born, but at another (random) position in the reference area. This new gust will have the same $\hat{u}_i$ as the previous one but will have a different duration $\hat{P}_i$, chosen at random within the population with same $\hat{T}_i$.

The generation of the velocity field starts with the gust in random phase.

The adjustable parameters in this model are thus

N, a, b, c, d, $\alpha$ and $\gamma_i$

For the sample calculations for which the results are given in fig 4 to fig 17, the following values have been attributed to these parameters

| | | | |
|---|---|---|---|
| N | = 10 | $\alpha$ | = 0.2 |
| a | = 0.28 | $\gamma_i$ | = 0.025 (same for all classes) |
| b | = 0.93 | | |
| c | = 0.5 | | |
| d | = 1.4 | | |

The preliminary results have been encouraging, and it is hoped, that through a continuing effort in developing and simplifying the model, it will become a useful and reliable tool for calculation of the loading on a wind turbine.

## MEASURED TIMESERIES

T = 172 SEC. ; 17 HZ

| | | MEAN | RMS | MIN | MAX |
|---|---|---|---|---|---|
| WINDSPEED | [M/S] | 8.9 | 1.52 | 5.0 | 13.1 |
| EL.POWER | [ KW] | 204 | 42.3 | 114 | 294 |
| FLAPWISE BENDING MOM. | [KNM] | -9.6 | 28.2 | -101.6 | 88.2 |
| "-"STOCHAST. | [KNM] | 0 | 23.9 | -80.8 | 81.0 |
| YAW MOM. | [KNM] | 2 | 34.1 | -102. | 135. |
| "-"STOCHAST. | [KNM] | 0 | 32.5 | -110. | 130. |

## SIMULATED WINDSPEED

T = 172 SEC.

| | | MEAN | RMS | MIN | MAX |
|---|---|---|---|---|---|
| WINDSPEED | [M/S] | 8.6 | 1.35 | 5.7 | 12.6 |
| EL.POWER | [ KW] | 193 | 60.5 | 86 | 410 |
| FLAPWISE BENDING MOM. | [KNM] | 10.9 | 47.0 | -136. | 180. |
| "-"STOCHAST. | [KNM] | 0 | 38.9 | -106. | 182. |
| YAW MOMENT | [KNM] | 2.8 | 46.2 | -159. | 153. |
| "-"STOCHAST. | [KNM] | 0 | 43.4 | -141. | 172. |

Figure 1.

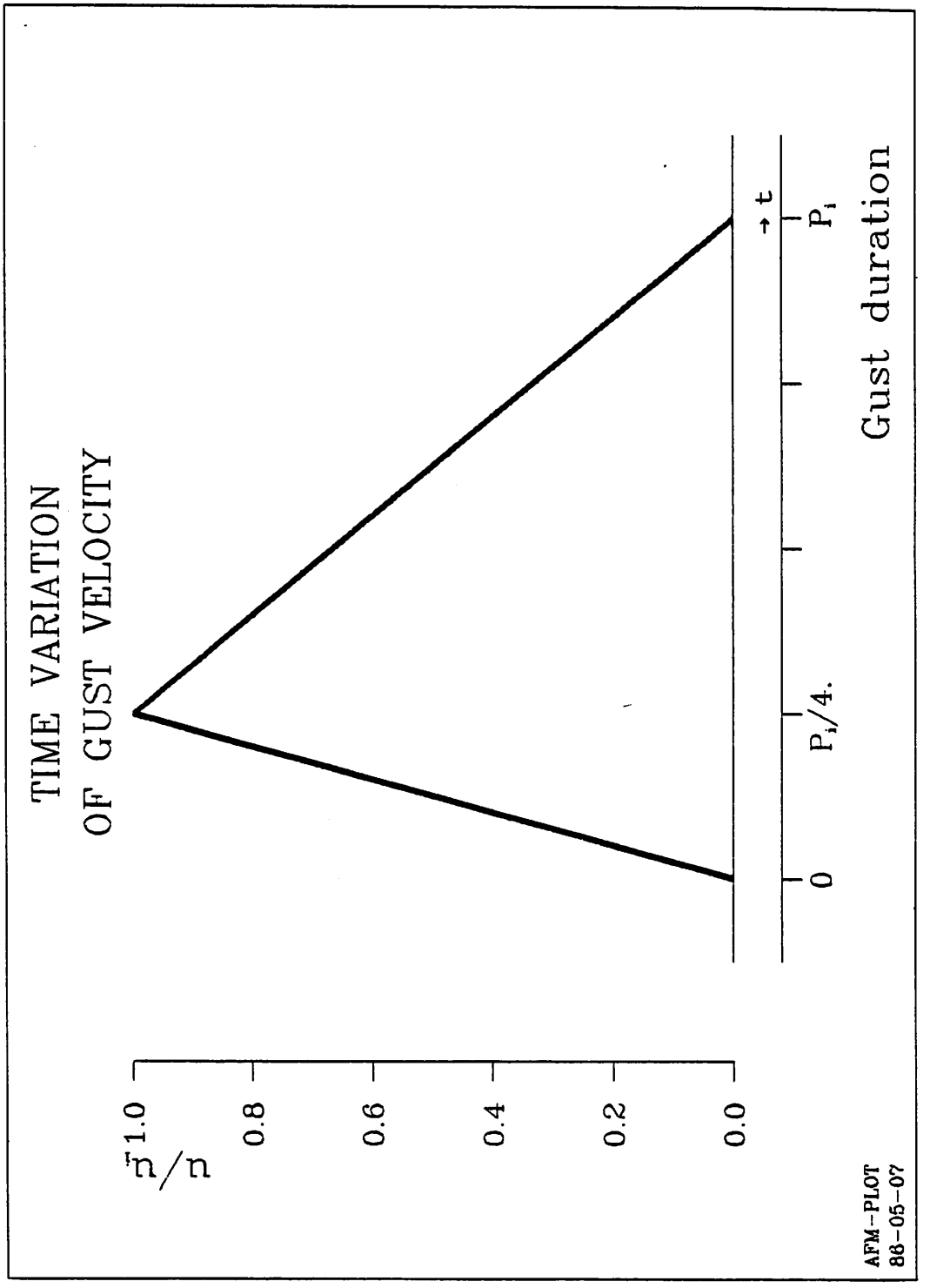
TIME VARIATION
OF GUST VELOCITY
n̄/n
1.0
0.8
0.6
0.4
0.2
0.0
0
$P_i/4.$
$P_i$
→ t
Gust duration
AFM-PLOT
88-05-07

Figure 2.

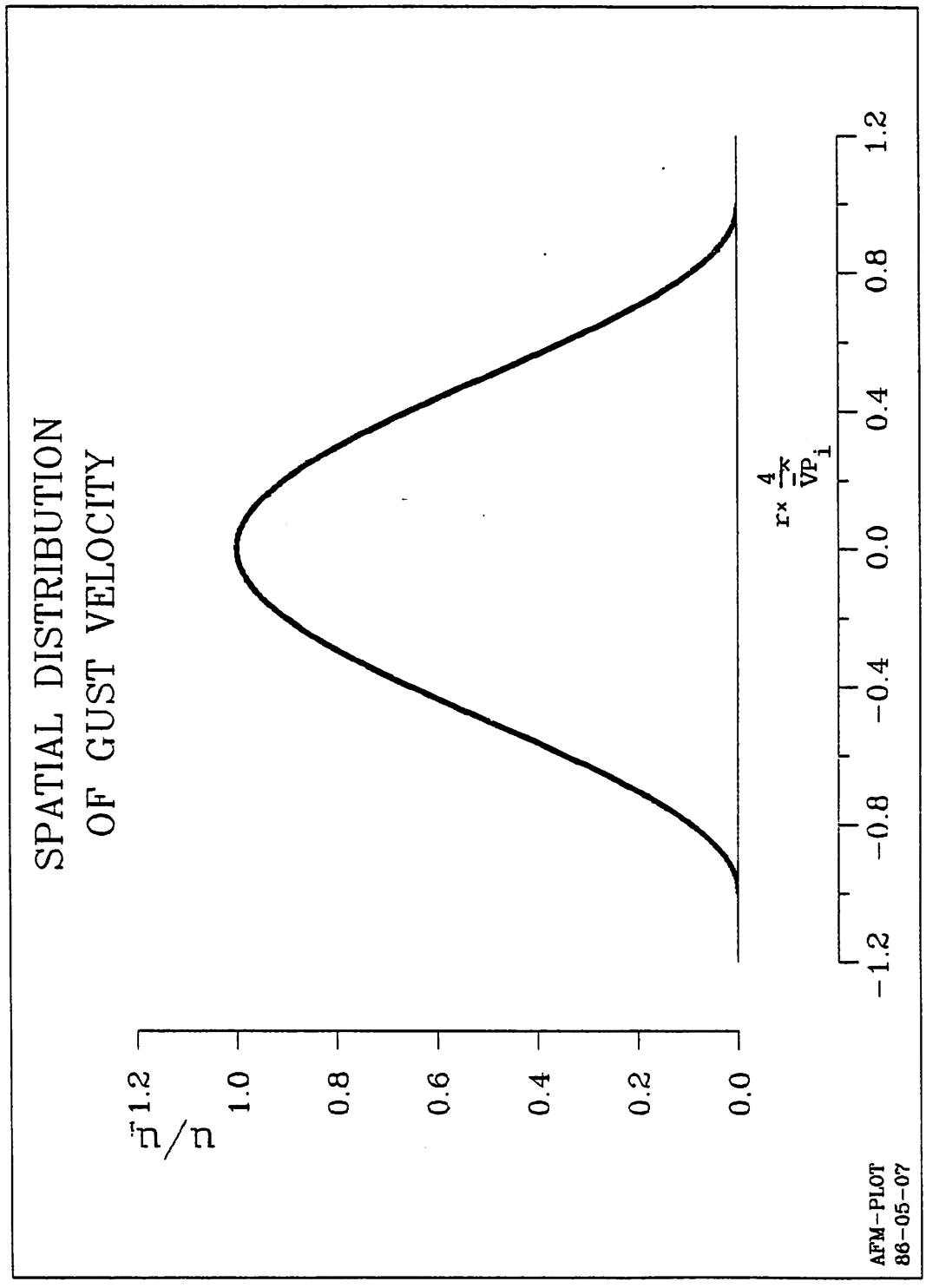
SPATIAL DISTRIBUTION
OF GUST VELOCITY
u/ū
1.2
1.0
0.8
0.6
0.4
0.2
0.0
-1.2
-0.8
-0.4
0.0
0.4
0.8
1.2
r× 4/L × x/VP_i
AFM-PLOT
86-05-07

Figure 3.

DEFINING THE AREA OVER WHICH GUSTS ARE ACTIVE

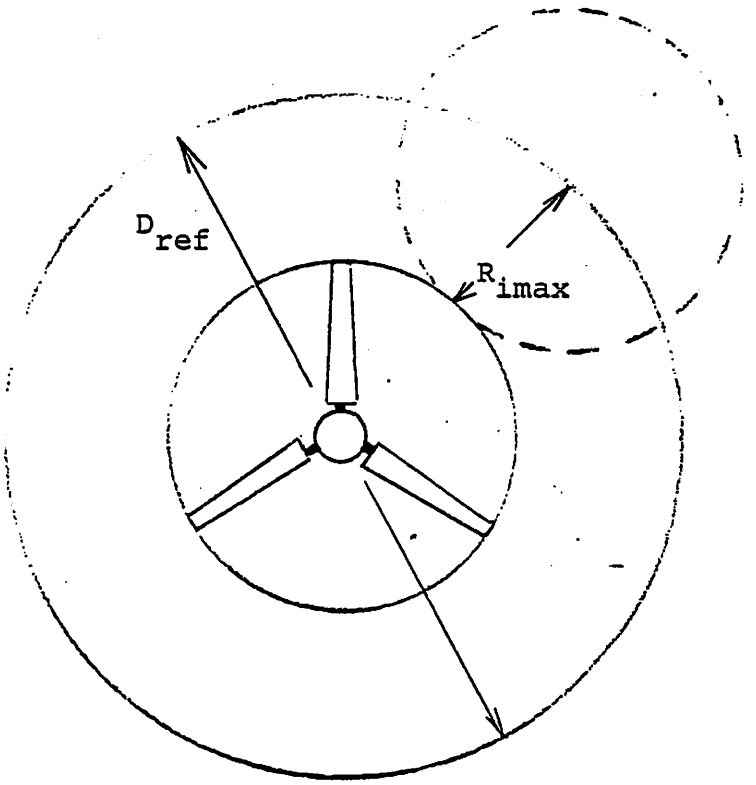


$$A_i = \frac{\pi}{4} D_{ref}^2$$

Figure 4.

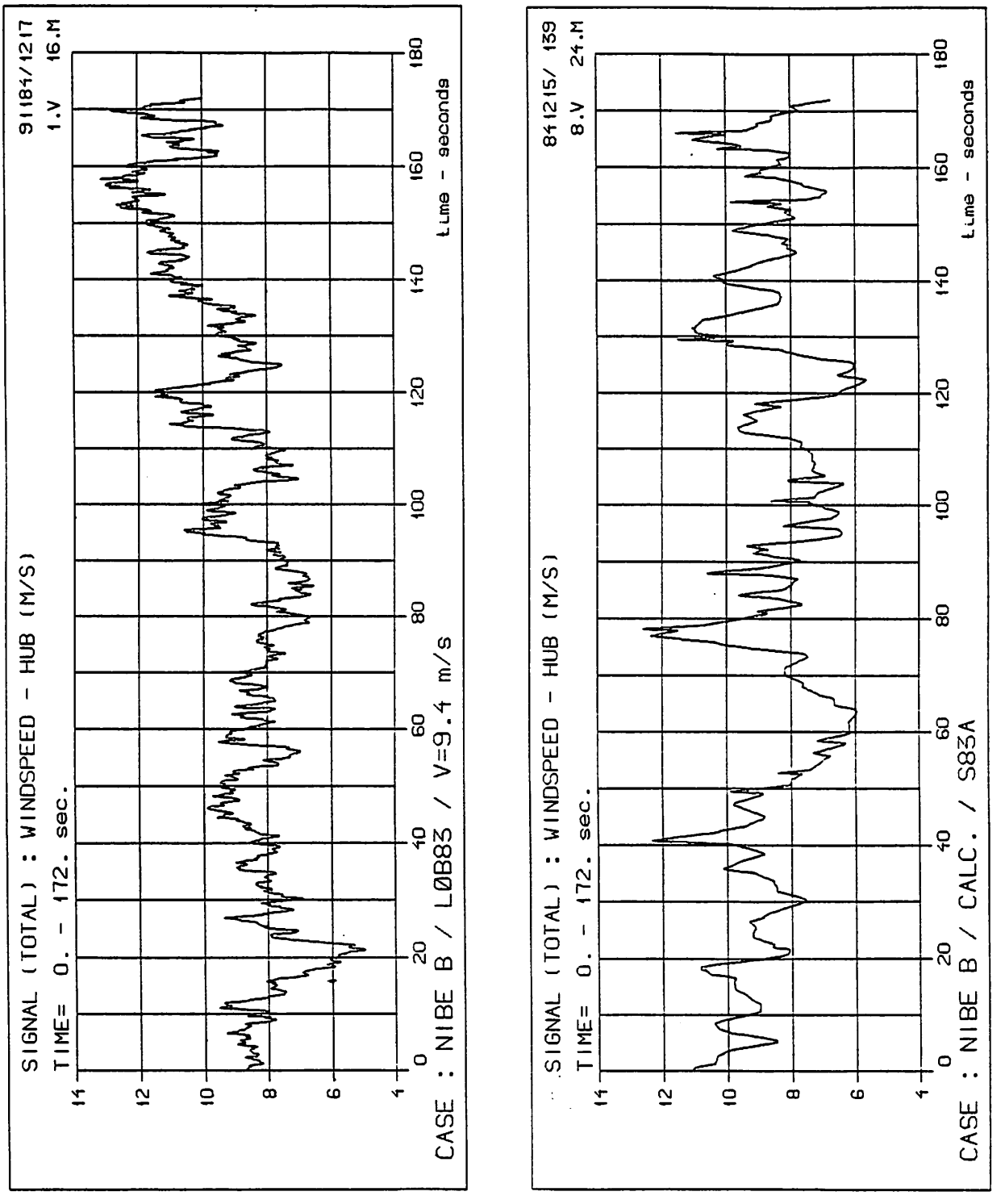
SIGNAL (TOTAL) : WINDSPEED - HUB (M/S)
TIME= 0. - 172. sec.
91184/1217
1.V 16.M
CASE : NIBE B / LØB83 / V=9.4 m/s
Time - seconds
SIGNAL (TOTAL) : WINDSPEED - HUB (M/S)
TIME= 0. - 172. sec.
841215/ 139
8.V 24.M
CASE : NIBE B / CALC. / S83A
Time - seconds

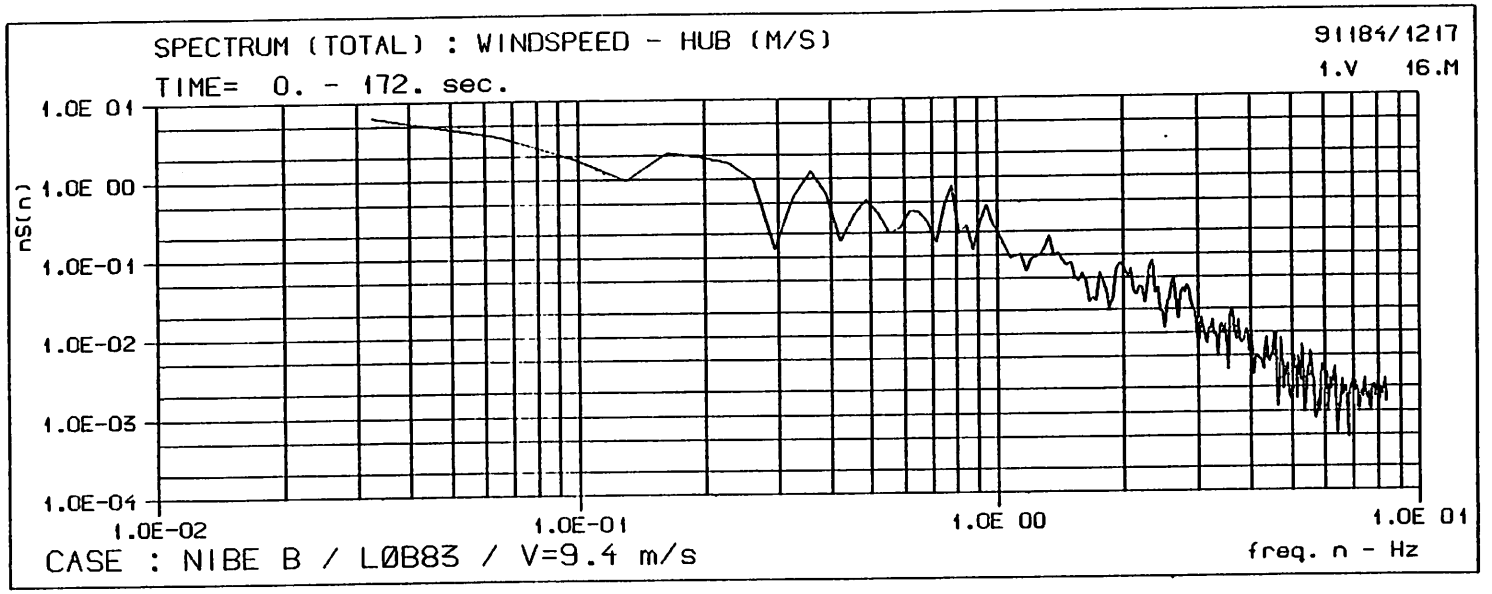
SPECTRUM (TOTAL) : WINDSPEED - HUB (M/S)
91184/1217
1.V 16.M
TIME= 0. - 172. sec.
1.0E 01
1.0E 00
1.0E-01
1.0E-02
1.0E-03
1.0E-04
nS(n)
1.0E-02
1.0E-01
1.0E 00
1.0E 01
freq. n - Hz
CASE : NIBE B / LØB83 / V=9.4 m/s

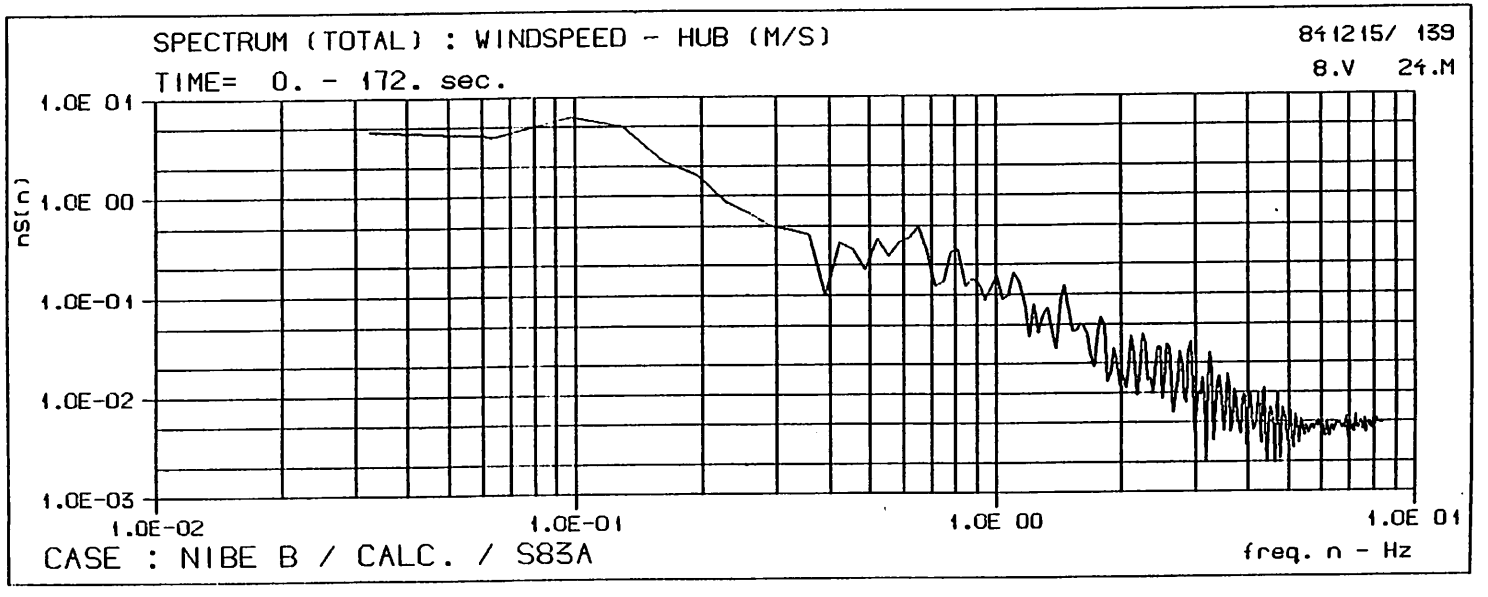
SPECTRUM (TOTAL) : WINDSPEED - HUB (M/S)
841215/ 139
8.V 24.M
TIME= 0. - 172. sec.
1.0E 01
1.0E 00
1.0E-01
1.0E-02
1.0E-03
nS(n)
1.0E-02
1.0E-01
1.0E 00
1.0E 01
freq. n - Hz
CASE : NIBE B / CALC. / S83A

Figure 5.

Figure 6.

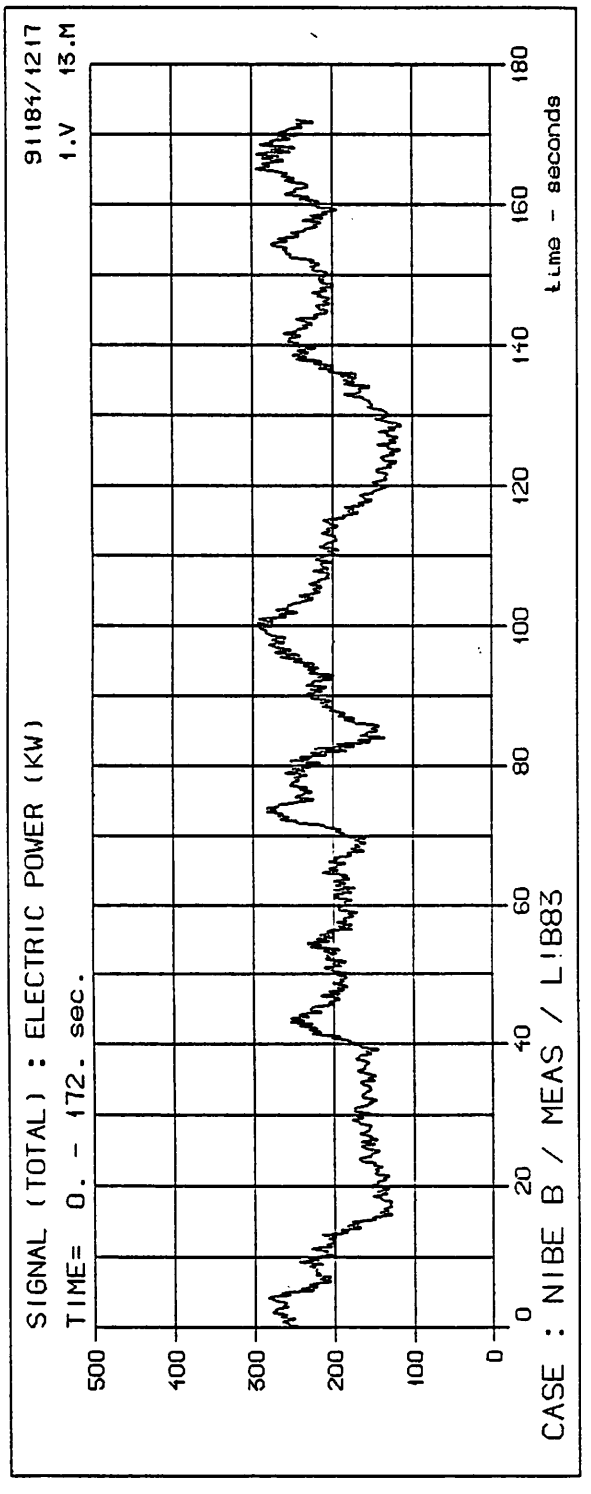
SIGNAL (TOTAL) : ELECTRIC POWER (KW)
TIME= 0. - 172. sec.
91184/1217
1.V 13.M
0
100
200
300
400
500
0
20
40
60
80
100
120
140
160
180
Time - seconds
CASE : NIBE B / MEAS / L1883

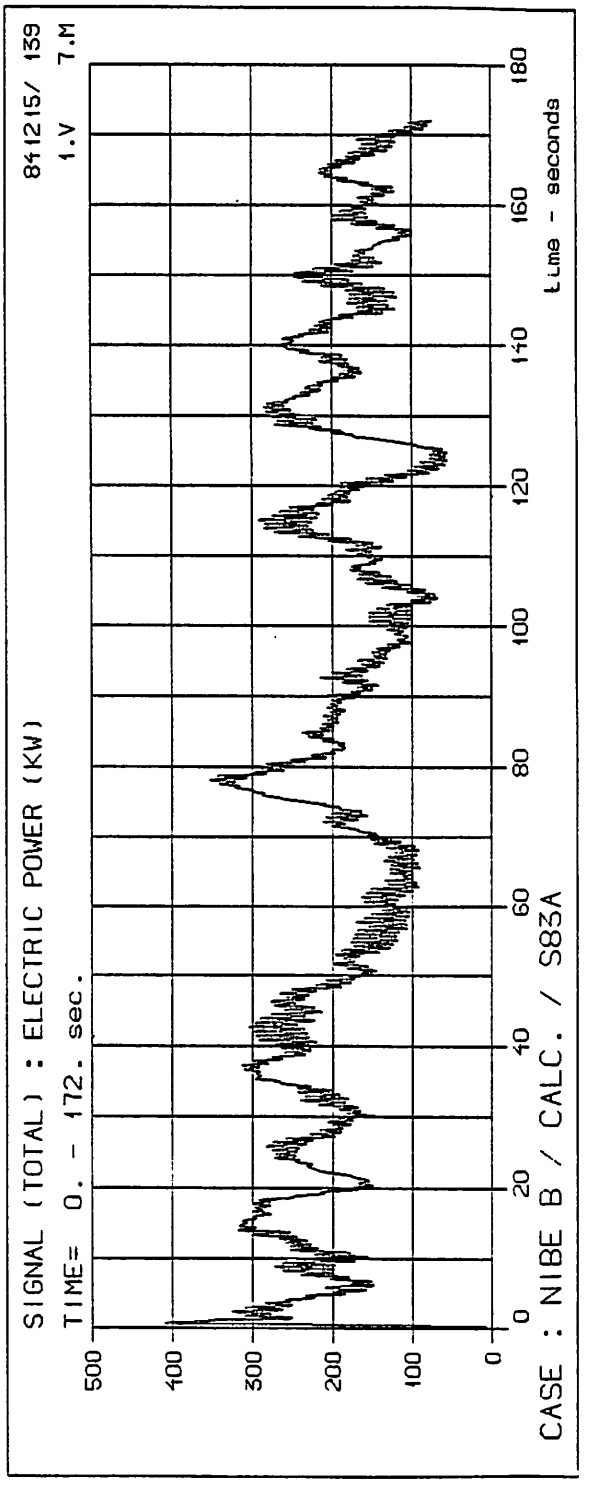
SIGNAL (TOTAL) : ELECTRIC POWER (KW)
TIME= 0. - 172. sec.
841215/ 139
1.V 7.M
0
100
200
300
400
500
0
20
40
60
80
100
120
140
160
180
Time - seconds
CASE : NIBE B / CALC. / S83A

Figure 7.

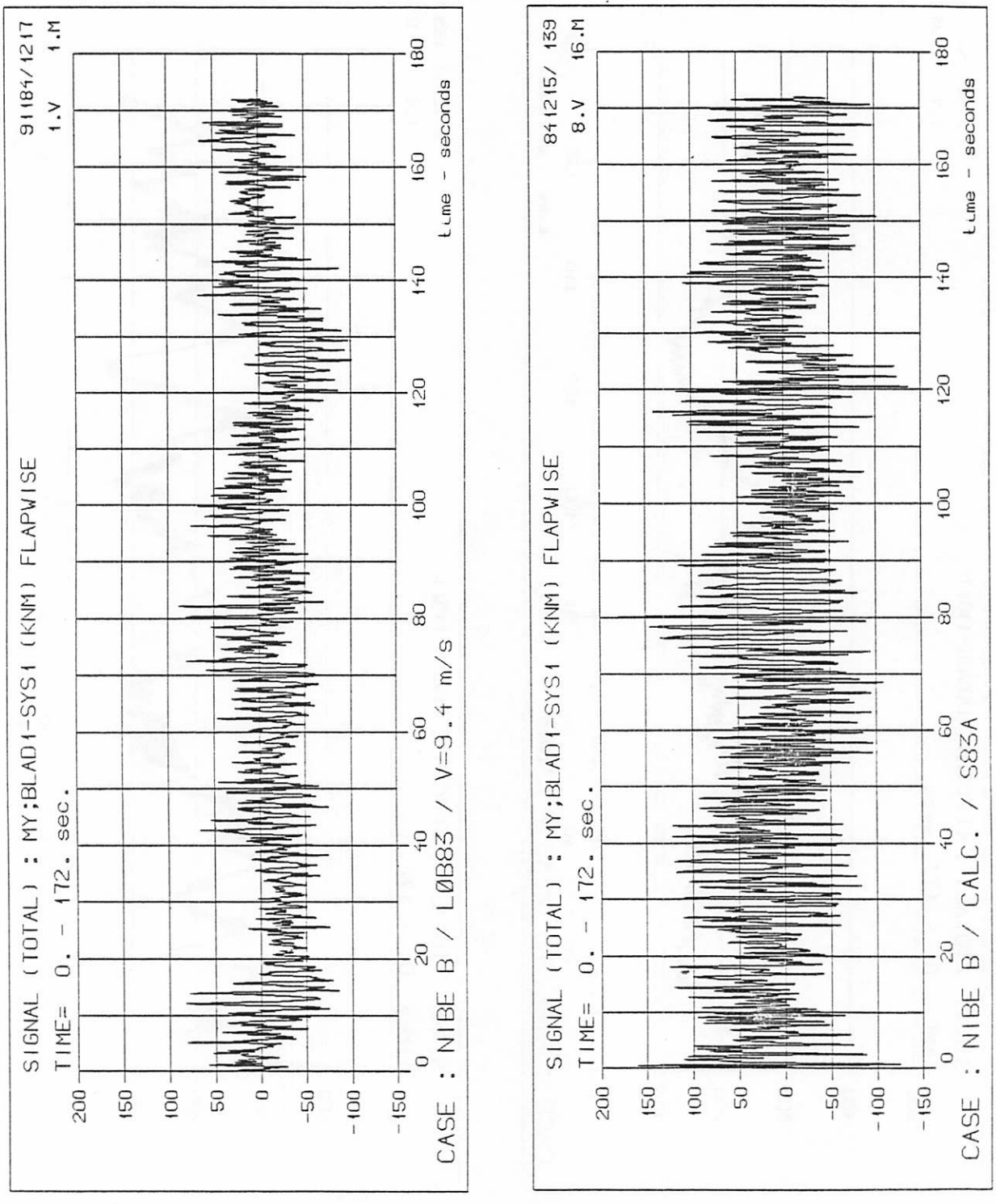
SIGNAL (TOTAL) : MY;BLAD1-SYS1 (KNM) FLAPWISE
TIME= 0. - 172. sec.
91184/1217
1.V 1.M
CASE : NIBE B / LØB83 / V=9.4 m/s
SIGNAL (TOTAL) : MY;BLAD1-SYS1 (KNM) FLAPWISE
TIME= 0. - 172. sec.
841215/ 139
8.V 16.M
CASE : NIBE B / CALC. / S83A
200
150
100
50
0
-50
-100
-150
0
20
40
60
80
100
120
140
160
180
Time - seconds

Figure 8.

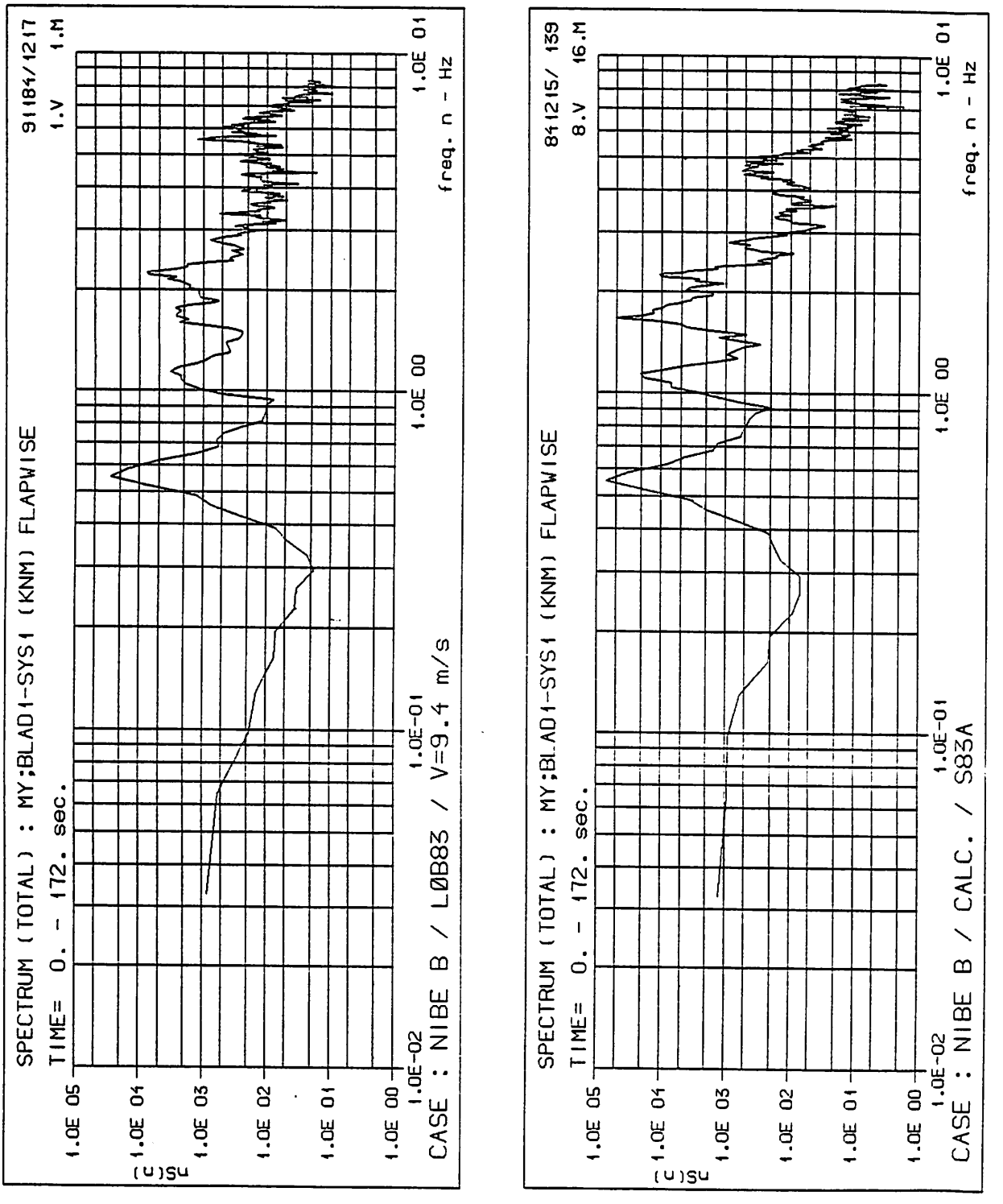
SPECTRUM (TOTAL) : MY;BLAD1-SYS1 (KNM) FLAPWISE
TIME= 0. - 172. sec.
91184/1217
1.V 1.M
CASE : NIBE B / LØB83 / V=9.4 m/s
841215/ 139
8.V 16.M
CASE : NIBE B / CALC. / S83A
freq. n - Hz
1.0E 05
1.0E 04
1.0E 03
1.0E 02
1.0E 01
1.0E 00
1.0E-01
1.0E-02
1.0E 01
1.0E 00
1.0E-01
1.0E-02

Figure 9.

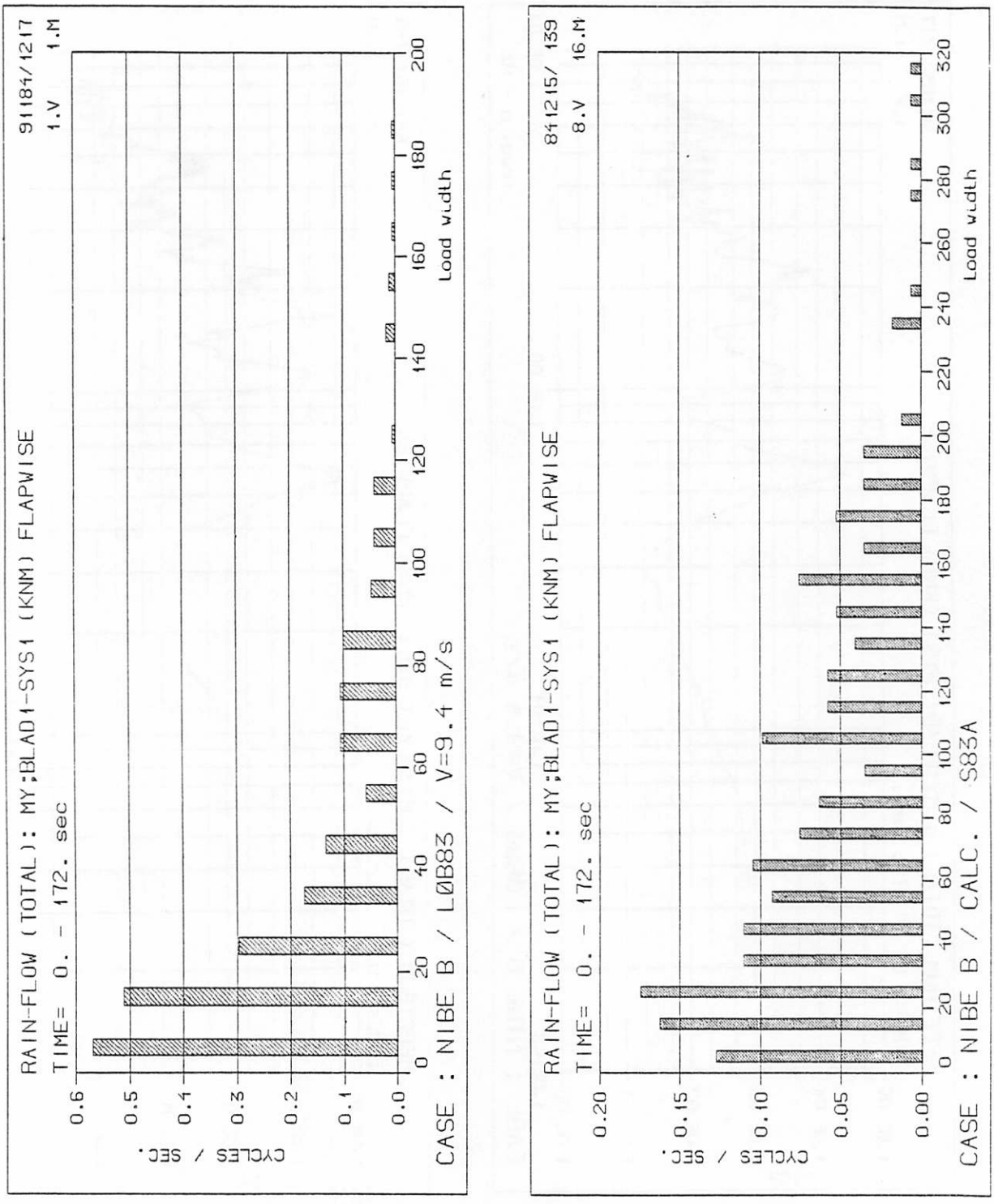
RAIN-FLOW (TOTAL): MY;BLAD1-SYS1 (KNM) FLAPWISE
TIME= 0. - 172. sec
91184/1217
1.V 1.M
CYCLES / SEC.
0.0
0.1
0.2
0.3
0.4
0.5
0.6
0 20 40 60 80 100 120 140 160 180 200
Load width
CASE : NIBE B / LØB83 / V=9.4 m/s
RAIN-FLOW (TOTAL): MY;BLAD1-SYS1 (KNM) FLAPWISE
TIME= 0. - 172. sec
841215/ 139
8.V 16.M
CYCLES / SEC.
0.00
0.05
0.10
0.15
0.20
0 20 40 60 80 100 120 140 160 180 200 220 240 260 280 300 320
Load width
CASE : NIBE B / CALC. / S83A

Figure 10.

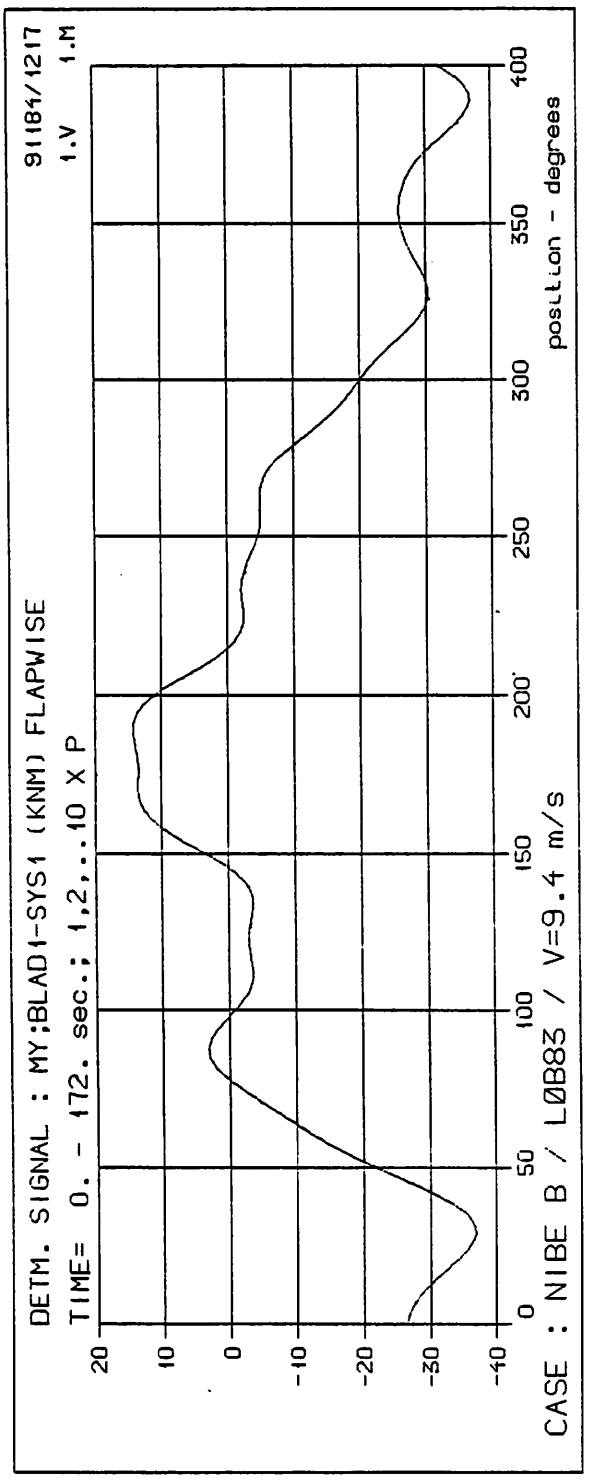
DETM. SIGNAL : MY;BLAD1-SYS1 (KNM) FLAPWISE
TIME= 0. - 172. sec.: 1,2,..10 X P
91184/1217
1.V 1.M
CASE : NIBE B / LØB83 / V=9.4 m/s
position - degrees
20
10
0
-10
-20
-30
-40
0
50
100
150
200
250
300
350
400

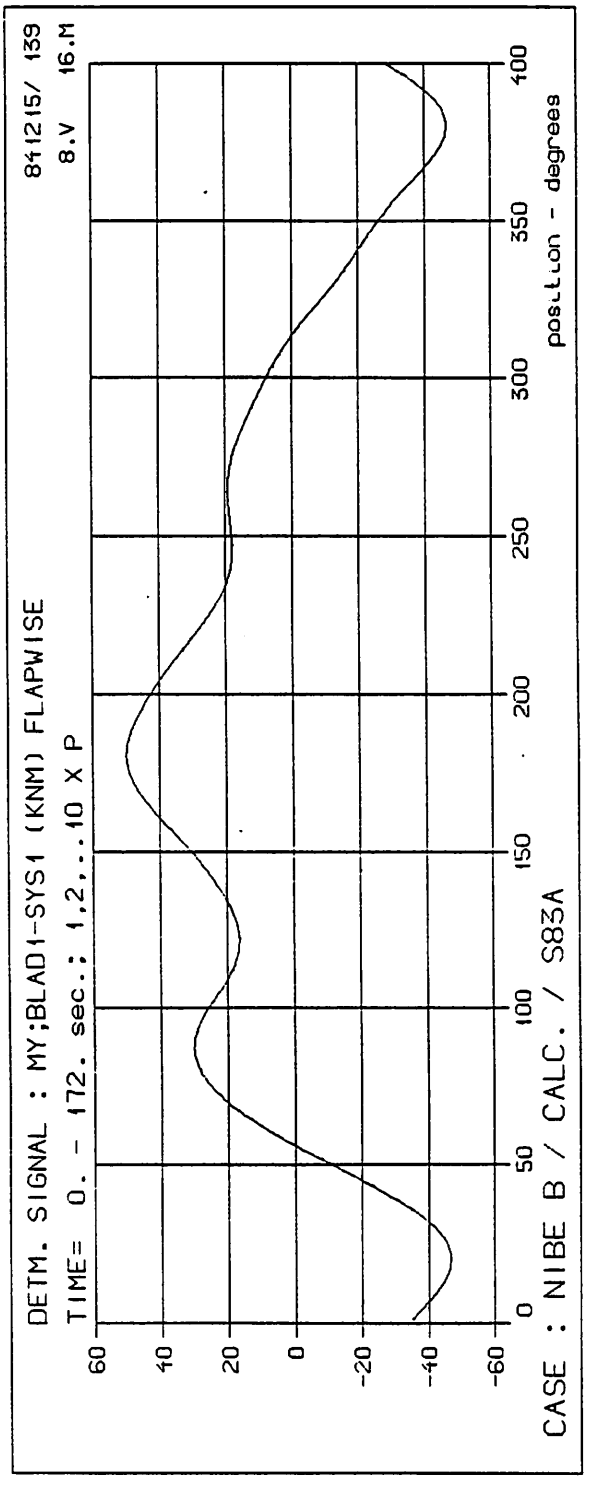
DETM. SIGNAL : MY;BLAD1-SYS1 (KNM) FLAPWISE
TIME= 0. - 172. sec.: 1,2,..10 X P
841215/ 139
8.V 16.M
CASE : NIBE B / CALC. / S83A
position - degrees
60
40
20
0
-20
-40
-60
0
50
100
150
200
250
300
350
400

Figure 11.

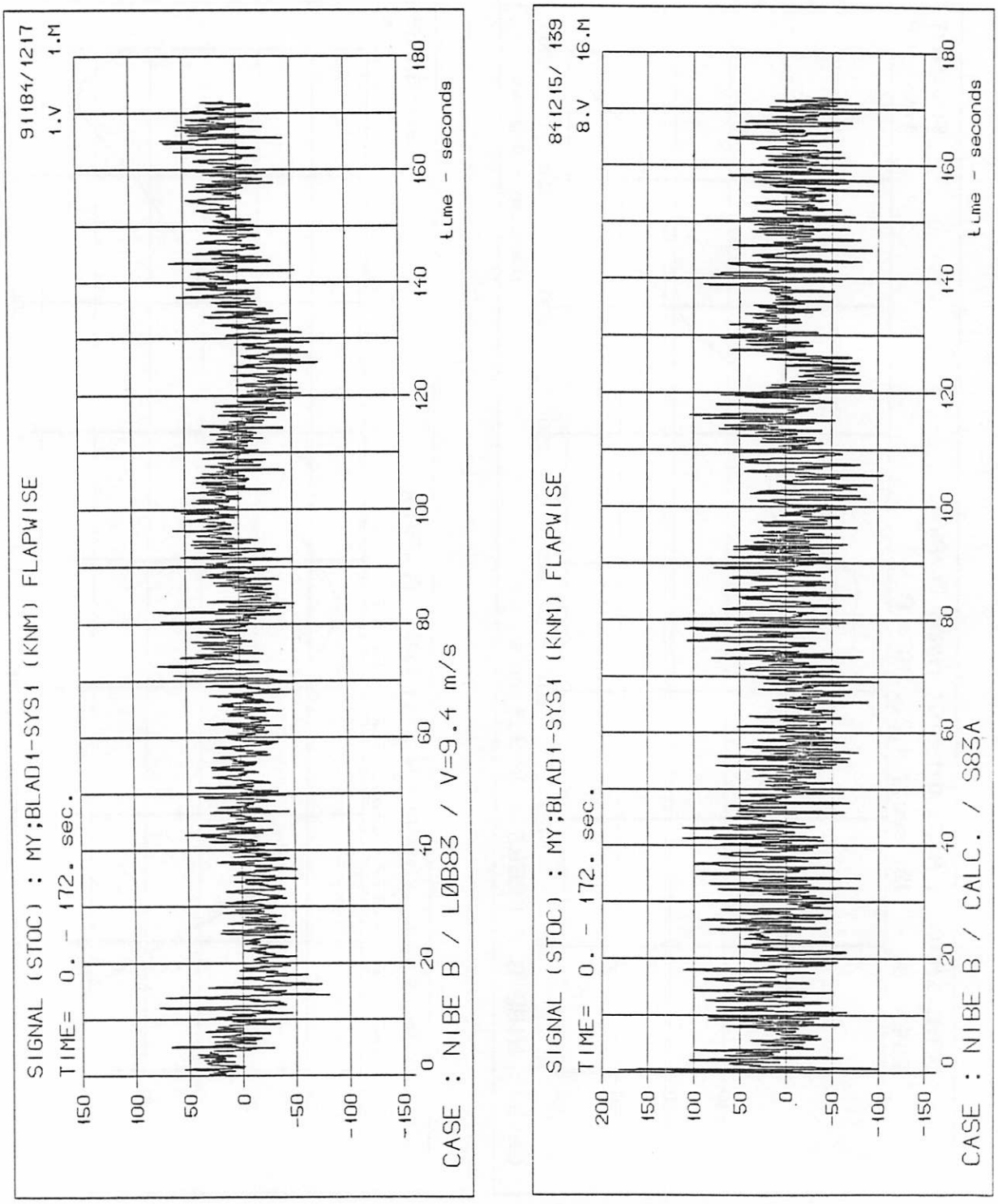
SIGNAL (STOC) : MY;BLAD1-SYS1 (KNM) FLAPWISE
TIME= 0. - 172. sec.
91184/1217
1.V 1.M
CASE : NIBE B / LØB83 / V=9.4 m/s
Time - seconds
SIGNAL (STOC) : MY;BLAD1-SYS1 (KNM) FLAPWISE
TIME= 0. - 172. sec.
841215/ 139
8.V 16.M
CASE : NIBE B / CALC. / S83A
Time - seconds

Figure 12.

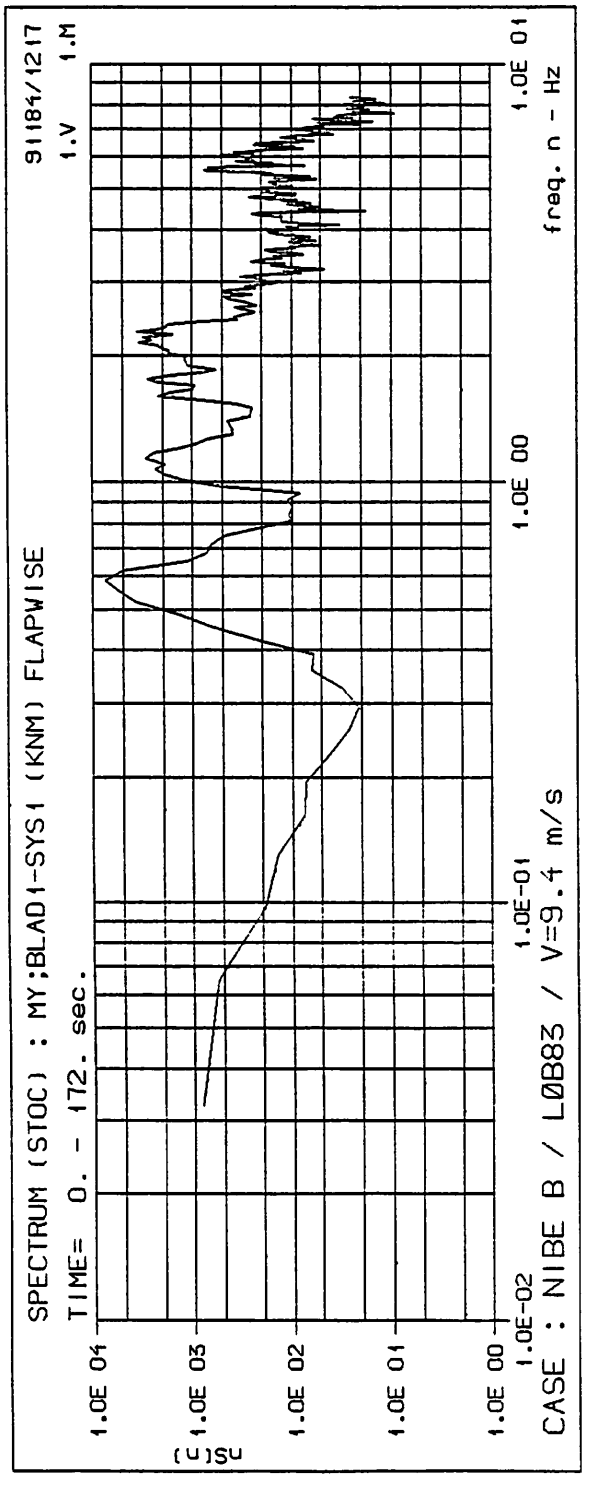
SPECTRUM (STOC) : MY;BLAD1-SYS1 (KNM) FLAPWISE
91184/1217
1.V 1.M
TIME= 0. - 172. sec.
1.0E 04
1.0E 03
1.0E 02
1.0E 01
1.0E 00
1.0E-01
1.0E-02
1.0E 01
1.0E 00
1.0E-01
freq. n - Hz
CASE : NIBE B / L0B83 / V=9.4 m/s

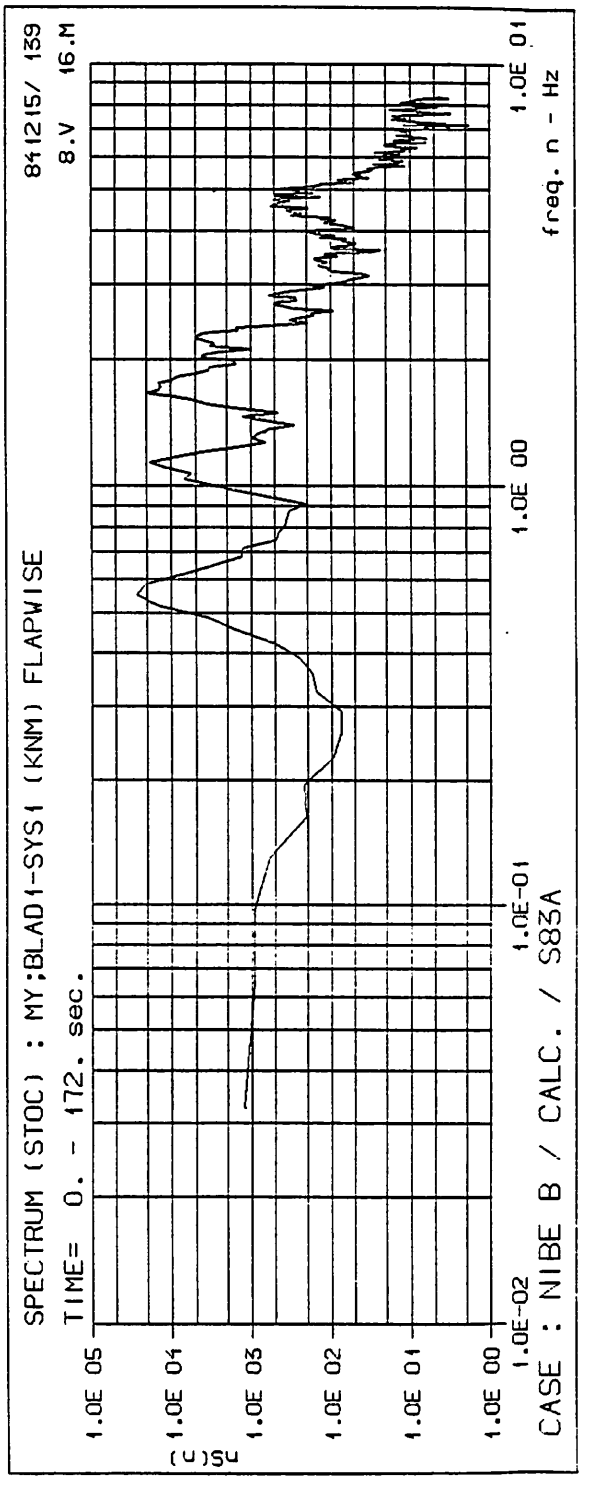
SPECTRUM (STOC) : MY;BLAD1-SYS1 (KNM) FLAPWISE
841215/ 139
8.V 16.M
TIME= 0. - 172. sec.
1.0E 05
1.0E 04
1.0E 03
1.0E 02
1.0E 01
1.0E 00
1.0E-01
1.0E-02
1.0E 01
1.0E 00
1.0E-01
freq. n - Hz
CASE : NIBE B / CALC. / S83A

Figure 13.

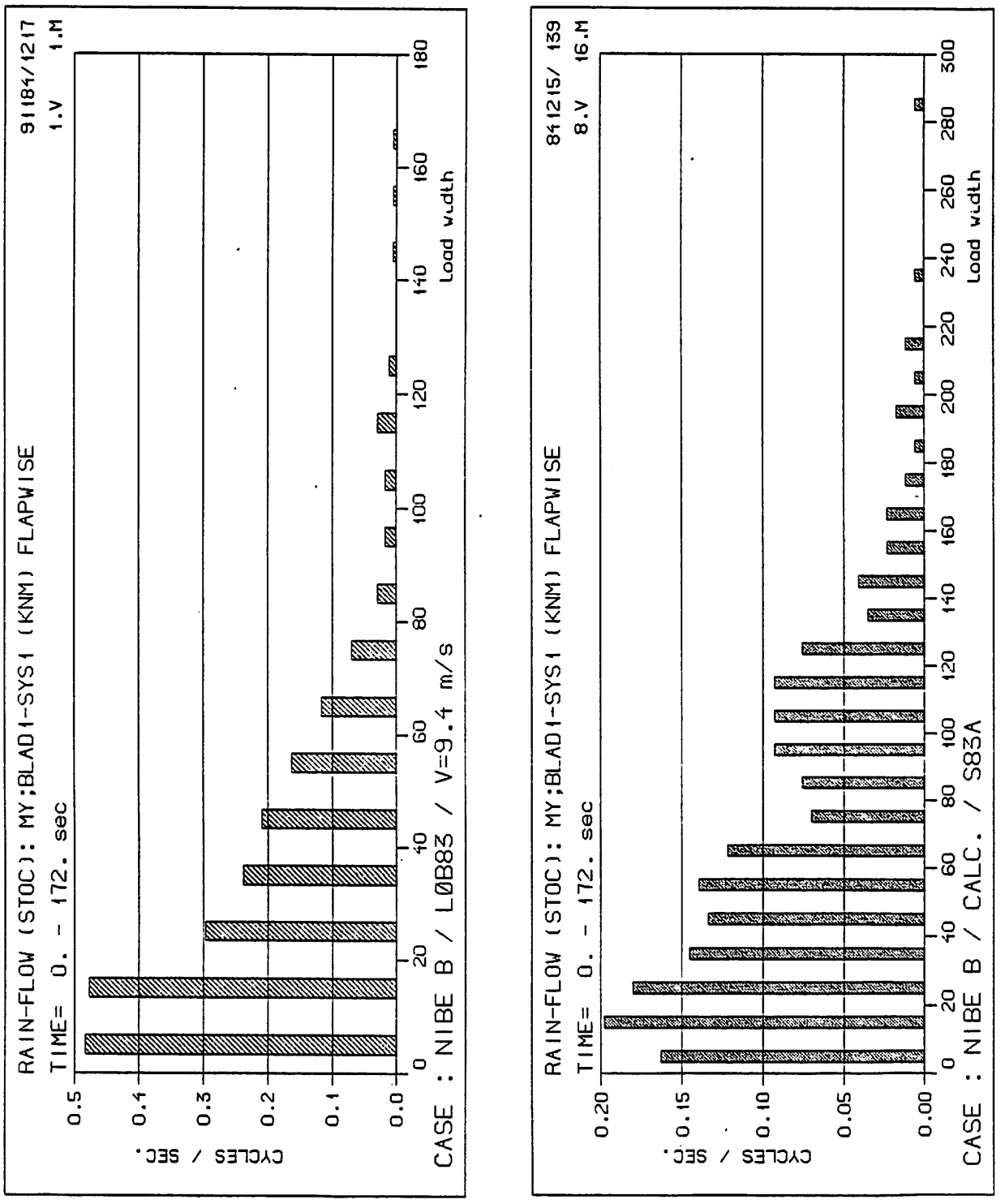
RAIN-FLOW (STOC): MY;BLAD1-SYS1 (KNM) FLAPWISE
TIME= 0. - 172. sec
91184/1217
1.V 1.M
CYCLES / SEC.
0.0
0.1
0.2
0.3
0.4
0.5
0
20
40
60
80
100
120
140
160
180
Load width
CASE : NIBE B / L0B83 / V=9.4 m/s
RAIN-FLOW (STOC): MY;BLAD1-SYS1 (KNM) FLAPWISE
TIME= 0. - 172. sec
841215/ 139
8.V 16.M
CYCLES / SEC.
0.00
0.05
0.10
0.15
0.20
0
20
40
60
80
100
120
140
160
180
200
220
240
260
280
300
Load width
CASE : NIBE B / CALC. / S83A

Figure 14.

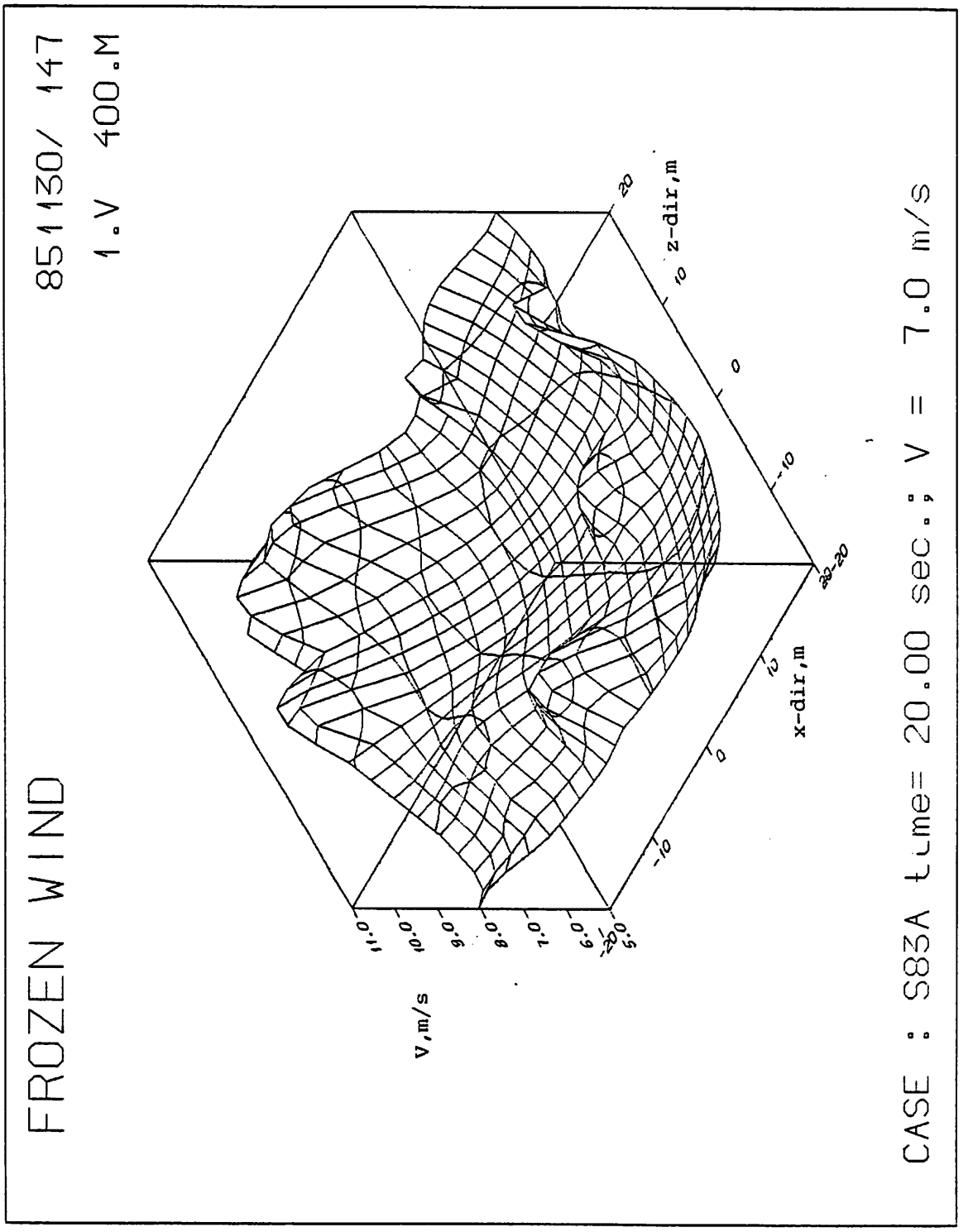
FROZEN WIND
851130/ 147
1.V 400.M
CASE : S83A time= 20.00 sec.; V = 7.0 m/s
z-dir,m
x-dir,m
V,m/s

Figure 15.

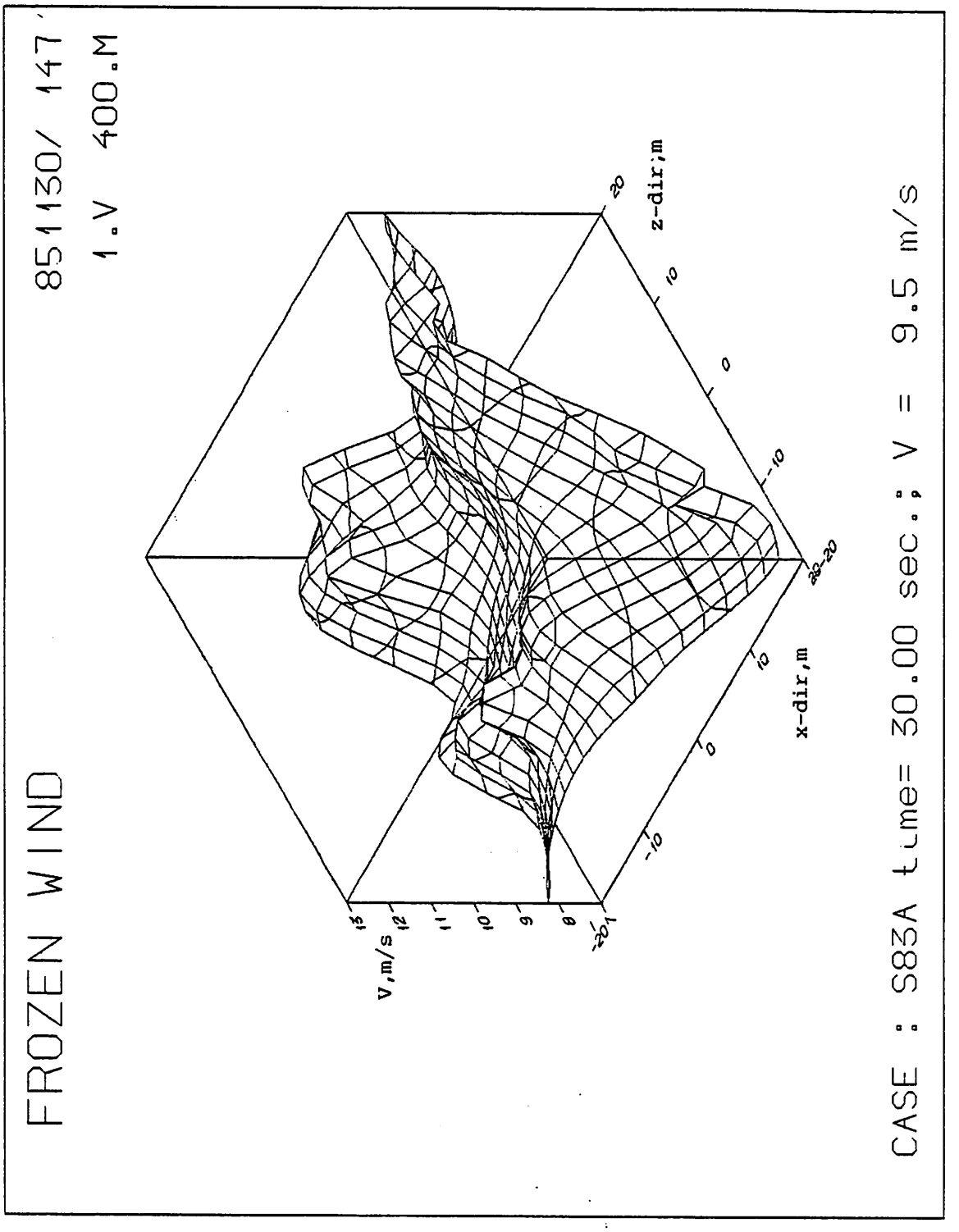
FROZEN WIND
851130/ 147
1.V 400.M
CASE : S83A time= 30.00 sec. ; V = 9.5 m/s
V,m/s
15
12
11
10
9
8
z-dir;m
20
10
0
-10
-20
x-dir,m
-20
-10
0
10
20

Figure 16.

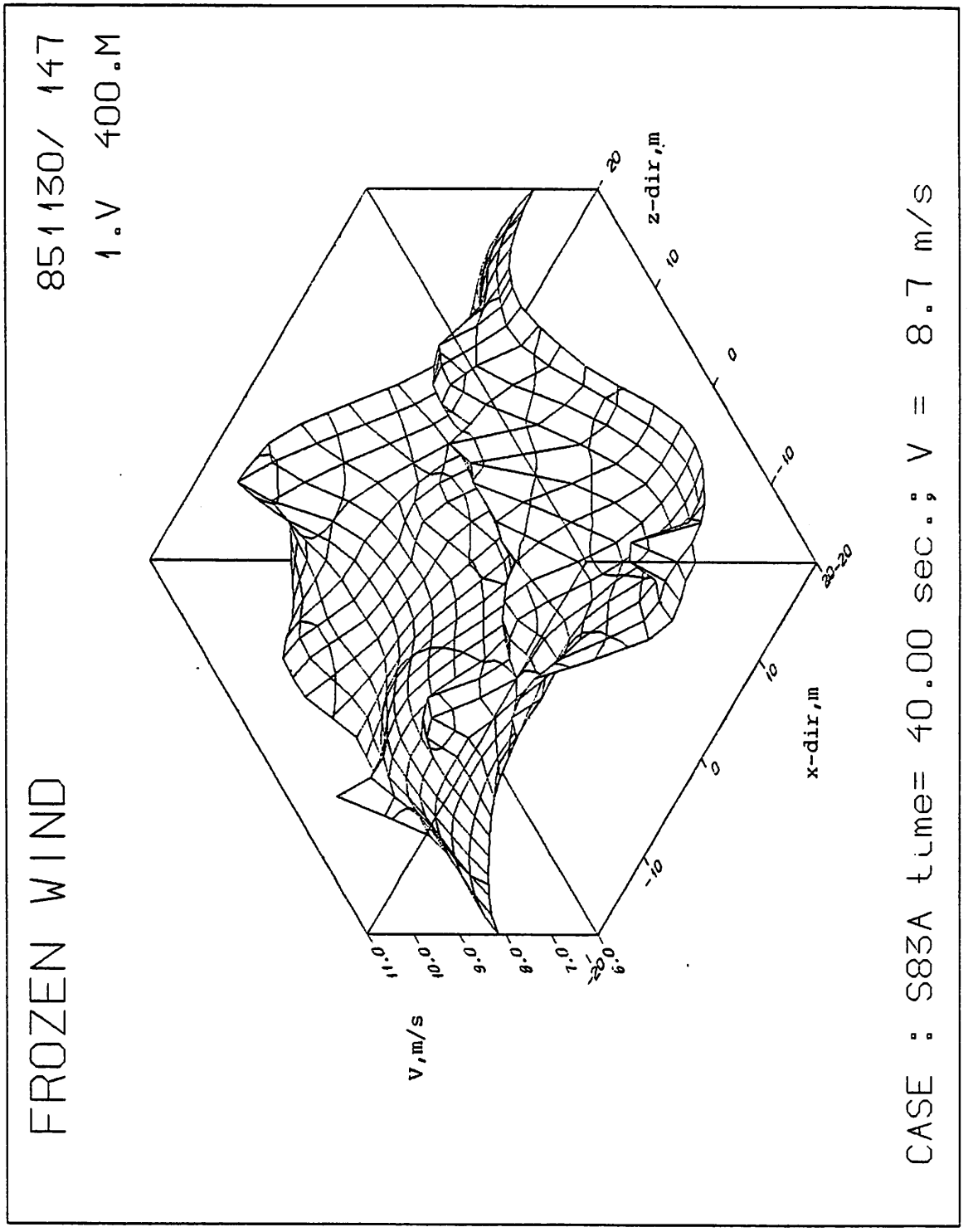
FROZEN WIND
851130/ 147
1.V 400.M
CASE : S83A time= 40.00 sec.; V = 8.7 m/s
V,m/s
11.0
10.0
9.0
8.0
7.0
6.0
z-dir,m
20
10
0
-10
-20
x-dir,m
-20
-10
0
10
20

Figure 17.

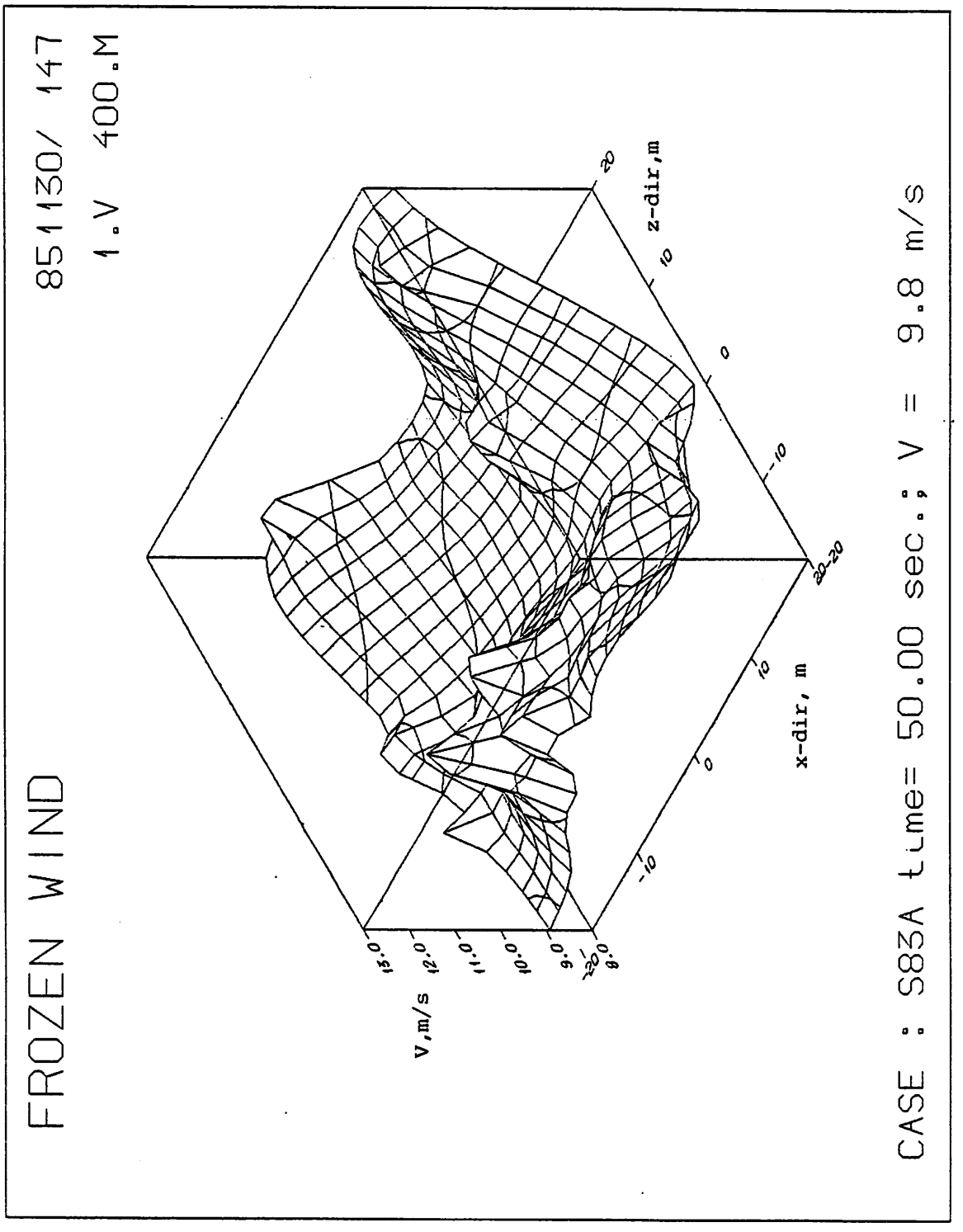
FROZEN WIND
851130/ 147
1.V 400.M
CASE : S83A time= 50.00 sec.; V = 9.8 m/s
V,m/s
x-dir, m
z-dir,m

# SOME THOUGHTS ON THE MODELING OF ATMOSPHERIC TURBULENCE FROM THE PERSPECTIVE OF A NON-EXPERT*

Dale Berg

## ABSTRACT

Recent work with a wind turbulence model has demonstrated that the effects of wind turbulence may be large. This work also illustrates that turbulence models do not need to accurately reproduce all the details in the physical wind to be of benefit to the wind turbine community. Their use, however, will be facilitated if they are packaged in easy-to-use codes that function as subroutines. Several U.S. projects which are now in the planning stages are designed to measure the turbulence in the incident wind and the resultant response of the turbine. Knowledge gained from these tests will enhance our understanding of the role of turbulence in turbine response.

## INTRODUCTION

The development of computer codes to model the aerodynamics and structural dynamics of wind turbines is an ever-evolving process. Initial aerodynamic models were very simplistic and did a poor job of estimating even the mean aerodynamic performance of the turbines. Aerodynamic codes have gradually improved with the development of the strip theory and vortex filament models for the Horizontal Axis Wind Turbines (HAWTs) and the development of the double-multiple streamtube, vortex filament, and local circulation models for the Vertical Axis Wind Turbines (VAWTs). Approximate models for dynamic stall effects are used in many HAWT and VAWT codes. These codes are now capable of predicting the performance of a machine quite well, and some do a good job of predicting the rotationally-resolved performance.

Early structural analysis programs were confined to predicting the natural frequencies of vibration of turbines, enabling the designers to avoid resonance problems. Later versions are

* This work supported by the U.S. Department of Energy under Contract DE-AC04-76DP00789.

capable of predicting the response of turbine components in terms of mean and vibratory stresses. These codes frequently incorporate aerodynamic models for calculating blade loads. Comparison of predictions with data from operating turbines has not been entirely satisfactory. The agreement is frequently rather poor, especially at high wind speeds. One possible source of error is the assumption of a steady wind in the aerodynamic model. Only recently have studies been performed on the effect of wind stochastics on the predicted structural loads.

## Turbulence Effects on Wind Turbines

Paul Veers performed the first qualitative study of the effects of turbulence on VAWTs in 1983[1]. He needed a numerical model of the atmospheric turbulence, and, not finding one in the wind community, he developed his own consisting of a Gaussian time series with a power spectral density which matches the form suggested by Frost, Long and Turner[2].

A fully three-dimensional spatially varying wind was simulated by producing time series of the wind speed at several points which lie in a plane perpendicular to the mean wind direction. The longitudinal variations were produced using Taylor's frozen turbulence hypothesis. The main difference between this turbulence simulation and other methods is that in this simulation the turbulence is based solely on its first and second order statistical moments without any reference to the fluid dynamics of the wind. There is no guarantee that this simulated flow field will be continuous, compatible, or physically realizable. However, by matching its first two statistical moments, the turbulence properties which have the most significant impact on the blade loads and, therefore, on the structural response of the wind turbine are accurately represented[1].

Veers used the multiple streamtube model of Strickland[3] to calculate the aerodynamic loading on VAWT blades with and without turbulence in the wind. The steady wind blade loads for a VAWT consist entirely of frequencies which are integer multiples of the turbine rotating frequency (per rev frequencies). The addition of turbulence distributes the loads across the spectrum. Veers found that the motion of the blade through the turbulence and the magnifying effect of small variations in angle of attack combine to shift the turbulent energy in the wind to higher frequencies in the blade loads. For high winds, he found that the loads due to the steady mean wind are significantly higher than the mean loads due to a turbulent wind. This is consistent with the difference between actual measured stresses and stresses calculated using the steady wind model. Veers' work did not extend to determining the quantitative impact of the stochastic wind on the actual structural response.

Lobitz[4] developed the HAWTDYN full dynamic model computer program for structural dynamic analysis of HAWTs. The PROP[5] strip theory code was used to calculate the aerodynamic forces acting on the rotor, and the Veers turbulent wind model[1] was used for calculating the incident wind. Lobitz utilized this code to analyze the response of the Boeing/NASA Mod 2 HAWT; in particular, the flapwise bending moment at station 370 on the blade. Figure 1 illustrates the effect of the turbulent wind model on the predicted bending moment at that location. For the first three revolutions, a steady wind is input. During the fourth revolution, the stochastic wind increments are included, and revolutions 5 through 23 reflect a turbulent wind input. The differences between the two responses are quite dramatic. The cyclic amplitude increases by a factor of nearly four, and the frequency content changes from 2/rev to predominately 4/rev. Predictions of the mean and cyclic loads are compared with MOD2 data in Figs. 2 and 3. Figure 3 also includes a single data point to illustrate the predicted cyclic load for a steady wind.

Lobitz's work demonstrates that the effect of turbulence on wind turbine response may be quite dramatic. In this case it amplified a 4/rev response. Veers' work indicates that its effect on VAWTs may be to lower the high wind loads and predicted structural response. Much additional work is required to gain a better understanding of these turbulence effects and to study the effects of different turbulence models. It is quite clear from these studies, however, that response predictions based on assuming a steady incident wind can differ significantly from response predictions based on a turbulent wind, and the turbulent wind predictions tend to agree better with the measured data.

## Some Thoughts on Turbulence Models

The Veers model may not be the best possible model of the atmospheric wind, but its use has shown that turbulence effects can be significant. A model does not need all the bells and whistles that might be desirable in order for it to be of use to the wind community. One which just recreates the gross features of the turbulent wind would be quite helpful. It could then be replaced by more refined models as they become available. Incorporation of rotational sampling is not necessary, because the aerodynamic codes (at least the ones with which I am familiar) vectorially add the rotational velocity of the blade to that of the incident wind to determine relative velocities. This is precisely equivalent to rotationally sampling the incident wind. HAWT and VAWT codes "sample" the wind in the appropriate manner for each type of turbine, so the same turbulence model could be used for both types of turbines (although the importance of lateral coherence is much greater for VAWTs than for HAWTs).

Any model that is developed, however, should be programmed so that it may be readily used in structural and aerodynamic codes. Ideally, the model would function as a "black box," i.e., the user interface would be in the form of a subroutine call which specifies a time and location and which returns the velocity (possibly three spatial components). The mechanism by which this is done is not important. Perhaps a large file of wind data is created prior to the first use of the model and the subroutine simply reads data from this file and interpolates to generate the necessary velocity. A simple user interface such as this would relieve the developers of structural and aerodynamic codes of the necessity of becoming experts on the particular turbulence model that they choose to use, as is now the case. It would greatly reduce the risk of these developers introducing errors into the turbulence models in the course of adapting these models to the particular application at hand. It would also greatly simplify the task of evaluating the effects of turbulence models and turbulence model parameters.

## Current U.S. Efforts

Within the U.S. wind research community, there exists a great deal of interest in gaining an understanding of the effect of wind turbulence on turbine structural response.

Recent tests on the WTS-4 turbine at Medicine Bow, Wyoming involved monitoring the structural response of several locations on the turbine over a significant period of time. Fatigue analysis of the machine utilizing these data yields an estimated lifetime in excess of 30 years. Detailed analysis of the data, however, reveals that it contains areas, at all wind velocities, where the response data are quite smooth with relatively little oscillation about the mean value. Is this due to low turbulence in the wind? The available data cannot answer that question. Comparisons of the fatigue life estimated with the smooth data and that estimated with the normal oscillatory data shows that the oscillatory data yields a life that is shorter by a factor of two to three. This is consistent with the findings of Lobitz[4] on the impact of turbulence on the MOD2. Additional tests incorporating detailed meteorological measurements will be conducted on the WTS-4 to further investigate this phenomena.

The 34-m VAWT[6] that Sandia National Laboratories is building will be instrumented with several three-dimensional anemometers located in close proximity to the turbine at equatorial height. These instruments will be used to determine the turbulent wind experienced by the equatorial section of the rotor in the rotating frame of reference. The structural response of the equatorial section of the turbine will also be determined. Correlations of the incident wind and structural response data will be performed to study the effect of turbulence on the turbine response and determine what characteristics of the turbulence are the most important.

Analytical studies of the effects of turbulence are also underway. Sandia is currently funding efforts to incorporate stochastic wind models into double-multiple streamtube, vortex filament, and local circulation aerodynamic models, and to enhance the VAWT structural response code to include stochastic wind effects. Studies of the relative contributions of the spatial turbulence components to the structural response will be conducted as part of the enhancement. The relative contributions of the low and high frequency components of the turbulence will also be determined.

## SUMMARY

Recent work has shown that the presence of turbulence in the incident wind can significantly affect the response of a turbine. An analytical study by Lobitz on the MOD2 HAWT found that including turbulence in the incident wind resulted in increasing the blade flapwise cyclic load by a factor of four, as compared to the predicted load for a steady incident wind. Veers, on the other hand, found that the presence of turbulence in the incident wind resulted in lower loading on VAWT blades.

Turbulence models do not have to be highly sophisticated and model all details of the atmospheric wind to be useful. However, they should be packaged for easy incorporation into aerodynamic models. A simple user interface makes user modifications unnecessary and avoids the possible introduction of errors during such a modification.

Several experimental and analytical efforts within the US wind community are studying the effect of turbulence on turbine structural response.

## REFERENCES

1. Veers, P. S., "Modeling Stochastic Wind Loads on Vertical Axis Wind Turbines," SAND83-1909, Sandia National Laboratories, September 1984.

2. Frost, W., Long, D. H., and Turner, R. E., "Engineering Handbook on the Atmospheric Environment - Guideline for Use in Wind Turbine Generator Development," NASA Technical Paper 1359, December 1979.

3. Strickland, J. H., "The Darrieus Turbine: A Performance Prediction Model Using Multiple Streamtubes," SAND75-0431, Sandia National Laboratories, October 1975.

4. Lobitz, D. W., "A NASTRAN-based Computer Program for Structural Dynamic Analysis of Horizontal Axis Wind Turbines," Presented at the HAWT Workshop in Cleveland, Ohio, April 1984.

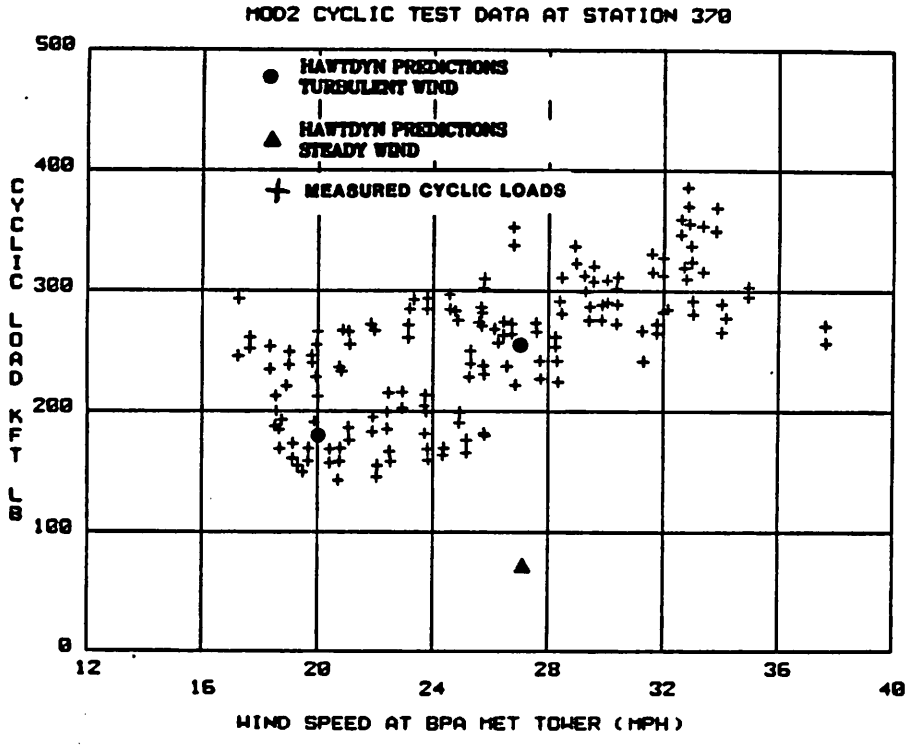


**Figure 3. Comparison of Predicted and Measured Cyclic Loads**

# THE MODELLING OF ATMOSPHERIC TURBULENCE IN RELATION TO VERTICAL AXIS WIND TURBINES

Dr. M.B. Anderson

# TURBULENCE - A FREQUENCY DOMAIN APPROACH FOR VERTICAL AXIS WIND TURBINES

## 1 INTRODUCTION

The effects of turbulence on loads, dynamic response, fatigue life and energy capture have been shown to be important for horizontal axis wind turbines, e.g. Anderson (1982), Powles and Anderson (1984). However, little work has been undertaken, to date, on the effects of turbulence on any of the above aspects for a vertical axis wind turbine. Veer's (1984) research, at Sandia Laboratories, deals with the effects of turbulence on the aerodynamic loads, for a 17m Darrieus turbine, using a time domain approach, but no account was taken of dynamic effects. The effects of turbulence becomes more important as the rotor size becomes comparable with turbulent length scales and as a result turbulence will :-

a) excite all modes of the turbine;

b) concentrate significant amounts of energy at and around integer multiples of the rotational frequency;

c) modify the peak aerodynamic loads;

d) reduce the amount of energy which the rotor can extract from the turbulent component.

A general methodology for analysing the effects of turbulence is shown in Table 1. Apart from the step designated "Rotational Sampling" standard techniques can be used (e.g. Bendat and Piersol 1980). A comparison between a horizontal and a vertical axis wind turbine of the physical and statistical properties and assumptions generally made for each step is shown in Table 2 and is exemplified below :

- Turbulence

  For both types of turbine it is generally assumed that atmospheric turbulence is a stationary Gaussian process which is homogeneous and isotropic. However, for a vertical axis wind turbine, it is necessary to consider both the longitudinal and lateral turbulent velocity components unlike a horizontal axis wind turbine where only

the longitudinal component is of importance (Jensen and Frandsen 1978). In practice turbulence is neither homogeneous or isotropic, but Fordham and Anderson (1982) have shown that these limitations do not affect the results significantly.

- Rotational Sampling

Owing to the turbines' rotational motion it is necessary to convert the turbulence, as seen by a stationary observer, into a rotating frame of reference. This technique is usually called "Rotational Sampling" and in principle is the same for both types of turbine. For a horizontal axis wind turbine the main feature of this transformation is that it shifts the turbulent energy to higher frequencies and particularly to the rotor speed and its harmonics. The transformed spectrum is however still stationary, i.e. independent of rotor position. As will be shown, in this paper, for a vertical axis wind turbine this transformation causes not only a redistribution of energy but, perhaps more importantly, the spectrum becomes non-stationary with respect to frequency. This effect can be explained by considering an observer rotating with the blade. As the observer approaches the oncoming wind the turbulent spectrum will be shifted to higher frequencies whereas when he is travelling in the same direction as the oncoming wind the converse will occur, the spectrum will be shifted to lower frequencies. This effect is very similar to the well known Doppler effect.

- Aerodynamic Loads

For both types of turbine the formulation of the aerodynamic loads is basically the same except that for a vertical axis wind turbine they are periodic. As a result of this the effect of turbulence is dependent on rotor position. In addition, both turbulent components have to be considered.

- Structural Response

Considering only the rotor, the formulation of the equations of motion are fundamentally the same. However, when the supporting structure is included the equations become periodic unless, for a rotor consisting of more than three blades, a multiblade co-ordinate system is adopted. For a vertical axis wind turbine the equations of motion may be simplified considerably if it is assumed that the

supporting structure co-rotates, i.e is isotropic relative to a fixed co-ordinate system.

- Statistics
  Similar techniques for both types of turbine can be used except with a vertical axis wind turbine the deterministic periodic aerodynamic loads must be combined with the stochastic turbulent components.

This paper presents results specifically for a straight bladed wind turbine but the techniques used are equally applicable for a Darrieus type turbine.

## 2. STRUCTURAL MODEL

The problem is approached by assuming a modal representation of the turbine. Given the normal mode shapes and frequencies, the response of a blade at a point 'l' and time 't' is given by

$$y(l,t) = \sum_i \phi_i(l)\, q_i(t) \qquad (1)$$

where $\phi_i$ and $q_i$ are the mode shape and co-ordinate of the 'i'th mode. The co-ordinate 'y' can represent either lagging, flapping or torsion of the blades assuming that they are mutually uncoupled by the effects of rotation or aerodynamics. The generalised co-ordinate of each mode is assumed to satisfy the following relationships :-

$$M_i \ddot{q}_i + C_i \dot{q}_i + K q_i = F_i \qquad (2)$$

where $M_i$, $C_i$ and $K_i$ are the generalised structural properties and $F_i$ is the generalised force.

Based on previous work it can be shown that the applied load is relatively insensitive to the displacement or its derivatives and hence the power spectrum of y(l,t) is given by

$$G_{yy}(\omega) = \sum_i \sum_j \phi_i \phi_j H_i H_j \iint \phi_i \phi_j G_{p_1 p_2}(l_1, l_2, \omega)\, dl_1\, dl_2 \qquad (3)$$

where $G_{P1P2}$ is the cross-spectral density matrix of the applied load for all points on the blade and

$$H_i(\omega) = \left\{ K_i \left[ 1 - (\omega/\omega_i)^2 + j 2\xi\omega/\omega_i \right] \right\}^{-1} \qquad (4)$$

where $w_i$ and $\xi_i$ are the undamped natural frequency and damping ratio of the ith mode.

## 3. STATISTICAL ANALYSIS

For a Gaussian process spectral moments may conveniently be used to characterise a spectral distribution just as probability moments are used to characterise a probability distribution. In general the n-th spectral moment is defined as

$$m_n = \int_0^\infty \omega^n G_{jj}(\omega)\, d\omega \qquad (5)$$

For an arbutary spectrum Cartwright and Longuet-Higgins (1956) have shown, based on the work of Rice (1944), that it is possible to determine the probability of peak values in terms of a spectral width parameter

$$\varepsilon = \left[ 1 - m_2^2 / m_0 m_4 \right]^{1/2} \qquad (6)$$

which takes values between 0 (narrow band spectrum) and 1 (wide band spectrum). The probability distribution of maxima (i.e. peak values), denoted by h, is given by

$$p(\gamma) = (2\pi)^{-\frac{1}{2}} \varepsilon \exp\left(-\tfrac{1}{2}\gamma^2/\varepsilon^2\right) - \tfrac{1}{2}(1-\varepsilon^2)^{\frac{1}{2}} \cdot \gamma \exp(-\tfrac{1}{2}\gamma^2)\left[1 + \operatorname{erf}\left(\gamma(1-\varepsilon^2)^{\frac{1}{2}}\right)/\varepsilon\sqrt{2}\right] \qquad (7)$$

where erf( ) is the error function and $\gamma = h/m_0^{\frac{1}{2}}$. From this distribution the mean of h, denoted $\bar{h}$, the root mean square value $h_{rms}$ are given respectively as

$$\bar{h}/m_0^{\frac{1}{2}} = (\pi/2)^{\frac{1}{2}}(1-\varepsilon^2)^{\frac{1}{2}} \qquad (8)$$

$$\bar{h}_{rms} / m_0^{1/2} = (2 - \varepsilon^2)^{1/2} \tag{9}$$

The expected value of $h_{max}$, that occurs within a specified time, T is given by

$$E(h_{max}) / m_0^{1/2} = [2\ln(\tau)]^{1/2} + \frac{1}{2} 0.5772 [\ln(\tau)]^{-1/2}$$

where $\tau = T(m_2/m_0)^{\frac{1}{2}}$. (10)

For the more general case of a Gaussian random process y(t) which is combined with a periodic signal s(t) = S sin wt of the form

$$z(t) = y(t) + s(t) \tag{11}$$

the probability density function, assuming both have zero means, is given by

$$p(z) = \frac{1}{\sigma_n \pi \sqrt{2\pi}} \int_0^{2\pi} \exp \frac{[-(z - S\cos\Omega)^2]}{16\sigma_n^2} \, d\Omega \tag{12}$$

where $\sigma_n$ is the standard deviation of the Gaussian noise. The probability of a value occurring which is greater than $h_{max} + S$ occurring is given by

$$P(h_{max} + S) = 2 \int_{h_{max} + S}^{\infty} p(z) \, dz \tag{13}$$

Therefore the expected maximum value of the combined process can be obtained from

$$E(h_{max} + S) = [2\ln(\tau')]^{1/2} m_0^{1/2} + \frac{1}{\tau} 0.5772 [\ln(\tau')]^{1/2} m_0^{1/2} + S \tag{14}$$

where $\tau' = P(h_{max} + S)$.

## 4. AERODYNAMIC LOADS

Neglecting the steady centrifugal loads the applied load due to the fluctuating aerodynamic forces can be considered to comprise three components. The first arises from the blades periodic motion through a steady flow, the second from turbulence and the third from aeroelastic effects.

For reasons which will become apparent the formulation of the aerodynamic forces, with the effects of turbulence included, are easier if derived in the rotating frame of reference. If the longitudinal and lateral turbulent velocity components, in the stationary frame, are respectively u and w then the velocity components relative to the rotating blade are (Figure 1).

$$V_x' = \bar{U}\cos\Theta + u'$$
$$V_y' = \bar{U}\sin\Theta + \Omega r - w' \qquad (15)$$

The turbulent velocity components in the rotating frame of reference are u' and w'. The blade aerodynamic normal and tangential forces are defined as

$$\begin{Bmatrix} dF_n \\ dF_t \end{Bmatrix} = \tfrac{1}{2}\rho c W^2 dL \begin{bmatrix} \cos\alpha & \sin\alpha \\ \sin\alpha & -\cos\alpha \end{bmatrix} \begin{Bmatrix} C_L \\ C_D \end{Bmatrix} \qquad (16)$$

where the usual symbol convention is applied. As a frequency domain solution is wanted it is necessary to linearise this equation through making the following assumptions :-

$$C_L \cos\alpha \gg C_D \sin\alpha \qquad W = \Omega R$$
$$C_L = C_{L_\alpha} \sin\alpha$$
$$C_D = C_{D_0}$$

which results in

$$\begin{Bmatrix} dF_N \\ dF_t \end{Bmatrix} = \frac{1}{2}\rho c\, dL \begin{Bmatrix} V_x' V_y' C_{L_\alpha} \\ V_x'^2 C_{L_\alpha} - \Omega R V_y' C_{D_0} \end{Bmatrix} \tag{17}$$

Substituting equation (13) into (15) gives for the normal force

$$dF_N = \frac{1}{2}\rho c C_{L_\alpha} dL \{ \bar{U}^2 \cos\Theta \sin\Theta + \bar{U}\cos\Theta\, \Omega R - \bar{U}\cos\Theta\, w' + \bar{U}\sin\Theta\, u' + u'\Omega R + u'w' \} \tag{18}$$

and assuming that u'w', u' $\bar{U}\sin\Theta$ and w'$\bar{U}\cos\Theta$ are small compared with the other terms leads to the following linear equation :

$$dF_N = \frac{1}{2}\rho c C_{L_\alpha} dL \{ \bar{U}^2 \cos\Theta \sin\Theta + \Omega R \bar{U}\cos\Theta + u'\Omega R \} \tag{19}$$

As a result of transforming the turbulent velocities into the rotating frame of reference it can be seen from equation (19) that the effect of turbulence is independent of azimuth angle. In addition the only component which effects the normal force is that component which is normal to the blade and hence if the turbulence is Gaussian then the loads will also be Gaussian.

Following a similar analysis, for the tangential force, results in the following equation :

$$dF_t = \frac{1}{2}\rho c\, dL \{ C_{L_\alpha} (\bar{U}^2 \cos^2\Theta + 2\bar{U}u'\cos\Theta) - C_{D_0} (\Omega R)^2 \} \tag{20}$$

Again only the turbulent component normal to the blade is important but unlike the normal force the effects of turbulence are now dependent on the azimuth angle. As a result of this it has not been possible to obtain a solution in the frequency domain without considerably more effort possibly involving Markov processes and the Fokker-Planck equation.

However, as the normal force is usually the design load this limitation may not be significant.

## 5. TURBULENCE

In order to determine $G_{P1P2}(w)$ and hence $G_{yy}(w)$ it is necessary to determine the cross-spectral density function of the turbulent velocity fluctuations.

Assuming that the turbulence is both isotropic and homogeneous then a similar method to that used by Rosenbrock (1955) and more recently by Anderson (1981) can be used. The correlation coefficent between two velocity components 'p' and 'q' at points P and Q in space (see Figure 2) can be shown (Karman (1937)) to be

$$R_{pq} = \langle u^2 \rangle \left[ f(r,t)\cos\alpha\cos\beta + g(r,t)\sin\alpha\sin\beta \right]\sin\gamma \qquad (21)$$

where $\langle u^2 \rangle$ is the variance of the turbulence and the angle brackets denote an ensemble average. The functions f(r,t) and g(r,t) are the correlation coefficients between velocity components parallel and at right angles to the line joining P and Q. In general 'f' and 'g' are functions of separation, i.e. 'r' and also time, however at the frequencies of interest atmospheric turbulence can be considered to be a stationary process and hence time invariant. The condition of fluid continuity provides a relationship between these two functions

$$g(r) = f(r) + \frac{r}{2}\frac{d}{dr}f(r) \qquad (22)$$

so that the specification of f(r) implies g(r). The form of f(r) will be discussed later.

In a time interval $\tau$, a point on a blade rotating at a constant angular velocity $\Omega$ will move, relative to an observer translating with the mean flow, between two points separated by a vector $\underline{r}$, (see Figure 3) given by :

$$\underline{r} = \left[ R\cos\Theta_0 - R\cos(\Omega\tau + \Theta_0) + \bar{u},\ R\sin\Theta_0 - R\sin(\Omega\tau + \Theta_0),\ z \right]^T \qquad (23)$$

where $[\ ]^T$ is the transpose, R the radius of the turbine, Z the vertical separation between the two points on the blade.

Even though we have assumed that f(r) and g(r), for a given r, are stationary the correlation coefficient $R_{pq}$ will not be stationary as $\underline{r}$ is a function of not only time lag $\tau$ but also $\Theta_o$ hence t (absolute time). It is fairly obvious from equations (21) through (23) that $R_{pq}$ is periodic, viz :-

$$R_{pq}(t+\tau, t) = R_{pq}(t+\tau-nT, t-nT) \tag{24}$$

where $t = \Theta_o / \Omega \ (\leq T)$ and skew symmetric viz :-

$$R_{pq}(t+\tau, t) = R_{pq}(-t-\tau, -t) \tag{25}$$

where T is the period of rotation and 'n' is an integer. An example of the single point (p=q) correlation coefficient for the case of the normal velocity component on a blade at a radius of 50m rotating at 0.7 rad/sec in a 10 m/s wind is shown in Figure 4. It can be observed from this figure that correlation coefficient is dependent on blade azimuth angle. Only half of the function has been plotted as the other will be skew symmetric according to equation (25). As the spectral density of stationary data can be defined by the Fourier transform of a stationary correlation function, so the spectral density of a non-stationary process can be defined by the double Fourier transform (Papoulis 1965) as

$$\Gamma(\omega_1, \omega_2) = \iint R(t_1, t_2)\, e^{-j(\omega_1 t_1 - \omega_2 t_2)}\, dt_1\, dt_2 \tag{26}$$

For the correlation function defined as in equation (24) we have

$$\Delta(\omega_1, \omega_2) = \iint R_{pq}(t+\tau, t)\, e^{-j(\omega_1 \tau - \omega_2 t)}\, dt\, d\tau$$

$$= \Gamma(\omega_1, \omega_1 + \omega_2) \tag{27}$$

Now from equations (25) and (27) it is possible to show that

$$\Delta(\omega_1,\omega_2) = e^{jn\tau\omega_2}\,\Delta(\omega_1,\omega_2) \tag{28}$$

for all $w_2$. This equality is possible only if the function $\Delta\ (w_1,w_2)$ equals zero everywhere except at the points $(w_1,w_2)$ such that

$$e^{jn\tau\omega_2} = 1 \tag{29}$$

for any integer 'n'. For this to be the case, we must have

$$n\tau\omega_2 = 2\pi k \qquad \text{k:integer} \tag{30}$$

This represents a family of straight lines in $(w_1,w_2)$ space which are parallel to the $w_1$ axis. As a result of this we can define the average correlation coefficient $\tilde{\bar{R}}(\tau)$ and hence its transform $\tilde{\bar{G}}(\omega)$, the average cross-spectral power density function :-

$$\bar{R}_{pq}(\tau) = \frac{1}{T}\int_0^T R_{pq}(t+\tau,t)\,dt \tag{31}$$

$$\bar{G}_{pq}(\omega) = \frac{1}{2\pi}\int_{-\infty}^{\infty} \bar{R}_{pq}(\tau)\cos\omega\tau\,d\tau \tag{32}$$

In addition the correlation coefficient is also ergodic. It remains to describe the functional form of f(r), which is not determined by the symmetry properties leading to equation (22). A number of different functional forms were examined :

a) simple exponential,
b) von Karman model,
c) Fourier inversion of the spectrum.

Based on the work of Fordham and Anderson (1982) and Anderson et. al. (1984) the von Karman model was adopted as a compromise between accuracy and computational speed; the form of which is

$$f(r) = 0.592\,\hat{r}^{1/3}\,K_{1/3}(\hat{r}) \tag{33}$$

and hence from equation (22)

$$g(r) = 0.592\left[\hat{r}_2^{1/3}\,K_{1/3}(\hat{r}_2) - \tfrac{1}{2}\,\hat{r}_2^{4/3}\,K_{2/3}(\hat{r}_2)\right] \tag{34}$$

where

$$\hat{r}_1 = 0.747\,r/{}^{x}L_u \;, \qquad \hat{r}_2 = 0.374\,r/{}^{x}L$$

$L^u_x$ is the longitudinal length scale and $K_n$ is a modified Bessel function of the second kind order 'n'.

The angles $\alpha$ and $\beta$ in equation (21) are determined by the velocity component of interest, in the case of the normal force it is the component normal to the blade. The angle $\gamma$ is a function of the vertical separtion between the points $p_1$ and $p_2$. If the points lie in the same horizontal plane the angle will be zero. If the points $p_1$ and $p_2$ are not on the same blade, but on blades separated by $\Theta_s$ , equation (23) is then

$$\underline{r} = \left[\, R\cos(\Theta_0) - R\cos(\Omega z + \Theta_0 + \Theta_s) + \bar{U}z \,,\; R\sin(\Theta_0) - R\sin(\Omega z + \Theta_0 - \Theta_s) \,,\; z \,\right]^T \tag{35}$$

## 6. RESULTS

To gain an understanding of the effects of turbulence and also substantiate the assumptions made regarding the removal of non-stationary effects it was decided to neglect the modal response and concentrate on integrated normal aerodynamic blade forces; this in effect assumes that the blade behaves like a rigid body. This assumption also allows a

certain amount of verification of the results, with a time domain simulation model. (Anderson et al. 1985).

The power spectrum of the turbulent component only for the integrated half blade normal aerodynamic force is

$$G_N(\omega) = A_N^2 \iint_{L\,L} G_{u_1 u_2}(L_1, L_2, \omega)\, dL_1\, dL_2 \qquad (36)$$

where

$$A_N = \tfrac{1}{2}\rho c C_{L_\alpha} \Omega R \qquad (37)$$

From equation (19) it can be observed that the variance of the normal force is directly proportional to the variance of the turbulence and the statistics will be Gaussian.

The following parameters will be used to describe a straight bladed 100m diameter vertical axis wind turbine :-

| | |
|---|---|
| Radius | 50 m |
| Chord | 5 m |
| Rotational Speed | 0.7 rad/sec |
| Blade Length (tip to tip) | 72 m |
| Mean Wind Speed | 10 m/s |
| Turbulence Intensity | 15% |

Equation (36) has been evaluated for the above parameters for a range of turbulent length scales and the results are presented in Figures 5 to 9. The spectra are shown plotted against the reduced frequency (i.e. non-dimensional with respect to the rotational frequency). For all the spectra it can be observed that a significant amount of energy is concentrated around 1P but not at the higher harmonics. Perhaps surprisingly there appears to be a removal of energy at 2P compared with adjacent frequencies. Increasing the length scale from 50m to 150m causes the 1P peak to become larger. A statistical analysis of these spectra, based on equations (6) to (9) is presented in Table 3. From this table a number of observations can be made :

i) The variance increases with increasing length scale.

ii) The spectral width, an indication of the distribution of energy, does not appear to have any obvious relationship with the length scale. This is not surprising as the calculation of this parameter is prone to numerical error.

iii) The mean and root-mean-square peak values, which are functions of the spectral width, are approximately 1.05 and 1.30 respectively.

iv) The maximum likely peak value decreases with increasing length scale.

v) The zero crossing rate decreases with increasing length scale.

Presented in Figures 10 to 12 are results obtained from Anderson et al 1985 using a time domain simulation technique for the turbulent component only; a direct comparison with results obtained from this analysis can be made. A turbulent length scale and intensity of 85m and 15% respectively was used in both computations. From Figure 10 it can be seen that the two spectra are in reasonable agreement especially in the prediction of the 1P peak and the trough at 2.5P. The spectra from the simulation is considerably more 'noisy', at higher frequencies, as a result of statistical errors. Both spectra also predict the existence of a peak at 3.5P even though the structure was considered to be rigid in both cases. The probability and level crossing distributions, for the turbulent normal force component from the simulation, are shown in Figures 11 and 12 respectively. Also shown are the predicted maximum peak value and the zero crossing frequency from this analysis. It can be clearly observed that good agreement exists and that the distributions are approximately Gaussian.

## 7. CONCLUSIONS

An analytical model has been developed, in the frequency domain, for predicting the modal response of a vertical axis wind turbine to turbulence. Unfortunately owing to non-stationary terms, in the tangential force equation which could not be removed, the model is limited to the normal force only. As discussed this is not a severe limitation as the normal force is usually the design load.

It has been shown that turbulence, as a result of rotational sampling, concentrates a significant amount of energy at 1P and and to a lesser extent at 2.25P and 3.5P. These latter two peaks are not thought to be real but the result of the numerical analysis. To a large extent it has been shown that the statistical properties of the turbulent induced normal forces can be assumed to be independent of the turbulent length scale. It has been shown that the maximum peak and root mean square peak values are 3.4 and 1.35 respectively times the standard deviation. Confidence in the assumptions made during the development of this model has been gained by comparing the results with a time domain simulation model.

## 8. REFERENCES

Anderson, M.B., 1981. 'An Experimental and Theoretical Study of Horizontal Axis Wind Turbines'. Ph.D. dissertation, University of Cambridge.

Anderson, M.B., 1982. 'The Interaction of Turbulence with a Horizontal Axis Wind Turbine'. Proc. of the 4th BWEA Conference, Cranfield.

Anderson, M.B., Garrad, A.D. and Hassan, U., 1984. 'Teeter Excursions of a Two-Bladed Horizontal Axis Wind Turbine Rotor in a Turbulent Velocity Field'. J. of Wind Eng. and Ind. Aero., Vol. 17, pp. 71-88.

Anderson, M.B., Bossanyi, E. and Powles, S.J.R., 1985. 'The Response of a Vertical Axis Wind Turbine to Fluctuating Aerodynamic Loads'. Proc of the 7th BWEA Conference, Oxford. Pub. M.E.P.

Bendat, J.S. and Piersol, A.G., 1980. 'Engineering Applications of Correlation and Spectral Analysis'. John Wiley & Sons Inc.

Cartwright, D.E. and Longuit-Higgins, M.S., 1956. 'The Statistical Distribution of the Maxima of a Random Function'. Proc. Roy. Soc., Ser. A, Vol. 237, pp. 212-232.

Fordham, E.J., 1984. 'Atmospheric Turbulence in Relation to Horizontal Axis Wind Turbines and the Construction of Two Research Machines'. Ph.D. dissertation, University of Cambridge.

Jensen, N.O. and Frandsen, S., 1978. 'Atmospheric Turbulence in Relation to Wind Generator Design'. Proc. 2nd Int. Symp. on Wind Energy Systems, Amsterdam.

Papoulis, A., 1965. 'Probability : Random Variables and Stochastic Processes'. New York : McGraw Hill.

Rosenbrock, H.H., 1955. 'Vibration and Stability Problems in Large Wind Turbines having Hinged Blades'. Electr. Res. Assoc., Rep., C/T 113.

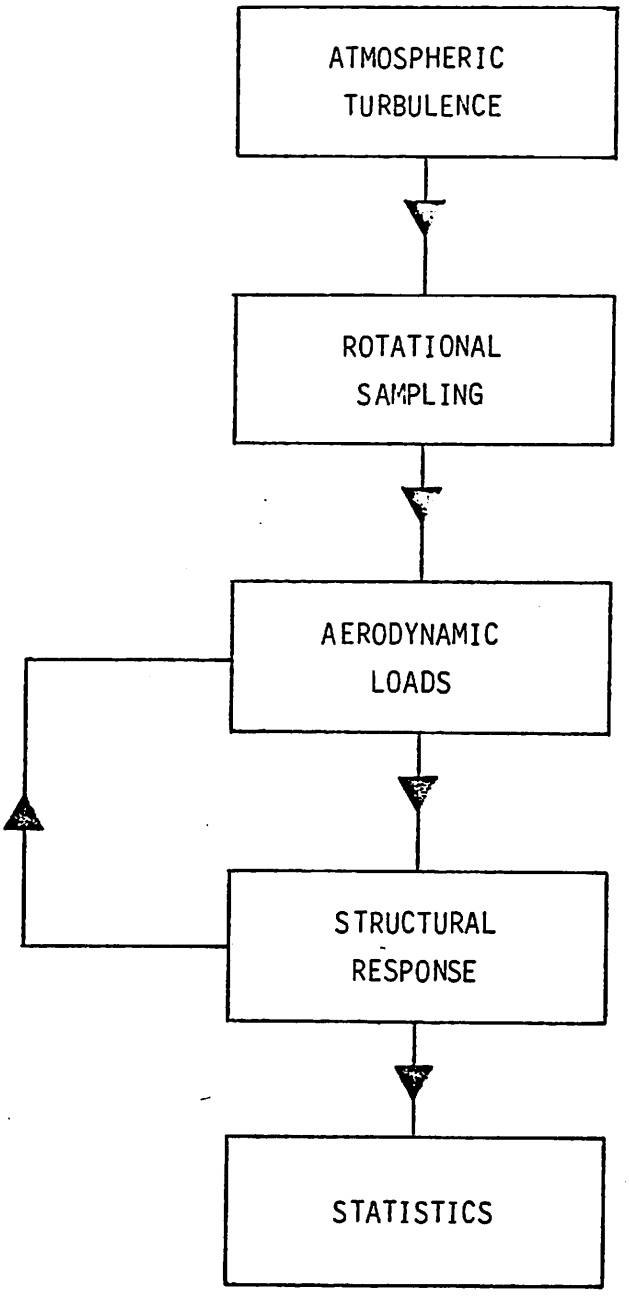


Table 1 General Method of Analysis

TURBINE TYPE

| COMPONENT | HORIZONTAL | VERTICAL |
|---|---|---|
| Atmospheric Turbulence | Gaussian distribution.<br>Stationary.<br>Only longitudinal component usually of interest.<br>Isotropic and homogeneous.<br>Wind shear neglected. | Gaussian distribution<br>Stationary.<br>Lateral and longitudinal components required.<br>Isotropic and homogeneous.<br>Wind shear neglected. |
| Rotational Sampling | gaussian distribution preserved.<br>Stationary. | Gaussian distribution preserved.<br>Non-stationary with respect to frequency. |
| Aerodynamic Loads | Gaussian distribution preserved.<br>Stationary.<br>Independent of blade position | Non-Gaussian distribution<br>Non-stationary.<br>Dependent on blade. position. |
| Structural Response | Linear structural model.<br>Gaussian distribution preserved.<br>Independent of blade posit/n except when tower is included for a two-bladed turbine. | Linear structural model.<br>Non-Gaussian distribution.<br>Non-stationary.<br>Dependent on blade position. |

Table 2 Comparison of Basic Assumptions

| Parameter | LENGTH SCALE ($^{x}L_u$) (m) 50 | 75 | 100 | 125 | 150 | Infinity |
|---|---|---|---|---|---|---|
| Variance ($m_o$) ($N^2$) | $9.07 \times 10^8$ | $9.94 \times 10^8$ | $10.04 \times 10^8$ | $10.07 \times 10^8$ | $10.97 \times 10^8$ | $12.17 \times 10^8$ |
| Spectral Width ($\epsilon$) | 0.600 | 0.349 | 0.482 | 0.542 | 0.585 | 0.456 |
| Mean Peak ($\bar{h}/m_o^{\frac{1}{2}}$) | 1.00 | 1.17 | 1.09 | 1.05 | 1.01 | 1.11 |
| R.M.S. Peak ($h_{rms}/m_o^{\frac{1}{2}}$) | 1.28 | 1.37 | 1.32 | 1.30 | 1.28 | 1.33 |
| Zero Crossing Rate (Hz) | 0.735 | 0.622 | 0.556 | 0.511 | 0.479 | 0.432 |
| Maximum Peak ($h_{max}/m_o^{\frac{1}{2}}$) | 3.48 | 3.44 | 3.41 | 3.40 | 3.36 | 3.33 |

Table 3 Variation of the Statistical Properties of the Aerodynamic Normal Force with Length Scale. (Turbulent Component Only)

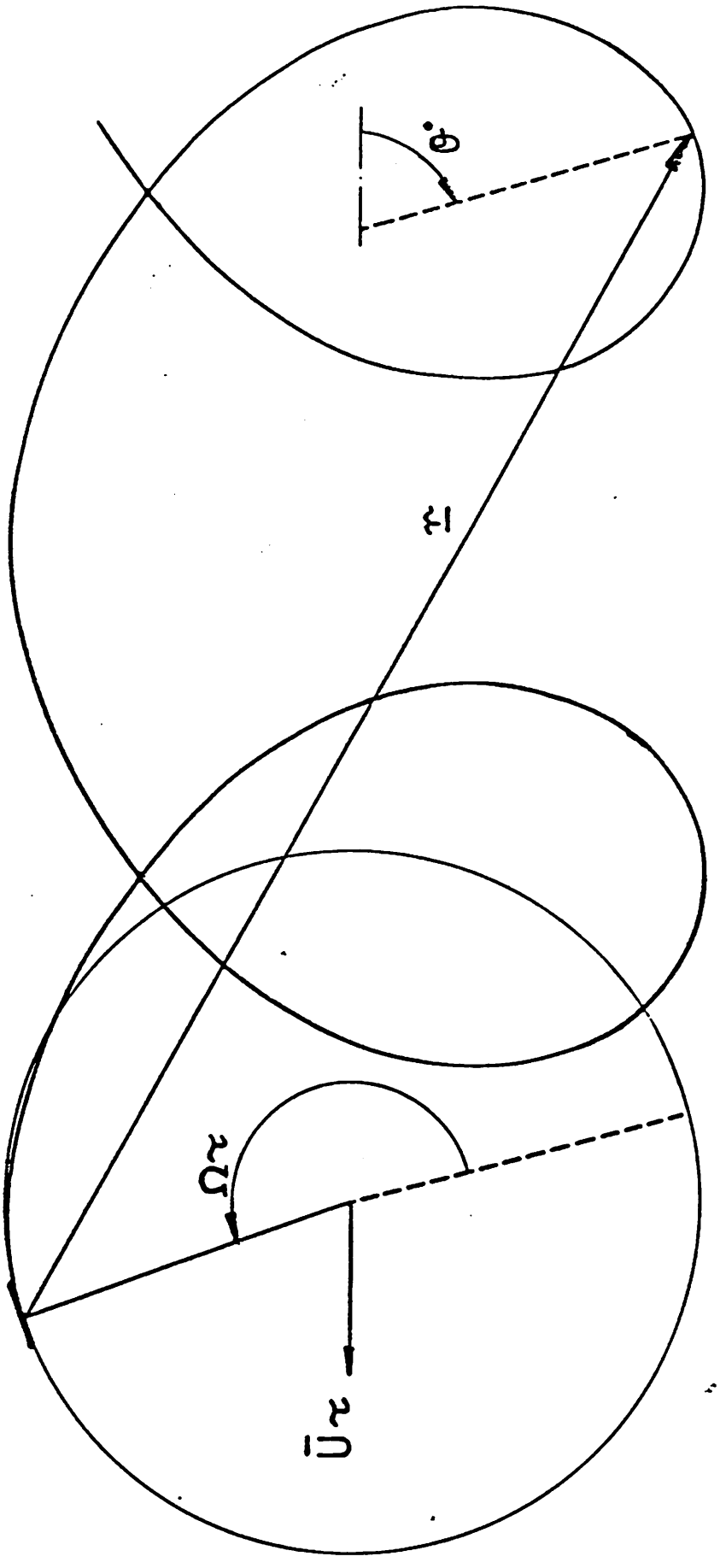


FIGURE 1 TRAJECTORY OF A POINT ON THE BLADE RELATIVE TO AN OBSERVER TRANSLATING WITH THE MEAN FLOW

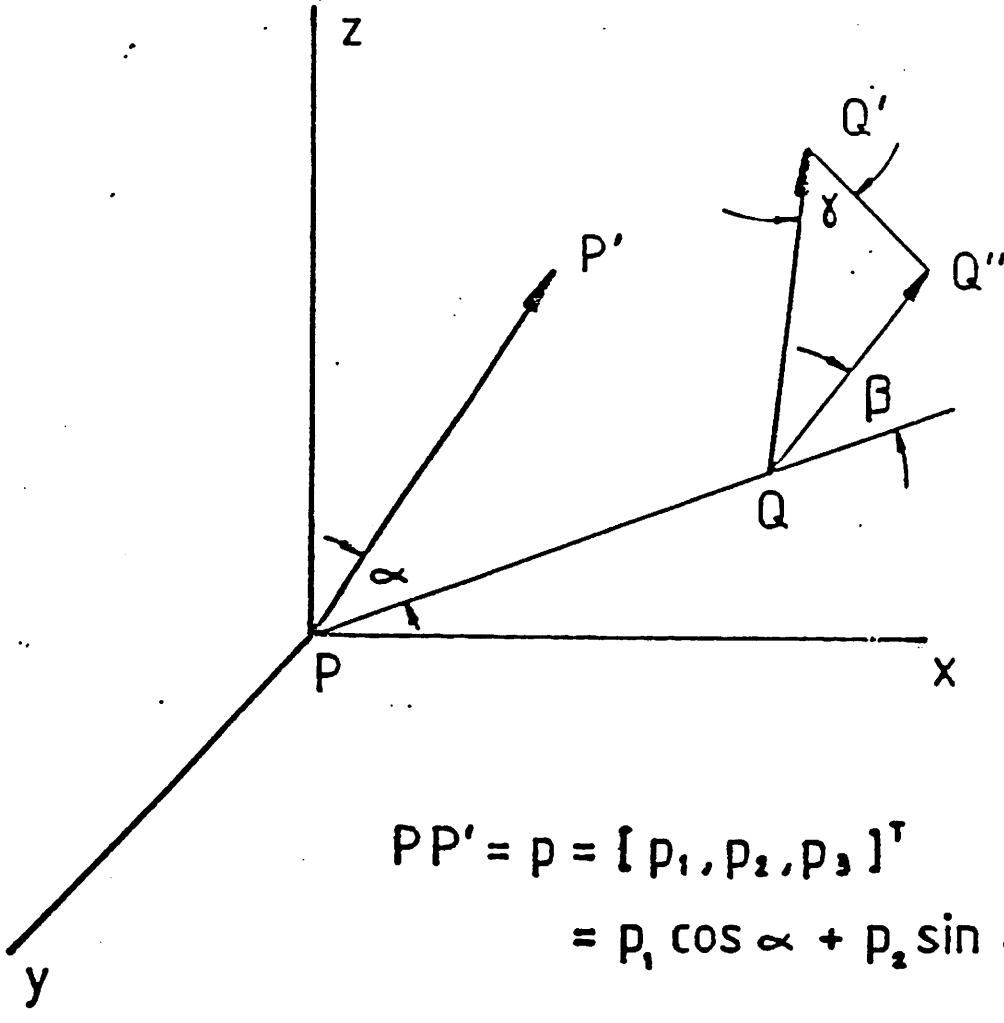


$$PP' = p = [p_1, p_2, p_3]^T$$
$$= p_1 \cos\alpha + p_2 \sin\alpha$$

$$QQ' = q = [q_1, q_2, q_3]^T$$
$$= q_1 \cos\beta \sin\gamma + q_2 \sin\beta \sin\gamma + q_3 \cos\gamma$$

FIGURE 2 CORRELATION

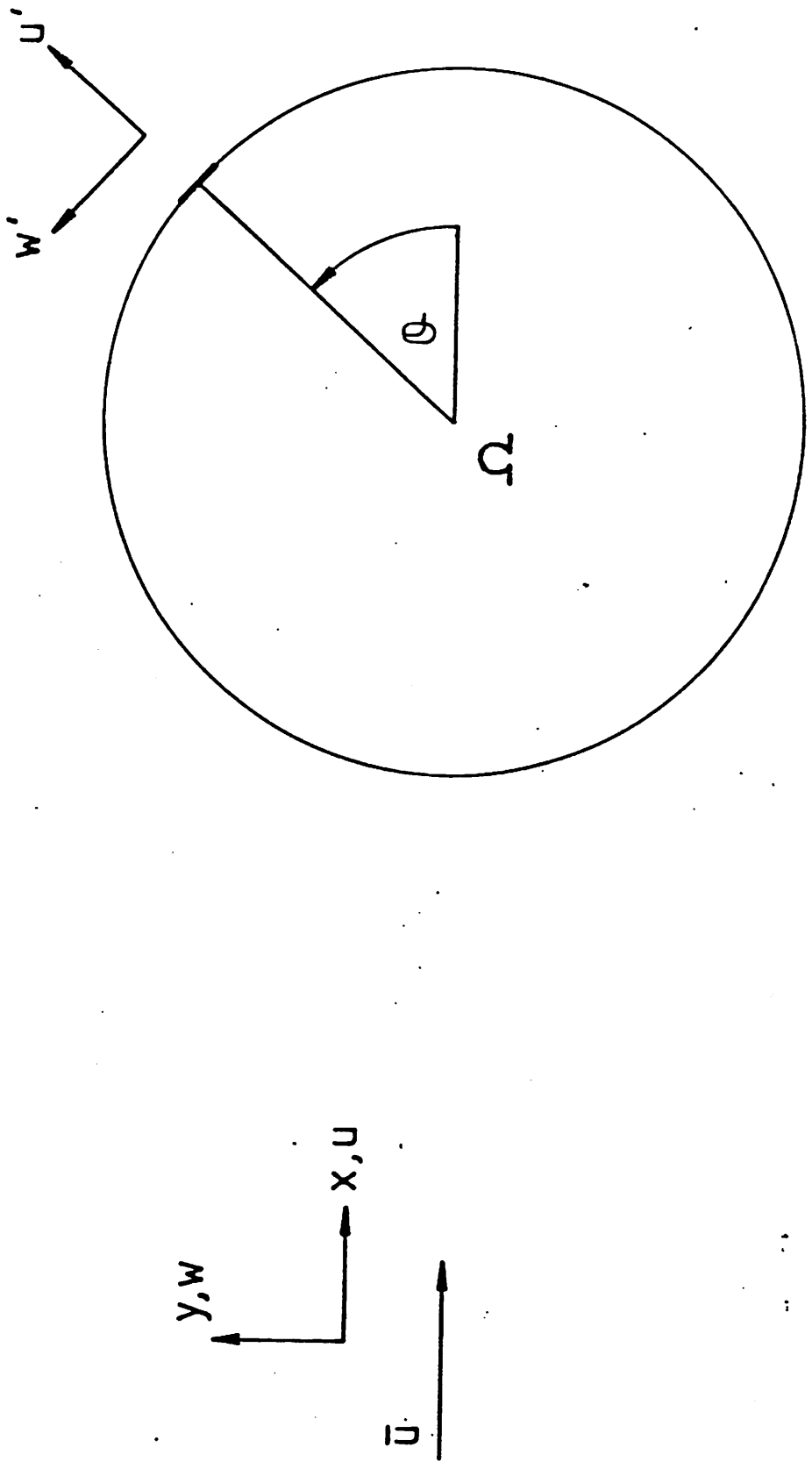


FIGURE 3 TRANSFORMATION OF TURBULENCE FROM STATIONARY TO ROTATING FRAMES OF REFERENCE

CORRELATION COEFFICIENT

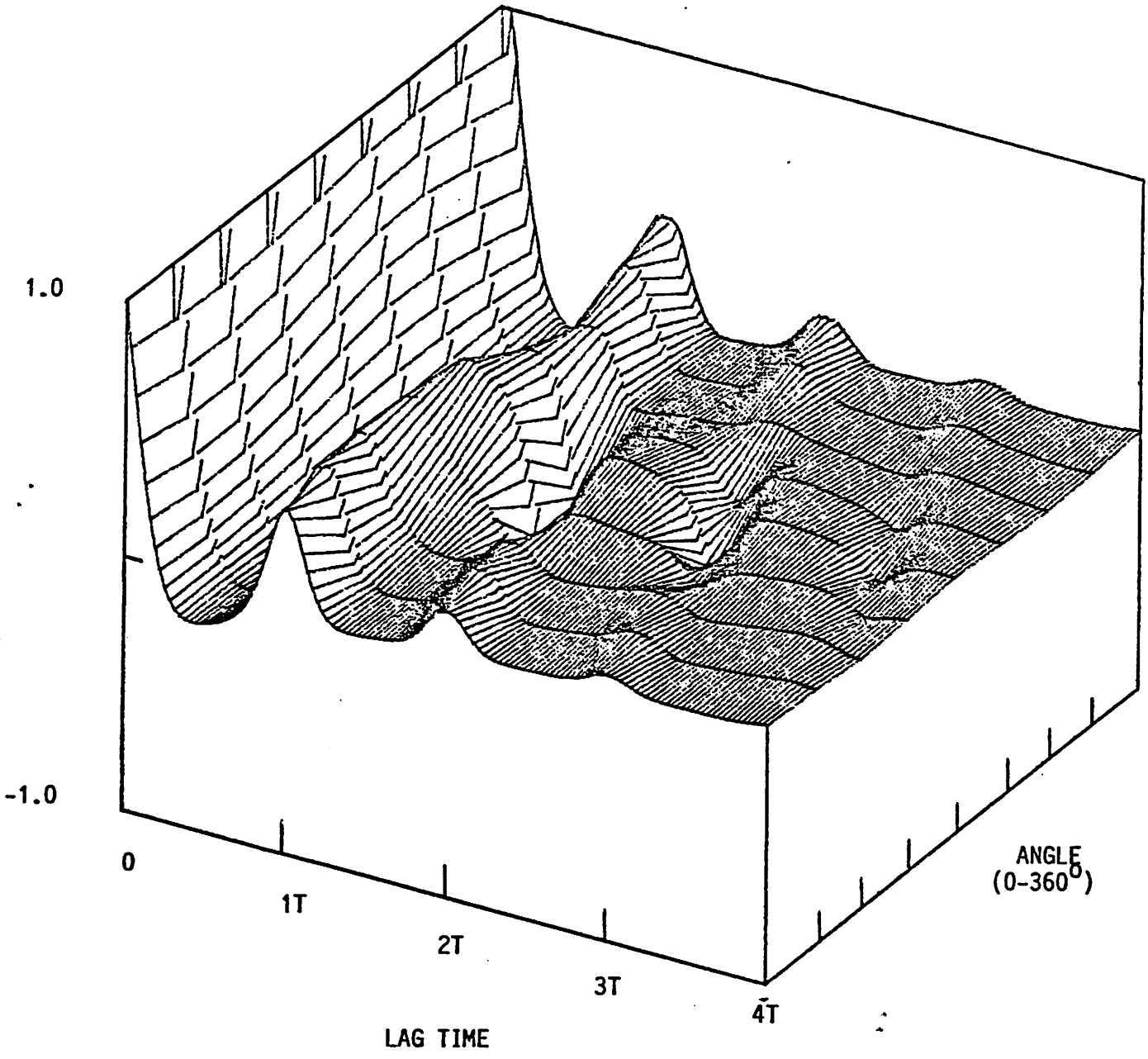


FIGURE 4 CORRELATION COEFFICIENT

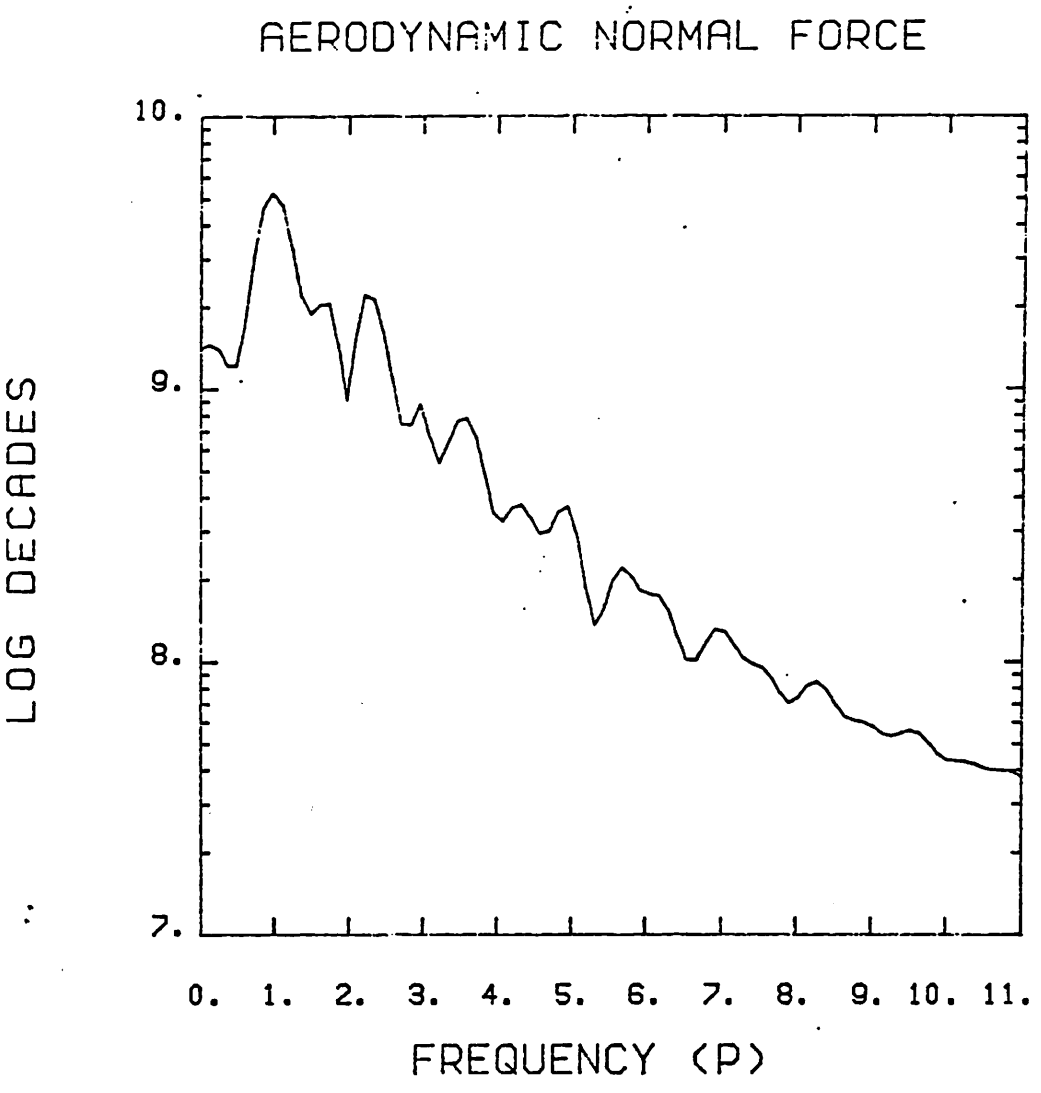


FIGURE 5 POWER SPECTRAL DENSITY FUNCTION OF NORMAL BLADE FORCE (turbulence only). LENGTH SCALE = 50m.

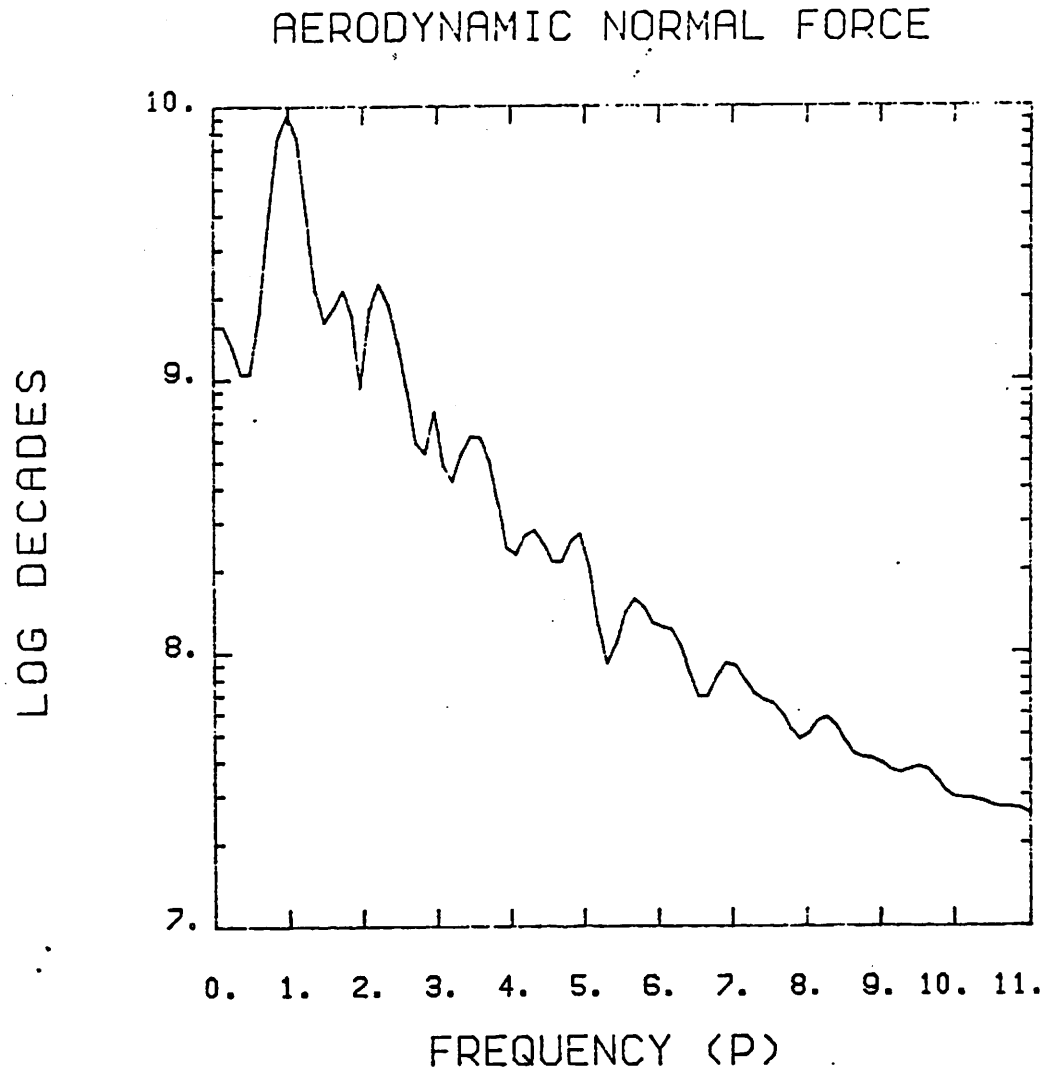


FIGURE 6 POWER SPECTRAL DENSITY FUNCTION OF NORMAL BLADE FORCE (turbulence only). LENGTH Scale = 75m.

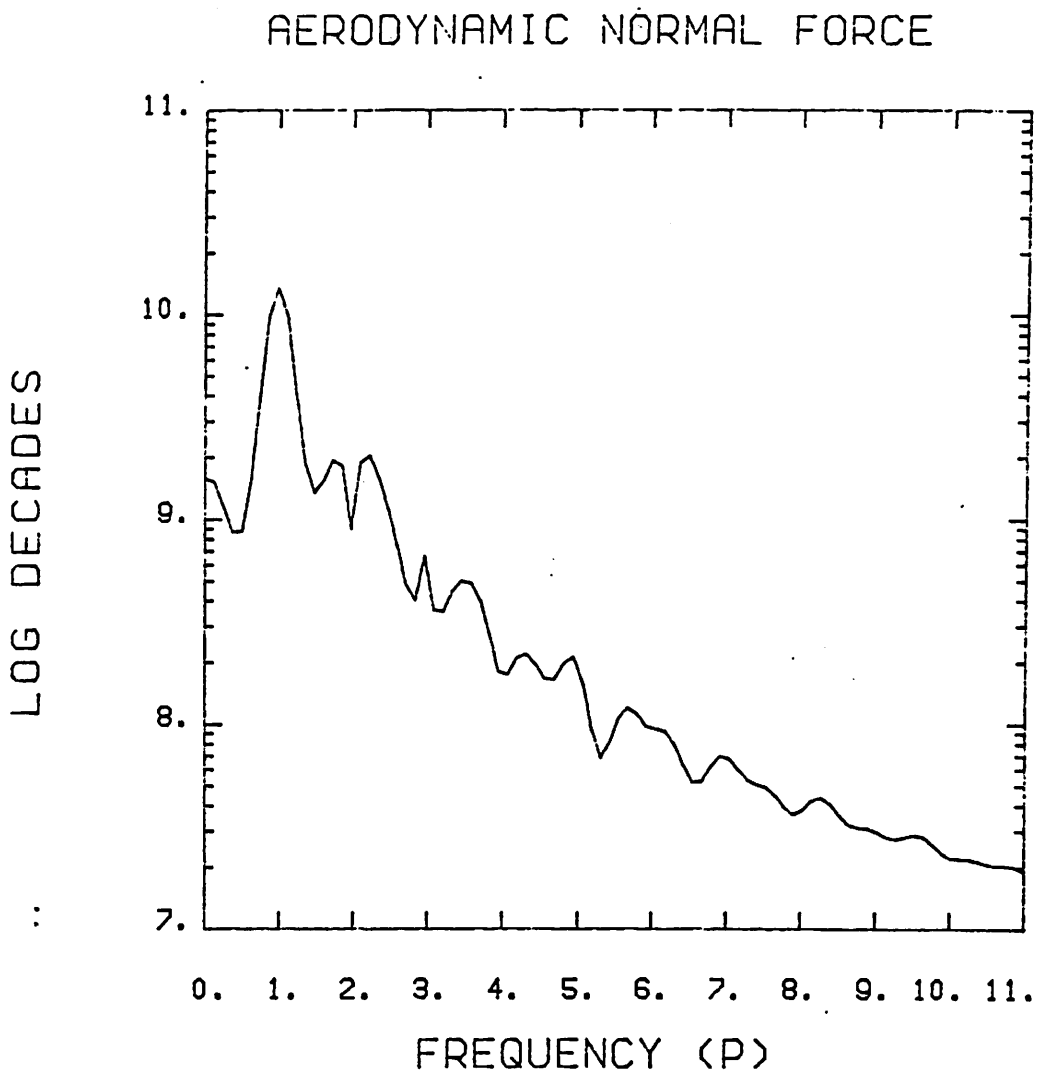


FIGURE 7 POWER SPECTRAL DENSITY FUNCTION OF NORMAL BLADE FORCE (turbulence only). LENGTH SCALE = 100m.

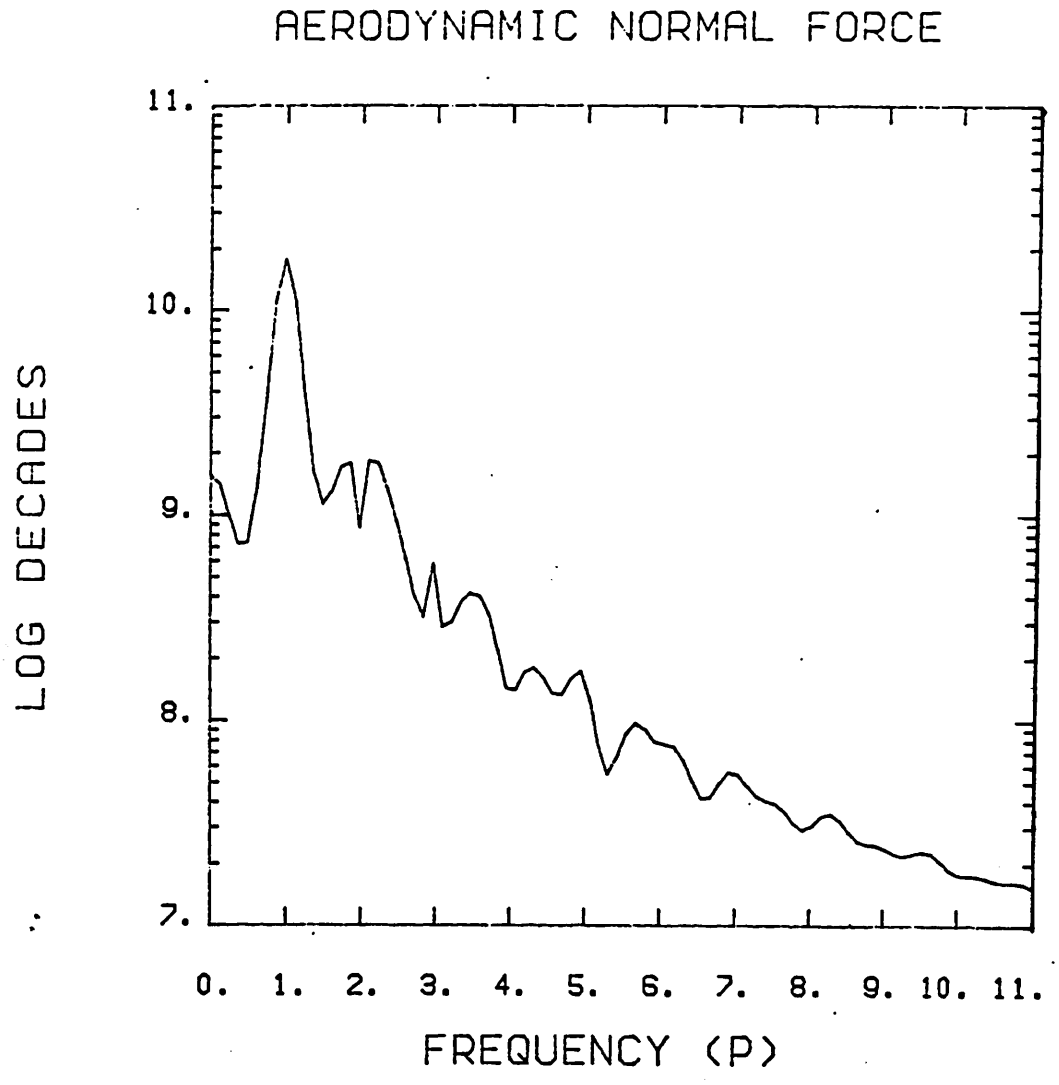


FIGURE 8 POWER SPECTRAL DENSITY FUNCTION OF NORMAL BLADE FORCE (turbulence only). LENGTH SCALE = 125m.

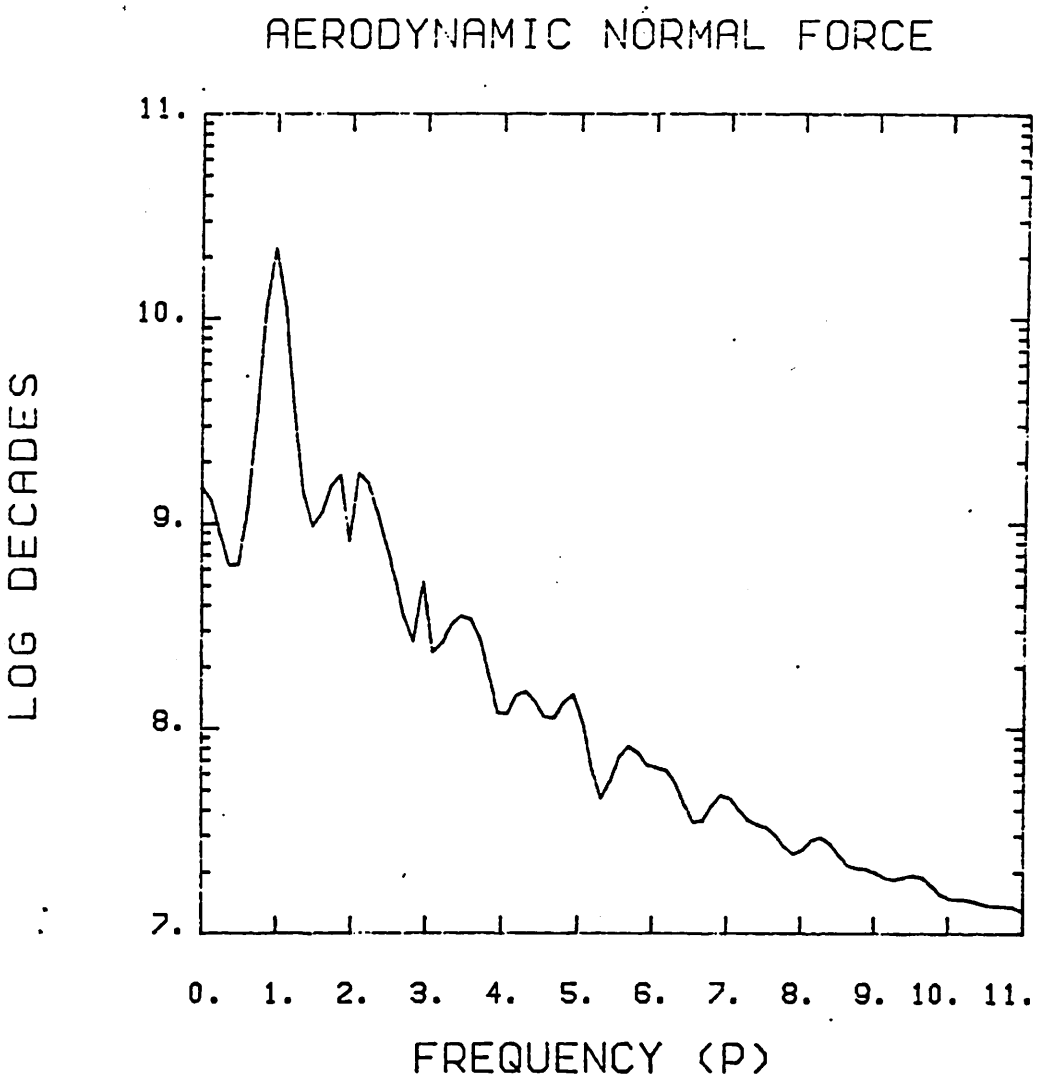


FIGURE 9 POWER SPECTRAL DENSITY FUNCTION OF NORMAL BLADE FORCE (turbulence only). LENGTH SCALE = 150m.

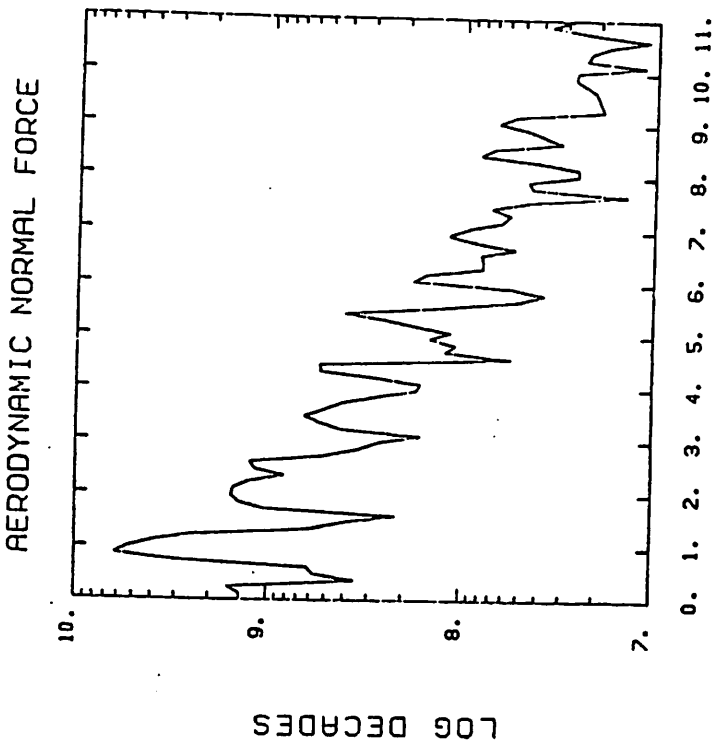


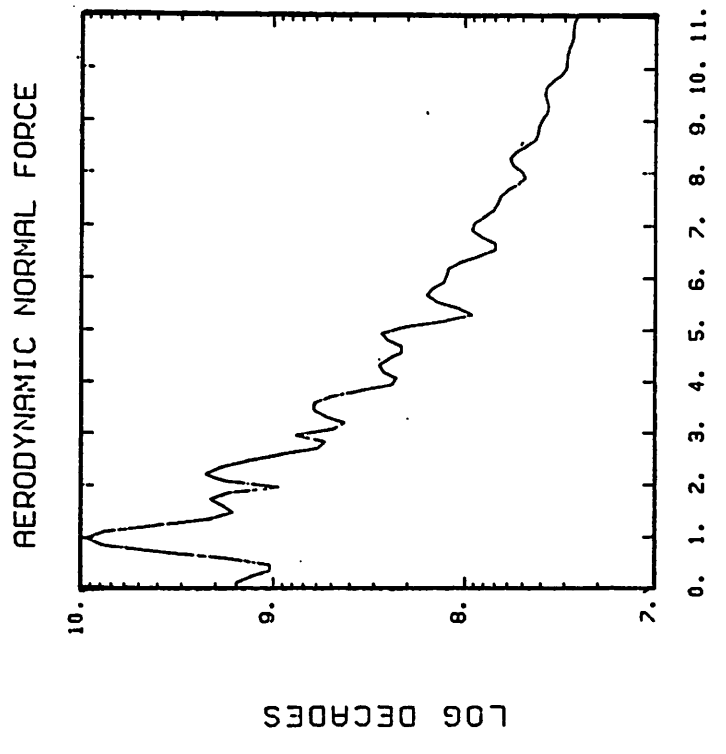


FIGURE 10 COMPARISON OF THE PREDICTED POWER SPECTRAL DENSITY FUNCTIONS OF THE NORMAL FORCE FROM A DIRECT FREQUENCY DOMAIN ANALYSIS AND INDIRECTLY VIA THE TIME DOMAIN.

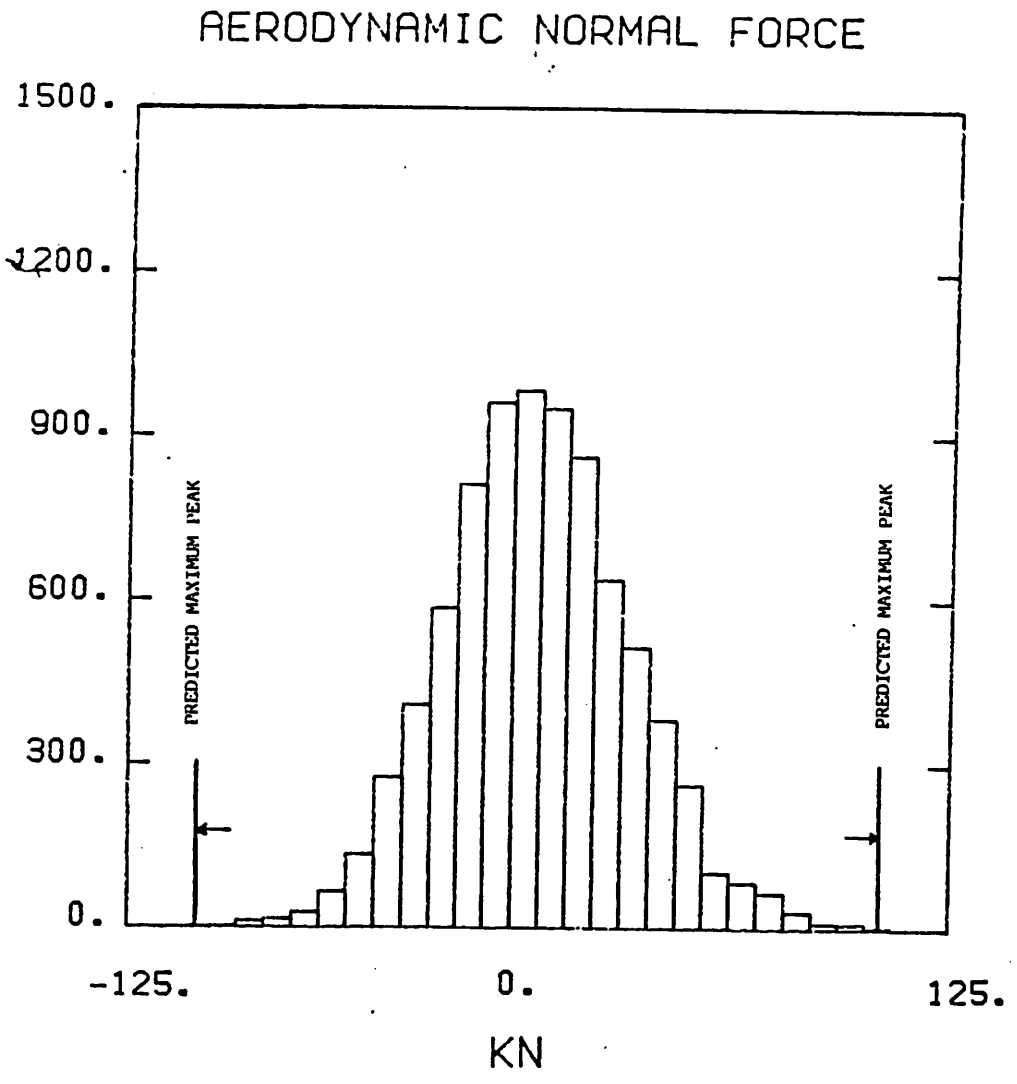


FIGURE 11 PROBABILITY DISTRIBUTION OF NORMAL FORCE (turbulence only) FROM TIME DOMAIN ANALYSIS. ALSO SHOWN PREDICTED MAXIMA FROM THIS ANALYSIS.

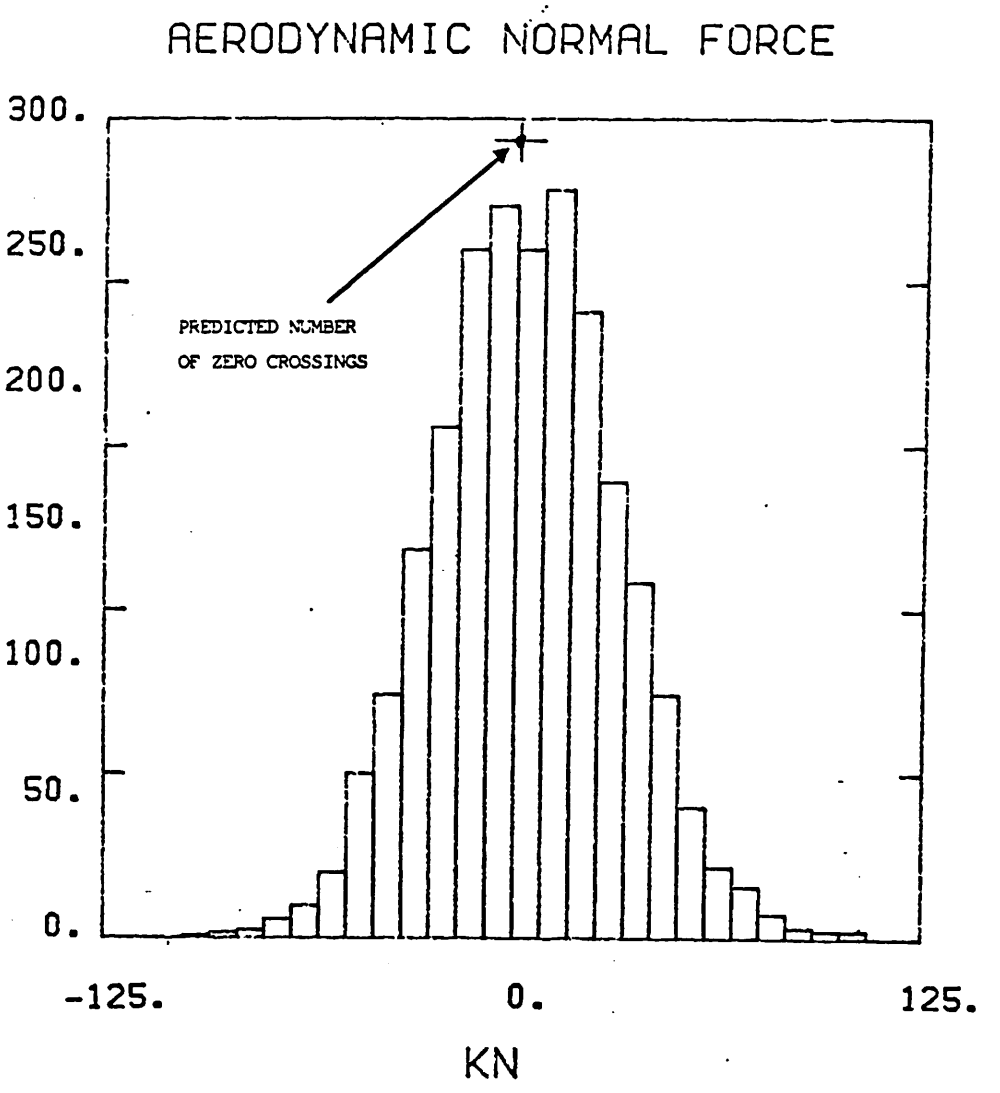


FIGURE 12 LEVEL CROSSINGS OF NORMAL FORCE (turbulence only) FROM TIME DOMAIN ANALYSIS. ALSO SHOWN PREDICTED NUMBER OF ZERO CROSSINGS FROM THIS ANALYSIS.

# THE SIMULATION OF TURBULENCE FOR USE IN WIND TURBINE ANALYSIS

## 1. INTRODUCTION

The main advantage of adopting an approach based on the numerical simulation of the turbulent velocity is that non-linear effects associated primarily with stall, whether it be dynamic or quasi-steady, can be included. In addition, once the velocity field has been synthesised it may be stored and used many times over as an input to structural/aerodynamic models of different complexity. The results from such a model are in general easier to interpret and are directly comparable with experiemental data. Care, must however be taken to ensure that this method does not become computationally very expensive.

## 2. METHODOLOGY

There are two basic avenues of approach for the numerical simulation of a three-dimensional turbulent velocity field :-

a) numerical solution of the Navier-Stokes equation;

b) 'Monte Carlo' simulation.

A detailed discussion of both these can be found in Frost and Moulden (1977) and the references cited therein. However, in summary the main difference between the two approaches is that the 'Monte Carlo' method is based solely on the first and second order statistical moments without any reference to the fluid dynamics of the flow and hence is considerably simpler. There is no guarantee that the 'Monte Carlo' approach will produce a velocity field which is continuous or physically realisable. However, in the context of aerodynamic/ structural dynamics the first and second order statistical moments have the most significant impact on loads. For these reasons the 'Monte Carlo' approach was adopted.

## 3. MONTE CARLO SIMULATION

To simulate a three-dimensional velocity field the method outlined by Shinozuka and Jan (1972) and more recently by Veers (1984) has been adopted. A three dimensional velocity field can be simulated by producing time series of wind speeds at 'q' points which lie in a plane perpendicular to the mean wind direction, Figure 1. To simulate it is necessary to have a knowledge of the spectral density matrix $S^x$. This is a matrix which represents the cross-spectral density function between two points in space; in general it is complex and Hermitian, hence

$$S_{jk} = \bar{S}_{kj} \tag{1}$$

where the overbar indicates the complex conjugate.

Assuming that Taylor's frozen turbulence hypothesis is applicable, and that the number of points at which the turbulence is simulated is q, then

$$S^x = \begin{bmatrix} S_{11} & S_{12} & \cdots & S_{1,2q} \\ S_{21} & S_{22} & \cdots & S_{2,2q} \\ \cdot & \cdot & & \\ S_{2q,1} & S_{2q,2} & \cdots & S_{2q2q} \end{bmatrix} \tag{2}$$

The $S^x$ matrix is of size 2q x 2q, not q x q, owing to the two velocity components. Conceptually, it is assumed that $S^x$ can bd produced by passing a set of 2q mutuaddy independent white noise sources $w_i = w_i(t)$, i=1,2,.....2q through a set of suitable linear systems $H_{ij}$, called the H matrix (see Figure 2) It can be shown that the H matrix satisfies the equation

$$S^x = H \bar{H}^T \tag{3}$$

where T indicates the transpose

To find the matrix H efficiently, it may be assumed that H is of lower triangular form hence :

$$H_{ii} = \left(S_{ii} - \sum_{j=1}^{i} H_{ij}^2\right)^{1/2} \quad i = 1, 2 \ldots, 2q \tag{4}$$

$$H_{ji} = \left(S_{ij} - \sum_{k=1}^{j-1} H_{ik} H_{jk}\right)/H_{jj} \quad j = 1, 2 \ldots i \tag{5}$$

All terms on the main diagonal of H are real-valued quantities while the other terms are, in general, complex.

The 2q white noise sources can be defined by a vector of the same length having individual terms given by

$$S^{W}_{ij} = (T)^{-1} E[\bar{W}_i W_i] = 1 \tag{6}$$

where T represents the simulation period of time, E is the expected value and $W_i$ is the Fourier transform of $w_i(t)$. To generate the noise vector, the Fourier transforms can be defined as

$$W_i(f) = (T)^{\frac{1}{2}} \exp)-j\alpha_i(f)) \tag{7}$$

The phase angles, $\alpha_i$ (f) are taken from a uniform distribution between 0 and $2\pi$ radians. The Fourier transform of the 2q time series is hence given by

$$\mathbf{X} = \mathbf{HW} \tag{8}$$

which is equivalent to

$$X_i = \sum_{k=1}^{i} H_{ik} W_k \quad i = 1,2 \ldots, 2q \tag{9}$$

The simulated time series can then be obtained from the inverse Fourier transform of equation (9).

To simplify matters it is possible to assume that the spectral matrix is real and that the lateral and longitudinal components are uncorrelated;

both of these assumptions can be justified in the light of experimental evidence, Kristensen and Jensen (1979) and Davenport (1961).

The individual terms within the $S^x$ can be calculated via the coherence function and a suitable form of the single point power spectrum.

The coherence function, for either component, is defined (ESDU 1971) as

$$\gamma^2_{ij}(\Delta r, \omega) = \frac{|S_{ij}(\Delta r, \omega)|^2}{S_{ii}(\omega)\, S_{jj}(\omega)} \tag{10}$$

but as we have assumed that the turbulence is homogeneous then

$$S_{ii}(n) = S_{jj}(n) \qquad i = 1,2 \ldots 2q \tag{11}$$

and hence

$$|S_{ij}(\Delta r, \omega)| = S_{ii}(\omega)\, \gamma_{ij}(\Delta r, \omega) \tag{12}$$

ESDU (1971) have proposed, based on experimental evidence, the following relationships for the coherence function for the two components,

$$\gamma^2_{ij}(\omega, \Delta r) = \exp\left(-r A_n \Delta r/(2\pi \bar{U})\right) \tag{13}$$

where

$$r_{A_n} = 3 + 270\,\Delta\, r^{\frac{1}{3}}/{}^{x}L_u \qquad \text{longitudinal} \tag{14}$$

$$r_{A_n} = 270\,\Delta\, r^{\frac{1}{3}}/{}^{x}L_u \qquad \text{lateral} \tag{15}$$

and ${}^{x}L_u$ is the longitudinal length scale. The single point power spectrum based on the von Karman spectrum was used for $S_{ii}(n)$ with the appropriate constants for each of the two velocity components. The restriction of Taylor's hypothesis can be removed by generating two uncorrelated velocity fields and interpolating between them.

However, even though this method is numerically very efficient, a considerable amount of core storage is required and therefore special software is required to enable disk storage to be used efficiently unless a virtual operating system is available.

## 4. RESULTS

To gain confidence with this technique a comparison, in statistical terms, was made with real wind data. This data consisted of measurements of three perpendicular components of the wind at 12 points, 8 in an outer ring, 4 in an inner ring. Positions and dimensions are shown in Figure 3. The anemometers used were Gill propellors, and the data were sampled every 0.2s. To effect a comparison the longitudinal length scale, turbulence intentsity and mean wind speed had to be determined. From the comprehensive analysis of this data carried out by Fordham (1984) the following values were taken; longitudinal length scale = 85m, turbulence intensity = 13.5%, mean wind speed = 10.78 m/s. Using these data a simulated wind field was generated using the above described technique. For both the real and simulated wind fields estimates of the single point power spectra and coherence functions were obtained by the method generally known as segment averaging. A Hanning window was applied to each segment prior to performing a FFT in order to reduce leakage effects. The results of this analysis (for the longitudinal turbulent component only) is shown in Figures 4 and 5. It can be observed from both figures that close agreement exists between the simulated and the real data. Presented in Figure 6 and 7 are isovent contour maps, of horizontal slices, of a simulated field; the contours are at 1 m/s intervals. The number of simulated points perpendicular to mean wind direction was 32 in a rectangular grid 4 (vertical) by 8 (lateral) spanning an area 72m by 100m respectively. The total length of the field was 8192 points spaced at equal intervals of approximately 20m.

Results from using this technique in conjunction with structural models of both horizontal and vertical axis wind turbines can be found in Anderson et al. 1985 and Powles and Anderson 1984.

## 5. REFERENCES

Anderson, M.B., Bossanyi, E. and Powles, S.J.R., 1985. 'The Response of a Vertical Axis Wind Turbine to Fluctuating Aerodynamic Loads'. Proc of the 7th BWEA Conference, Oxford. Pub. M.E.P.

Davenport, A.G., 1961. 'The Spectrum of Horizontal Gustimes near the Ground in High Winds'. Quarterly Journal Meteorological Society, Vol. 87.

ESDU, 1971. 'Characteristics of Atmospheric Turbulence near the Ground'. Eng. Sci. Data Unit, Data Item 74031.

Fordham, E.J. and Anderson, M.B., 1982. 'An Analysis of Results from an Atmospheric Experiment to Examine the Structure of the Turbulent Wind as seen by a Rotating Observer'. Proc. 4th BWEA Wind Energy Conference, Cranfield.

Frost, W. and Moulden, T.H., 1977. 'Handbook of Turbulence : Volume 1, Fundamentals and Applications'. Plenum Press, New York.

Kristensen, L and Jensen, N.O., 1979. 'Lateral Coherence in Isotropic Turbulence and in the Natural Wind'. Boundary Layer Meteorology, Vol. 17.

Powles, S.J.R. and Anderson, M.B., 1984. 'The Effect of Stochastic and Deterministic Processes on Fatigue Damage in a Large Horizontal Axis Wind Turbine'. Proc. of the European Wind Energy Conference, Hamburg.

Rice, S.O., 1944-45. 'Mathematical Analysis of Random Noise'. Bell Systems Tech. 5, Vol. 23, pp. 282-332; Vol. 24, pp. 46-156.

von Karman, T. and Howarth, L., 1937. 'On the Statistical Theory of Isotropic Turbulence'. Proc. Roy. Soc. Ser. A, Vol. 164, pp 192 et seq.

Shinozuka, M., and Jan, C.M., 1972. 'Digital Simulation of Random Processes and its Applications'. Journal of Sound and Vibration, Vol. 25, 111-128.

Veers, P.S., 1984. 'Modelling Stochastic Wind Loads on Vertical Axis Wind Turbines'. Sandia Report SAND83-1909.

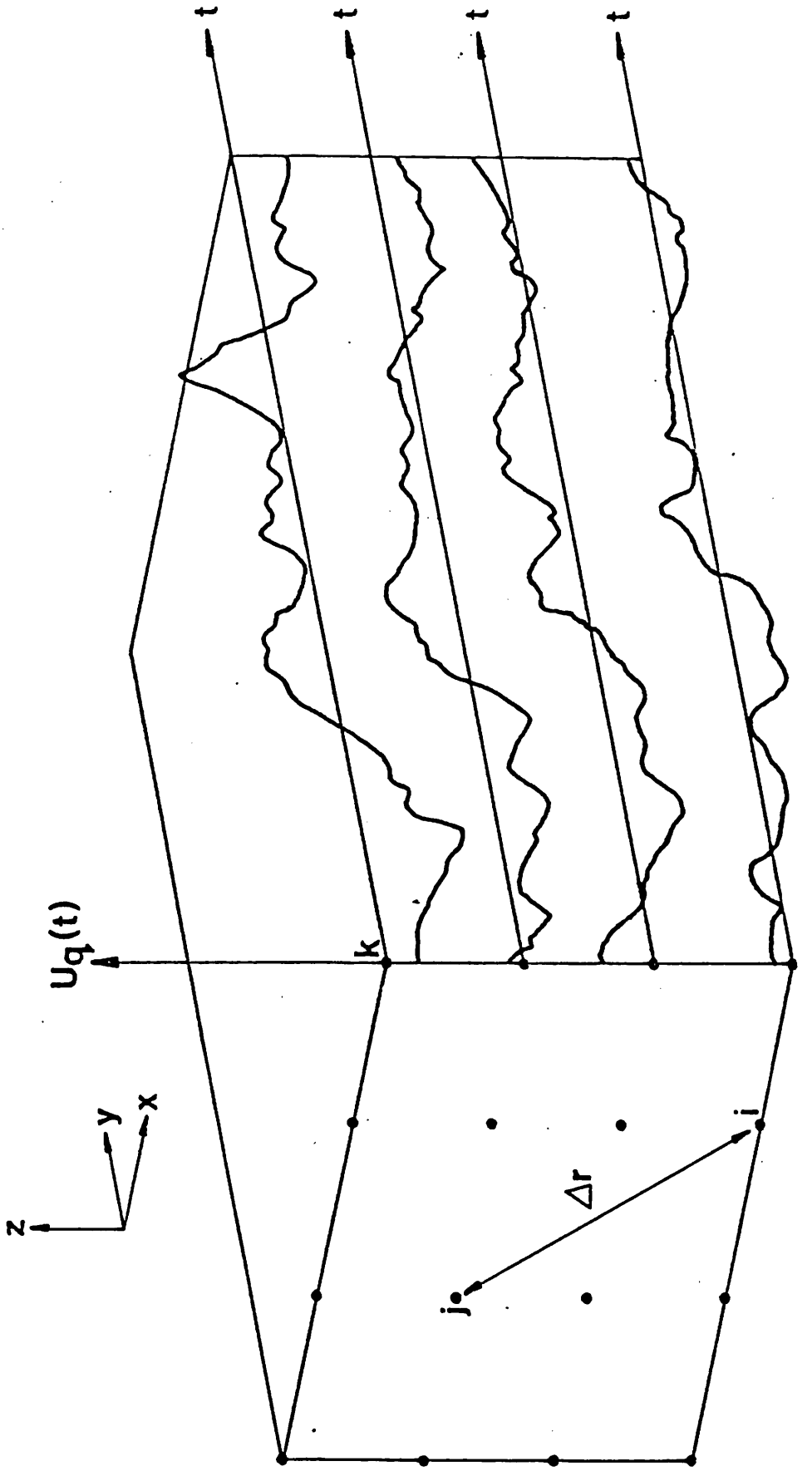


FIGURE 1 SCHEMATIC REPRESENTATION OF SPATIAL STRUCTURE

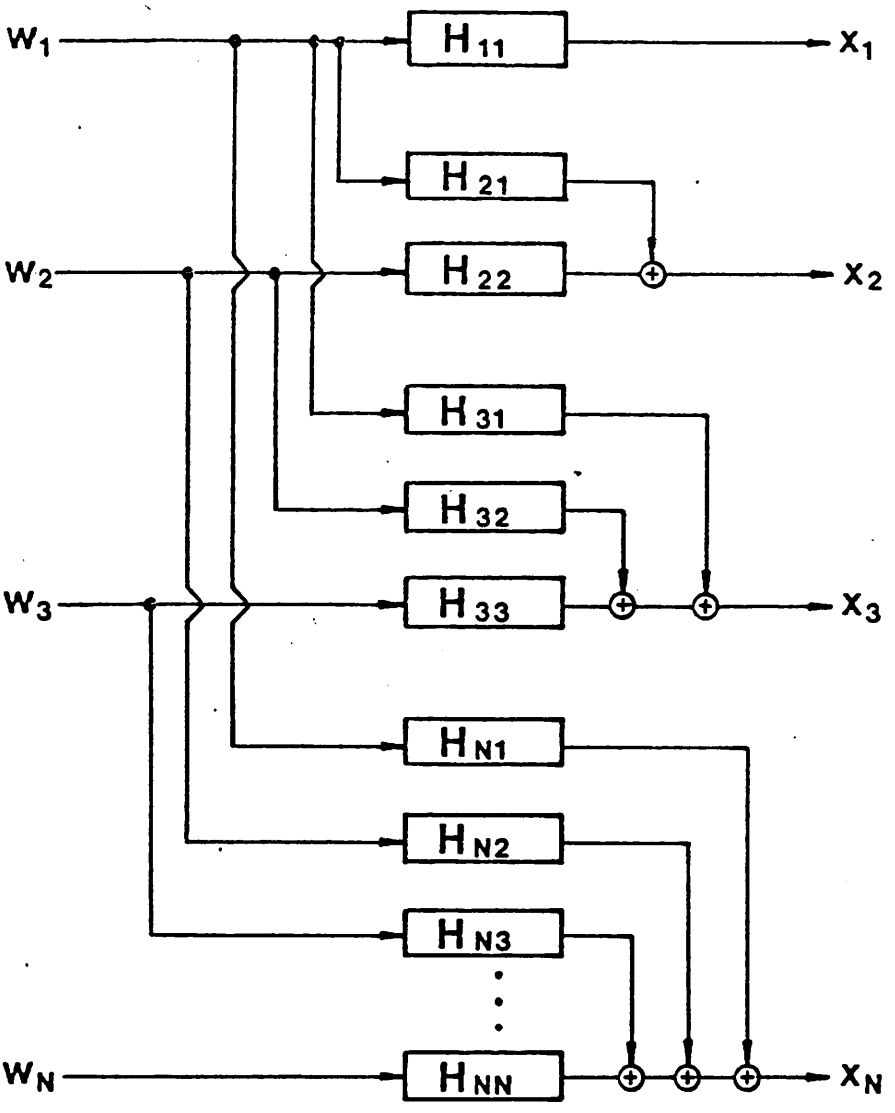


FIGURE 2 LINEAR FILTER REPRESENTATION OF SIMULATION MODEL.

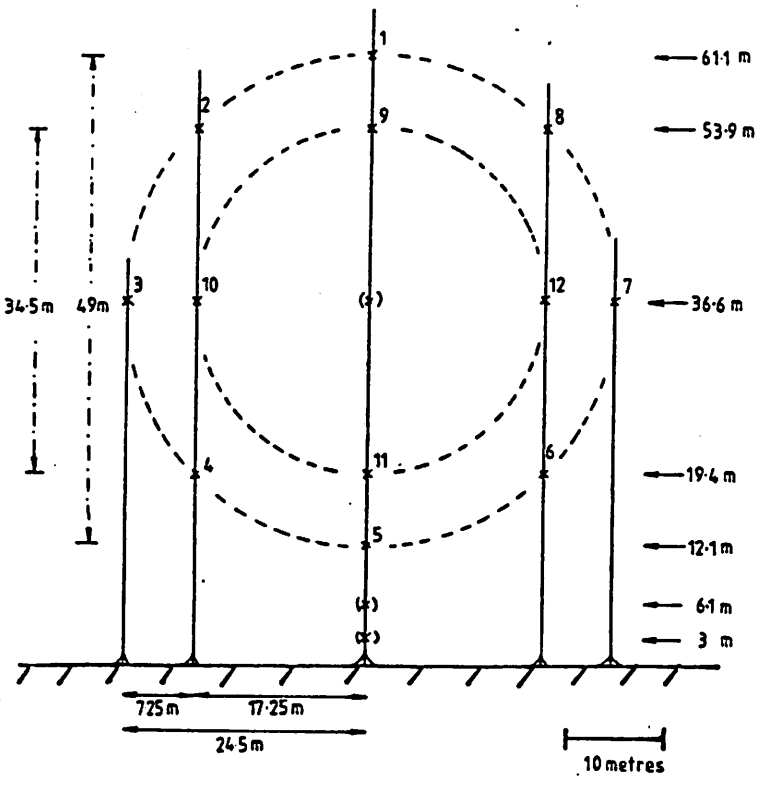


Fig. 3 Geometry of Battelle vertical plane array.

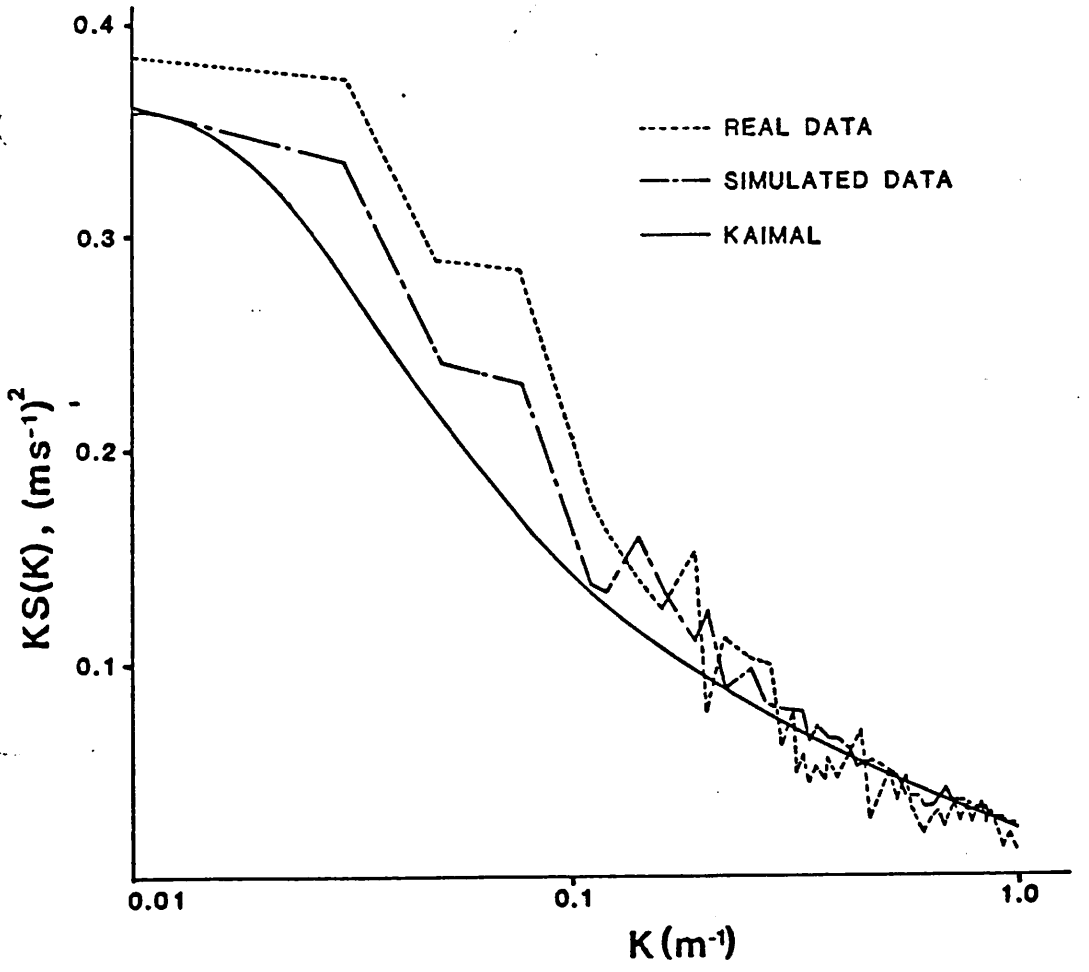


Fig. 4 A comparison of the real, simulated and theoretical estimates of the single point power spectra of the wind velocity fluctuations for anemometer position 1.

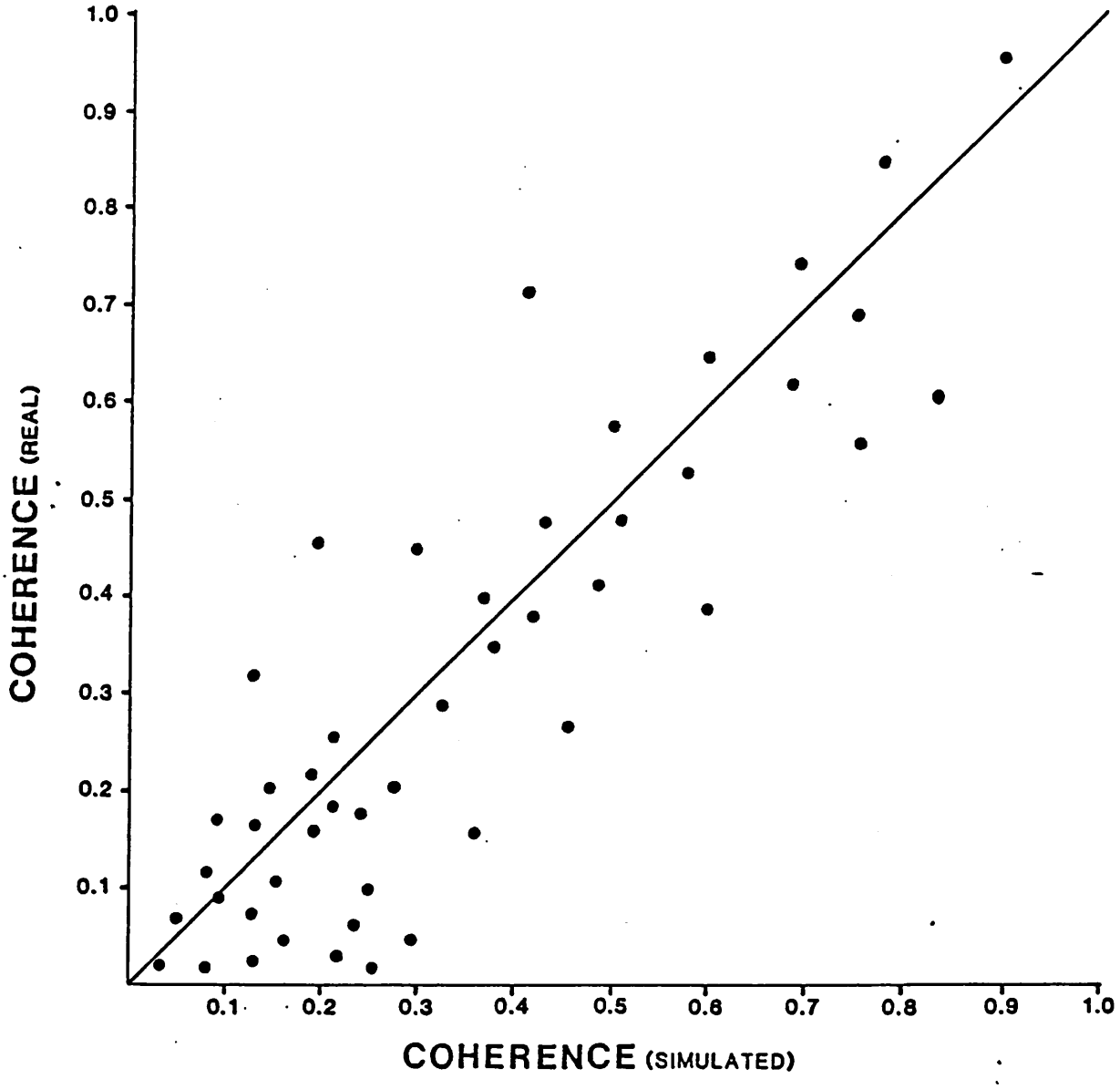


Fig. 5 A comparison of the coherence function estimtes of the real and simulated wind fields.

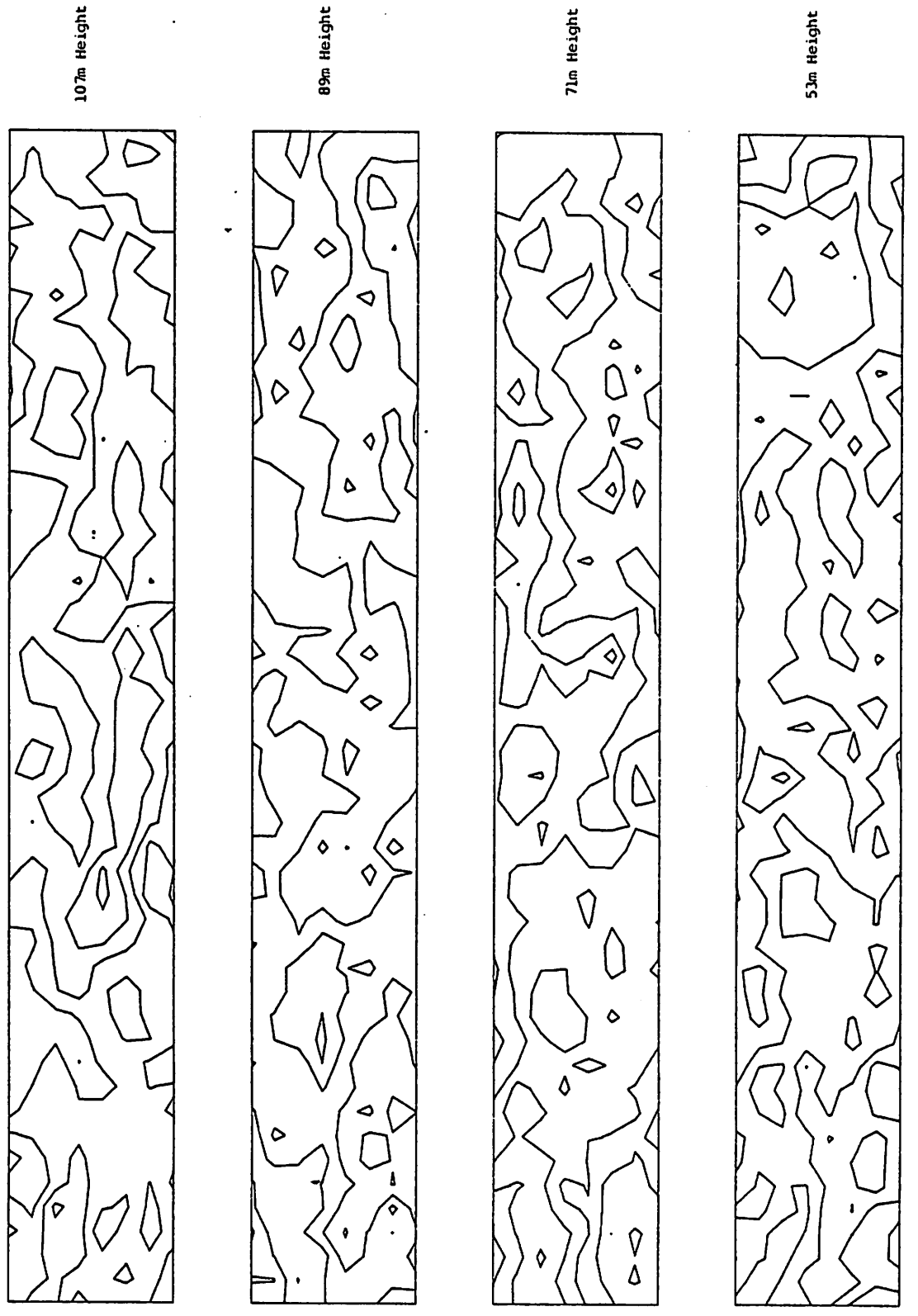


Fig. 6 Contours of the Longitudinal Component of Turbulence. Horizontal Slices 100m x 700m at Equally Spaced Height Intervals; Contours at 1 m/s Intervals.

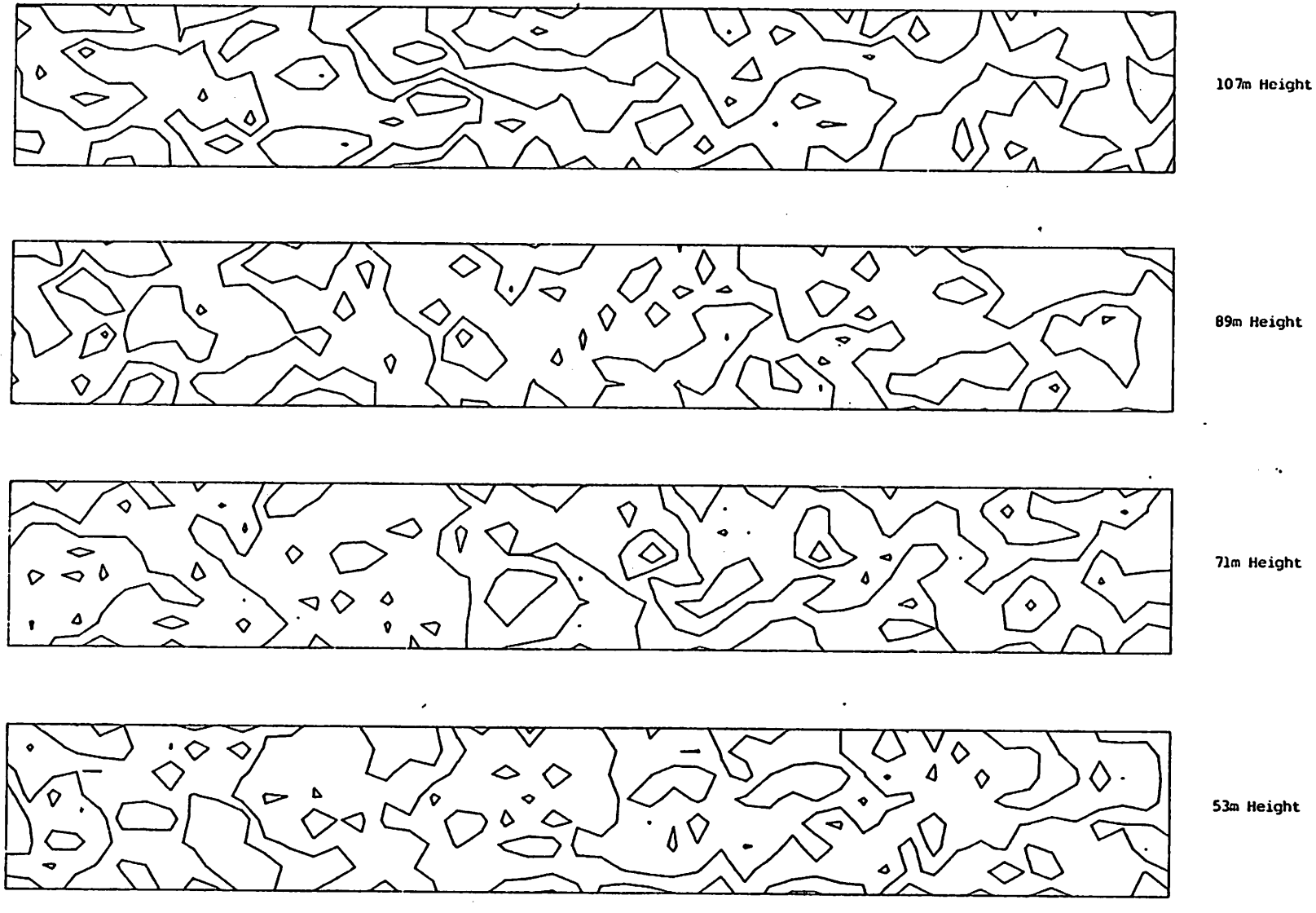


Fig. 7 Contours of the Lateral Component of Turbulence : Horizontal Slices 100m x 700m at Equally Spaced Height Intervals; Contours at 1 m/s Intervals

# WIND CHARACTERISTICS IN THE TURBINE WAKE.

Jan-Ake Dahlberg

Information about the wind characteristics in the turbine wake has been obtained by measurements in the fixed meteorological towers at the Swedish prototype sites WTS 3 at Maglarp and WTS 75/2 at Nasudden.

The towers are located approximately 3 turbine diameters from the turbines.

The towers are equipped with sensors according to:

| Sensor: | Number of levels: | Updated every: |
|---|---|---|
| Wind speed | 7 (x2) | 10 sec |
| Wind direction | 3 | 10 |
| Turbulence | 3 (x3,X,Y & Z) | .5 |
| Temperature | 7 | 10 |
| Humidity | 1 | 10 |
| Air press | 1 | 10 |
| Ice | 1 | 10 |

Figure 1 and 2 show the locations of the sensors.

All the signals from the meteorological tower are fed into the data aquisation system together with signals from the turbine.

Recordings are automaticly "triggered" when the wind direction is pointing to the tower or the wind direction is sweeping past the tower.

A number of such occasions were presented during the meeting by means of Video recorded sequences of animated wind profiles including turbulence level, wind direction and power output.

An example of the presentation is shown in figure 3.

Copies of the Video tape are avaliable at FFA.

Figure 1

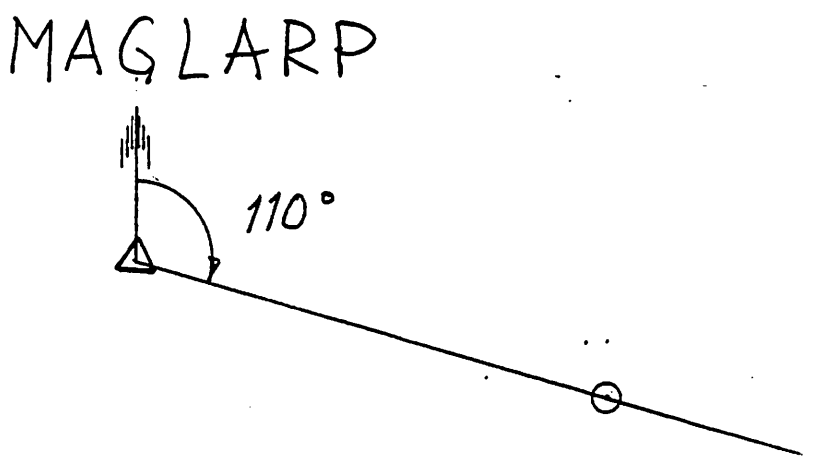


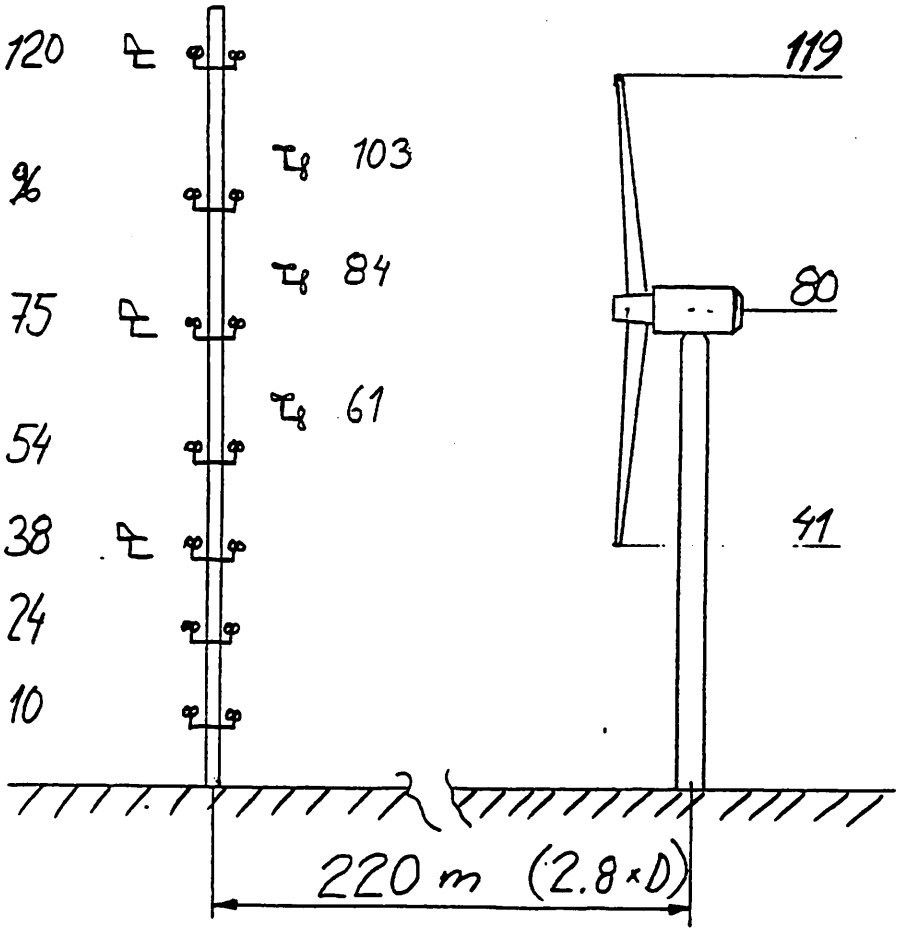

Figure 2

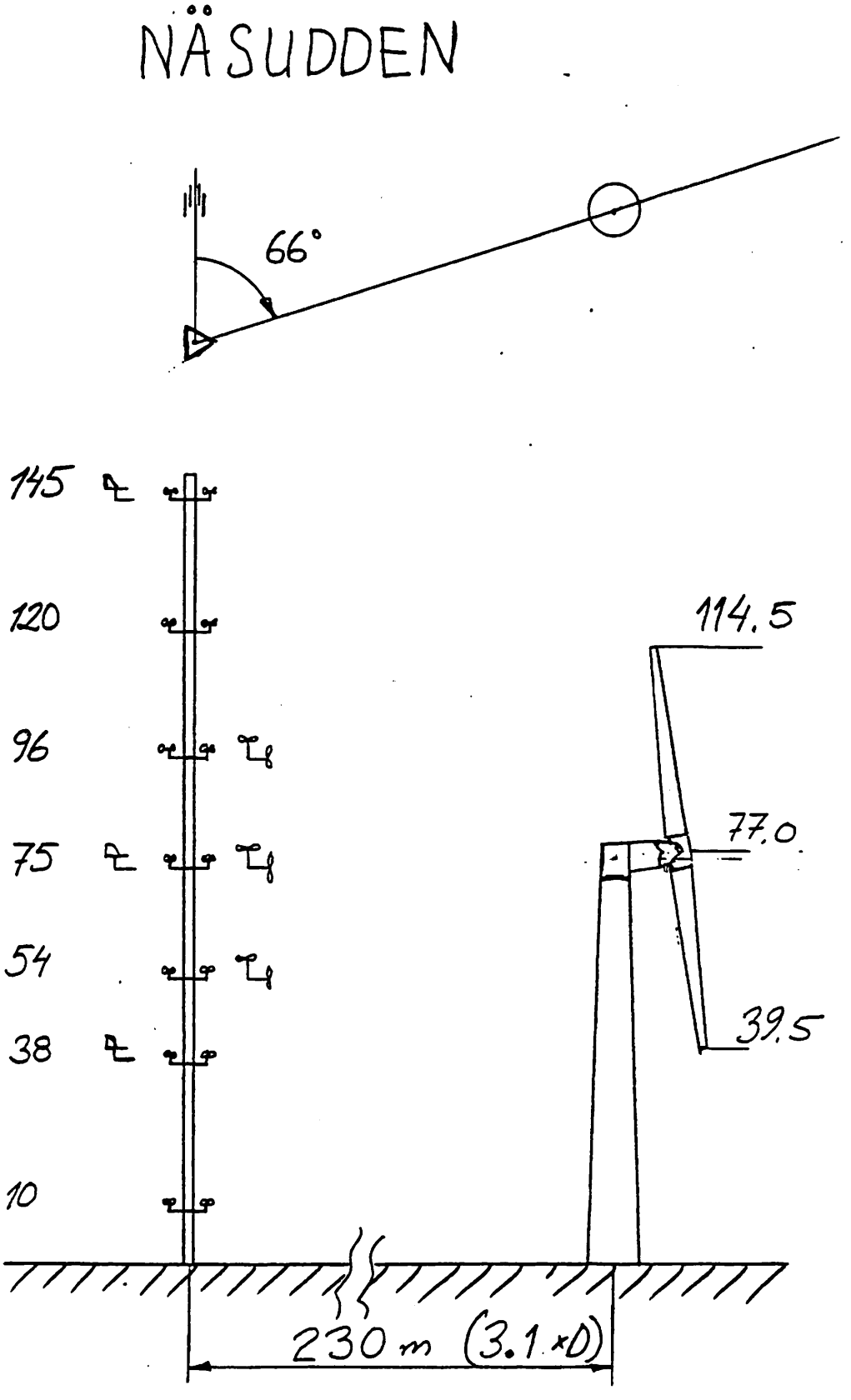

Figure 3

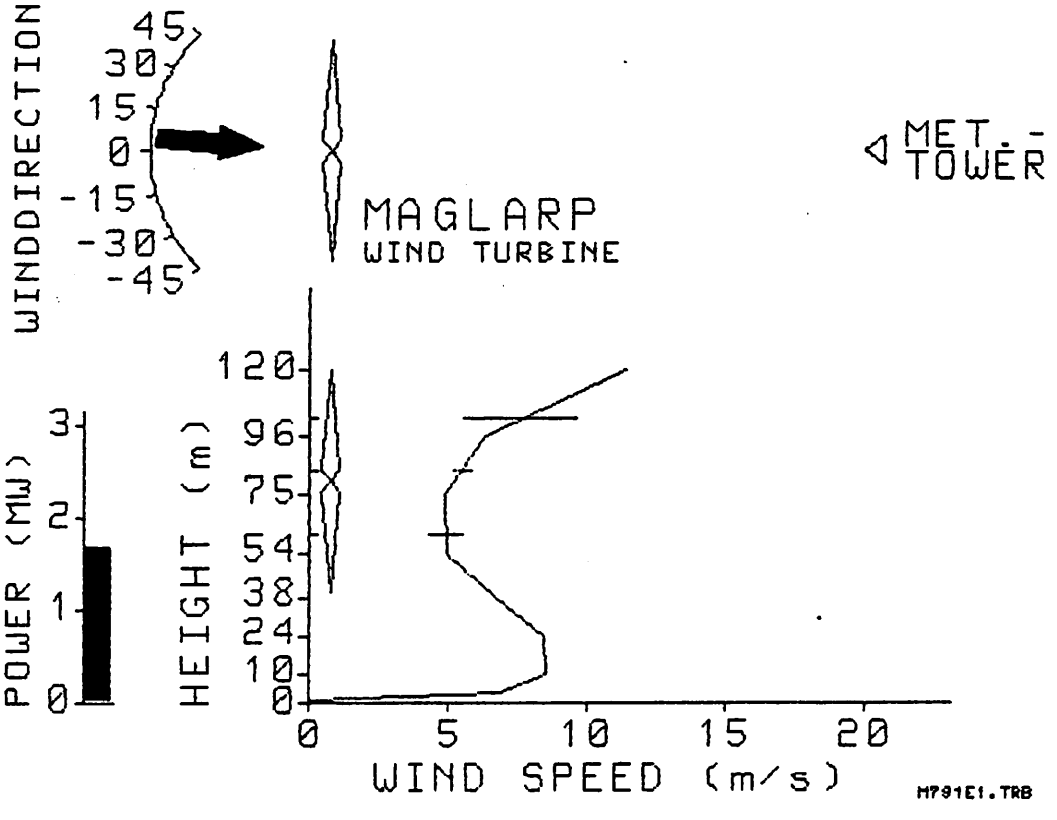
WINDDIRECTION
45
30
15
0
-15
-30
-45
MAGLARP
WIND TURBINE
MET.-
TOWER
POWER (MW)
3
2
1
0
HEIGHT (m)
120
96
75
54
38
24
10
0
0
5
10
15
20
WIND SPEED (m/s)
M791E1.TRB

# Wind Measurement and Evaluation Methods

J. P. Molly

Summary

Different wind measurement and data evaluation methods are explained briefly. These methods are applied or under consideration on the test site of the DFVLR. They are used to describe the spatial and transient behaviour of gusts and the correlation of wind and wind energy converter (WEC) load responses. Recording wind and load real time data with a sufficent time resolution needs large storage capacities, which normally not exist at the test sites. Therefore methods for on-line data reductions are necessary. Those which are applied by DFVLR are reported.

## General Problems

Experiences on the WEC test site of DFVLR showed the difficulty of recording high speed wind and WEC load data for sufficient long periods which are necessary for the statistical description of the typical wind and WEC response behaviour. Dependent on the quantity of data channels the storage capacity of common data recording systems are only sufficient for recording some minutes or hours of high speed data streams. The collected data therefore are limited to some spot checks and the chance to record extraordinary occurances are quite small. To increase the observed time, statistical

on-line reduction methods are necessary, but using them the transient gust behaviour will be lost. On the other hand a statistical data evaluation could simplify the correlation problem between measured wind speed and the time delayed response of the WEC which is dependent on wind direction and velocity.
To get good compromises between the needed on-line data reduction and the loss of information, DFVLR developed special data reduction technics and wind measuring systems.

Measurement of the Wind Speed

All systems which use a certain grouping of anemometers to measure the wind speed across the rotor disk area have the disadvantage of a strong influence on the correlation between wind measurement and WEC response if the both measuring sites are not aligned with the wind. To avoid this, DFVLR has a wind measurement system in preparation, which will be mounted on the rotor blade of a WEC transmiting the relative wind velocity along its rotational path of the rotor blade by a telemtry system.
Dependent on the applied reduction, spatial wind field informations can be gained by this measuring method for a longer time period under nearly always perpendicular flow conditions through the measuring plane. The equipment is designed for the use on the DEBRA-25 WEC which has a diameter of 25 m. With the pitch control system it is possible to operate the rotor under various rotation speeds and under zero load conditions with the advantage of very low influences on the flow field caused by the power extraction of the rotor. Under rated speed conditions and only one rotor blade equiped with wind sensores all 1.2 s a wind speed average for the measured rotor cross section can be built up. The measurement accuracy for the calculated incoming wind speed is about 0.5 m/s at low wind speeds. At higher wind speeds the resolution will become better.
Flow speed and direction relative to the chord direction of the blade will be registered with a maximum data sampling rate of 10 ms or every $3^{o}$ of rotor azimuth angle under rated rotor speed condition.
The sensor for the flow speed measurement is a Prandtl pipe which

is mounted in front of the leading edge of the rotor blade. Parallel to the speed sensor a wind vane is fixed to measure the incoming flow direction (Fig. 1). Both signals together with the rotor speed are used to calculate the actual flow perpendicular to the rotor plane.

Determination of the Transient Gust Behaviour

The knowledge of the time history of gusts is quite important for the load calculations of rotor blades and drive train. Wind speed accelerations and decelerations during gust conditions have a WEC dependent influence on the loads that means the load maximum depend on the reaction time of the pitch control and on the changing speed of the aerodynamic flow condition.

To find out the typical transient behaviour of wind gusts, DFVLR developed a wind data evaluation programme which classifies the gusts due to their speed difference between beginning and maximum speed of the gust. For the gusts collected in one class an average transient gust behaviour is calculated, which specifies the acceleration of the gust front, the duration of the maximum speed the deceleration at the gust back and the speed after the gust. The definition of what a gust is can be chosen by selecting accelerations or magnitudes.

All gusts of each class are counted as well as maximum values are registered. By this method typical gust shapes and frequencies for example for different weather conditions or/and different sites can be evaluated from raw data tapes. An on-line processing using this method is in preparation and can be applied in conjunction with the existing data acquisition system at the DFVLR testfield Schnittlingen. Fig. 2 shows an example of a data evaluation using this method.

Relation Method Between Wind Speed and Load Measurement

Significant difficulties exist in relating the wind speed with the load reaction of the WEC due to the time delay between wind speed measurement point and WEC.
To avoid the necessity of calculating the time delay with which the wind reaches the WEC it seems to be possible to register both with the same statistical reduction method and than compare the typical shape of the data pattern. Such a method of course also would include the possibility of an on-line data compression with the advantage of a long-term data acquisition.This increases the chance of measuring really extraordinaire and therefore design relevant gusts

The existing data processing system of DFVLR, which is in use at the test site already offers such statistical data reduction methods, which can be applied on-line or off-line. The simpliest method is the normal procedure of counting up the frequencies of wind speed and load bins (power, stresses, moments etc.). With the comparison of the load and wind speed pattern a certain relation can be found. The main disadvantage is the loss of all transient informations because the frequency distribution allows no longer any statements, if the wind speed laid down in a certain bin was taken during a constant, change or peak condition.
To solve that problem DFVLR installed a Markov-matrix as an on- or off-line data processing method by which again wind and load data can be evaluated. In the Markov-matrix transitions from one level to an other level are registered and laid down at the specified place. Transition from one wind speed to an other can occure with different accelerations which are lost in a normal Markov-matrix.
Therefore the wind speed transitions can be classified into up to five different acceleration classes. By this method it is possible to concentrate the data recording on the most significant transitions. Fig. 3 and 4 show such a data evaluation for the wind speed and for the corresponding power output of a WEC. In both graphs the diagonal values are suppressed because they do not represent load changes.

## Conclusion

The different methods presented in this report are an attempt to find measurement and evaluation methods which can be applied on the data on- or off-line. On-line data reductions enclose the possibility of long term data recordings, which have to be done in a way that the important transient information are not totally lost. The application of these methods on the test site of DFVLR will show their suitability. Dependent on the results, a combination of the three data collecting and measurement systems is planned.

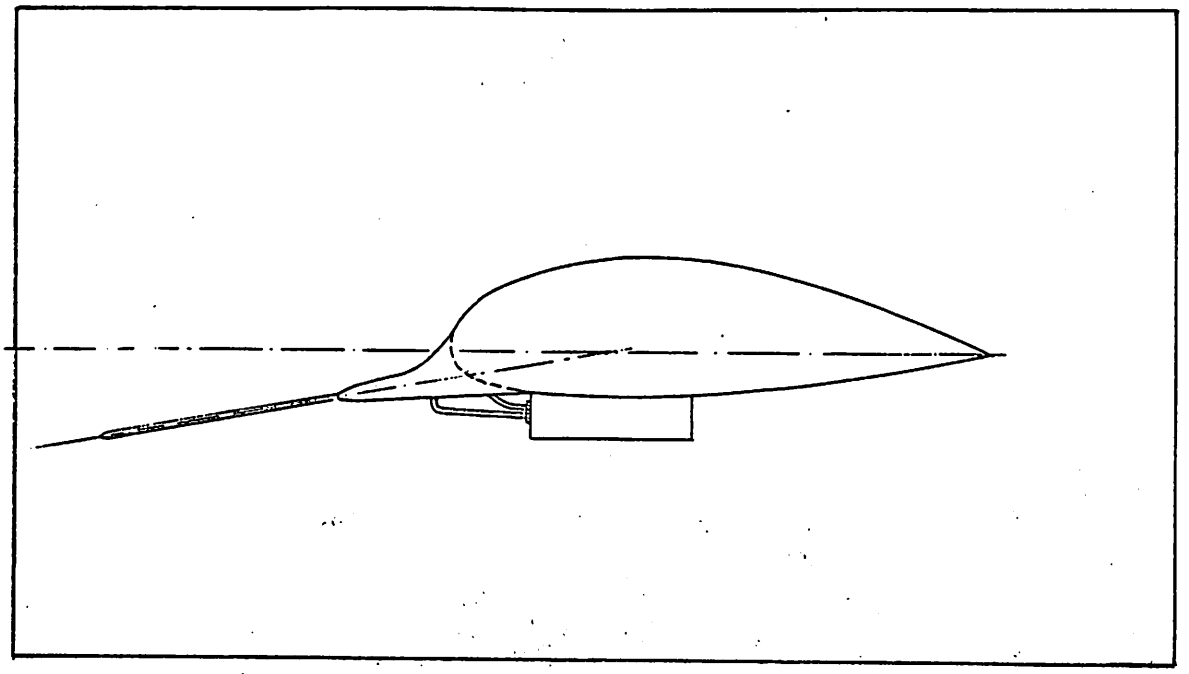

Fig. 1 Flow speed sensor for measurement at the rotor blade

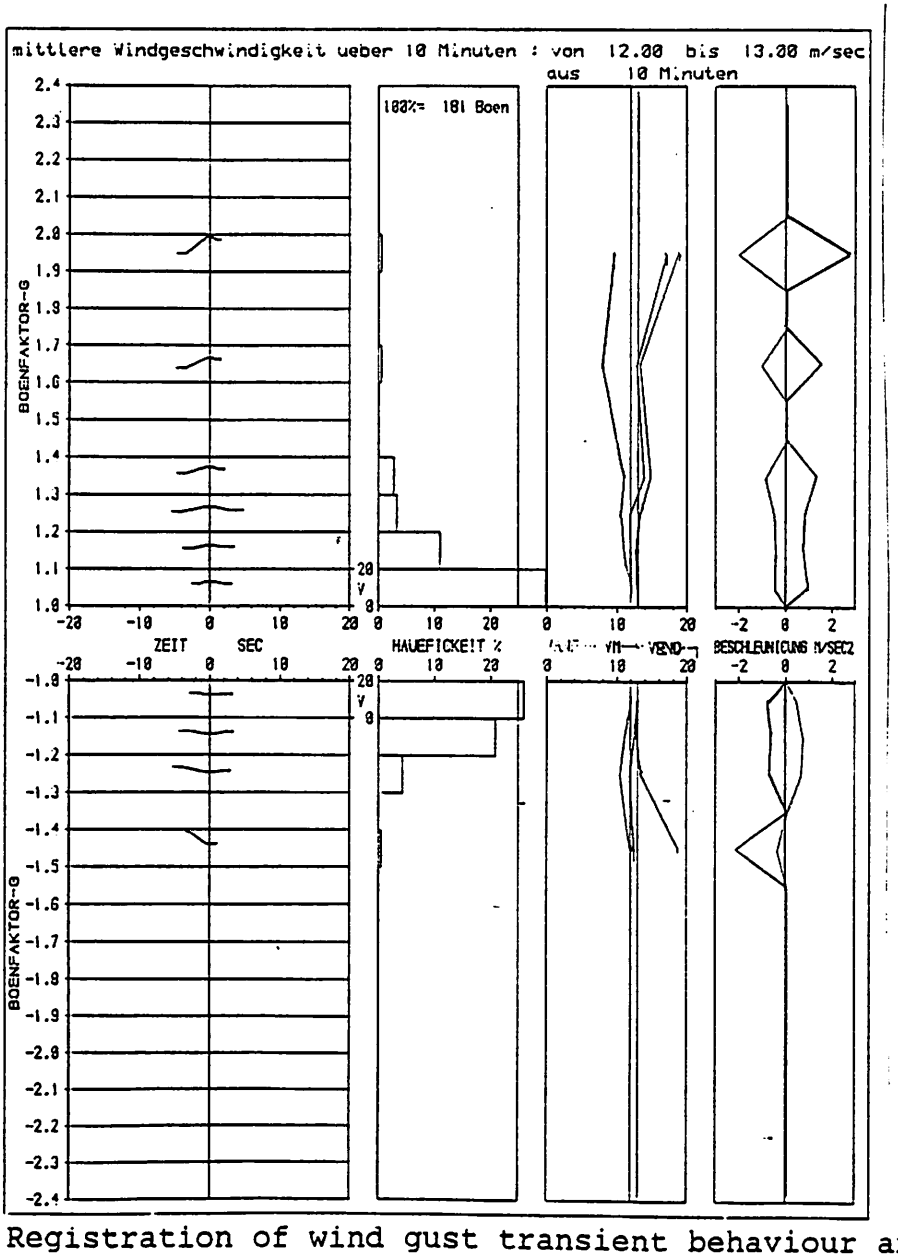


Fig. 2 Registration of wind gust transient behaviour and classification in magnitude classes

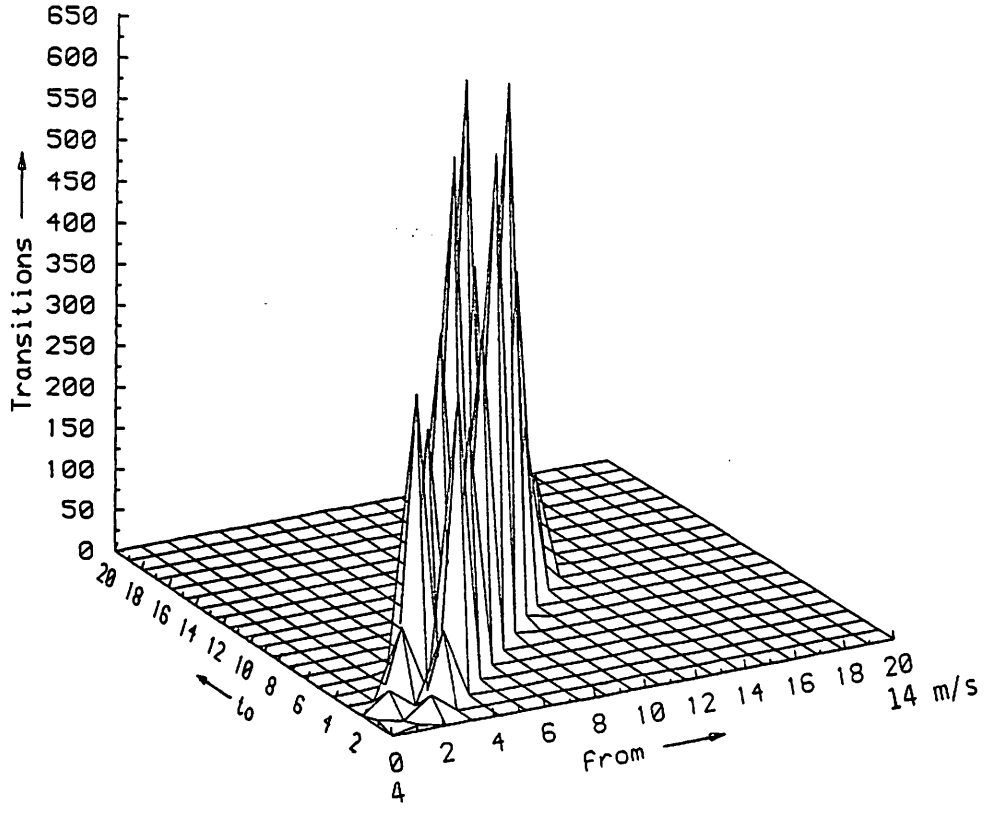


Fig. 3 Markov matrix applied on wind speed

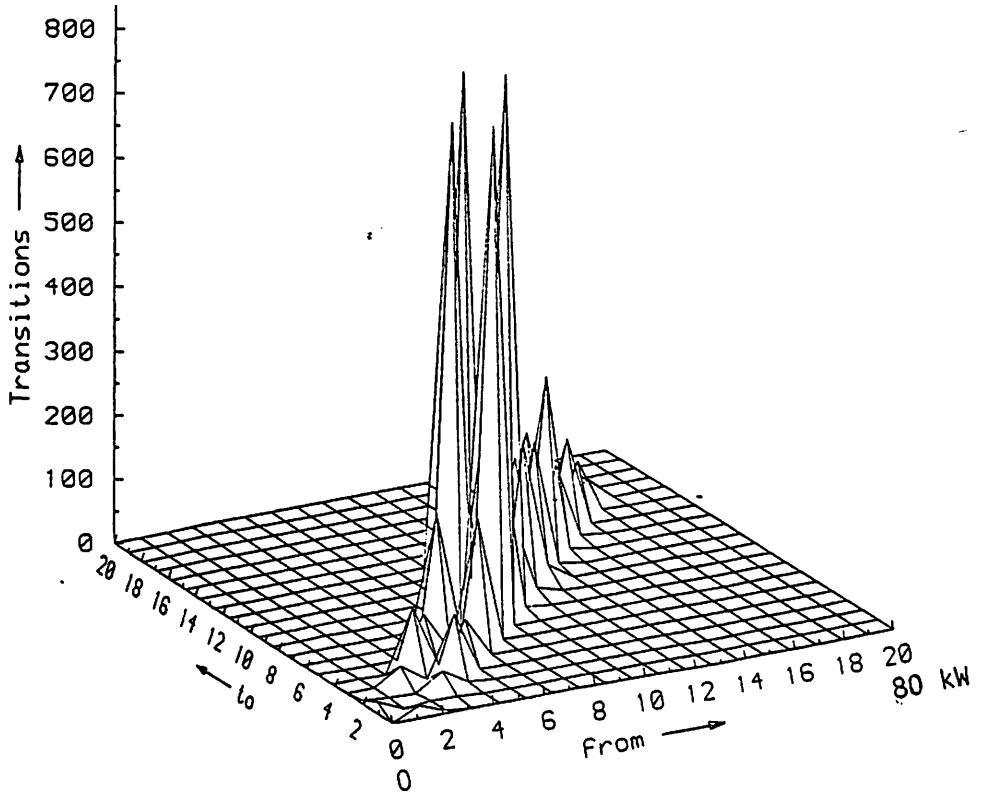


Fig. 4 Markov matrix applied on power output corresponding to the wind of Fig. 3.

Fig. 6 gives some typical gust structures. The steplike velocity change is preceeded by a slow velocity decrease respectively increase depending if the gust is positive or negative. The step is followed by a slow velocity change back to the mean value. The relative number of gusts is typically larger for positive gusts as is shown in Fig. 7. The gust amplitude, defined as the difference between the maximum and minimum value of the velocity step, can be normalized with the square root of the variance multiplied by the detection level factor, and becomes approximately constant, Fig. 8.

Figs. 9-10 shows results for wind components making an angle $\varphi$ relative to the mean wind direction. In Fig. 11 the relative gust amplitude has been plotted against $\varphi$. The amplitude ratio does not follow the cosine-function which one would expect if the gust front is plane. So this is an indication on that the gust front is curved.

Fig. 12 shows gust samples for different integration time intervals, 1.4-20.25 s. The data in this case have been sampled with 20 Hz frequency (recorded by MIUU with hot wire probe).

Fig. 13 shows gust samples for time interval 9 s. These data have been sampled with 1 Hz frequency (recorded by SMHI with Gill turbine anemometer). It is found that the most distinct gust structure is found for time interval 5 - 10 s indicating that this should be a characteristic time scale for gusts.

A continued work on gust structure studies should include a comparison of the gusts detected with conditional sampling with other gust models e.g. the velocity difference model. Also analysis of multipoint measurements ought to be made in order to get a better description of the spatial structure.

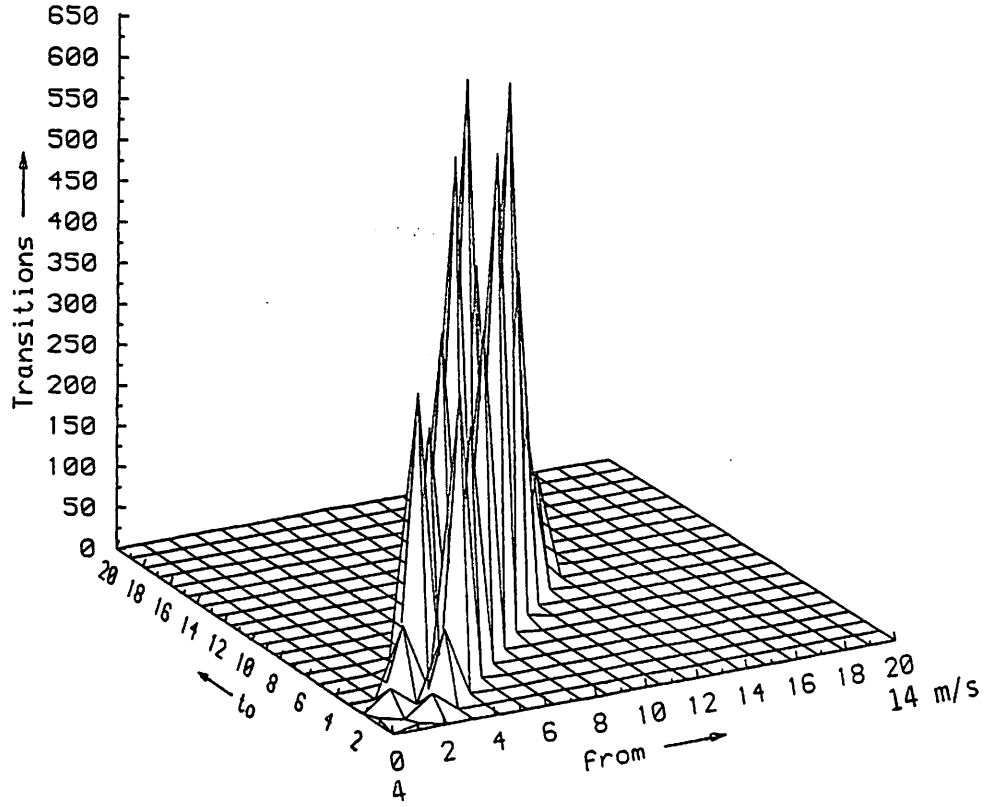


Fig. 3 Markov matrix applied on wind speed

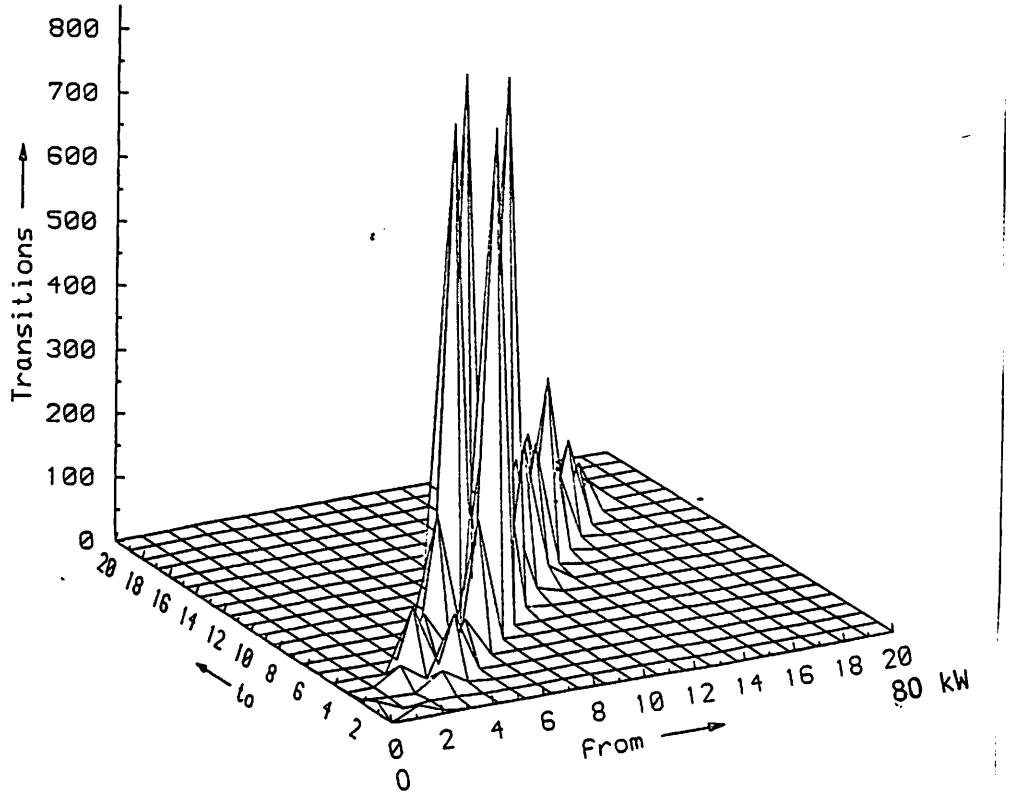


Fig. 4 Markov matrix applied on power output corresponding to the wind of Fig. 3.

# GUST STRUCTURE

Magnus Linde

An analysis has been made of wind turbulence measurements using conditional sampling technique. Wind data from the Swedish WECS test sites have been used. The data has been collected by MIUU, Uppsala University and SMHI, Norrköping.

The gust structure is defined as the time history of the wind velocity in one or several points in space, in a fixed or a rotating frame (Fig. 1). The present analysis is limited to fixed points in space.

Conditional sampling technique has earlier been used in turbulent boundary research in order to study characteristic events or "well-ordered structures" as the term has sometimes been. In the present work it is used as a tool to study characteristics of gusts. Some work has earlier been done by the author and some others (Fig. 2).

The VITA-technique (Variable-Interval-Time-Averaging) uses the short-time variance as a detection function for events with strong fluctuations (Fig.3). All detected events are collected in a sample and this sample function is presented in following figures. The events are separated in positive and negative ones using an additional criterion shown in Fig. 4. Fig. 5 shows an example of a sample where separation ahs not been made and then the negative respectively the positive events separated.

Fig. 6 gives some typical gust structures. The steplike velocity change is preceeded by a slow velocity decrease respectively increase depending if the gust is positive or negative. The step is followed by a slow velocity change back to the mean value. The relative number of gusts is typically larger for positive gusts as is shown in Fig. 7. The gust amplitude, defined as the difference between the maximum and minimum value of the velocity step, can be normalized with the square root of the variance multiplied by the detection level factor, and becomes approximately constant, Fig. 8.

Figs. 9-10 shows results for wind components making an angle $\varphi$ relative to the mean wind direction. In Fig. 11 the relative gust amplitude has been plotted against $\varphi$. The amplitude ratio does not follow the cosine-function which one would expect if the gust front is plane. So this is an indication on that the gust front is curved.

Fig. 12 shows gust samples for different integration time intervals, 1.4-20.25 s. The data in this case have been sampled with 20 Hz frequency (recorded by MIUU with hot wire probe).

Fig. 13 shows gust samples for time interval 9 s. These data have been sampled with 1 Hz frequency (recorded by SMHI with Gill turbine anemometer). It is found that the most distinct gust structure is found for time interval 5 - 10 s indicating that this should be a characteristic time scale for gusts.

A continued work on gust structure studies should include a comparison of the gusts detected with conditional sampling with other gust models e.g. the velocity difference model. Also analysis of multipoint measurements ought to be made in order to get a better description of the spatial structure.

## GUST STRUCTURE

THE TIME HISTORY OF WIND VELOCITY

- IN A FIXED POINT IN SPACE
- IN SEVERAL FIXED POINTS IN SPACE
- IN A ROTATING FRAME

IS IT IMPORTANT TO KNOW THE GUST STRUCTURE?

WHAT IS NEEDED - WHAT CAN BE USED?

FIG. 1.

HYPOTHESIS: "WELL-ORDERED" STRUCTURES EXIST IN THE ATMOSPHERIC SURFACE LAYER (CF. TURBULENT BOUNDARY LAYERS)

ANALYSIS USING CONDITIONAL SAMPLING TECHNIQUE
VITA (VARIABLE INTERVAL TIME AVERAGING)

| | |
|---|---|
| GUSTAVSSON H<br>LINDE M | THE GUST AS A COHERENT STRUCTURE IN THE TURBULENT BOUNDARY LAYER. 1979 |
| LINDE M | ANALYSIS OF GUST STRUCTURE IN THE ATMOSPHERIC BOUNDARY LAYER BY USING CONDITIONAL SAMPLING. 1981 |
| LINDE M | GUST STRUCTURE AND GUST STATISTICS... 1983 |
| ANTONIA RA ET AL | CONDITIONAL SAMPLING OF TURBULENCE IN THE ATMOSPHERIC SURFACE LAYER. 1983 |
| SCHOLS JLJ | THE DETECTION AND MEASUREMENT OF TURBULENT STRUCTURES IN THE ATMOSPHERIC SURFACE LAYER. 1984 |

FIG. 2.

# CONDITIONAL SAMPLING MODEL

VITA - TECHNIQUE

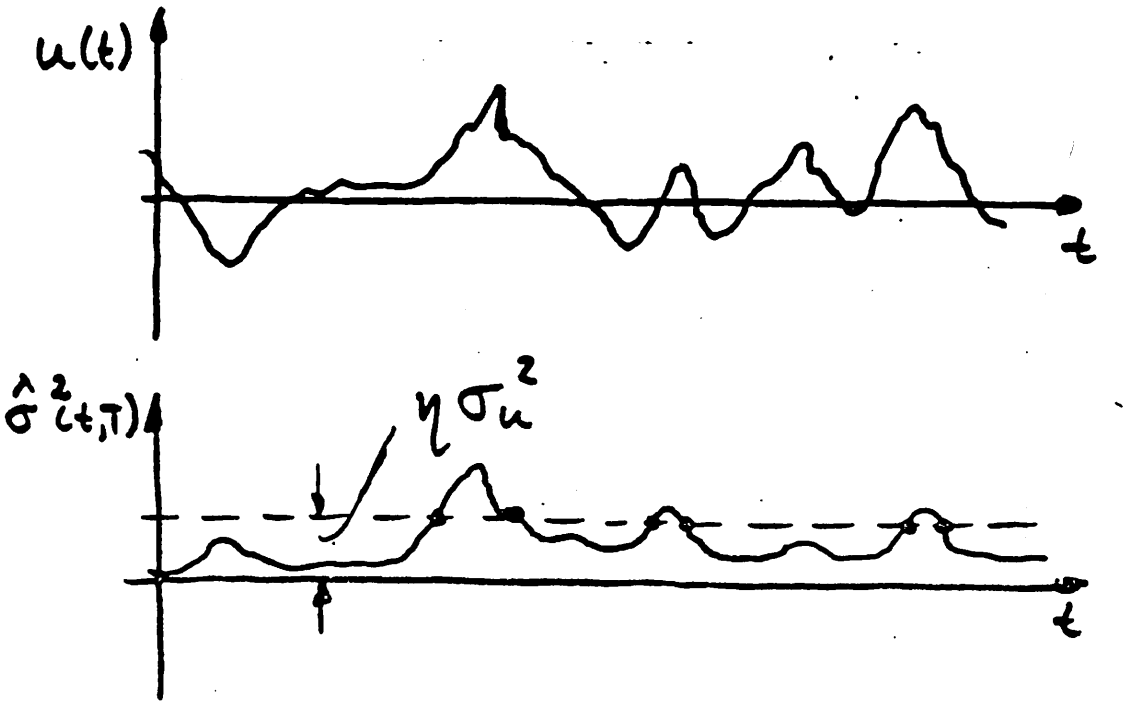


$$\hat{\sigma}^2(t,T) = \frac{1}{T}\int_{t-T/2}^{t+T/2} \left[ u(t) - \hat{u}(t,T) \right]^2 dt$$

$$\hat{u}(t,T) = \frac{1}{T}\int_{t-T/2}^{t+T/2} u(t)\, dt$$

FIG. 3.

ADDITIONAL CRITERION FOR THE SEPARATION OF "POSITIVE" AND "NEGATIVE" GUSTS

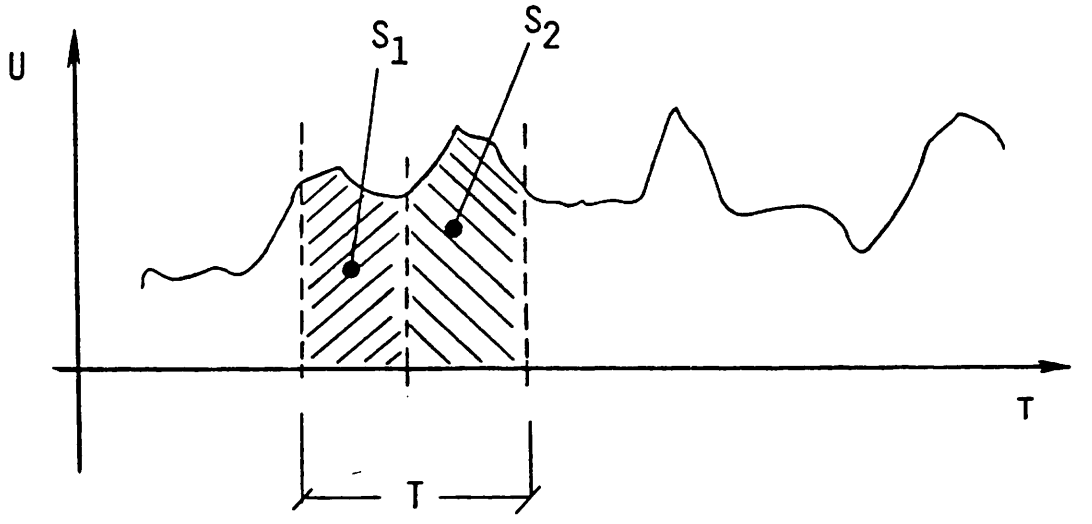


AREA $S_1$ < AREA $S_2$ ⇒ POSITIVE GUST

FIG. 4.

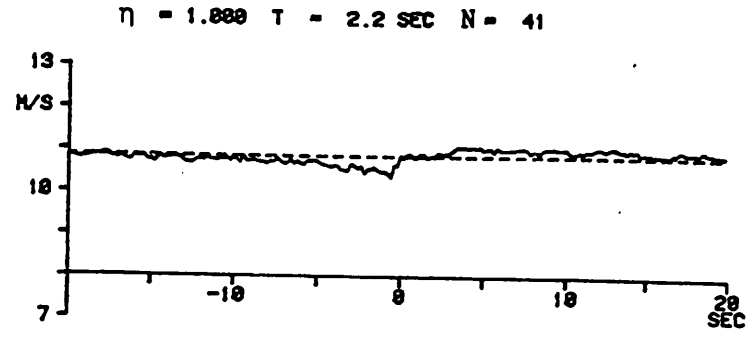


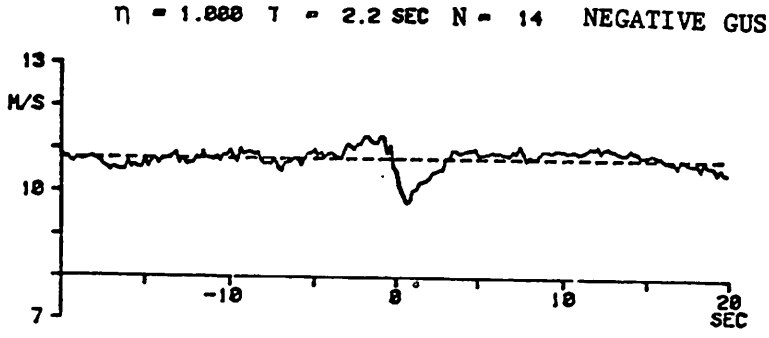


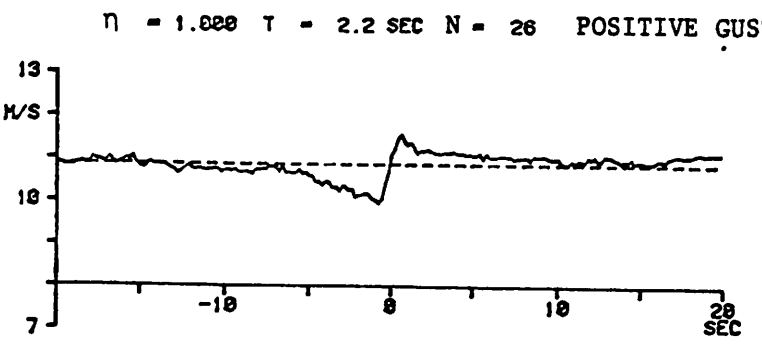


TURBN2, conditional averages. Positive and negative gusts separated.

FIG. 5.

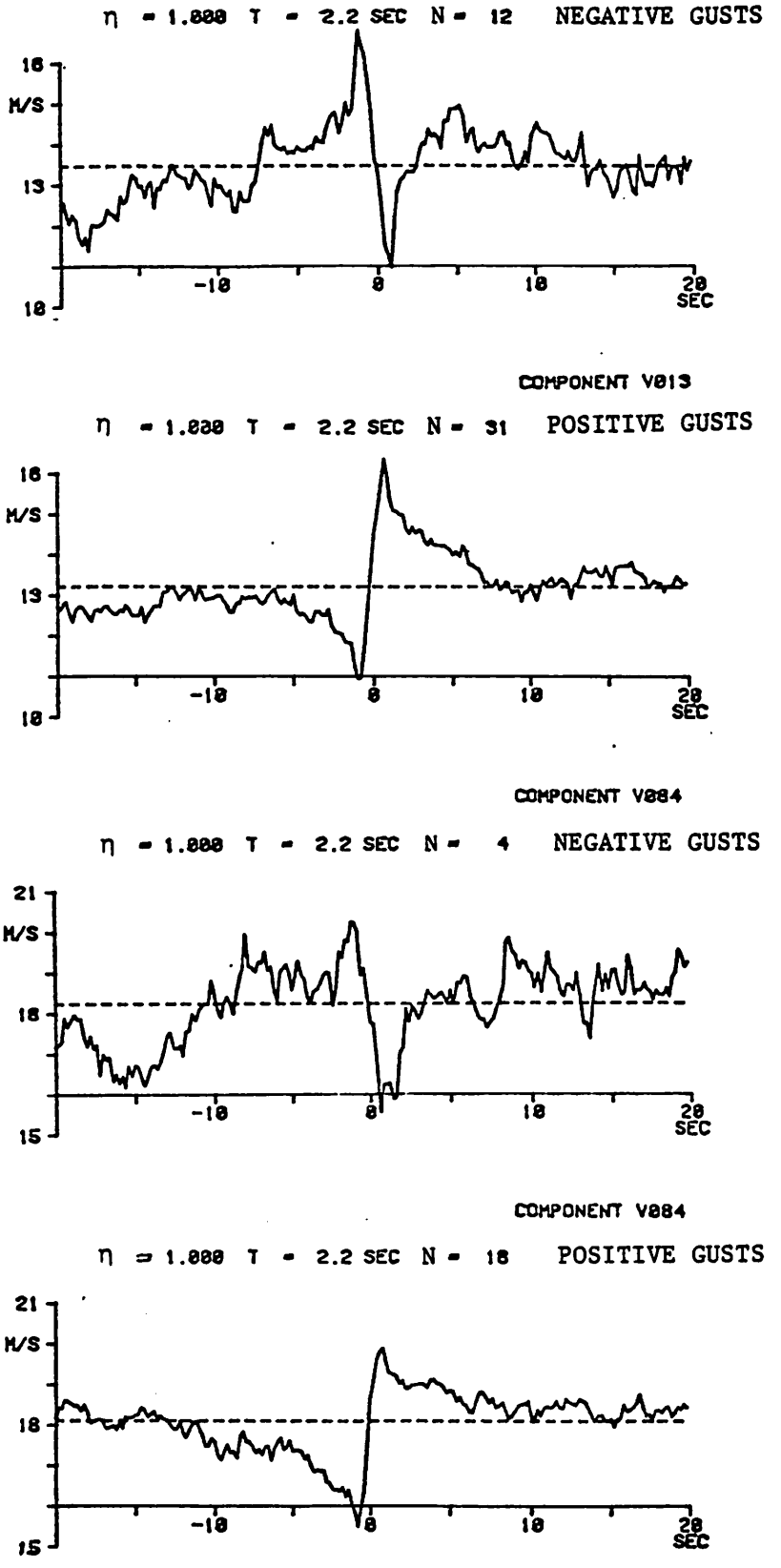


TAXUS, conditional averages. Positive and negative gusts separated.

FIG. 6.

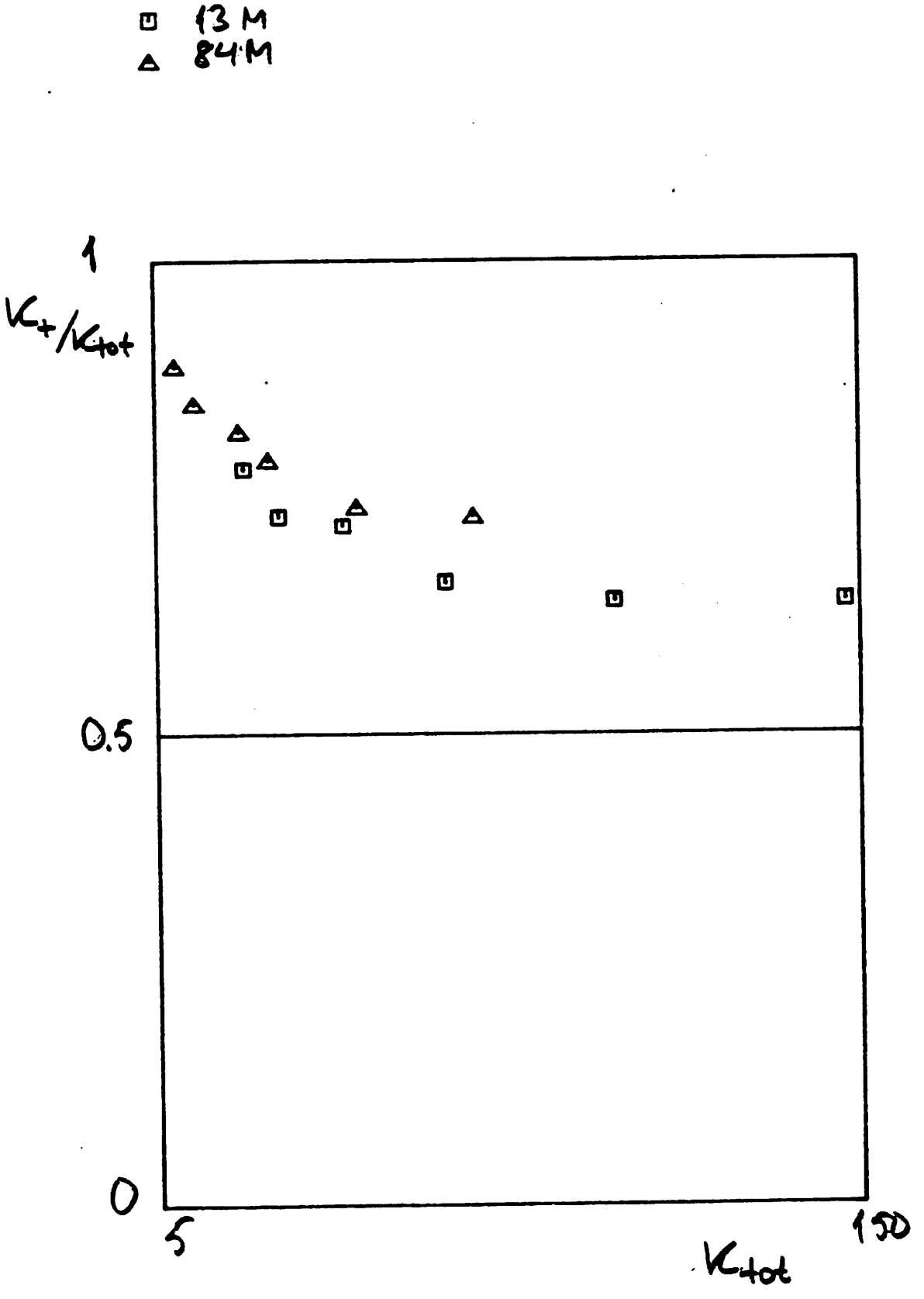


FIG. 7.

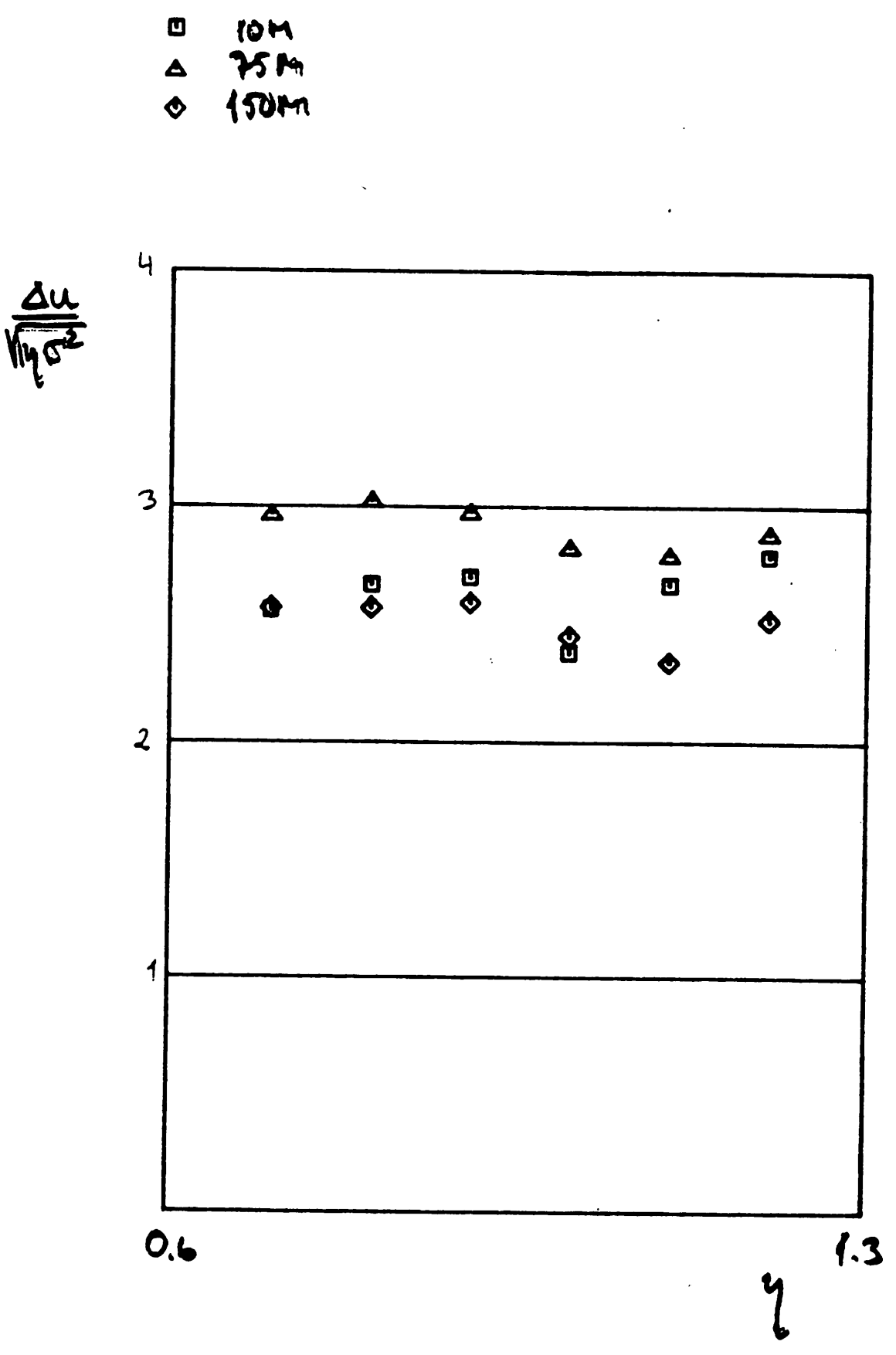


FIG. 8.

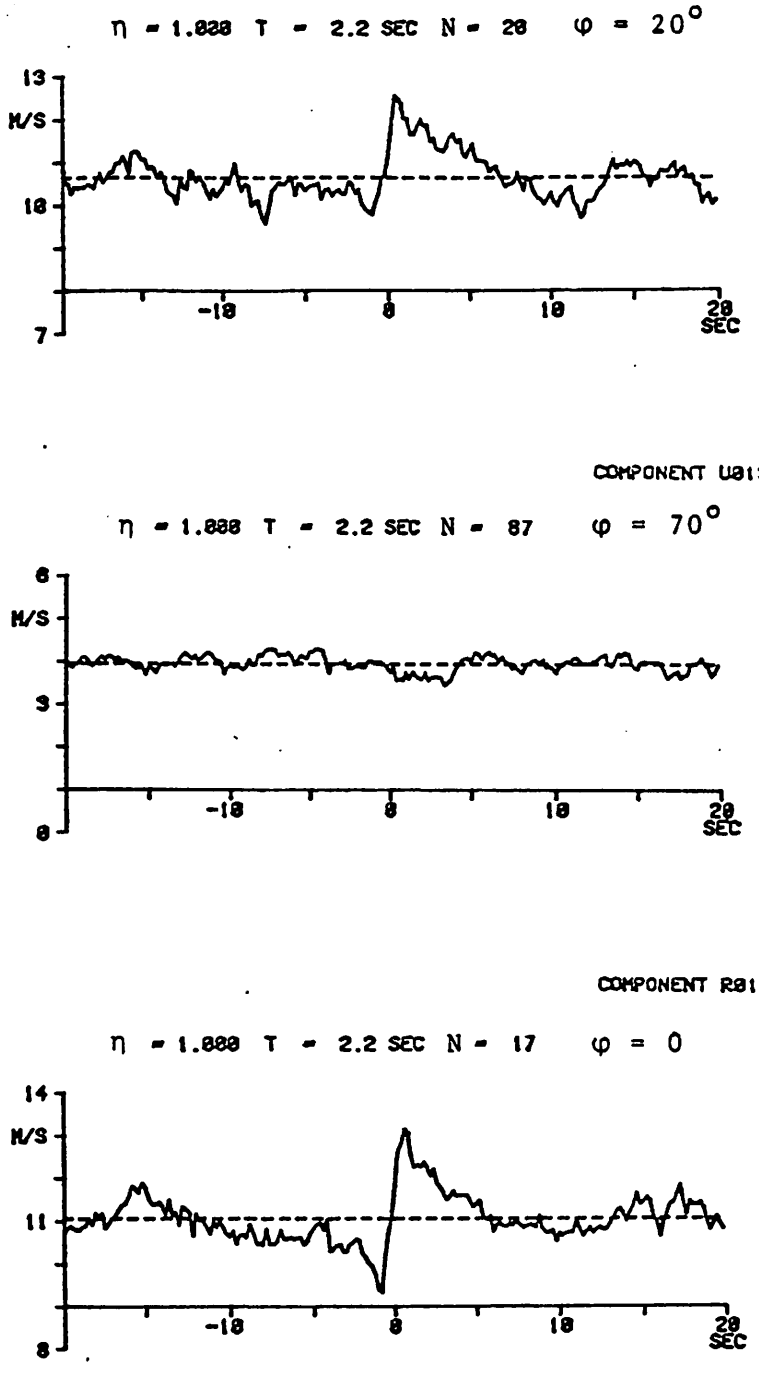


STRIX, conditional averages.

FIG. 9.

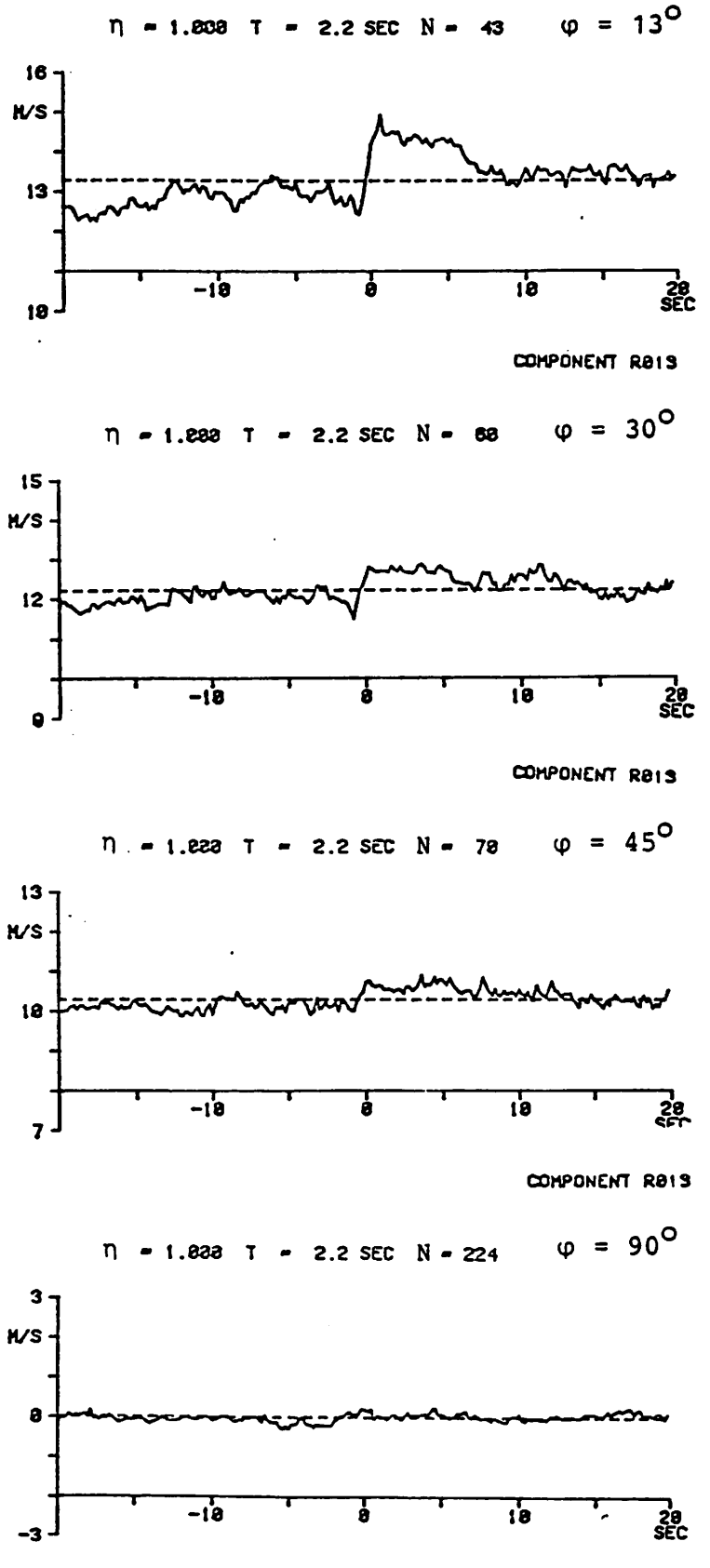


TAXUS, conditional averages.

FIG. 10.

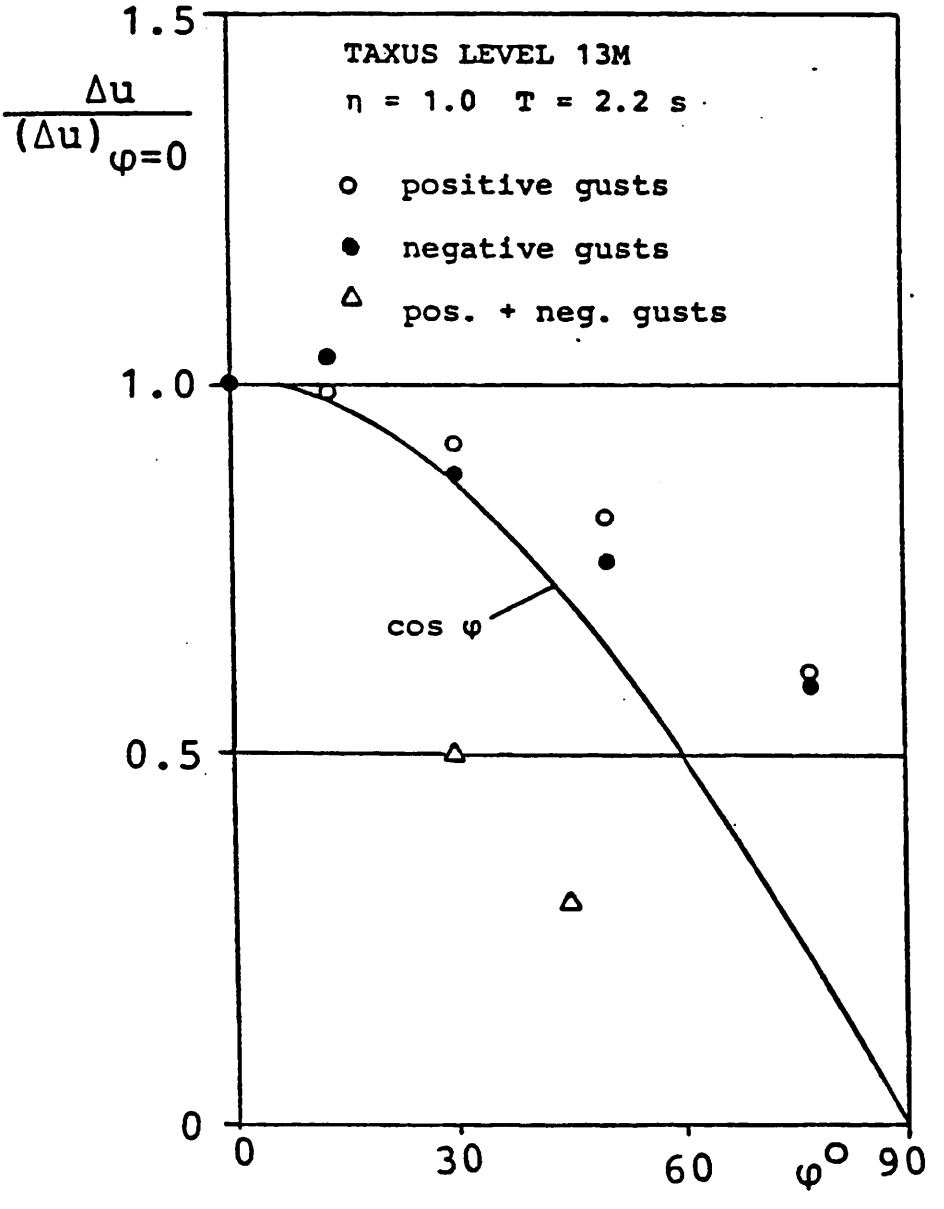


Gust amplitude variation.

φ = angle relative to mean wind direction.

FIG. 11.

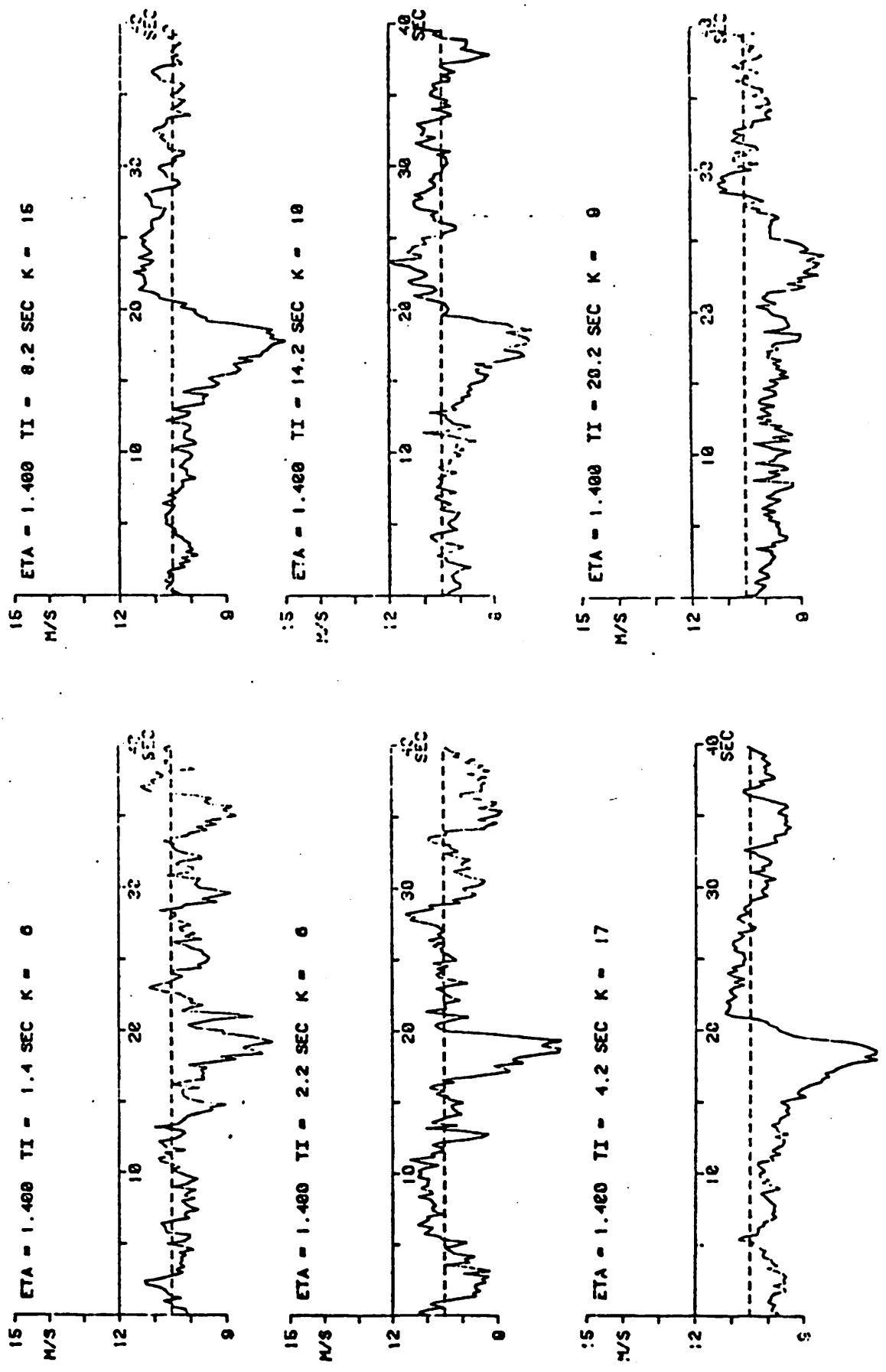


Fig. 2. Conditional average, longitudinal component, detected in longitudinal component. $\eta = 1.4$, TI = 1.4 - 20.2 s

FIG. 12.

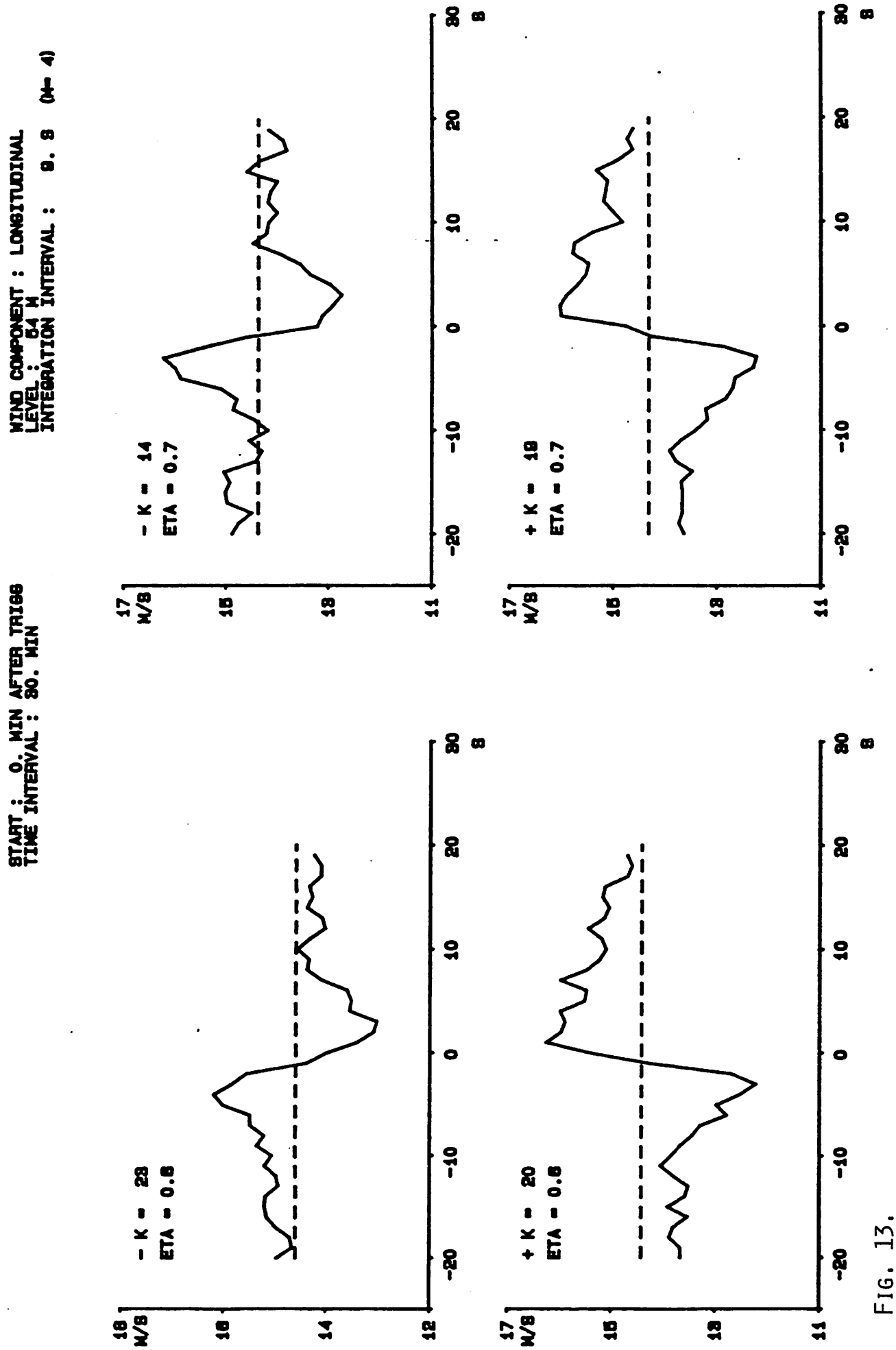
START : 0. MIN AFTER TRIGG
TIME INTERVAL : 30. MIN
WIND COMPONENT : LONGITUDINAL
LEVEL : 64 M
INTEGRATION INTERVAL : 0. 8 (N= 4)
- K = 28
ETA = 0.8
- K = 14
ETA = 0.7
+ K = 20
ETA = 0.8
+ K = 10
ETA = 0.7
M/S
S

FIG. 13.

## SUMMARY

- CHARACTERISTIC TIME - VELOCITY RELATION
- GUST AMPLITUDE RELATION
- DOMINANT TIME SCALE FOR GUSTS?
- INDICATIONS OF GUST SPACE STRUCTURE?

CONTINUED WORK:

- COMPARISON WITH OTHER GUST MODEL (VELOCITY DIFFERENCE)
- ANALYSIS OF MULTIPOINT MEASUREMENTS

FIG. 14.

## CONCLUDING DISCUSSION

The concluding discussion after the presentation of all papers was led by Jim Connell.

One major question that was raised reveral times during the sessions and also during the discussion was, "How well do we have to describe the wind?". Obviously this is not same questions as, "How well can we describe the wind?".

Those who work in the frequency domain when making load calculations seem to have the same, quite simple, turbulence modelling (Garrad). If one wants to find out if the turbulence description is satisfactory one has to verify what the effects of the turbulence are (Gustafsson). The paper presented by Ganander showed some results for how stochastic loads could be separated from the periodic ones. Ganander, however, remarked that the test campaigns have to be long enough so that the complete dynamics of the turbuelnce is included. Someone suggested that it could be interesting to compare the sum of a number of shorter campaigns with one long campaign.

Turbulence is of great importance for the fatigue of a wind turbine (Berg). A more detailed turbulence modelling then should be motivated (Smedman). The calculation of the fatigue life of a wind turbine however also includes several other important and difficult parts, e.g. load calculation and material fatigue data. Efforts to improve these parts of fatigue calculation of course are going on so, as Connell remarked, also work for the improvement of turbulence modelling should continue.

Dragt made a remark on the importance of the coherence function. Some calculations with different assumptions for the coherence were presented showing how much this effects the result. Further measurements in order to get a better knowledge of the coherence function was suggested.

Most load calculations seem to be made in the frequency domain. A linear system then is assumed. When working in the time domain the complete dynamics of the system is achieved as pointed out by Ganander. Discrete gust models should only be used for extreme events and not for fatigue calculations (Anderson).

It was remarked that the meeting almost entirely had been devoted to turbulence modelling for HAWT:s without much attention to VAWT:s which probably is even more difficult. Another remark was that wind turbines with variable speed, which look very promising, will need more sophisticated turbulence modelling. A third remark was that perhaps more attention should be paid to the turbulence modelling in wind farms. If a large scale utilization of wind power comes a more or less windfarm like configuration will have to be used. Then most wind turbines will not work in the undisturbed atmospheric surface layer, but in a turbulent flow field which is influenced by other wind turbines.

# RESEARCH ON TURBULENT WIND IN THE U.S. WIND ENERGY TECHNOLOGY PROGRAM

J. R. Connell

Work Supported by
the U.S. Department of Energy
under Contract DE-AC06-76RLO 1830

# RESEARCH ON TURBULENT WIND IN THE U.S. WIND ENERGY TECHNOLOGY PROGRAM

James R. Connell

## 1. INTRODUCTION

The typical procedure in the initial design of a wind turbine uses a modest description of the turbulent wind. However, redesign and analytical testing of turbine rotors, after the fluctuating forces of operating in the turbulent wind have been experienced, often place a high priority on accounting for the details of turbulence. Thus the part of the U.S. Department Of Energy (DOE) wind energy technology program dedicated to turbulent wind characterization has found a strong coupling with the primary DOE program elements of aerodynamics and mechanical design and testing of wind turbines. The responsibility for turbulence research and the characterization and modeling of turbulence experienced by wind turbines has been assigned to DOE's Pacific Northwest Laboratory (PNL)(Connell 1979). Inter-laboratory cooperative activities with Sandia National Laboratories (SNL)(Veers 1984) and the National Aeronautics and Space Administration (NASA)(Spera 1984), and more recently with the Solar Energy Research Institute (SERI) (Thresher and Holley 1981), have transformed some of the basic research done by PNL (Connell 1981, 1982) into interim models of turbulent wind specialized for their particular use of aerodynamics models.

This paper outlines the U.S. DOE wind energy technology program's past progress in turbulence wind research, current activity and future directions.

## 2. A BRIEF HISTORY OF U.S. DOE RESEARCH ON TURBULENCE AT WIND TURBINE ROTORS

Research in the United States on turbulence effects on wind turbines started with Eulerian descriptions, both theoretical and empirical, of the wind observed at single nonmoving points. Only slightly later, measurements with a circular array of anemometers placed in a crosswind vertical plane were made, to more completely describe the wind that would cross the disk space of a horizontal-axis wind turbine (Verholek 1978). This research developed

quickly into analysis of turbulence as it would be observed from a point rotating around a circle, matching the rotation of a wind turbine blade. The term "rotational sampling" was coined to describe the process of sequential observation from a point moving at constant speed in a circle in a rotating frame of reference. An empirical spectral model and the outline of an approach to a theoretical model of the rotationally sampled wind velocity were developed (Connell 1980, 1981, 1982).

In late 1979, at an International Energy Agency (IEA) meeting in Linköping, I presented the PNL model of the measured spectrum of rotationally sampled turbulence. I also brought a copy of the 1955 Ph.D. thesis in which Rosenbrock formulated a theoretical model of a rotationally sampled wind spectrum as a small part of a much larger work on wind turbine dynamics (Rosenbrock 1955). Figure 1 shows the spectral density function generated by Rosenbrock's theoretical model of the "free stream" axial wind speed fluctuations viewed from the rotational sampling frame of reference. It suggests that there would be more high-frequency fluctuations than are predicted by an Eulerian wind model. Returning to the United States by way of Risø I was delighted to find that the spectrum of measured blade root bending moment of the Gedser mill had the structure that I predicted for turbines from the new PNL model of the rotationally sampled wind (Lundsager, Christensen and Frandsen 1979).

A vertical plane array was erected by PNL in front of a 200-kW horizontal-axis wind turbine in order to develop the correlation between turbine response and the turbulent wind (Connell and George 1983; George and Connell 1984). At the same time, three separate approaches to modern theoretical modeling of the rotationally sampled turbulent wind were initiated to keep pace with the measurements (Connell 1981, 1982; Fichtl 1980; Thresher and Holley 1981). Figure 2 contains spectral density functions generated for three cases of the axial wind speed rotationally sampled from PNL's vertical plane array in front of the MOD-0A at Clayton, New Mexico (Connell and George 1983a). Figure 3 gives one example of the corresponding spectrum derived from the PNL theretical model. The similarity between measured and theoretical wind spectra is very strong. Figure 4 shows three cases of the spectral density function of the flatwise root bending

moment of the MOD-0A downwind of the vertical plane array in the top row and of power output in the bottom row (Connell and George 1983; George and Connell 1984). Its similarity to the wind spectrum is also very strong. Simple aerodynamic arguments lead to the conclusion that the rotational sampling model of wind advanced substantially our understanding of fluctuating aerodynamic forces on a wind turbine rotor. This piece of research established the validity of the rotationally sampled wind model of turbulence for wind turbine aerodynamics as a replacement for the Eulerian wind model.

## 3. RECENT ADVANCES IN TURBULENCE MEASUREMENT AND MODELING

Models and measurements of the rotationally sampled wind for the "free stream" do not provide the winds that actually force the rotor blade, because the rotor itself induces upwind flow distortion. Further, the wind information they provide does not correlate, instant by instant, with blade response because of the time required for wind to get from the "free stream" to the rotor and because of the transitory nature of the detailed flow in turbulence (Connell, George and Sandborn 1985). To help understand this phenomenon, some measurements of the turbulent wind velocity just ahead of the leading edge of rotor blades have been made with special anemometers (Sandborn and Connell 1984). The use of the turbulence measurements made with these hotfilm anemometers has resulted in the only successful computation of the bending moment fluctuations measured on the MOD-2 blades (Connell, George and Sandborn 1985; Miller 1984).

Figure 5 shows an example of the spectra of the axial wind speed measured with a hotfilm anemometer protruding from four locations on the leading edges of the MOD-2 wind turbine blades (Connell, George and Sandborn 1985). The wind was measured in the flow distortion region relative to a sensor that moved with the teetering, flapping blade at the 0.7 radius. This is the wind that the blade actually experienced, and it does not need to be corrected by a model of the flow distortion caused by the rotor. The similarities to and differences from the "free-stream" rotationally sampled wind are evident and raise some important questions about how closely the flow distortion for the steady aerodynamics of a rotor must be modeled. Research efforts to find out more about the changes in turbulence and mean wind velocity caused by flow distortion near the rotor have recently been begun by PNL.

In order to accurately compute the aerodynamic force on a rotor blade as a function of time, the wind velocity must be known at several radial locations. To find this information, the most practical method is to measure the turbulence simultaneously with several hotfilm anemometers placed at different radial locations on a rotating system. Figure 6 shows six pairs of time series of wind speed measured by two hotfilms on a rotating boom. Figure 7 shows the amplitude and phase spectra for one example of radial separation from the tip location on the boom. Up to a certain frequency, the spectral relationships are linear. These preliminary results are being used in the design of further measurement and theoretical research into the two-point, two-time analysis of rotationally sampled turbulent wind.

## 4. CURRENT ACTIVITIES

Mean wind and turbulence measurements have been initiated at PNL to study the effect of flow distortion caused by a rotor. The early phases of this research used a small wind turbine model in a large wind tunnel. Some preliminary measurements of the power coefficient of the model are shown along with the locations of wind measurements being made in Figures 8 and 9. No scaling is planned. We are using these results to guide our design of experiments for measurement of flow distortion in front of a larger turbine in the real atmosphere in later phases.

In addition to performing basic research, PNL is active in simplifying models of the rotationally sampled wind and providing time series of the spectrally modeled wind for use in design analyses. We are also evaluating and developing instruments for measurement of turbulent wind for wind turbine design and response purposes. Some of these models and instruments will be discussed below.

Figure 10 shows spectra of a simplified model time series graph of rotationally sampled wind speed for three wind cases in the free stream ahead of a MOD-0A wind turbine, derived from turbulence measurements taken from a single tower (Connell 1985; Connell and George 1983a,b). The data were transformed into a rotationally sampled wind speeds by a PNL method called the Single

Tower Rotationally Sampled model, type 2 (STRS-2). Use of the STRS-2 computer program can be learned readily, although knowledge of turbulence physics is helpful for setting the amount of artificial expansion used in stretching single-tower measurements to the crosswind plane in which a rotor turns. In the three cases where the single-tower model was compared to the corresponding 7-tower measurement of the rotationally sampled wind, the spectra were reasonably well modeled at frequencies of up to three times the rotation rate of the sampling (or the rotor). The accuracy degenerated to very poor beyond five times the rotor's rotation rate. Figure 11 contrasts STRS-2 wind time series from a single tower and from a laser anemometer both rotationally sampled corresponding to a large (MOD-2) turbine. Figure 12 shows the corresponding spectra. It would appear that, overall, the two methods give about the same result. However, to the experienced eye, the detailed structure looks more realistic for the laser measurements. No clear test of either method has been made on this scale of rotation.

A recent simulation of time series, derived from the PNL theoretical spectrum model of rotationally sampled wind, is shown in Figure 13. The simulated time series retains the spectrum of the theory from which it was derived, which is based upon the integral scale. Other statistical parameters of the time series would not be expected to match those of measured turbulence, except by chance. One example of a simplified model of this time series is shown in Figure 14. The time series is reduced to a set of five sine waves.

Turbulence at a coastal sand dune site has been measured in a pilot study using five levels of anemometry between 19 and 46 m AGL on a single meteorological tower. These results indicate very different distributions of mean wind speed and turbulence variance for different wind directions. Figure 15 shows several examples of the vertical profiles of these average variables. Excess wind speed in the middle heights of measurement is indicated for certain wind directions. The data can be rotationally analyzed for use in wind turbine response estimation using STRS-2.

One of our other tasks has been to assess the quality of wind velocity values and their time series measured in turbulence with kite anemometers and

with cup or hotfilm anemometers attached to tethered balloons. Theoretical results and corresponding measured results obtained during accuracy tests for the kite anemometer are shown in Figures 16 and 17. It appears that neither the kite nor the tethered balloon system is capable of accurately measuring turbulent wind velocity on the scales important for blade fluctuations. Interestingly, the kite anemometer sometimes produces a time series having a spectrum that looks somewhat like a rotationally sampled wind spectrum (Figure 17). Considering the kite's motion in turbulence, some type of moving sampling is expected, but it would not be sampling around a circle at a constant rotation rate and radius.

## 5. FUTURE ACTIVITIES IN THE U.S. DOE TURBULENCE AND WIND TURBINE RESPONSE PROGRAM OF RESEARCH

The U.S. DOE wind turbine research program is at a point where new initiatives are beginning at the field measurement stage and where a few of the older wind turbine research tests are winding down. New activities are beginning for the measurement of the turbulent wind with single meteorological towers at older sites like that of the MOD-2 in Washington State and the WTS-4 in Wyoming. The physical arrangement of anemometers at the WTS-4 site is shown in Figure 18. The anemometers are spaced uniformly across the height span of the disk at a distance of 1.7 rotor diameters upwind from the turbine. We cannot expect to correlate turbine rotor response on an instantaneous basis with the turbulence measured so far away, but we may hope to relate the measured spectrum of the rotor response to the spectrum of the rotational time series of the turbulence modeled from these measurements, using STRS-2. The measurement phase of the microscale turbulence research at the WTS-4 will be completed by the end of April 1986.

The primary tool for our research on the rotationally sampled turbulent wind has been a rotating boom apparatus at the PNL. The boom may be rotated in the horizontal-axis wind turbine (HAWT) or the vertical-axis wind turbine (VAWT) mode and carries a pair of three-dimensional hotfilm anemometers that may be placed at selected radial distances along the boom. This permits controlled studies of the phase and coherence of two-point, two-time turbulence

properties. We plan on further developing the methods of accurate turbulence measurement from rotating systems using the rotating boom. Figure 19 is a drawing of an originally planned version of the apparatus. The actual apparatus had a truss tower, a helicopter blade and other rudimentary features. We are now upgrading the apparatus substantially. Some of the results from the existing apparatus have already been discussed.

The measurement of turbulence from HAWTs is being extended to include three-dimensional turbulence measurements taken simultaneously at two points on a blade of the Howden turbine installed at San Gorgonio, California, where there is a good research test site in a good wind regime. This will provide turbulence information for a non-teetered rotor, intermediate size machine. Our previous results were for a teetered-rotor megawatt machine and for a small, flexible rotor of 8-m diameter.

Theoretical modeling will be extended to include two-point, two-time information corresponding to some of the most recent turbulence measures. This will likely close our theoretical efforts for a while, since it will be important to assess their accuracy and usefulness in aerodynamic computations for design and to verify them with new measurements before continuing to develop theories.

## 6. CLOSING REMARKS

Three areas of fundamental research on turbulent winds seem to merit future attention. The first is a fuller description of the size and shape of the coherent structures, or eddies, that make up the field of turbulent flow that interacts with turbine rotors. Coherence and spatial correlation analyses will be done in relation to theoretical modeling needs. Out of this research will come more information on phase relationships in the wind that are important in calculating the aerodynamic forces that rotate and bend the rotor.

The second area of fundamental research has to do with the unsteady, three-dimensional aerodynamic forces as they are influenced by the turbulent wind. For this research, it is expected that a combination of turbulence measurements

made with hotfilms, pressure measurements along the surface of the blade and advanced aerodynamic flow calculations will be integrated with measurements of the effects on and near the rotor.

The third area of research is measurement of the flow distortion effects a turning rotor has on the energy and the sizes and shapes of elements of turbulence approaching a rotor.

Much of the planned future research could be classified as refinement of present knowledge and might not be viewed as having basic value for turbine design. However, as turbines become more successful in their current, rugged forms, refinement may well be the name of the design game. We would prefer to be prepared with useful turbulence information for that time, some years away, when it will be called for. Such turbulence information will not otherwise appear rapidly when, say, five years from now, it may be needed.

## 7. POSTSCRIPT

It will come as no surprise, at this technical meeting with a strong international flavor, that I hope that we in the United States will be able to keep informed of the advancements in research on the turbulent wind, steady and unsteady aerodynamics, aeroelastics and mechanics and the testing of the response of turbines that will clearly all be part of the international research now going on. I look forward to a lively continuing exchange of results and ideas.

## Acknowledgment

This work was supported by the U.S. Department of Energy under Contract DE-AC06-76RLO 1830. The Pacific Northwest Laboratory is operated for the U.S. Department of Energy by Battelle Memorial Institute.

REFERENCES CITED

Connell, J. R. 1979. "Overview of Wind Characteristics for Design and Performance." In Proceedings of the Conference and Workshop on Wind Energy Characteristics and Wind Energy Siting, pp. 5-12. American Meteorological Society, Boston, Massachusetts.

Connell, J. R. 1980. Turbulence Spectrum Observed by a Fast-Rotating Wind Turbine Blade. Report PNL-3426, Pacific Northwest Laboratory, Richland, Washington.

Connell, J. R. 1981. The Spectrum of Wind Speed Fluctuations Encountered by a Rotating Blade of a Wind Energy Conversion System: Observations and Theory. Report PNL-4083, Pacific Northwest Laboratory, Richland, Washington.

Connell, J. R. 1982. "The Spectrum of Wind Speed Fluctuations Encountered by a Rotating Blade of a Wind Energy Conversion System." Solar Energy 29:363-375.

Connell, J. R. 1985. "A Primer of Turbulence at the Wind Turbine Rotor." Paper presented at the Windpower '85 Conference, September 1985, San Francisco, California.

Connell, J. R., and R. L. George. 1983a. "A New Look at Turbulence Experienced by a Rotating Wind Turbine." In Proceedings of the Second ASME Wind Energy Symposium, pp. 455-479. American Society of Mechanical Engineers, New York, New York.

Connell, J. R., and R. L. George. 1983b. "Scaling Wind Characteristics for Designing Small and Large Wind Turbines". In Proceedings of the Sixth Biennial Wind Energy Conference and Workshop, pp. 513-524. American Solar Energy Society, Boulder, Colorado.

Connell, J. R., R. L. George, and V. A. Sandborn. 1985. Rotationally Sampled Wind and MOD-2 Wind Turbine Response. EPRI Research Project Report RP 1996-12, Electric Power Research Institute, Palo Alto, California.

Fictl, G. H. 1980. Covariance Statistics of Turbulence Velocity Components for Wind Energy Conversion System Design--Homogeneous, Isotropic Case. Report PNL-3499, Pacific Northwest Laboratory, Richland, Washington.

George, R. L., and J. R. Connell. 1984. Rotationally Sampled Wind Characteristics and Correlations with MOD-OA Wind Turbine Response. Report PNL-5238, Pacific Northwest Laboratory, Richland, Washington.

Lundsager, P., C. J. Christensen, and S. Frandsen. 1979. Interim Report on the Measurements on the Gedser Wind Mill. Risø National Laboratory Report to NASA/Lewis Research Center, Cleveland, Ohio.

Miller, R. D. 1984. Theoretical Structural Dynamic Loads Prediction with Rotationally Sampled Wind. EPRI Research Project, RP-1996-6, vol. 3, Electric Power Research Institute, Palo Alto, California.

Rosenbrock, H. H. 1955. Vibration and Stability Problems in Large Wind Turbines Having Hinged Blades. Report C/T 113, ERA, Surrey, England.

Sandborn, V. A., and J. R. Connell. 1984. Measurement of Turbulent Wind Velocities Using a Rotating Boom Apparatus. Report PNL-4888, Pacific Northwest Laboratory, Richland, Washington.

Spera, D. A. 1984. "Application of Rotationally Sampled Turbulence Data to Rotor Analysis." Paper presented at the DOE/NASA Horizontal-Axis Wind Turbine Technology Workshop, May 1984, Cleveland, Ohio.

Thresher, R. W., and W. E. Holley. 1981. The Response Sensitivity of Wind Turbines to Atmospheric Turbulence. Report DOE/ET/23144-81, National Technical Information Service, Springfield, Virginia.

Veers, M. G. 1984. Modeling Stochastic Wind Loads on Vertical-Axis Wind Turbines. Sandia Report SAND 83-1909, Sandia National Laboratory, Albuquerque, New Mexico.

Verholek, M. G. 1978. Preliminary Result of a Field Experiment to Characterize Wind Flow Through a Vertical Plane. Report PNL-2518, Pacific Northwest Laboratory, Richland, Washington.

## ADDITIONAL LITERATURE

Anderson, M. B., and E. J. Fordham. 1982. "An Analysis of Results from an Atmospheric Experiment to Examine the Structure of the Turbulent Wind as Seen by a Rotating Observer." Paper presented at the Fourth British Wind Energy Association Workshop, Cranfield, England.

Connell, J. R., contributing author. 1981. "Meteorological Aspects of the Utilization of Wind as an Energy Source." Technical Note 175, World Meteorological Organization, Geneva, Switzerland.

Connell, J. R. 1984. "Basic Principles and Recent Observations of Rotationally Sampled Wind." Paper presented at the DOE/NASA Horizontal-Axis Wind Turbine Technology Workshop, May 1984, Cleveland, Ohio.

Connell, J. R., and R. L. George. 1982. The Wake of the MOD-OA1 Wind Turbine at Two Rotor Diameters Downwind on December 3, 1981. Report PNL-4210, Pacific Northwest Laboratory, Richland, Washington.

George, R. L. 1984. Simulation of Winds as Seen by a Rotating Vertical-Axis Wind Turbine Blade. Report PNL-4914, Pacific Northwest Laboratory, Richland, Washington.

Hardesty, R. M., J. A. Korrell, and F. F. Hall. 1981. Lidar Measurement of Wind Velocity Turbulence Spectra Encountered by a Rotating Turbine Blade. Report DOE/RL/10236-81/1, National Technical Information Service, Springfield, Virginia.

Powell, D. C., J. R. Connell, and R. L. George. 1985. Verification of Theoretically Computed Spectra for a Point Rotating in a Vertical Plane. Report PNL-5440, Pacific Northwest Laboratory, Richland, Washington.

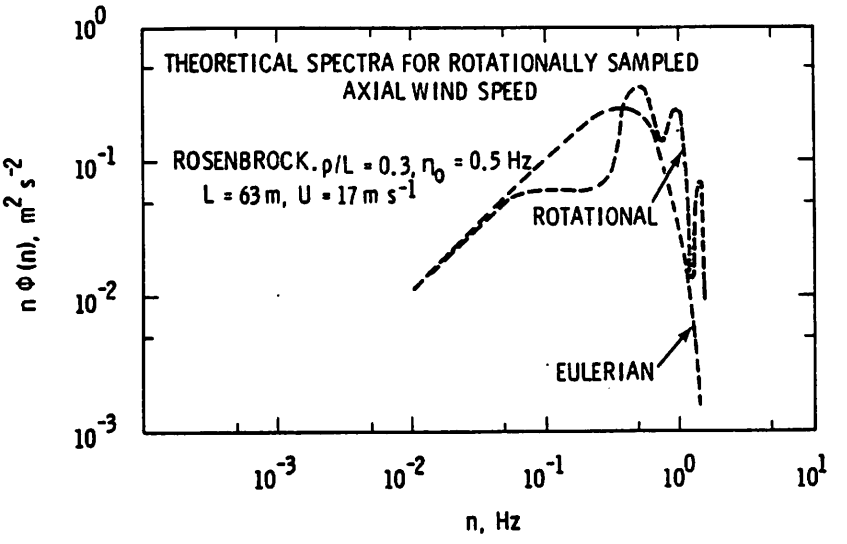


Figure 1. Theoretical spectra for rotationally sampled axial wind speed

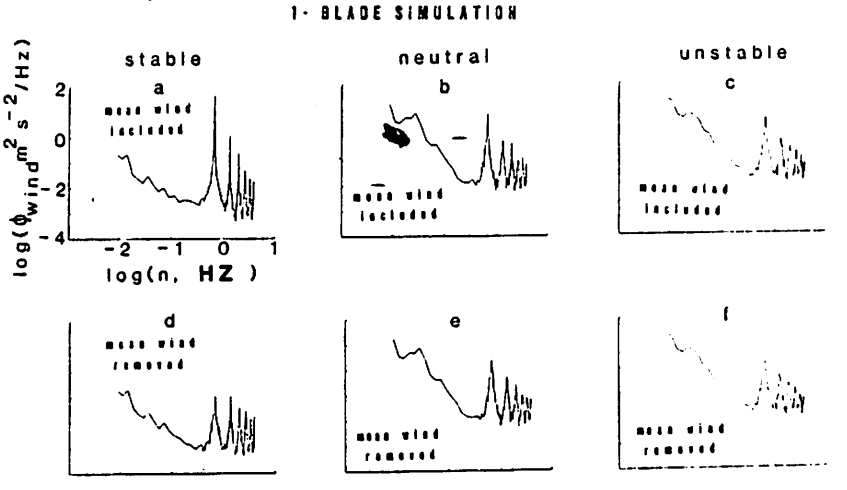


Figure 2. Spectral density function for rotationally sampled winds

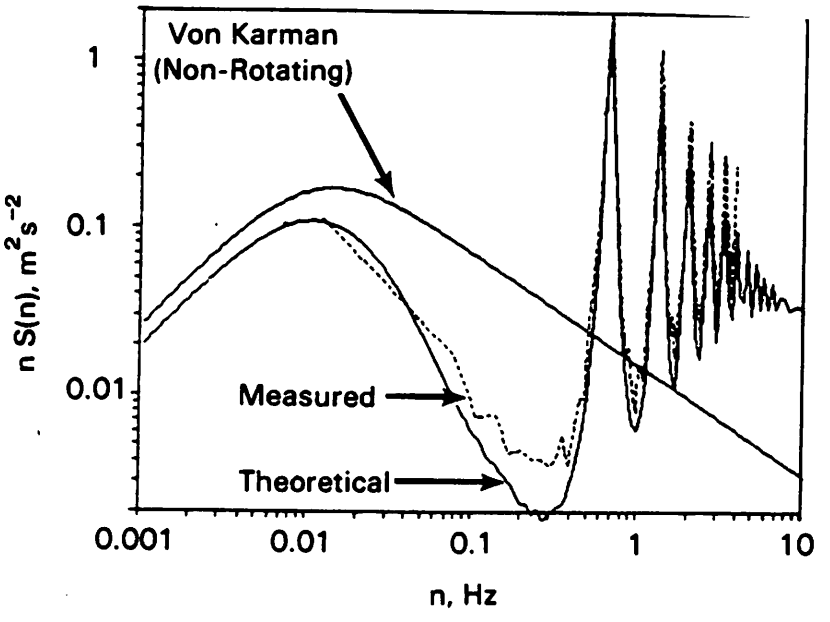


Figure 3. Verification of theory of rotationally sampled wind speed

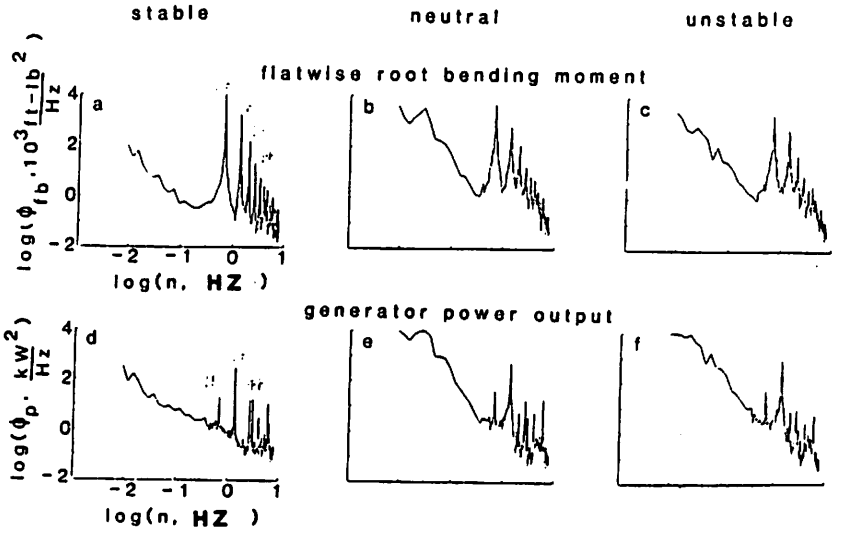


Figure 4. Spectral density functions of turbine blade and generator fluctuations

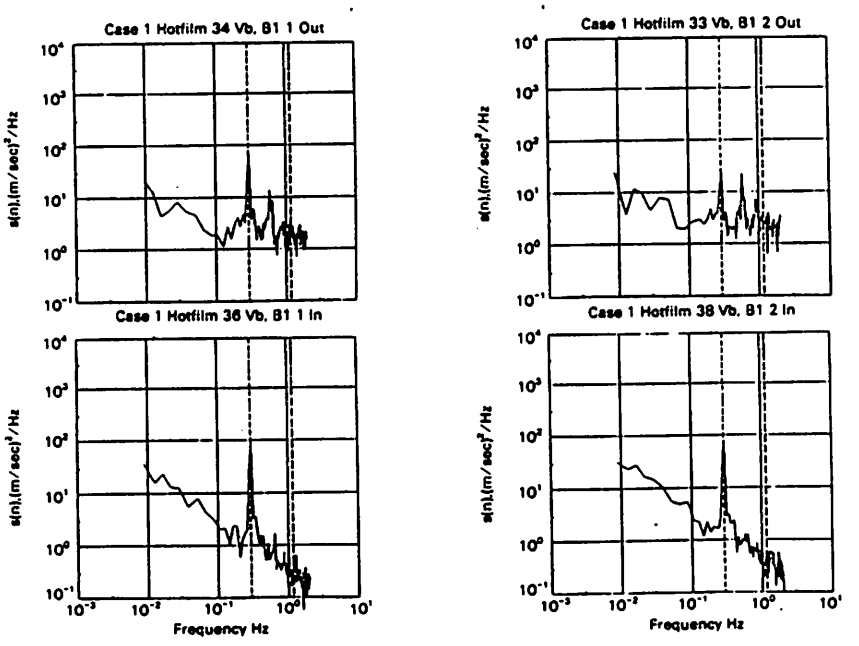


Figure 5. Rotationally measured wind spectra

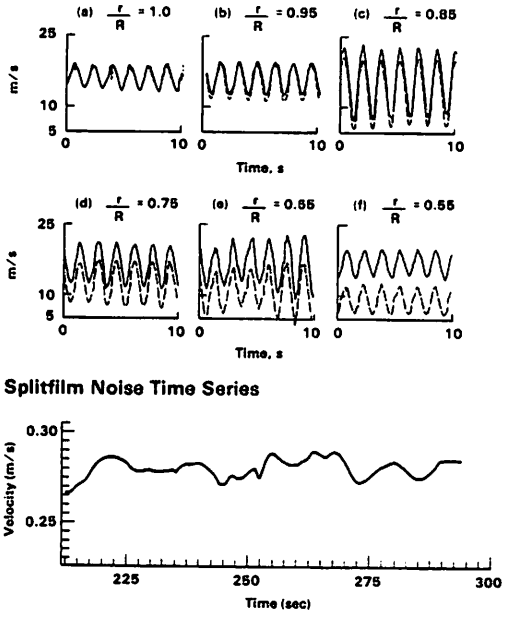


Figure 6. Time series for rotationally measured tangential wind speed at six radial locations on a blade

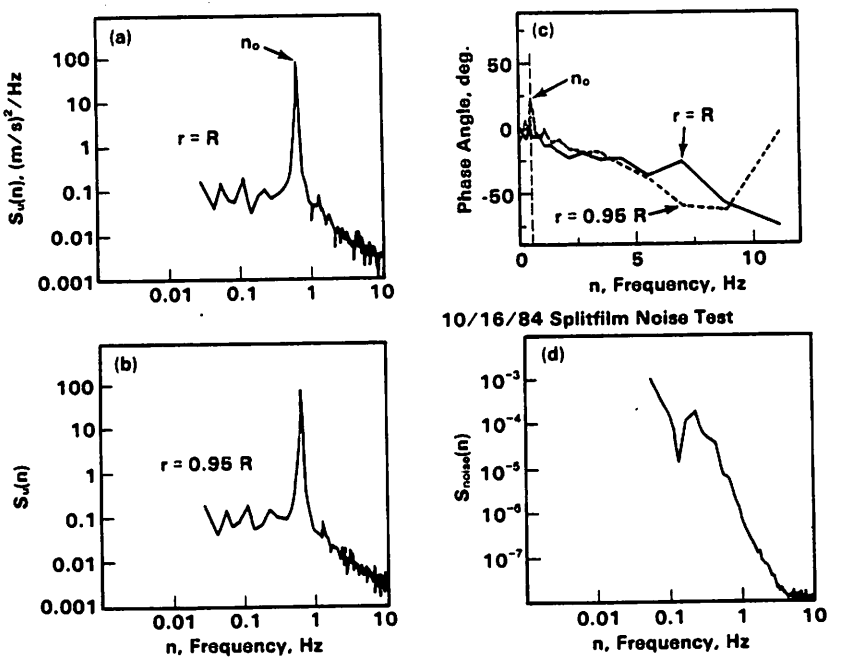


Figure 7. Rotationally measured wind amplitude and phase spectra for two radial locations

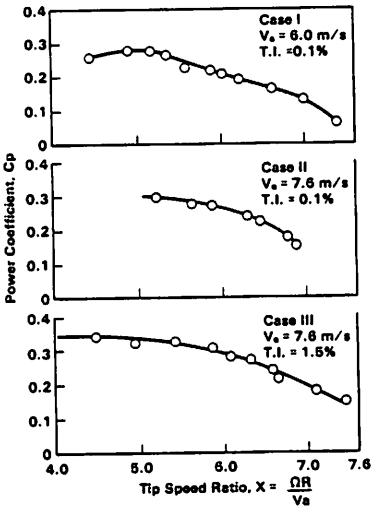


Figure 8. Power coefficient measured against tip speed ratio

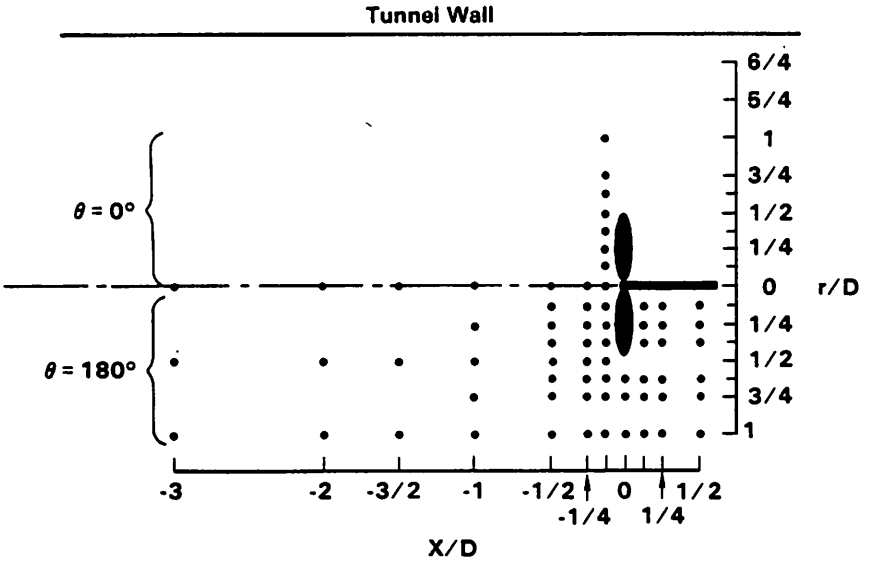


Figure 9. Positions where measurements were taken

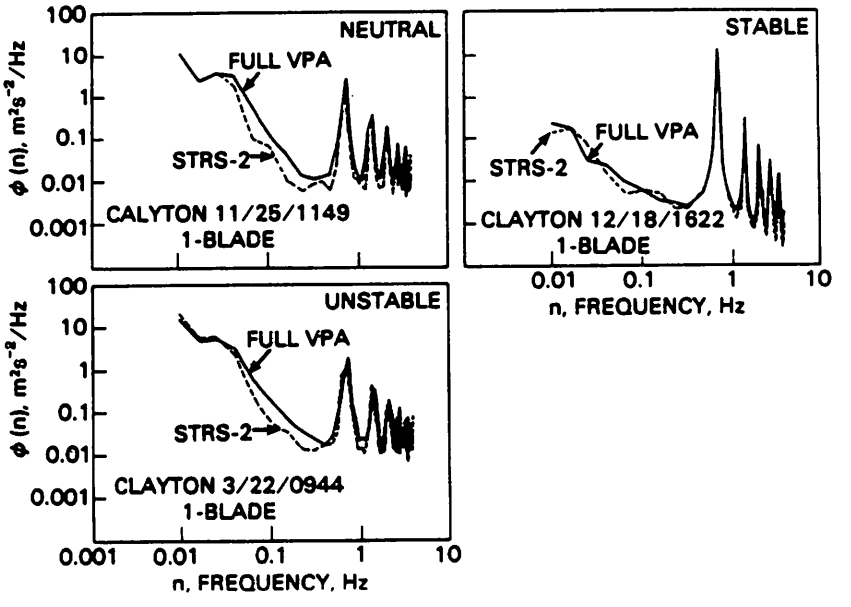


FIGURE 10. Simplified model time series of rotationally sampled wind speed

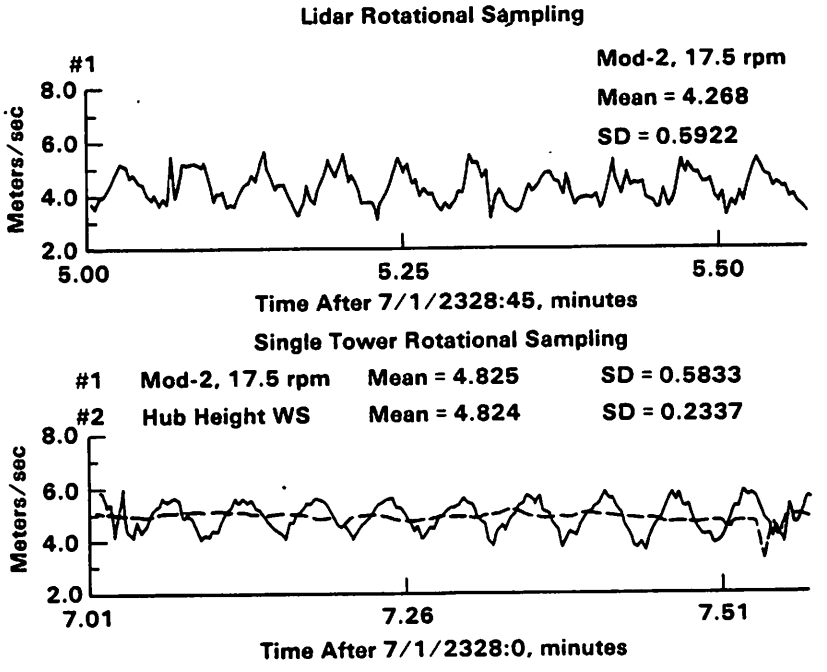


Figure 11. Time series comparison of laser rotational measurement with single tower sampling of rotational turbulence

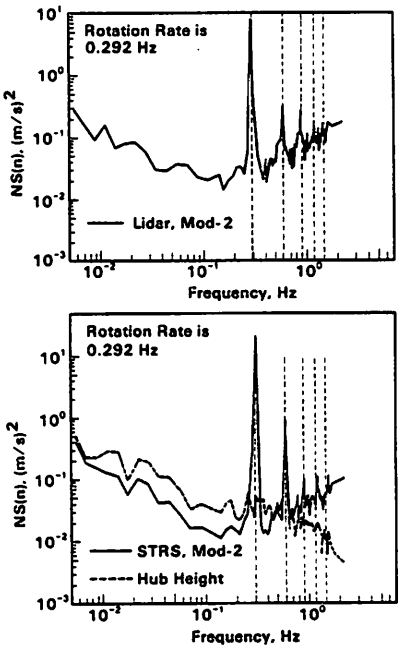


Figure 12. Turbulence spectra comparison of laser rotational measurement with single tower rotational sampling

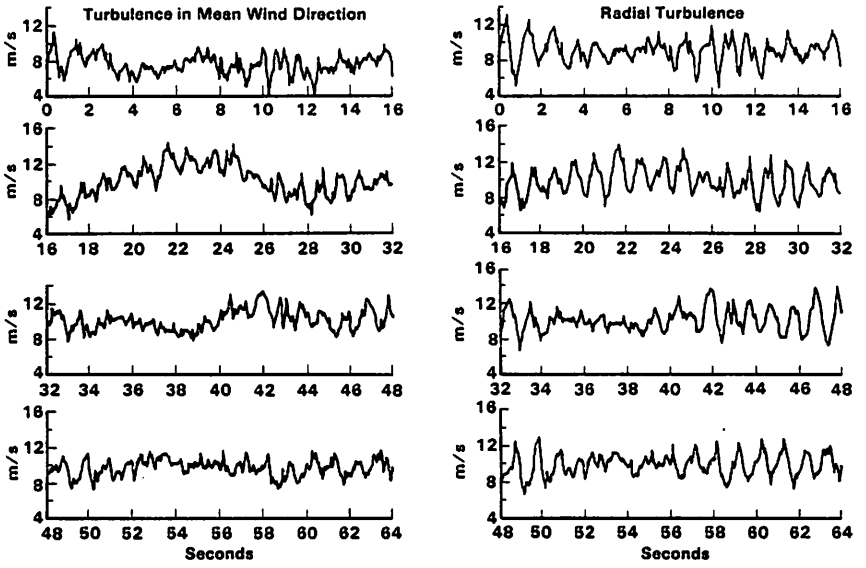


Figure 13. Simulation of turbulent time series for one rotating point on a VAWT

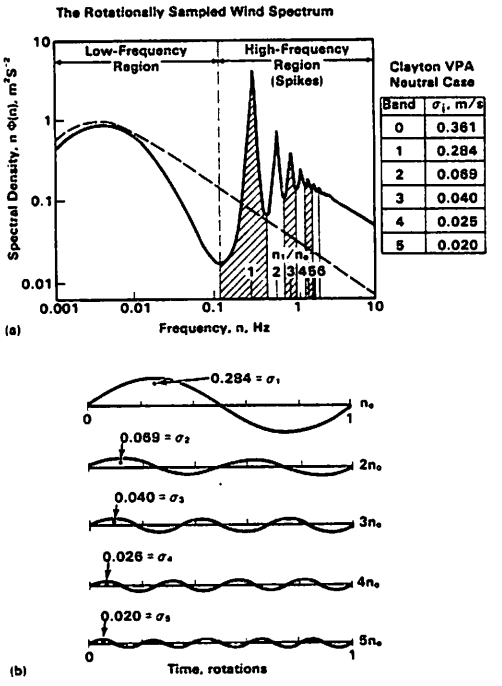


Figure 14. Simplified model of simulated turbulent time series

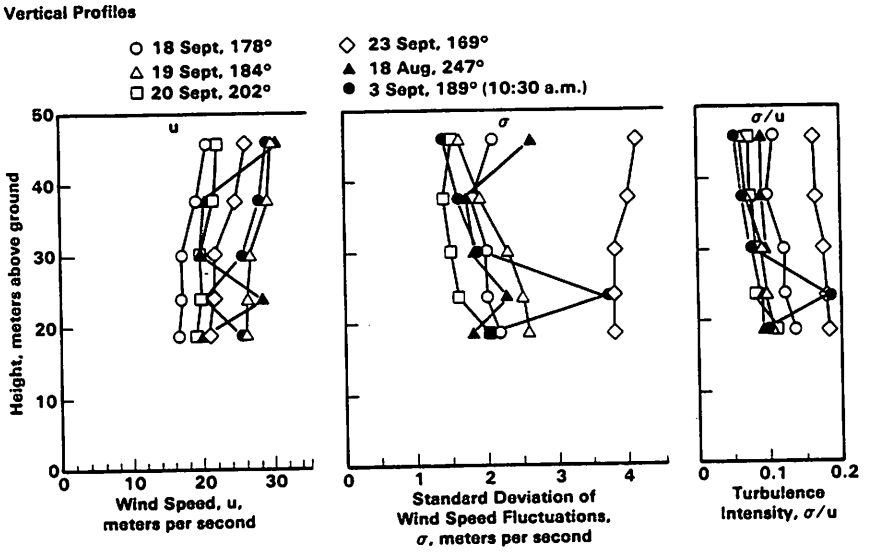


Figure 15. Turbulent wind at a coastal sand dune site

$$\sigma_t^2 = T^2 \left( 4 \frac{U'^2}{U^2} + C^2 \frac{W'^2}{U^2} + 4C \frac{U'W'}{U^2} \right)$$

(longitudinal) (vertical) (cross correl.)

Where $\sigma_t^2$ = Variance of kite-tether tension

$U'$ = ($\mu$ + $l\Omega$ sur $\Theta$)

$W'$ = ($W$ + $l\Omega$ cos $\Theta$)

$U$ = Mean wind speed

$\mu$ = Along-mean wind fluctuation speed

$w$ = Vertical fluctuation wind speed

$l$ = Kite-tether string length

$\Theta$ = String elevation angle

$\Omega$ = $\frac{d\Theta}{dt}$ (where t = time)

**Significance of Turbulence Components and Kite Motion:**

**Magnitude of Terms in $\sigma_t^2$ Equation**

| Ω (Kite Motion Rate) | (Longitudinal Velocity) | (Vertical Velocity) | (Cross Correlation of Velocities) |
|---|---|---|---|
| 0 | 0.069 | 0.0067 | 0.014 |
| $0.001 s^{-1}$ | 0.185 | 0.0404 | 0.054 |

Figure 16. Mathematical relation between kite string tension and turbulent wind velocity

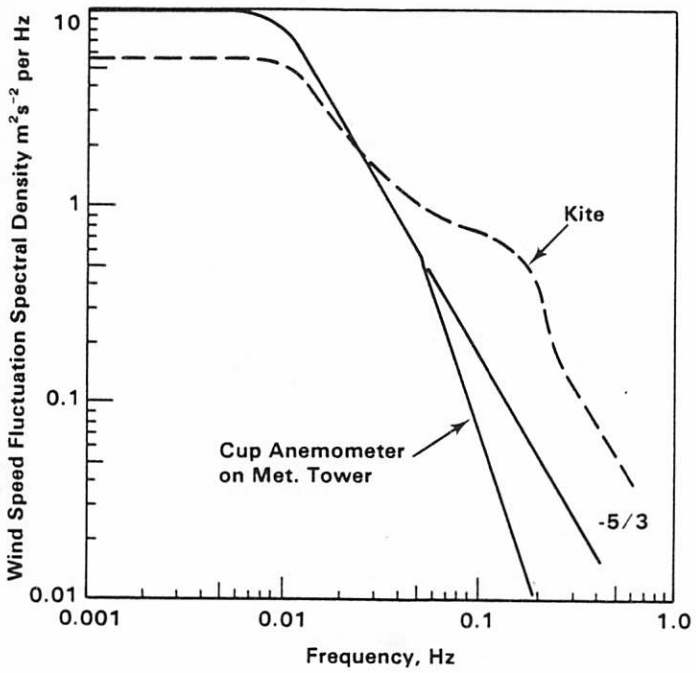


Figure 17. Test of kite anemometer using comparison of wind spectra

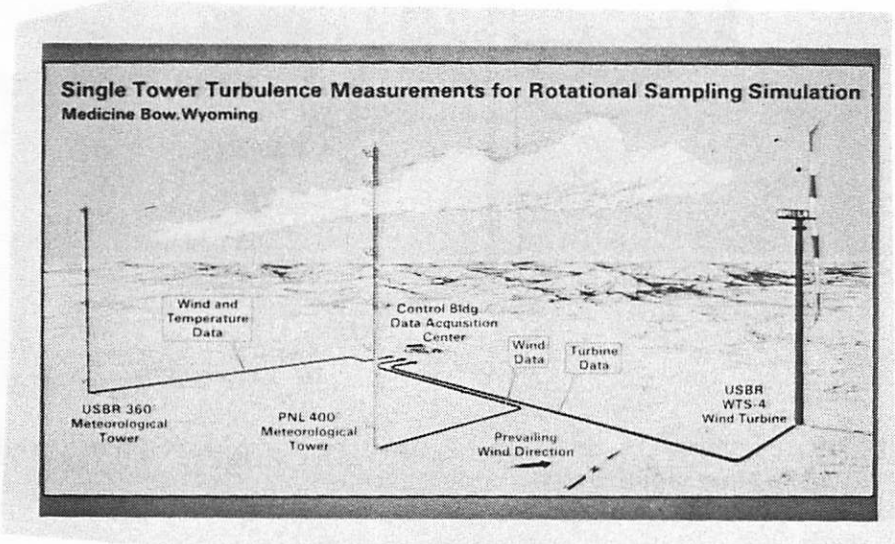


Figure 18. Arrangement of anemometers for single tower turbulence measurements

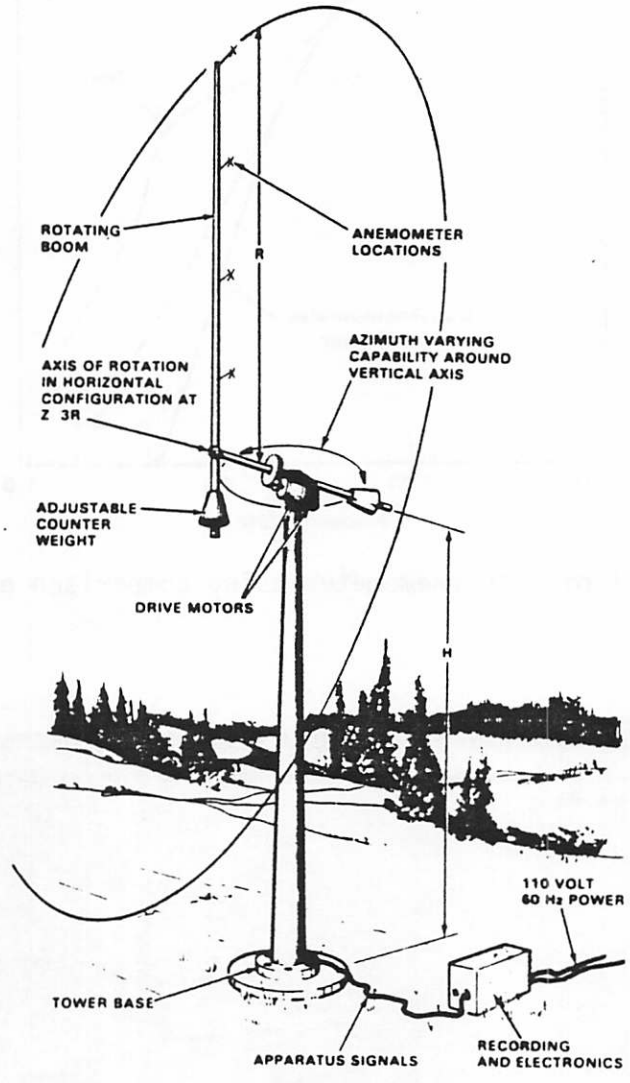


Figure 19. Schematic drawing of originally planned rotating boom apparatus

LITERATURE:

PNL-4083
UC-60

# The Spectrum of Wind Speed Fluctuations Encountered by a Rotating Blade of a Wind Energy Conversion System: Observations and Theory

J. R. Connell

November 1981

Prepared for the U.S. Department of Energy
under Contract DE-AC06-76RLO 1830

Pacific Northwest Laboratory
Operated for the U.S. Department of Energy
by Battelle Memorial Institute

Battelle

PNL-4083

PNL-4210
UC-60

# The Wake of the MOD-OA1 Wind Turbine at Two Rotor Diameters Downwind on December 3, 1981

J. R. Connell
R. L. George

November 1982

Prepared for the U.S. Department of Energy
under Contract DE-AC06-76RLO 1830

Pacific Northwest Laboratory
Operated for the U.S. Department of Energy
by Battelle Memorial Institute

Battelle

PNL-4210

PNL-3499
UC-60

# Covariance Statistics of Turbulence Velocity Components for Wind Energy Conversion System Design-Homogeneous, Isotropic Case

G. H. Fichtl

September 1983

Prepared for Pacific Northwest Laboratory
under Agreement B-29086-A-L

Pacific Northwest Laboratory
Operated for the U.S. Department of Energy
by Battelle Memorial Institute

PNL-3499

PNL-5238
UC-60

# Rotationally Sampled Wind Characteristics and Correlations with MOD-OA Wind Turbine Response

R. L. George
J. R. Connell

September 1984

Prepared for the U.S. Department of Energy
under Contract DE-AC06-76RLO 1830

Pacific Northwest Laboratory
Operated for the U.S. Department of Energy
by Battelle Memorial Institute

Battelle

PNL-5238

PNL-5440
UC-60

# Verification of Theoretically Computed Spectra for a Point Rotating in a Vertical Plane

D. C. Powell
J. R. Connell
R. L. George

March 1985

Prepared for the U.S. Department of Energy
under Contract DE-AC06-76RLO 1830

Pacific Northwest Laboratory
Operated for the U.S. Department of Energy
by Battelle Memorial Institute

Battelle

PNL-5440

EPRI
Electric Power
Research Institute

Topics:
Wind turbines
Technology assessment
Performance testing
Power generation planning
Research programs
Wind power

EPRI AP-4335
Project 1996-12
Final Report
November 1985

# Rotationally Sampled Wind and MOD-2 Wind Turbine Response

Prepared by
Battelle, Pacific Northwest Laboratories
Richland, Washington

# GUSTS

# A STATISTICAL ANALYSIS

HANS BERGSTRÖM

ABSTRACT

Turbulence measurements from the Näsudden peninsula, Gotland, during near-neutral stratification, are used to study the instantaneous wind gradients, the wind velocity difference $\Delta U = U(t+\tau) - U(t)$ using different time lags $\tau$ (1 - 10 s), and the amplitudes and durations of gusts as defined by a gust model.

The observed wind gradient distribution is found to be well approximated by the normal distribution and the standard deviation may be determined through its relation to the standard deviation of the longitudinal wind component, $\sigma_u$. By using the observed two dimensional mean wind speed — mean wind shear distribution, the long term probabilities of encountering large differences in wind velocity between the 38 m and 120 m levels are estimated.

The observed $\Delta U$-values are also found to be normally distributed for the data used here, provided the period studied is short enough (1 h or less) for non-stationary effects to become unimportant. Especially in these cases the probabilities of finding large $\Delta U$-values may be underestimated, when using the normal distribution. Relations between the standard deviation of the $\Delta U$-distribution and $\sigma_u$ are given.

Finally it is shown that the gust amplitude and duration distributions may be described by the normal distribution, provided that the wind data are filtered with e.g. a 5 s/50 s band-pass filter. The standard deviation of the amplitude may be determined through the relation $\sigma_A = 1.35 \cdot \sigma_u$.

## 1 INTRODUCTION

The turbulence of the atmospheric wind field is usually analysed in terms of 'moments', such as the standard deviations of the wind components ($\sigma_u$, $\sigma_v$, $\sigma_w$) and the friction velocity ($u_* = \sqrt{-\overline{u'w'}}$). Often spectra of the turbulence moments are also calculated, in order to find out at which frequencies the turbulent fluctuations predominantly occur. In this report, however, we more directly want to investigate the gustiness of the wind. In order to do this, turbulence measurements from the 145 m high tower at Näsudden, Gotland, have been used. The instruments are equipped with hot-wire probes with very high frequency response [Högström et al. 1980]. The maximum sampling rate is set by the data logging system at 20 Hz. The data used here are wind speed and wind direction sampled once every second at three levels in the tower (11 m, 77 m and 135 m). Both instantaneous values and 5 s-mean values have been employed when studying wind gradient fluctuations and changes in wind velocity over short time intervals (1 - 10 s). The distributions of amplitude and duration of gusts as given by a gust model are also shortly described.

## 2 FLUCTUATIONS OF THE WIND GRADIENT

The mean wind gradient, or the wind shear, varies quite a lot depending primarily on the roughness of the underlying surface, on the thermal stratification of the atmosphere and on the wind velocity itself. According to an investigation of the wind shear distribution between the 38 m and 120 m levels at Näsudden [Kvick et.al. 1983] the most common values are found in the interval $0.01 - 0.04\ s^{-1}$, equivalent to a difference in wind speed of 0.8 - 3.3 m/s between the two levels. The lowest observed value is about $-0.04\ s^{-1}$ and no value is greater than $0.16\ s^{-1}$. The greatest wind shears are usually observed during nocturnal conditions with very stable thermal stratification, when sometimes a maximum can be observed in the wind velocity at about 100-200 m height. The *mean* wind profile may, at least during fairly horizontally homogeneous conditions, be predicted from the Monin-Obukhov similarity theory [Monin and Yaglom, 1971], provided we know the roughness length ($z_0$), the thermal stratification and the wind speed at least at one level. The aim of the present study is, however, to investigate the *fluctuations* in the gradient.

To do this we are going to make use of the turbulence measurements taken in the 145 m high tower at Näsudden. First we look at the wind gradient between 11 m at 77 m, simply by taking the difference in wind speed between the two levels,

$$\frac{\Delta U}{\Delta z} = \frac{U_{77} - U_{11}}{66} = G \qquad (1)$$

In Figures 1 and 2, two examples of the resulting distributions are shown. The data used in Figure 1 are unfiltered, i.e. the wind values used is practically instantaneous, while in Figure 2 the wind velocity is prefiltered by calculating 5 s-mean values before the wind gradient is computed. As a comparison to the observed distribution, the normal probability (Gaussian) distribution is also included in the figures, and we may conclude that the agreement between the two is quite good. This is evident also from Figure 3 showing the cumulative frequency distribution. We can see in this figure that even at very small probabilities the agreement between the observed and the Gaussian distribution is rather good. From Figure 3 we may also draw the conclusion that the probability of en-

countering very large wind gradients is reduced by about one order of magnitude when we consider 5 s-mean values instead of momentary values.

As indicated by the above examples, we may establish from the analysed data that the normal probability distribution is a good approximation to the observed wind gradient distribution. To be able to calculate this distribution one only needs to know the mean wind gradient and the standard deviation of the gradient distribution, where upon the probability may be estimated from the relation

$$P(G) = \frac{1}{\sigma_g \cdot \sqrt{2\pi}} \cdot \exp\left[-\frac{1}{2}\frac{(G-\overline{G})^2}{\sigma_g^2}\right] \qquad (2)$$

where G denotes the magnitude of the wind gradient, $\overline{G}$ is the mean value and $\sigma_g$ is the standard deviation.

The corresponding cumulative probability that G is greater than a given value $G_i$ is then given by

$$P(G > G_i) = \frac{1}{\sigma_g \sqrt{2\pi}} \int_{G_i}^{\infty} \exp\left[-\frac{1}{2}\frac{(G-\overline{G})^2}{\sigma_g^2}\right] dG \qquad (3)$$

## 2.1 *The standard deviation of the wind gradient distribution*

We will now try to find the standard deviation of the wind gradient distribution, provided that the mean value is either observed or calculated from for instance the Monin-Obukhov similarity theory. That this standard deviation in some way must be related to the atmospheric turbulence is clear. It may thus be dependent both on the mean wind velocity, on the thermal stratification of the atmosphere, and on the surface roughness.

In Figure 4, where the standard deviation of the wind gradient is plotted against $\sigma_u$, we see that the relationship between the two is quite well established and consequently, if we do know the stability dependence of $\sigma_u$, we have found a possible way to include both the velocity and the stability dependence in the $\sigma$-values of the wind gradient distribution. As the largest wind gradient fluctuations are found for large $\sigma_u$-values, and consequently most frequently in situations with high wind velocity, an assumption of neutral stratification should, however, not seriously affect the results. The relation between $\sigma_u$ and the wind speed U which was given by Högström [1984] has consequently been used here

$$\sigma_u = U/\ln (z/0.04) \qquad (4)$$

As the data analysed in this report are all from situations with not far from neutral stratification, the range in z/L at 11 m being from -0.08 to 0.28, it is, however, impossible to draw any definitive conclusions about the wind gradient distribution other htan for near neutral stratification.

## 2.2 *Long term probabilities of large wind gradients*

Having outlined a method to calculate the wind gradient distribution during a specific situation, we will now try to get some estimates of the long term probabilities of finding large differences in wind velocity between the 38 m and 120 m levels, i.e. roughly across the diameter of the 2.5 MW wind turbine, which is located at Näsudden. To do this we are going to use the bivariate mean wind velocity – mean wind shear distribution, see Table 1, observed at Näsudden between these two levels during the period 1980-08-01 to 1982-07-31 [Kvick et.al. 1983].

Table 1. The bivariate mean wind velocity – mean wind shear distribution observed at Näsudden 1980-08-01 to 1982-07-31. The number given for each class, is the observed percentage of the total number of observations (17136 hourly mean values). The midpoints of the classes are given. After Kvick et.al. 1983.

| Mean wind speed at 75 m [m/s] | Mean wind shear between 38 m and 120 m [$s^{-1}$] | | | | | |
|---|---|---|---|---|---|---|
| | -0.055 | -0.015 | 0.025 | 0.065 | 0.105 | 0.145 |
| 2.95 | 0.006 | 16.52 | 18.72 | 0.263 | 0.006 | 0 |
| 7.95 | 0 | 3.922 | 30.90 | 2.609 | 0.012 | 0 |
| 11.95 | 0 | 0.321 | 14.81 | 4.137 | 0.082 | 0 |
| 15.95 | 0 | 0.006 | 4.173 | 1.972 | 0.018 | 0 |
| 19.95 | 0 | 0 | 0.957 | 0.338 | 0.006 | 0.006 |
| 22.95 | 0 | 0 | 0.163 | 0.058 | 0 | 0 |

Although the class widths are somewhat large these observations will be used directly, without any attempt to model this mean value distribution.

As we have seen above, the standard deviation of the wind gradient distribution is very well determine through its relationship to $\sigma_u$.

If we now denote the instantaneous wind gradient by G, its mean value for a given class by $\overline{G}_i$ and if we let G' denote some high value which we want

to know how often G exceeds, then the probability that $G > G'$ for that class may be expressed from Equation (3) as

$$P(G > G') = \frac{1}{\sigma_g \sqrt{2\pi}} \int_{G'}^{\infty} \exp\left[-\frac{1}{2}\frac{(G - \overline{G}_i)^2}{\sigma_g^2}\right] dG \qquad (5)$$

But each class in Table 1, besides corresponding to a given mean wind shear $\overline{G}_i$, also corresponds to a mean wind speed $\overline{U}_j$, i.e. the probability given by Equation 5 is with the two conditions $\overline{G} = \overline{G}_i$ and $\overline{U} = \overline{U}_j$. To get the 'true' probability that $G > G'$ for that class, we have to multiply by the probability that $\overline{G} = \overline{G}_i$ and $\overline{U} = \overline{U}_j$. This gives us

$$P_c(G > G') = P(G > G') \cdot P(G = \overline{G}_i / \overline{U} = \overline{U}_j) \qquad (6)$$

As an example, the values of $P_c$ with $G' = 0.122\ s^{-1}$, i.e. the difference in wind speed between the 38 and 120 m levels is 10 m/s, are given in Table 2. To get the *total* probability we finally have to sum over all the classes, both $\overline{G}$-classes and $\overline{U}$-classes, which yields

$$P_T(G > G') = \sum_{i,j} P_c(G > G') \qquad (7)$$

Consequently we have added to the observed *mean* wind velocity gradient given in Table 1, the fluctuations in the gradient due to the turbulence and come up with some estimates of the probability for the *fluctuating* gradient to exceed some given values. The result is presented in graphical

Table 2. The probabilities as given by Equation 6 (in parts per million) for each class of Table 1, that the difference in wind speed between the 38 m and 120 m levels is greater than 10 m/s ($G' = 0.122\ s^{-1}$).

| $\overline{U}(75)$ | $\overline{G}$ (38 - 120 m) [$s^{-1}$] | | | | |
|---|---|---|---|---|---|
| [m/s] | -0.015 | 0.025 | 0.065 | 0.105 | 0.145 |
| 2.95 | 0 | 0 | 0 | 0.002 | 0 |
| 7.95 | 0 | 0 | 0.009 | 8.151 | 0 |
| 11.95 | 0 | 0 | 20.23 | 133.0 | 0 |
| 15.95 | 0 | 0.545 | 132.9 | 40.38 | 0 |
| 19.95 | 0 | 3.715 | 81.68 | 16.22 | 45.94 |
| 22.95 | 0 | 2.844 | 2.510 | 0 | 0 |

form in Figure 5, which gives the number of hours per year you could expect to find a given values of the difference in wind velocity between 38 m and 120 m. Two curves are given, one for momentary values and one for 5 s-mean values. Some numbers are also given in Table 3.

Table 3. Number of minutes per year the wind velocity difference between 38 m and 120 m exceeds some given values.

| $U_{120} - U_{38}$ | minutes/year using | |
|---|---|---|
| greater than | momentary values | 5 s-mean values |
| 10 m/s | 260 | 150 |
| 12 m/s | 30 | 20 |
| 14 m/s | 7 | 5 |
| 16 m/s | 1.3 | 0.7 |

## 3 WIND VELOCITY DIFFERENCE

In this section we are going to study the statistical behaviour of the difference in wind velocity over some given separation in time, $\tau$. Thus our new data will consist of a series of $\Delta U$-values, defined as

$$U(t,\tau) = U(t+\tau) - U(t) \tag{8}$$

This makes it possible to study the velocity fluctuations of different time-scales in a more direct way than by making a spectral analysis, although the two methods of course are interchangeable. It is notable that the variance of the velocity difference series, $\sigma^2_{\Delta U}$, is identical to what in the mathematical description of turbulence often is called the structure function, $D(\tau)$,

$$\sigma^2_{\Delta U} = D(\tau) = \overline{\left[U(t+\tau) - U(t)\right]^2} \tag{9}$$

and that $D(\tau)$ is related to the spectral density function $S_u(n)$ by the relation

$$D(\tau) = 2 \int_0^\infty (1 - \cos 2\pi n \tau)\, S_u(n)\, dn \tag{10}$$

where n is the frequency [Monin & Yaglom, 1975].

It should accordingly be possible to estimate the variance $\sigma^2_{\Delta U}$ from the ordinary energy spectra and then calculate the distribution of the velocity differences, provided that they are normally distributed. In fact. according to the analysed data, this seems to be the case, as can be seen from the examples in Figures 6-7, which show the observed $\Delta U$-distributions at the 11 m and 77 m levels from one hour of measurements. No smoothing of the data have been done, and the time step $\tau$ is 10 s. The agreement between the observations and the normal distribution, given by the full lines, is quite good, and there is consequently reason to believe that we may calculate the $\Delta U$-distribution provided that we are able to get some estimate of its stnadard deviation $\sigma_{\Delta U}$.

It must be pointed out, however, that a condition for this to be true seems to be fairly stationary conditions, because otherwise the normal distribution will underestimate the probabilities of finding large $\Delta U$-values.

This is illustrated by Figure 8, which results from an analysis of a 3.5 hour period when the wind speed decreased from 6.1 m/s to 4.0 m/s at 11 m. The influence of this non-stationarity is that the normal distribution, with the $\sigma_{\Delta U}$-value measured during this very period, gives a probability of finding e.g. $|\Delta U| > 3$ m/s, which is about twice smaller than the observations give. If the $\Delta U$-analysis is confined to the first hour of this 3.5 hour period, the agreement between the observed probabilities and the normal distribution is much better, as can be seen from Figure 9.

The agreement between observations and the normal distribution may, however, not be general as other investigations indicate that this is not the case. No definite conclusions may be drawn from the limited data set analysed here. Use of the normal distribution will, however, enable us to calculate the probability distributions of $\Delta U(\tau)$.

The problem remaining, is how to determine the standard deviation, $\sigma_{\Delta U}$, of the velocity difference distribution. As mentioned above it is possible to integrate the spectral density function $S_u(n)$ according to Equation 10, using for example some non-dimensional form of $S_u(n)$. A more direct way is to make use of the relation which must obviously exist between $\sigma_{\Delta U}$ and $\sigma_u$, the standard deviation of the longitudinal wind component. Two examples of this are shown in Figure 10. The full line result from linear regression using the least square method. This type of calculations have been made for both unfiltered data ('momentary values') and for data filtered by a 5 s running average. The time lags $\tau$ used are 1 s, 2 s, 5 s and 10 s. The quotient $\sigma_{\Delta U}/\sigma_u$ as a function of time lag $\tau$ is plotted in Figure 11.

We are now ready to estimate the probability distribution of the velocity different $\Delta U$. To do this we make use of the turbulence intensities, $\sigma_u/\bar{u}$, determined from our measurements as a function of height. Thus, using the observed mean wind velocity distribution at Näsudden, cf. Table 4, we are able to calculate the distribution of $\sigma_{\Delta U}$.

Table 4. Frequency distribution of the wind velocity (hourly mean values) at Näsudden 1980-08-01 to 1982-07-31. After Kvick et.al. 1983.

| Height | wind velocity interval [m/s] | | | | | | | | | | | |
|---|---|---|---|---|---|---|---|---|---|---|---|---|
| [m] | 0 - 2.4 | 2.5- 4.4 | 4.5- 6.4 | 6.5- 8.4 | 8.5 10.4 | 10.5- 12.4 | 12.5- 14.4 | 14.5- 16.4 | 16.5- 18.4 | 18.5- 20.4 | 20.5- 22.5 | 22.5- |
| 10 | 0.140 | 0.332 | 0.264 | 0.151 | 0.072 | 0.028 | 0.010 | 0.002 | | | | |
| 75 | 0.045 | 0.115 | 0.208 | 0.204 | 0.149 | 0.108 | 0.066 | 0.034 | 0.020 | 0.008 | 0.002 | 0.001 |

Computations of the probability of finding ΔU-values greater than 2, 3, 4 and 5 m/s are then made with the time lags 1, 2, 5 and 10 s. The results from the 11 m and 77 m level are illustrated graphically in Figures 12-15, for unfiltered data ('momentary values'), as well as for data filtered with a 5 s running mean value. One must, however, remember that these results are estimates made assuming both neutral stratification ($\sigma_u \propto \bar{u}$) and that the velocity differences are normally distributed. It should also be pointed out that this analysis does only account for the fluctuations in the wind velocity caused by the atmospheric turbulence, while phenomena such as heavy cumulonimbus clouds or thunderstorms may well be accompanied by gusts giving rise to large ΔU-values outside the scope of the ordinary turbulence.

## 4 STATISTICS USING A GUST-MODEL

In this section the longitudinal wind component, u, alone will be studied. A gust is defined according to Figure 16, having an amplitude A and a duration T. Comparing the observed amplitude distribution, using non-filtered data, with the Gaussian distribution we find that the two disagree markedly, as shown in Figure 17. This result is in agreement with the findings of e.g. Powell and Connell (1980).

By band-pass filtering the data, the normal distribution will quite well agree with the observations, as shown in Figure 18. We have here used a 5 s low-pass filter and a 50 s high-pass filter. The standard deviation of the amplitude distribution is in this case given by the relation

$$\sigma_A \approx 1.35 \cdot \sigma_u \tag{11}$$

where $\sigma_u$ is the standard deviation of the longitudinal wind component. The constant 1.35 is the mean value from 4 hours of measurement.

An example of the gust duration distribution is shown in Figure 19. Assuming this to be one half of a normal distribution, it may be shown that the standard deviation of the whole normal distribution will be given by

$$\sigma = \frac{\sigma_T}{\sqrt{1 - \frac{2}{\pi}}} \tag{12}$$

where $\sigma_T$ is the observed standard deviation of the duration. As shown in Figure 20, the agreement between observations and the normal distribution is rather good also in this case. The correlation between amplitude and duration varied between 0.62 and 0.71 for our data.

Also the wind velocity differences, as defined in Section 2, may be analysed in terms of the gust model defined above. Two examples of the observed $\Delta U$-amplitude distributions are shown in Figure 21, where the corresponding normal-distributions are also included. The agreement between the two is quite good in this case too.

## 5 CONCLUSIONS

An analysis of measurements of the atmospheric turbulence at Näsudden, Gotland, during near-neutral conditions, has shown the fluctuating part of the wind gradient to be normally distributed. The standard deviation of this distribution was found to be well defined through its relation to the standard deviation of the longitudinal wind component, which makes it possible to estimate the long term probability fo finding large wind gradients of short duration. In doing this the observed two dimensional mean wind shear — mean wind velocity distribution at Näsudden was also used. Assuming neutral stratification, the computations indicate that the instantaneous difference in wind velocity between the 120 m and the 38 m levels exceeds 12 m/s about 0.5 hour/year, 16 m/s about 1 minute/year.

Cases with extremely stable thermal stratification, when the mean wind gradient may be very large, are not taken account of, but during such situations the atmospheric turbulence is weak and consequently the wind gradient does not deviate very much from the mean value. In situations with highly unstable stratification, the longitudinal standard deviation is much larger than during neutral conditions. The quotient $\sigma_u/u_*$, being about 2.5 for neutral conditions, may increase by a factor two. This in turn causes an increase in the standard deviation of the wind gradient and consequently larger instantaneous deviations from the mean wind gradient than during neutral stratification. During unstable conditions, however, the mean wind gradient is rather small, and consequently large momentary gradients are probably not very common. But the measurements analysed, all being from situations with near-neutral stratification, do not permit us to draw any finai conclusions about the behaviour of the wind gradient fluctuations during very stable and very unstable conditions. Some uncertainties also arise from using the two dimensional mean wind speed — mean wind shear distribution observed during jusg two years. A longer observational series and modelling of this distribution may give a different result.

The fluctuations of the wind velocity with time have also been studied. This has been done by looking at the distributions of the wind velocity difference $\Delta U$, using the time lags 1, 2, 5 and 10 seconds. It is shown that the $\Delta U$-values are approximately normally distributed, provided short

enough periods are analysed (shorter than about one hour). If longer periods are used, non-stationary effects may imply that the normal distribution gives too few large ΔU-values. This bias may also be caused by the autocorrelation. As the time lags are small, the two wind velocities entering the difference are in fact correlated. Using the normal distribution and unfiltered data we arrive at the result that the momentary wind velocity difference over the time interval 10 s exceeds 5 m/s about 10 hours/year at the 11 m level and about 10 minutes/year at the 77 m level. Taking into account the uncertainties introduced using the normal distribution, these figures may be raised to about 20 hours/year and 20 minutes/year respectively.

Using a gust model, the fluctuating wind speed may be analysed in forms of amplitude and duration for individual gusts. These two parameters may also be described by the normal distribution if the wind signal is prefiltered using a band-pass filter with a width of about one decade, e.g. 5/50 s. The standard deviation of the amplitude may be determined through its relation to $\sigma_u$, which for the analysed data is $\sigma_A = 1.35 \cdot \sigma_u$. The correlation between amplitude and duration is, as may be expected, positive. It is, however, not larger than 0.6-0.7, indicating that gusts with large amplitudes may in some cases have very short duration. A more complete investigation of the two-dimensional amplitude-duration distribution requires much more data than have been used here.

ACKNOWLEDGEMENTS

The data used were gathered through the joint effort of several members of the Department of Meteorology at the University of Uppsala. The work was sponsored by the National Energy Administration, Sweden.

REFERENCES

Högström, U. 1984: Analysis of turbulence and wind measurements at the Näsudden peninsula during two periods with near-neutral stratification. Report No 75, Department of Meteorology, University of Uppsala.

Högström, U., Enger, L. & Knudsen, E. 1980: A complete system for probing the detail structure of atmospheric boundary layer flow. Report No 60, Department of Meteorology, University of Uppsala.

Kvick, T., Andersson, H. & Fredriksson, U. 1983: Vindarna över Sverige (in Swedish). Projektresultat, NE 1983:16.

Monin, A.S. & Yaglom, A.M. 1971: Statistical Fluid Mechanics, Mechanics of Turbulence, Volume 1. The MIT Press.

Monin, A.S. & Yaglom, A.M. 1975: Statistical Fluid Mechanics, Mechanics of Turbulence, Volume 2. The MIT Press.

Powell, D.C. & Connell, J.R. 1980: Definition of Gust Model Concepts and Review of Gust Models. PNL-3138, Pacific Northwest Laboratory, Richland, Washington.

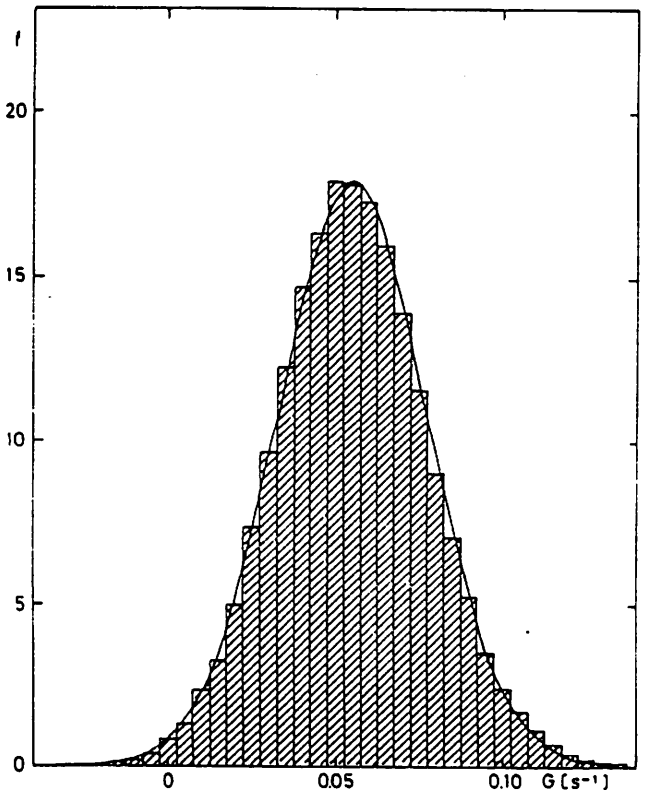


Figure 1. Histogram showing the observed distribution of the instantaneous difference in wind velocity between 11 m and 77 m, unfiltered data from 14.5h. The curve gives the corresponding normal distribution.

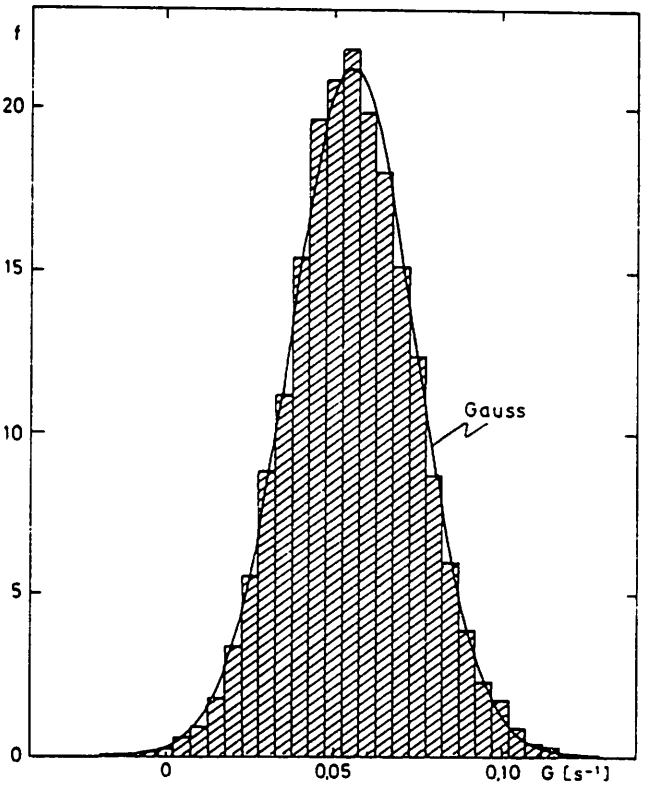


Figure 2. Same as Figure 1 but data filtered by a 5 s running average.

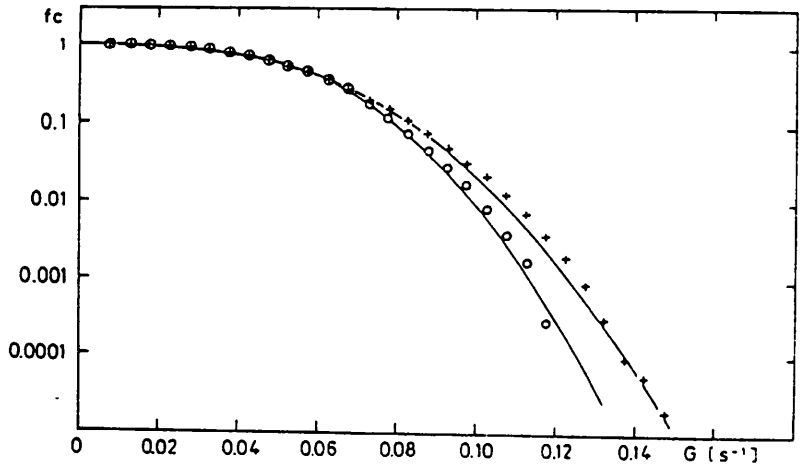


Figure 3. Same as Figure 1-2, but cumulative frequency; +: unfiltered data; o: data filtered by a 5 s running average.

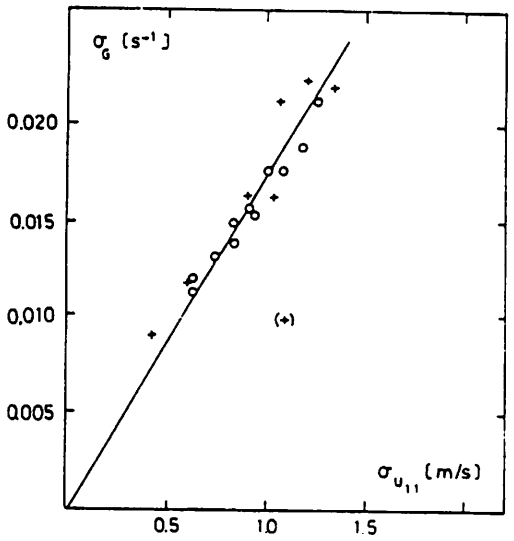


Figure 4. The standard deviation of the instantaneous wind gradient between 11 m and 77 m as a function of $\sigma_u$ at 11 m, (o: data from 1980, +: data from 1982).

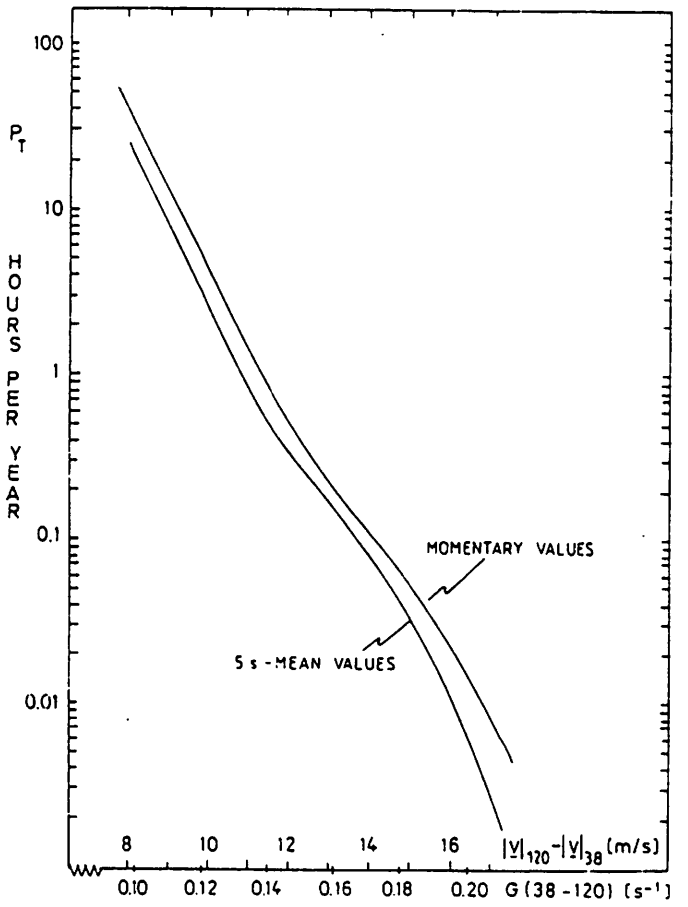


Figure 5. The total probability (hours/year) of large differences in wind speed between 38 m and 120 m, using momentary data and data filtered by a 5 s running average.

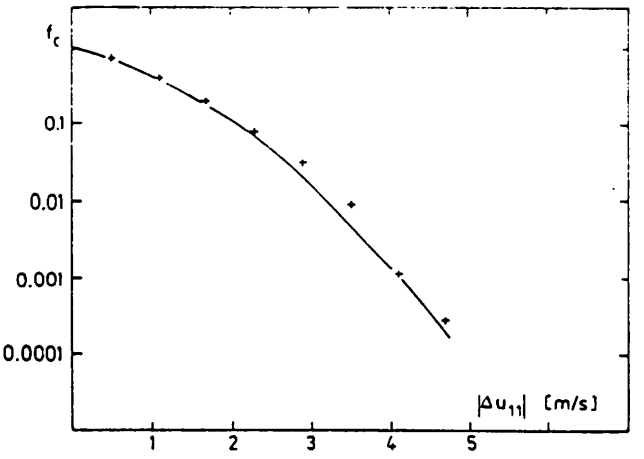


Figure 6. The observed cumulative frequency distribution of $|\Delta U|$ at the 11 m level, unfiltered data. The curve gives the corresponding normal distribution.

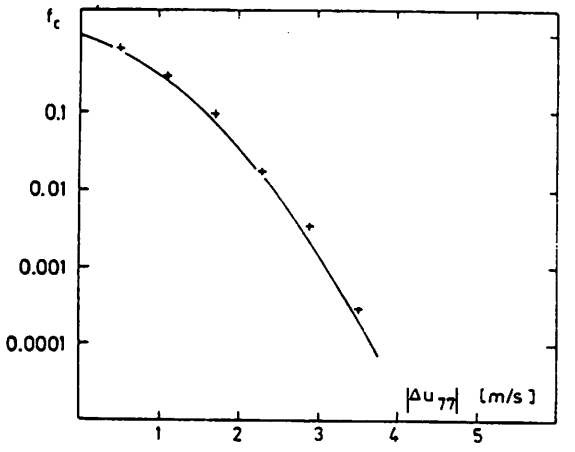


Figure 7. Same as Figure 6, but at the 77 m level.

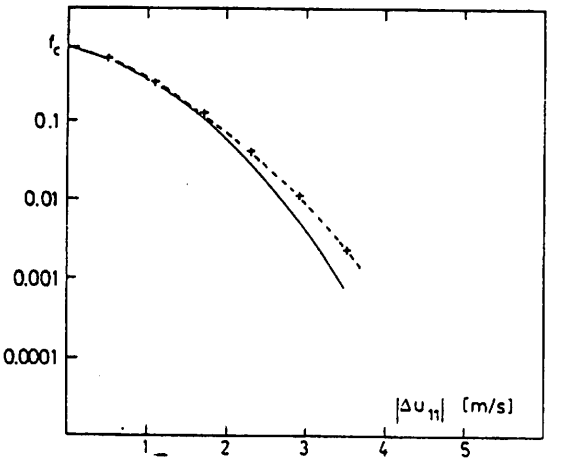


Figure 8. Observed cumulative frequency distribution of $|\Delta U|$ at the 11 m level during a period of 3.5h, unfiltered data. The full curve gives the corresponding normal distribution.

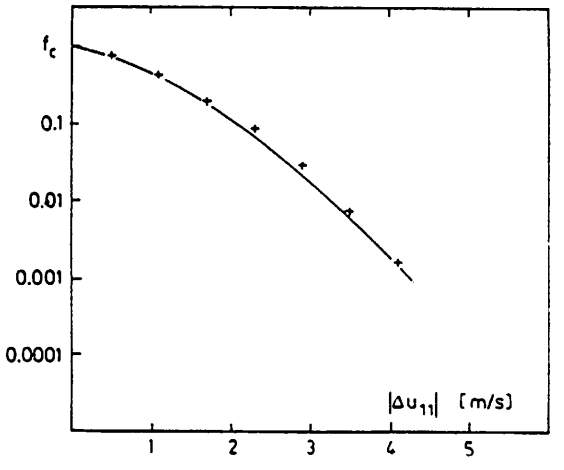


Figure 9. Same as Figure 8, but only the first hour is used.

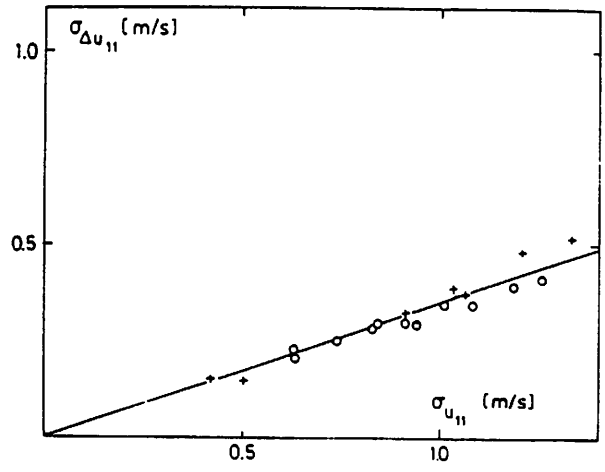


Figure 10. The relation between $\sigma_{\Delta U}$ and $\sigma_u$ at the 11 m level (o: data from 1980, +: data from 1982), data filtered by a 5 s running average used, time lag $\tau$ = 2 s.

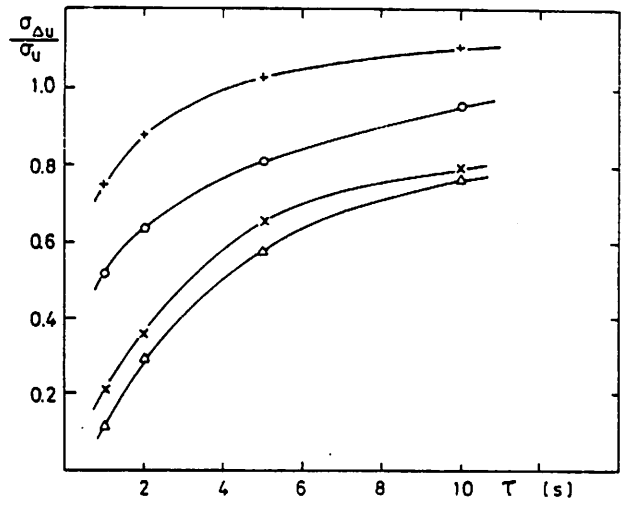


Figure 11. The quotient $\sigma_{\Delta U}/\sigma_u$ as a function of time lag $\tau$ (unfiltered data at 11 m (+) and at 77 m (o): data filtered by a 5 s running average at 11 m (x) and at 77 m ($\Delta$)).

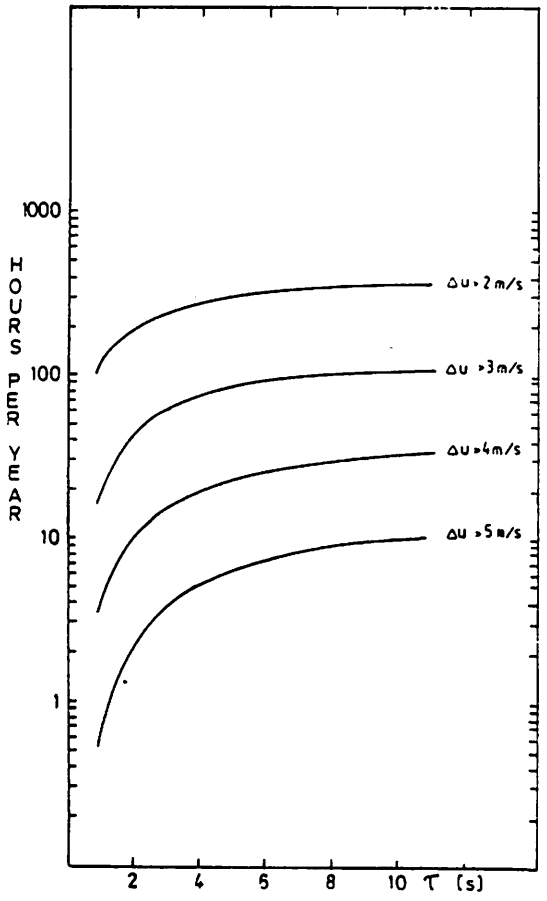


Figure 12. The probability of some large velocity difference ΔU as a function of time lag τ, height 11 m unfiltered, data.

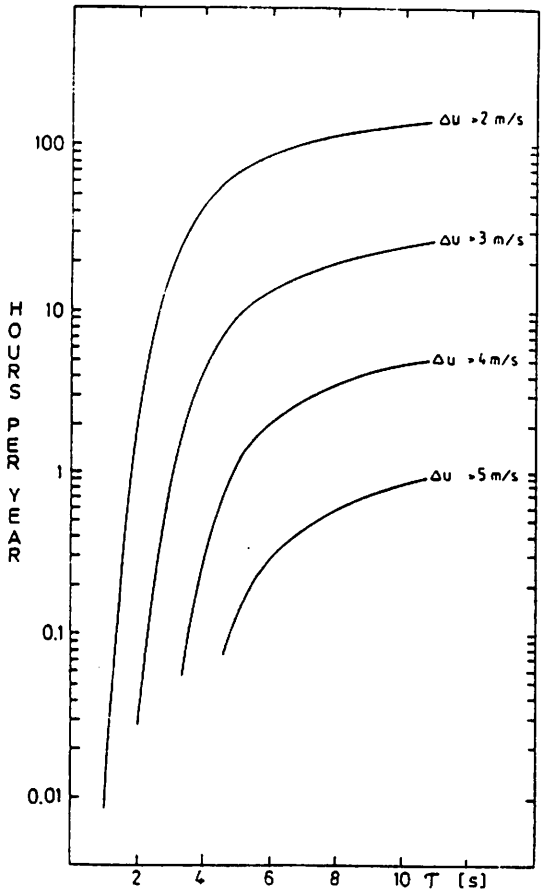


Figure 13. As in Figure 12, height 11 m, data filtered by a 5 s running average.

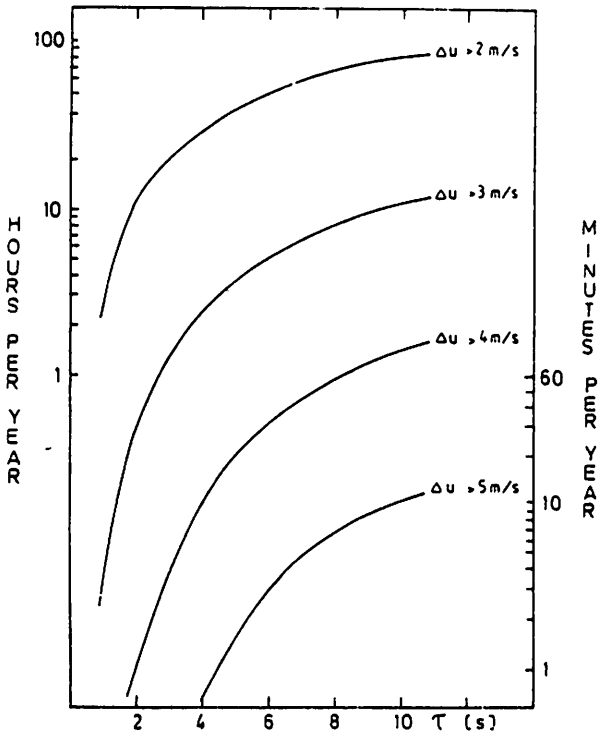


Figure 14. As in Figure 12, height 77 m, unfiltered data.

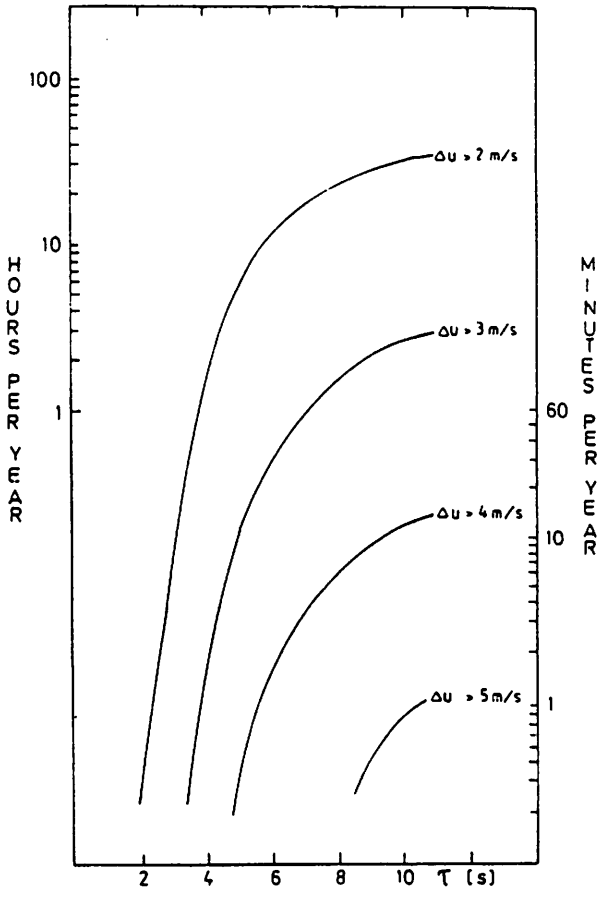


Figure 15. As in Figure 12, height 77 m, data filtered by a 5 s running average.

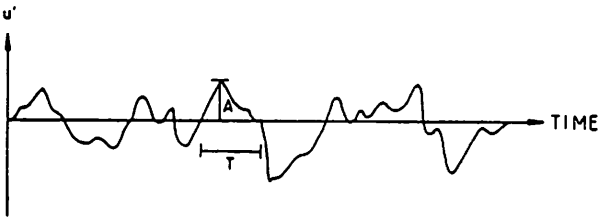


Figure 16. Definition of a gust with amplitude A and duration T.

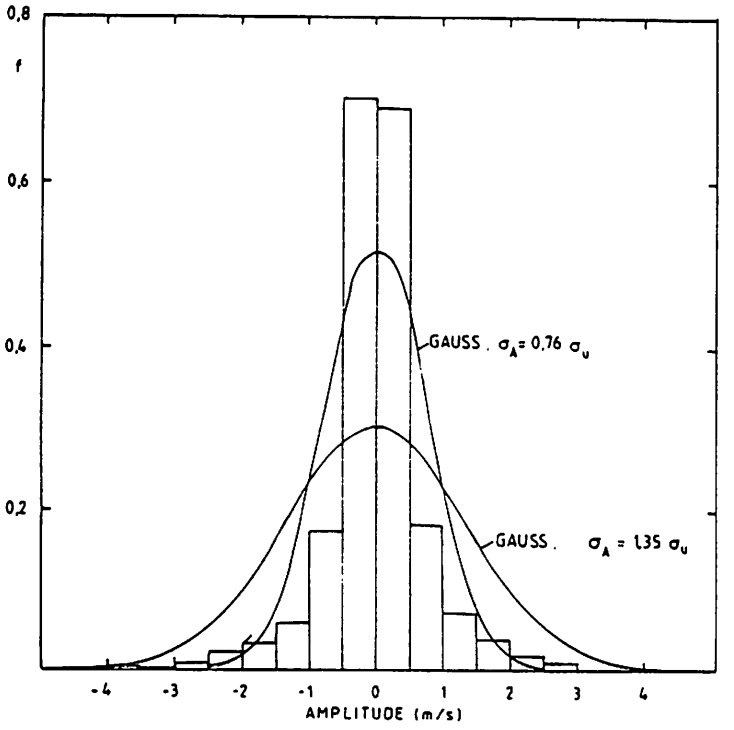


Figure 17. Distribution of the amplitude using non-filtered data.

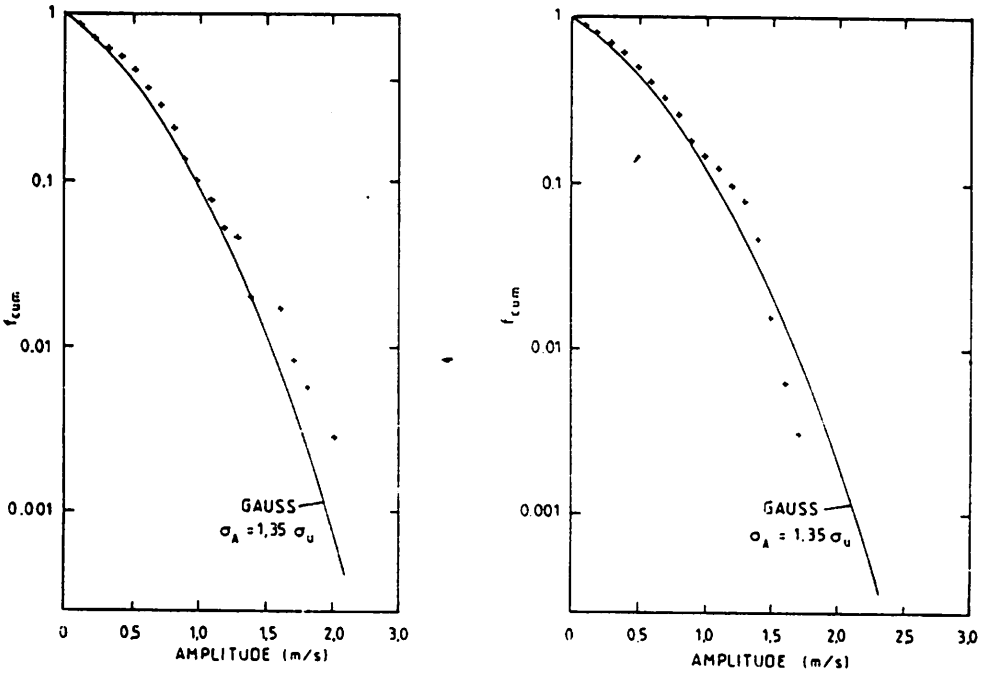


Figure 18. Cumulative frequency distribution of gust amplitude from two runs, compared with the Gaussian distribution, 5 s/50 s band-pass filtered data.

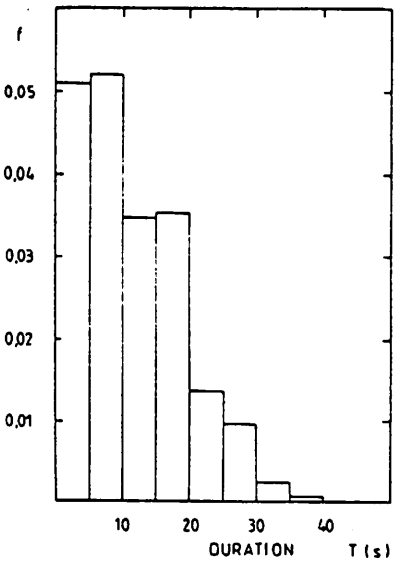


Figure 19. Frequency distribution of gust duration, using 5 s/50 s band-pass filtered data.

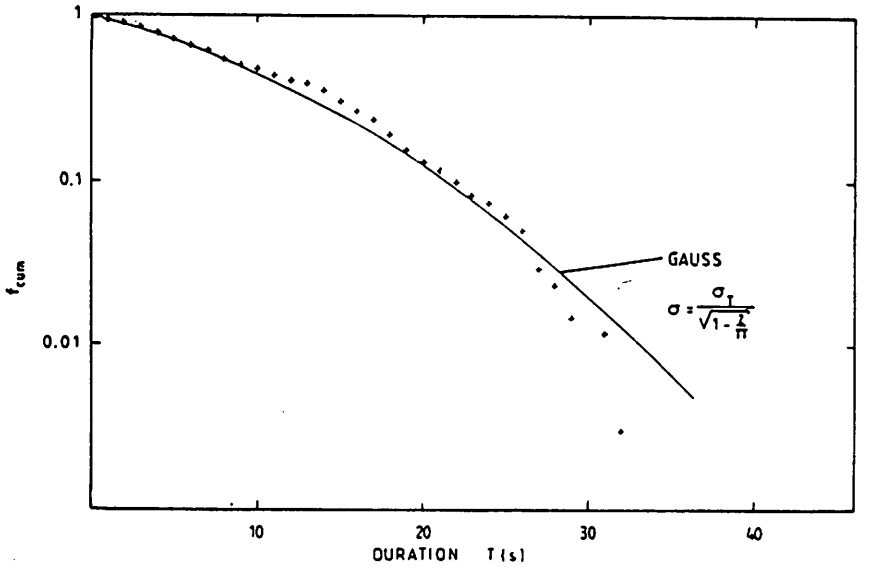


Figure 20. Same as Figure 19, but cumulative frequency distribution and compared with the Gaussian distribution.

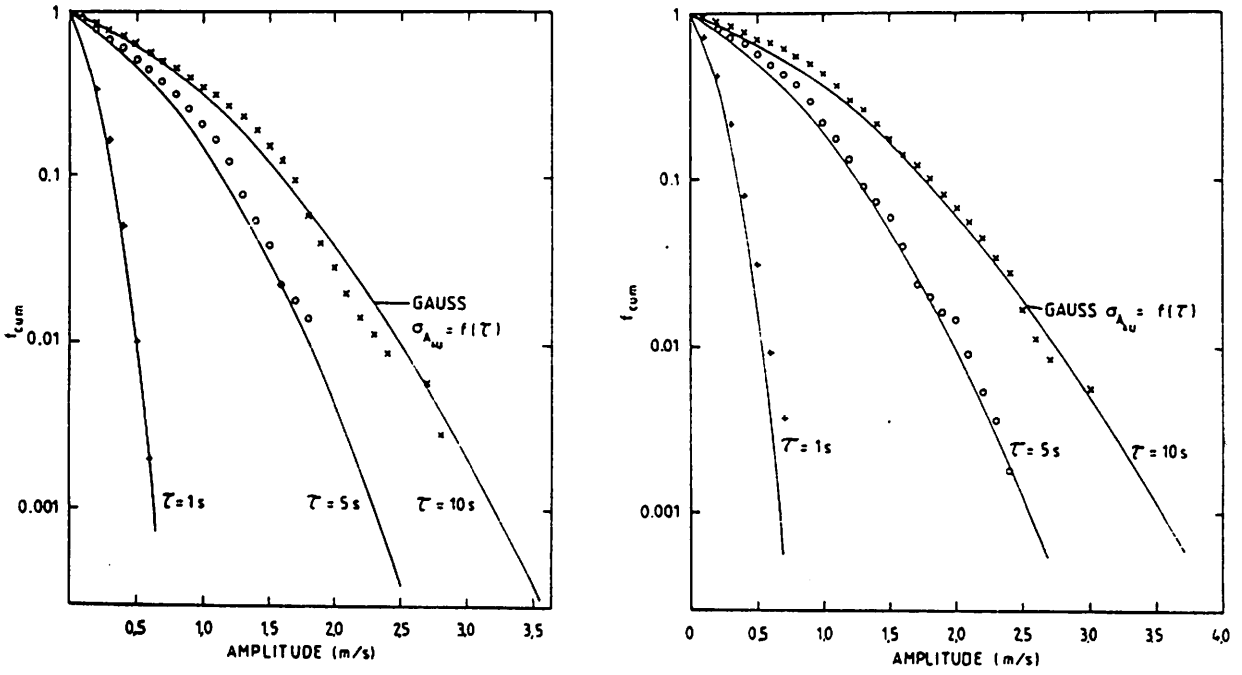


Figure 21. Cumulative frequency distribution of wind velocity difference amplitudes from two runs, compared with the Gaussian distribution.

# Turbulence Time Series Modelling with Different Spectra

Hermann G. Matthies

Spectra of wind turbulence give important information needed in WECS loading calculations. They can be used in at least three different ways:

1) Frequency domain computations, where the spectrum is multiplied by the squared modulus of the transfer-function to give the spectrum of the output quantity.

2) Time domain simulations with pseudo-random wind time series derived from a spectrum.

3) Time domain computations with discrete gusts; here the frequency of occurence of these gust is derived from the spectral moments:

$$\lambda_n = \int_0^\infty f^n S(f)\, df$$

$\lambda_n$ - n-th spectral moment
f - frequency
S(f) - one-sided power spectrum

The frequency of zero up-crossings is given by

$$\nu = (\lambda_2/\lambda_0)^{1/2}$$

and the frequency of maxima by

$$\mu = (\lambda_4/\lambda_2)^{1/2}$$

If the wind turbulence is assumed as homogeneous and isotropic, the general shape of the wave-number spectrum can be sketched as follows /1/:

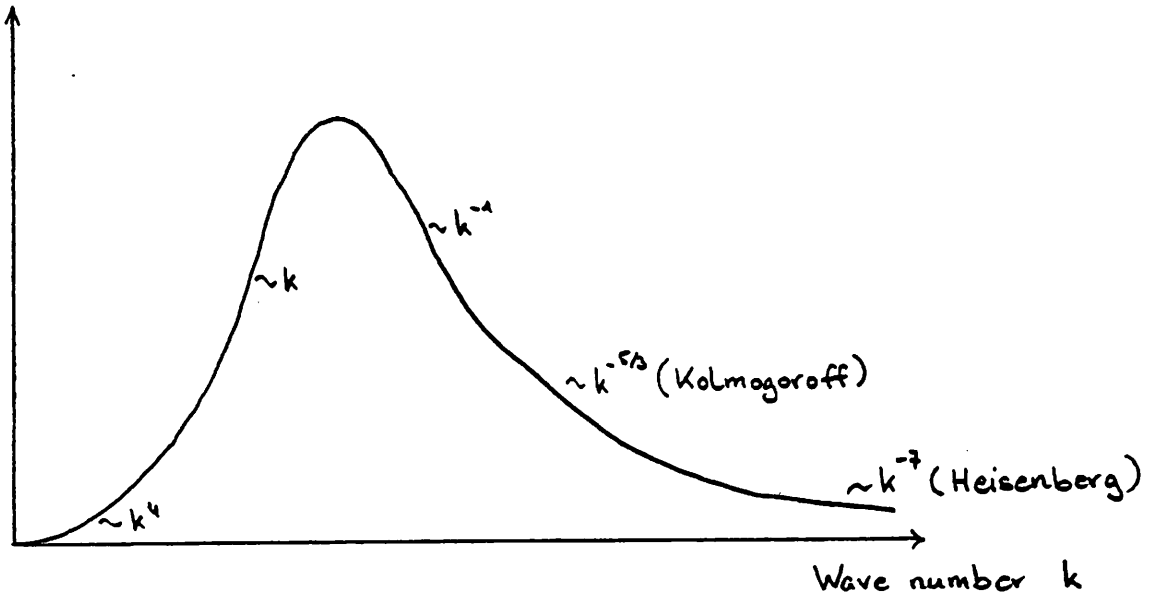


The energy peak is followed by the Kolmogoroff $k^{-5/3}$ range, which then melts into the $k^{-7}$ Heisenberg range.

To use this in calculations, we have to convert from wave-numbers to frequencies; this is usually done with the aid of Taylor's hypothesis:

$\omega / k$ = Phase speed = $\bar{u}$ (mean wind velocity)

This hypothesis is valid when the turbulence intensity $I_u = \sigma/\bar{u} \ll 1$. Looking at the spectra available in the literature, e. g.

- $$\frac{S_k(f) \cdot f}{\sigma^2} = \frac{11.4\ \tilde{n}}{1 + (23.5\ \tilde{n})^{5/3}}$$

  the "Kaimal" spectrum /2/ with $\tilde{n} = f \cdot z / \bar{u}$

  z = height

- $$\frac{S_H(f) \cdot f}{\sigma^2} = \frac{4\ \tilde{n}}{(1 + 70.8 \cdot \tilde{n}^2)^{5/6}}$$

  the "Harris" spectrum /3/ with $\tilde{n} = f \cdot L_x / \bar{u}$

  ($L_x$ = turbulence integral scale), derived from the von Kármán correlation function for homogenous isotropic turbulence.

- $\frac{S_D(f)\cdot f}{\sigma^2} = \frac{96\,\tilde{n}^2}{(1+144\,\tilde{n}^2)^{4/3}}$

  the "Davenport" spectrum /4/, modified such that the maximum coincides with the "Harris" spectrum.

- the original spectrum of /4/.

- $\frac{S_S(f)\cdot f}{u_*^2} = \frac{105\,\tilde{n}}{(1+33\tilde{n})^{5/3}}$

  the "Smedman" spectrum /5/ with

  $u_* = 0.4\,\bar{u} / \ln(z/z_0)$

  $z_0$ = surface roughness parameter.

These spectra are shown in fig. 1. They look very similar and only model the $k^{-5/3}$ Kolmogoroff range, since this is where the eigenfrequencies of most usual structures are.

1) In frequency domain computations there will be hardly any differences with any of the above spectra for usual structures. This changes if rotational sampling has to be considered /6/. The low frequency part is "folded" up to multiples of the rotation frequency.

2) The same is true for time domain simulations, if the spatial coherence is taken into account /7/.

3) The moments necessary to compute zero crossings etc. do not exist in a strict sense for the above spectra, a cut-off frequency has to be introduced /2/ at the beginning of the Heisenberg range, or averaging over the rotor disk with the coherence function /8/ to filter out the high frequencies.

The spectra of fig. 1 are shown in fig. 2 on a linear scale, and we see considerable difference in the low frequency end, while for higher frequencies they are all practically equal. For a wind measurement which was done on the GKSS test field on the island of Pellworm (cf. /9/ for a description of the test field), it was tried to simulate a time series which would look similar to the measured one. In figs. 3 and 4 the comparison between measured and simulated time series is shown for two spectra. By a visual inspection it may be seen that they are different. This and the other measurement shown later were performed at 10 m height with a cup

anemometer and a high sampling rate of over 50 /s (due to simultanious recording of structural data). The recording times were all in excess of 20 min. In fig. 5 we compare the measured spectrum with the ones of fig. 2, and it can be clearly seen where they differ. For higher frequencies not shown the shapes were much more similar. Looking at the time domain and comparing the auto-correlation functions in figs. 6 and 7 for different time lengths, the differences are also clearly to be seen.

Before computing spectra and auto-currelation functions, the mean value and linear trend had been removed from the data. In fig. 7 there is a recurrence with a period of approx. 140 s, which may be an instance of postulated gravity waves /9/. In table 1 we show for another measurement comparisons of the frequency of zero up-crossings and maxima for different cut-off frequencies, showing the sensitivity to the cut-off frequency.

Conclusion:

Comparison of measured wind data with spectra available in the literature shows sometimes pronounced differences, as there may be much more energy in the low-frequency range than predicted. These frequency contributions could potentially contribute significantly to WECS fatigue loading due to rotational sampling. More information is needed on the probability and shape of these spectral deformations, and on their causes. The comparison also shows the need for reliable cut-off frequencies if spectral moments are to be computed.

**References**

/1/ J. C. Rotta, Turbulente Strömungen, B GTeubner, Stuttgart 1972

/2/ W. Frost et al., Engineering handbook on the atmospheric environmental guidelines for use in wind turbine generator development, NASA TP 1359, 1978

/3/ ESDU Wind engineering subseries volume 1, London, 1984

/4/ A. G. Davenport, Gust loading factors, Proc. ASCE, ST3, 93 (1967) 11 - 34

/5/ B. Dahlroth, Load cases for medium sized wind power plants, 9th IEA meeting of experts - structural design criteria for LS WECS, Greenford, 1983

/6/ J. B. Dragt, The spectra of wind speed fluctuations met by a rotating blade and resulting load fluctuations, European Wind Energy Conference, Hamburg, 1984 (EWEC'84)

/7/ S. J. R. Powles and M. B. Anderson, The effect of stochastic and deterministic loading on fatigue damage in a large horizontal-axis wind turbine EWEC'84, Hamburg

/8/ W. E. Holley et.al., Atmospheric turbulence inputs for horizontal axis wind turbines, EWEC'84, Hamburg

/9/ S. Fries et. al., Windkraftanlagen-Versuchsfeld Pellworm, Abschlußbericht GKSS 85/E/42, Geesthacht, 1985

## Wind Spectra z=10.0m z0=.0065m, v= 8.3m/s L=76m

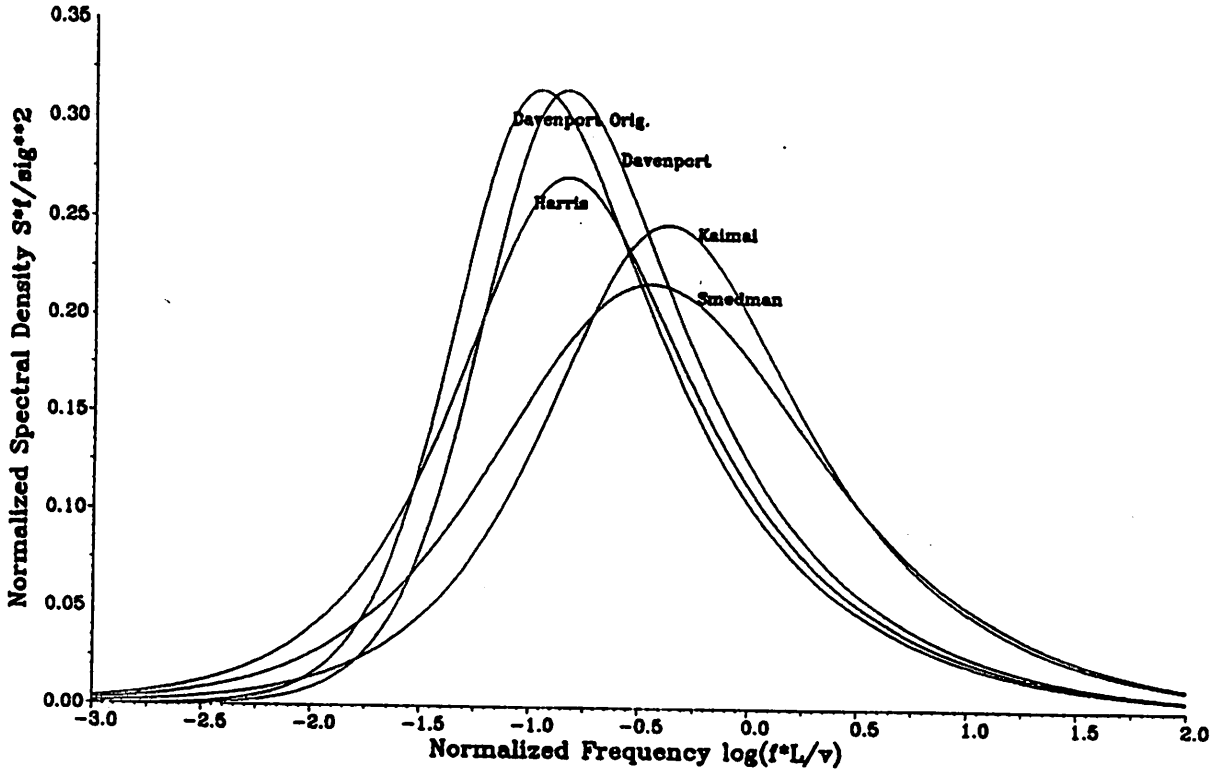


fig. 1

## Wind Spectra z=10.0m z0=.0065m v= 8.3m/s

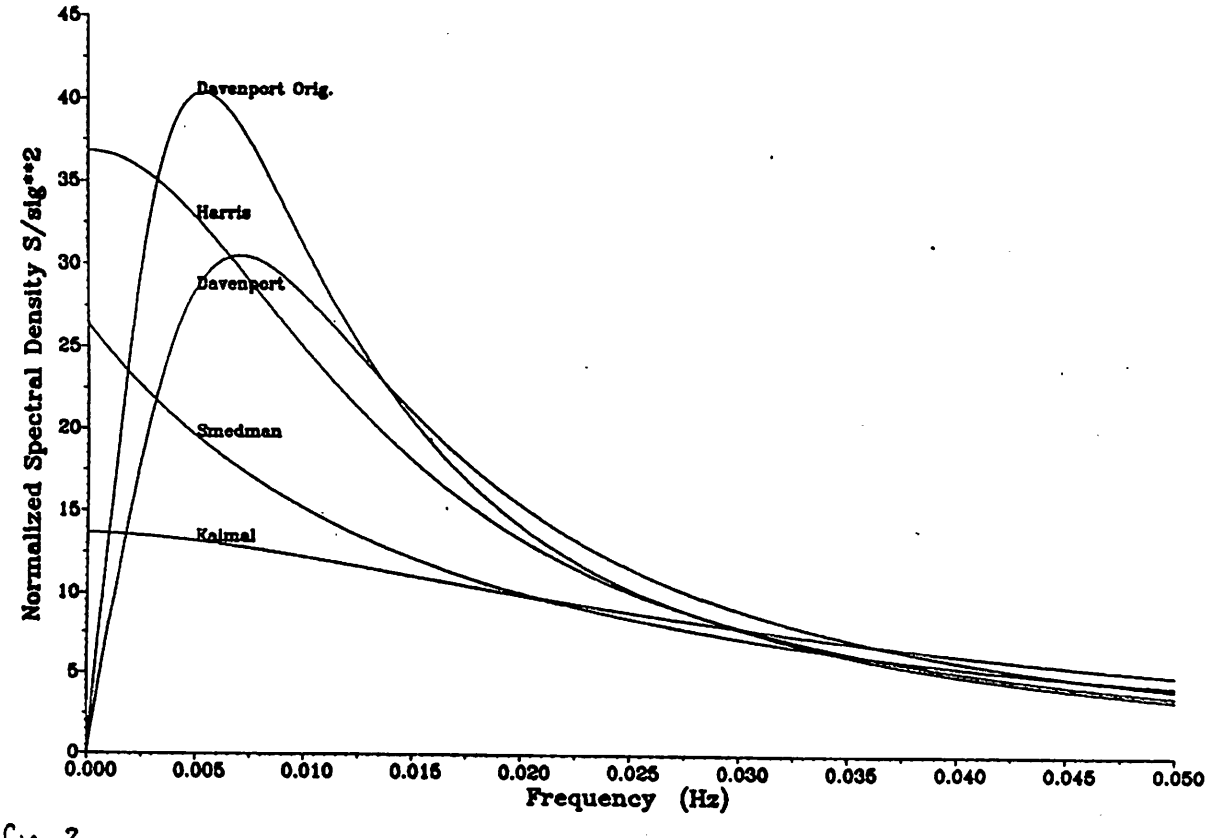


fig. 2

Measured Time History sig=1.33m/s

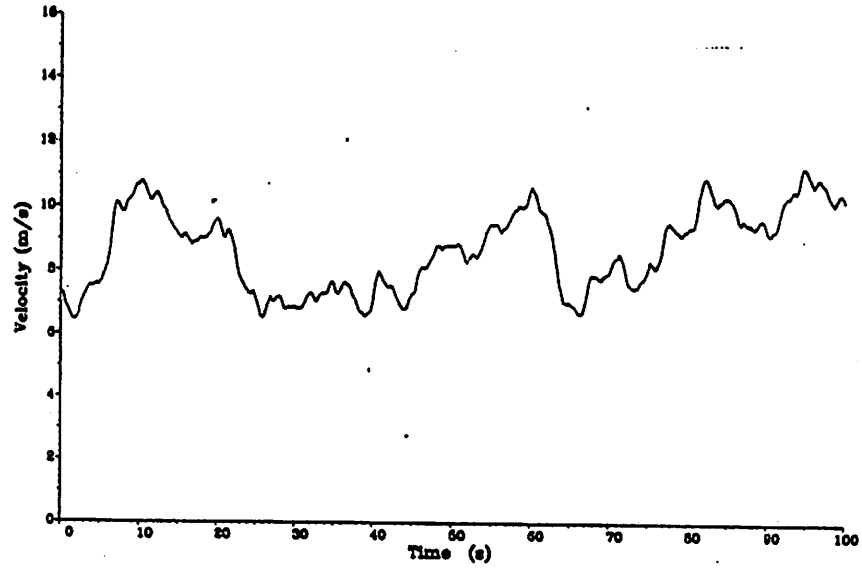


fig. 3

Simulated Time History sig=1.33m/s Harris

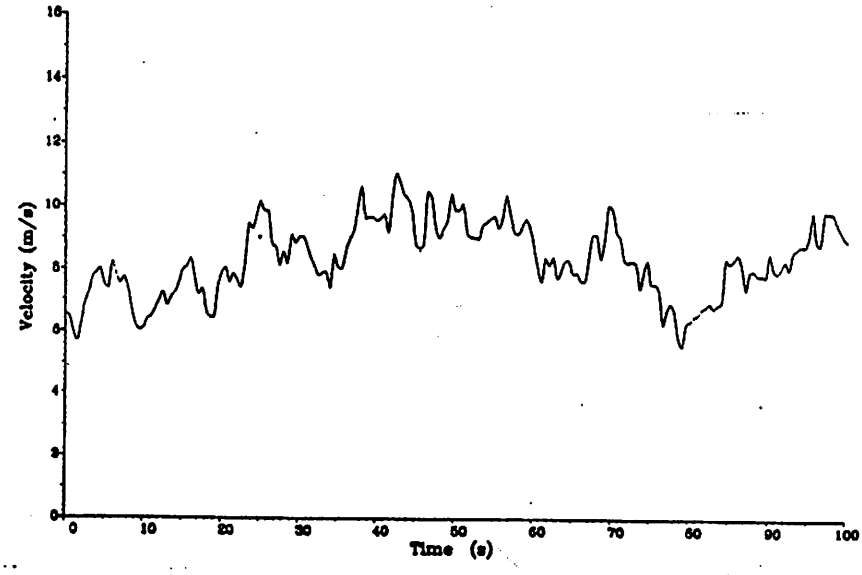


fig. 4

Simulated Time History sig=1.33m/s Smedman

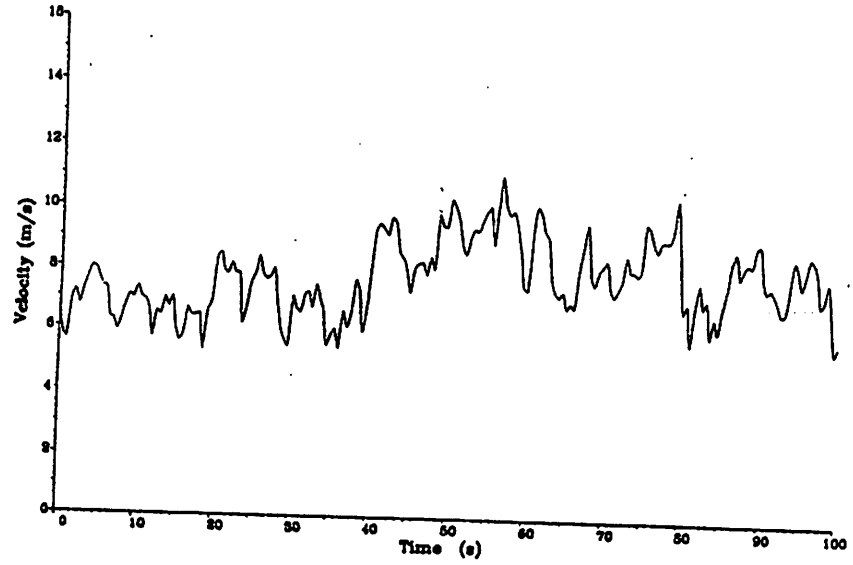

## Wind Spectra z=10.0m z0=.0065m v= 8.3m/s

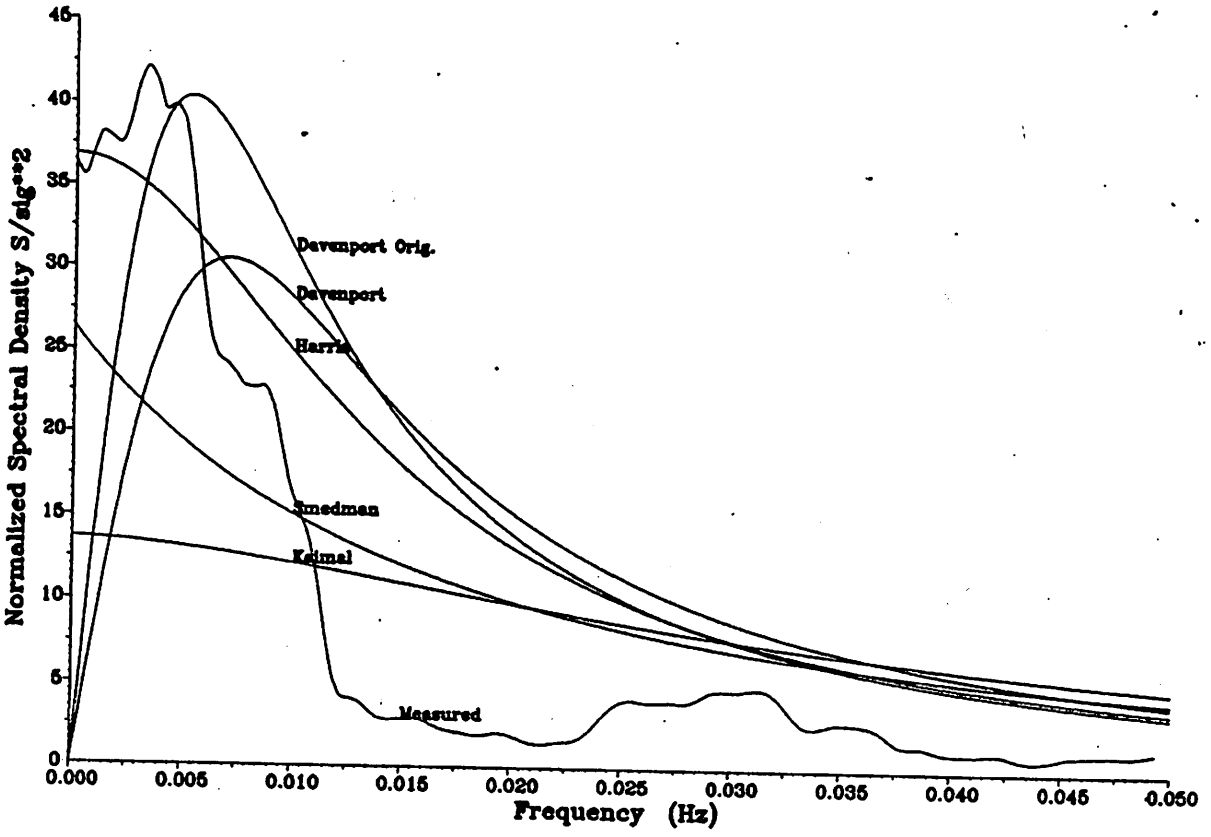


fig. 5

## Auto-Correlation Functions sig=1.33m/s L=76m

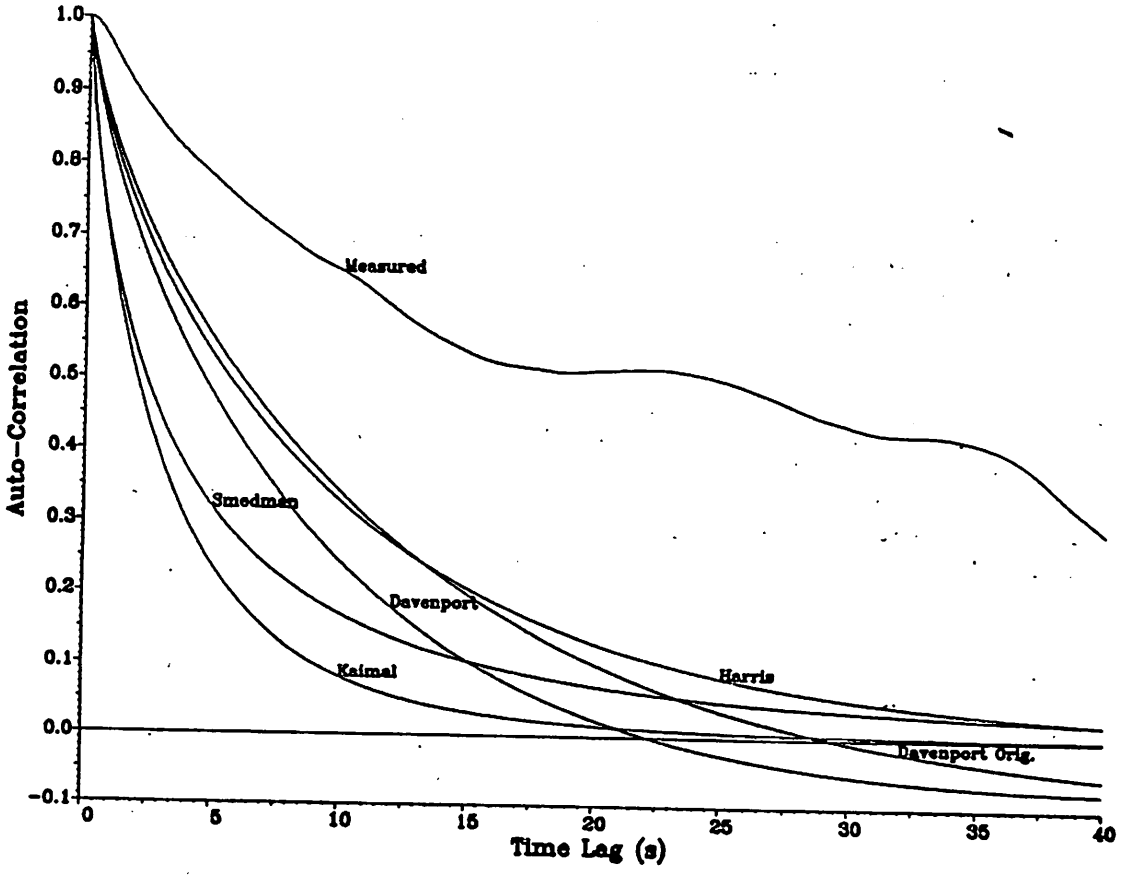


fig. 6

**Auto–Correlation Functions sig=1.33m/s L=76m**

fig. 7

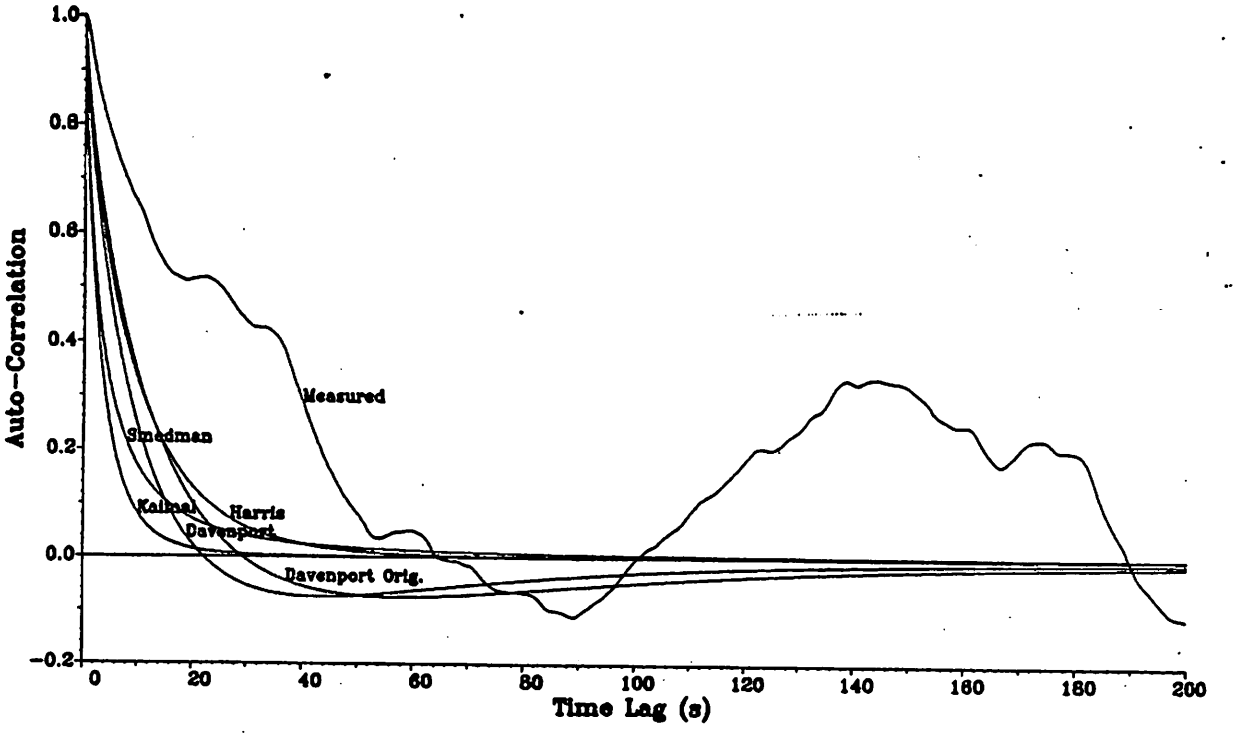


table 1

Measurement 18 : Vz = 13.06 m/s sig. = 1.783 m/s z0 = 0.002 m

Zero Up–Crossing Frequency (Hz) Measured: 0.169

| | Harris | Davenport | Davenport O. | Smedman | Kaimal |
|---|---|---|---|---|---|
| from 0.0 to 4 Hz | 0.4037 | 0.4252 | 0.3964 | 0.3010 | 0.2941 |
| 0.01 to 4 Hz | 0.4633 | 0.4596 | 0.4410 | 0.4411 | 0.4121 |
| 0.0 to 1 Hz | 0.1621 | 0.1711 | 0.1593 | 0.1194 | 0.1174 |
| 0.01 to 1 Hz | 0.1869 | 0.1854 | 0.1778 | 0.1767 | 0.1659 |

Frequency of Maxima (Hz) Measured: 0.803

| | Harris | Davenport | Davenport O. | Smedman | Kaimal |
|---|---|---|---|---|---|
| from 0.0 to 4 Hz | 2.5318 | 2.5316 | 2.5312 | 2.5349 | 2.5307 |
| 0.01 to 4 Hz | 2.5319 | 2.5316 | 2.5312 | 2.5351 | 2.5309 |
| 0.0 to 1 Hz | 0.6354 | 0.6351 | 0.6345 | 0.6368 | 0.6337 |
| 0.01 to 1 Hz | 0.6355 | 0.6352 | 0.6350 | 0.6371 | 0.6340 |

# MODELLING ATMOSPHERIC TURBULENCE

Ann-Sofi Smedman

## 1. INTRODUCTION

In wind energy engineering knowledge of the turbulence characteristics of a proposed or real site is vital. To describe atmospheric turbulence, which is a stochastic phenomenon, one has to make use of statistical models. The calculation methods for predicting the response of a WECS structure to a fluctuating wind have been improved rapidly during the last years and these models can now handle fairly complicated statistical turbulence models as input.

The turbulent fluctuations of the wind can be described by using

a) The energy spectrum of turbulence.
   The spectra of the velocity components depend on the atmospheric conditions as well as terrain, roughness and height above ground.

A very simple method to take these facors into account is shown in this paper.

b) The cross-correlations of the velocity fluctuations at different points in space.
   The correlation of velocity over different spatial separations can be expressed by a spectral correlation coefficient (coherence).

Some examples from measurements in Sweden, which are shown here, support the fact that the coherence of the wind velocity components are depending on the atmospheric integral scale.

## 2. SPECTRA OF ATMOSPHERIC TURBULENCE

During the last few decades appreciable knowledge of atmospheric spectra has accumulated - in particular so for the conditions of flat, homogeneous terrain. In wind energy applications high wind conditions are of particular interest. This simplifies matter, as the atmospheric conditions can then often be considered as nearly neutral. For such conditions i.e. near neutral conditions over flat, homogeneous ground and for heights below, say 100 m,

the following expressions, according to Kaimal et al (1972), are valid:

$$\frac{nS_u(n)}{u_*^2} = \frac{105f}{(1+33f)^{5/3}} \quad (1)$$

$$\frac{nS_v(n)}{u_*^2} = \frac{17f}{(1+9.5f)^{5/3}} \quad (2)$$

$$\frac{nS_w(n)}{u_*^2} = \frac{2f}{1+5.3f^{5/3}} \quad (3)$$

where $S_u(n)$, $S_v(n)$ and $S_w(n)$ are, respectively the power spectra for the longitudinal, the lateral and the vertical wind components and

$n$ = frequency (Hertz)

$f = \frac{nz}{\bar{u}}$ = non dimensional frequency

$z$ = height above the ground (meters)

$\bar{u}$ = the wind-speed (m/s) at z

$u_*$ = the friction velocity (m/s); it can be obtained from the logarithmic wind law:

$$u_* = \frac{k \cdot \bar{u}(z)}{\ln(z/z_o)} \quad (4)$$

where k = von Karman's constant = 0.4 and $z_o$ = the roughness length (meters).

As stated above, these formulas are valid only for flat, homogeneous terrain. In the real world, however the terrain is likely to be more or less inhomogeneous in some respect or other and the stratification is not always neutral. Now when calculation models have been improved it may be time to take these factors into consideration.

In this paper we will not deal with mountainous terrain but instead with relatively flat terrain with highly varying roughness - a typical case being that of a coastal site. At many WECS sites there is a more of less pronounced variation in elevation as well. This causes important modification of the local turbulence structure, even in cases with very slight height relief (see

Smedman and Bergström, 1984). As shown in e.g. Hunt (1980), Panofsky et al (1982) there are methods available to estimate the modification of the turbulence field over gently sloping terrain at least approximately. The reader is referred to these papers for sites on hills or on sloping terrain.

## 3. THEORETICAL FRAMEWORK

In 1982 two groups of scientists (Panofsky et al, 1982 and Högström et al, 1982) discovered independently of each other a fundamental phenomenon which has been termed *the spectral lag* and *local equilibrium* effect. In essence it means that the high frequency turbulent fluctuations adjust rapidly to a 'new' environment, i.e. when the air passes from an area characterized by a certain roughness $(z_o)_1$ to an area with different roughness $(z_o)_2$ - as an example $(z_o)_1$ can be less than a millimetre, in the case of a water surface and $(z_o)_2$ almost a metre, for a forest; as seen from Eq (4) this has great implications on the friction velocity - whereas the low frequency fluctuations (the big eddies) adjust only very slowly to the new environment, thus giving rise to *spectral lag*. Fig. 1 illustrates this. The dots in the two figures represent spectral measurements taken at 14 m above ground at the site Kalkugnen in Sweden - see Fig. 3. The spectra represent cases with the wind coming from the north, wich means that the air has long traveled over the sea when it encounters the relatively rough land area between the shoreline and the meteorological mast, about 200 m inland. The measurements have been obtained with a wind vane based three-axial hot-wire anemometer instrument (see Högström 1980). The friction velocity used for normalization in the diagram, $u_{*\ell}$, is the value $u_*$ attains locally at the site. The curves drawn in the two diagrams have been obtained from Eq (1) and (3). As clearly seen from Fig 1 the curves that are valid for the flat, homogeneous case agree very well with the measurements in the high frequency range ($n > 1$ Hz) but come much above the measurements in the low frequency range. Thus we see the local equilibrium in the high frequencies and the spectral lag in the low frequencies - the spectra behave as if they "remember" the conditions over the flat sea surface in this spectral range. As seen in the next Section it is possible to obtain the spectra dispayed in Fig. 1 from simple physiographical data of the site. But before doing that it is necessary

to introduce the concept of *internal boundary layers* (IBL).

When air flows from an area characterized by a certain $z_0$-value, $(z_0)_1$ say, to an area with different $z_0$-value, $(z_0)_2$ say, its turbulent characteristics are being modified gradually, the influence of the 'new' surface spreading from the ground upwards in a progressive way, as shown schematically in Fig. 3. The sloping line in the Figure indicates the boarder between the lower, modified internal boundary layer and the upper layer which as not yet been modified. Thus this outer layer is in principle fully charcteristic of the $(z_0)_1$-surface - i.e. spectra measured over land at the site M at a height z larger than h are expected to look exactly teh same as the spectra measured at that height at a point situated above the sea. Spectra measured at the land site M at heights lower than h are, however, modified in the manner described above, i.e. they exhibit spectral lag and local equilibrium. From this it is seen that we need a way to determine the height of the IBL, h as a function of distance from the line of discontinuity, see next Section.

## 4. THE METHOD TO CALCULATE SPECTRA IN AREAS WITH VARYING ROUGHNESS

Consider first the situation schematically depicted in Fig. 3, and let M be the proposed WECS site. In conclusion of the previous Section, in order to arrive at a practicable method to calculate wind spectra at relevant heights above the ground z for this site, we have to consider the following points:

. We must get a method to determine the height of the IBL at M.

When we have this information:

. *If* $z > h$: Spectra can be calculated with the aid of Eq (1) - (4) with $z_0 = z_{01}$

. *If* $z < h$: We must devise a method to construct a relevant spectrum characterized by spectral lag and local equilibrium. As will be seen below, this can be done by matching one spectrum for the high frequency parts and one for the low frequency parts.

For the determination of the rate of growth of a neutral internal boundary layer, we will use a simple method originally suggested by Pasquill (1972), i.e. the height h is given as a power law of the distance from the discontinuity x:

$$h = a \cdot x^b \qquad (5)$$

Empirical values of the parameters a and b are presented in Table I as a

function of the roughness length of the rougher of the two surfaces at a discontinuity. Relevant $z_0$-values for various types of terrain can be obtained from a table in Smedman-Högström and Högström (1978), which was originally presented in a report (ESDU 72026, 1972).

In order to calculate u-, and v-spectra for the case $z < h$ we adopt the following proceedure (a similar proceedure can be applied to w-spectra, but it requires certain modification, and is not given here).

For the *high frequency part*, i.e. for $n > 0.05$ Hz, we apply Eq (1) and (2) with $u_*$ determined with Eq (4) and the $z_0$-value relevant for the site M, i.e. $z_0 = z_{02}$ (cf. Fig. 3).

For the *low frequency part*, i.e. for $n < 0.01$ Hz, we use the same Eq-s but with $u_*$ being determined (with Eq (4)) for a surface with $z_0 = z_{01}$. We then obtain two curve parts which can be easily connected by hand (see the example in next Section).

Now we can apply the above method to a more general case. Fig. 4 illustrates a generalized geographical situation. Here we can identify three sectors with very different characteristics. But for each of these sectors we can apply the method as described above, i.e. we must determine relevant $z_0$-values for every type of surface - farmland, sea and forest in this particular example, we must also determine the distances from the WECS site to the various discontinuities.

## 5. AN EXAMPLE ILLUSTRATING THE APPLICATION OF THE METHOD DESCRIBED IN SECTION 4

Figure 2 shows the WECS site Kalkugnen in Sweden. With northerly winds we have the situation depicted in Fig. 5. At about 170 m distance from the shoreline there was a meteorological tower where turbulence measurements were taken at two heights: 14 m and 36 m above the ground (Smedman, 1983).

In this case, when we have access to turbulence measurements, we get a direct estimate of $u_* = \sqrt{-\overline{u'w'}}$ for the two measuring levels. For 36 m we obtain the following data:

$\bar{u} = 7.1$ m/s

$u_* = 0.26$ m/s

$z = 36$ m

Putting this into Eq (4) enables us to determine $z_0 = 6.5 \cdot 10^{-4}$ m. For the lower measuring height we get:

$\bar{u}$ = 5.0 m/s

$u_*$ = 0.50 m/s

z = 14 m

and we deduce (from Eq (4) that $z_0$ = 0.26 m/s. These $z_0$-values are clearly indicative of the sea surface ($z_0 = 6.5 \cdot 10^{-4}$ m) and the clearing ($z_0$ = 0.26 m) respectively. Applying Eq (5) and Table I with $z_0$ = 0.26 m gives:

h = 31 m

which thus shows that the upper measurements should be outside the IBL. We thus expect Eq (1) to hold for the longitudianl spectrum, with $u_*$ being determined from Eq (4) with $z_0 = 5 \cdot 10^{-4}$ m. Fig. 6A shows the normalized curve (Eq (1)) and Fig. 6B the actual spectrum $nS_u(n)$, the curve in that Figure being obtained from the curve in Fig. 6A by multiplication with $u_*^2$, where this quantity has been obtained from Eq (4). The dots in Fig. 6B are the actually measured spectral points. The agreement is very good.

In order to get spectra for the lower measuring height, 14 m, we apply the matching proceedure. In Fig. 7A the curve a - a' is obtained with Eq (1) and the $u_*$-value derived with Eq (4) with $z_0$ = 0.26 m. In accordance with the proceedure outlined above we terminate, however, this curve at n = 0.05 Hz. Curve b has been calculated with Eq (1) and with $u_*$ obtained from Eq (4) with $z_0 = 6.5 \cdot 10^{-4}$ m. We terminate this curve at n = 0.01 Hz and connect the curves a and b by hand. Fig. 7B shows the curve a - b - c and the measured spectral points. The agreement is excellent.

## 6. THE COHERENCE FUNCTION

Calculations of loads, stresses etc. of WECS also require knowledge of the statistical relations between the wind velocity components at two points separated in space. The most common way to describe this relation is, as mentioned above, to use the coherence function.

The coherence is defined

$$\mathrm{Coh}(n) = \frac{Co^2(n) + Q(n)}{S_1(n) \cdot S_2(n)} \qquad (6)$$

where

n = frequency

Co = cospectrum for velocity components at two points in space

Q = quadrature spectrum for velocity components at the same two points in space

s = energy spectrum in one point

The coherence approaches unity when $n \to 0$ (big turbulence elements) and it falls off rapidly when the frequency increases (small turbulence elements).

Davenport (1967) suggested that the coherence can be expressed as an exponential function of frequency, wind-speed ($\bar{u}$) and the distance between the points in space (D).

$$Coh(D,n) = e^{-a \cdot n \cdot D/\bar{u}} \qquad (7)$$

where a is an empirical constant which has to be determined.

The coherence can be calculated for the three components of the wind (u, v, w) in three directions (x, y, z). That will give us nine empirical constants i.e. for lateral separation

$a_y^u$, $a_y^v$, $a_y^w$

The values of these constants vary very much between different investigations (5 - 70) depending on the stability of the atmosphere, height above ground and the roughness parameter $z_o$.

Fig. 8 shows vertical coherence measurements performed at Gränby, Uppsala. The data fit an exponential curve well, and the constant ($a_z^u$) is determined to 20.

There are, however, a lot of cases where the coherence decay is not exponential. Fig. 9 shows a case where the decay is much faster. The measurements are taken at the WECS test site Kalkugnen, about 150 km north of Stockholm, and the coherence is calculated for a vertical separation of 22 m for the u-component.

However, 1979 Kristensen and Jensen (KJ) presented a theoretical model for isotroptic turbulence where they express the coherence as a function of D/L where L is the so called integral scale, defined as

$$L = \bar{u}/2\pi n_{max} \qquad (8)$$

$n_{max}$ is the frequency where the longitudinal wind spectra has its maximum. In the atmosphere the integral scale (L) varies with the stratification of the atmosphere as well as the height above ground and is usually in the range 10 - 1000 m.

KJ show that the coherence has an exponential decay only if D<<L, otherwise the coherence is much lower and will not approach unity. Fig. 10 shows two of their calculated curves (D/L = 0 and D/L = 0.5) for lateral separation, together with measurements from Kalkugnen (D/L ≈ 1). The agreement between the curves is very good. For vertical separation they find the same dependence of D/L in the coherence. Their theoretical curves for the three wind components and for D/L = 0.50 (Fig. 11A) can be compared with measurements taken at Maglarp (Fig. 11B). The general behaviour of the curves agree well.

As stated above the integral scale and thus the coherence varies strongly with the stratification in the atmosphere. It is in this case quite necessary to take the temperature variation with height into account and not always presume neutral condition.

## 7. CONCLUSIONS

Analytical expressions for turbulence spectra valid for flat homogeneous terrain during neutral condition have been widely used as input to different calculations of WECS response to a fluctuating wind field. Now perhaps it is time to use a slightly more complicated turbulence model as input. Somehow one must take local surface irregularities, such as water/land discontinuities, minor hills, escarpments and variations of surface roughness in different directions, into account.

The stratification of the atmosphere will influence the shape of the velocity spectra as well as the total variances and the integral scale.

Thus the coherence function will vary very much according to stability. For a certain distance of separation the coherence decay can i.e. be exponential in unstable condition where L is large but be almost zero during very stable condition.

ACKNOWLEDGEMENT

The field experiment was sponsored by the National Swedish Board for Energy Source Development (NE contract No 5061 472). The analysis effort was supported by Kraftverksföreningens utvecklingsstiftelse VAST and by the National Energy Administration Sweden (contract No 506226-3).

REFERENCES

Davenport, A.G. 1967: 'The dependence of wind loads on meteorological parameters'. Proceedings from Int. Res. Sem. on Wind effects on Buildings and Structures, Ottawa, Canada, Sept 1967.

ESDU 72026:1972 (Engineering Science Data Item Number 72026) 'Characteristics of wind speed in the lower layers of the atmosphere near the ground: strong winds'.

Hunt, J.C.R. 1980: 'Wind over hills'. Survey paper for NOAA-NSF Workshop, Boulder, Colorado.

Högström, U., Enger, L. and Knudsen, E. 1980: 'A complete system for probing the detailed structure of atmospheric boundary layer flow'. Report No 60. Meteorol. Dept., Uppsala, Sweden.

Högström, U., Bergström, H. and Alexandersson, H. 1982: 'Turbulence characteristics in a near neutrally stratified urban atmosphere'. Bound. Layer Met. 23, p 449-472.

Højstrup, J. 1981: 'A simple model for the adjustment of velocity spectra in unstable conditions down stream of an abrupt change in roughness and heat flux. Bound. Layer Meteor. 21, p 344-356.

Kaimal, J.C., Wyngaard, j.C., Izumi, Y. and Coté, O.R. 1972: 'Spectral Characteristics of Surface Layer Turbulence'. Quart. J. Roy. Meteorol. Soc. 98, p 563-589.

Kristensen, L., Jensen, N. 1979: 'Lateral coherence in isotropic turbulence and in neutral winds'. Bound. Layer Meteor. 17, p 353-373.

Panofsky, H.A., Larko, R., Lipschulz, R., Stone, G. 1982: 'Spectra of velocity components over complex terrain'. Quart. J. Roy. Meteorol. Soc. 98, p 215-230.

Pasquill, F. 1972: 'Some aspects of boundary layer description'. Quart. R. Roy. Meteorol. Soc. 98, p 469-494.

Smedman, A. and Högström U. 1978: 'A pracitcal method for determining wind frequency distributions for the lowest 200 m from routine meteorological data. J. of Appl. Meteorol. Vol 17, No 7, p 942-954.

Smedman, A. 1983: 'Some observations of turbulence structure near a wooded coast line. Report No 68. Meteorol. Dept., Uppsala, Sweden.

Smedman, A. and Bergström, H. 1984: 'Flow characteristics above a very low and gently sloping hill. Bound. Layer Meteorl. 29, p 21-37.

Table I. The constants a and b in Eq(5) given for certain intervals of the roughness length parameter $z_o$ for the rougher of the two surfaces of discontinuity.

| $z_o$ | a | b |
|---|---|---|
| > 1.5 | 0.83 | 0.73 |
| 0.5 - 1.5 | 0.73 | 0.75 |
| 0.2 - 0.5 | 0.55 | 0.79 |
| 0.06 - 0.2 | 0.38 | 0.83 |
| < 0.06 | 0.20 | 0.87 |

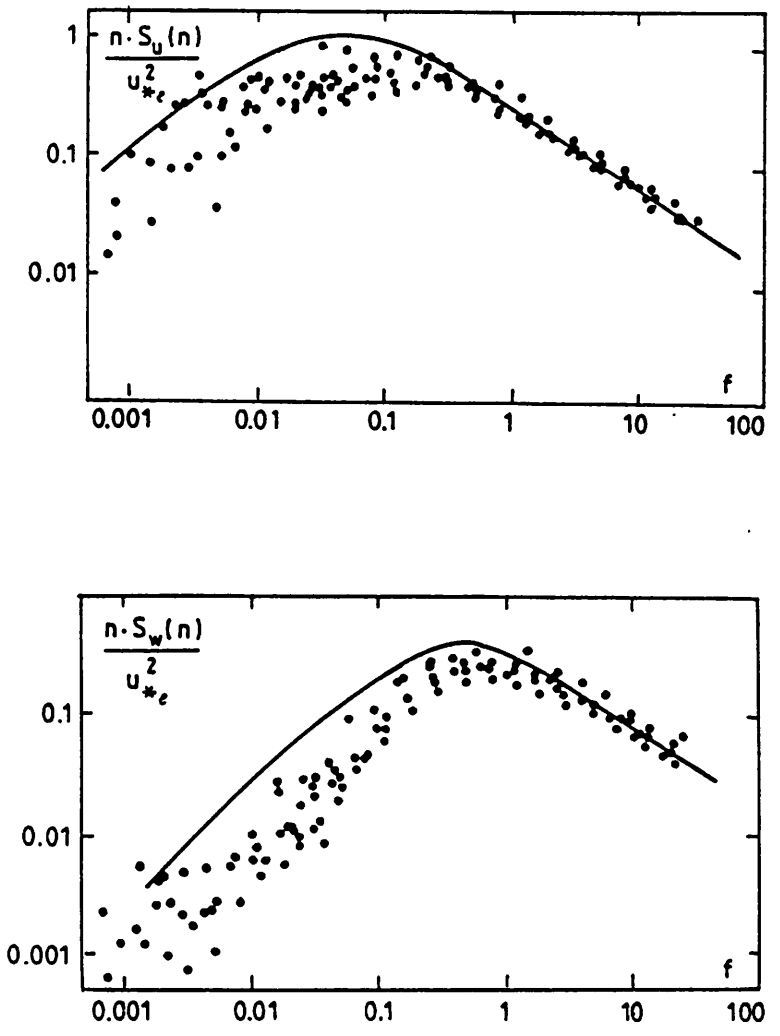


Figur 1. Normalized spectra for the longitudinal component $nS_u(n)$ and the vertical component $nS_w(n)$ respectively. The dots are measurements at 14 m from Kalkugnen. The curves are Eq-s (1) and (3).

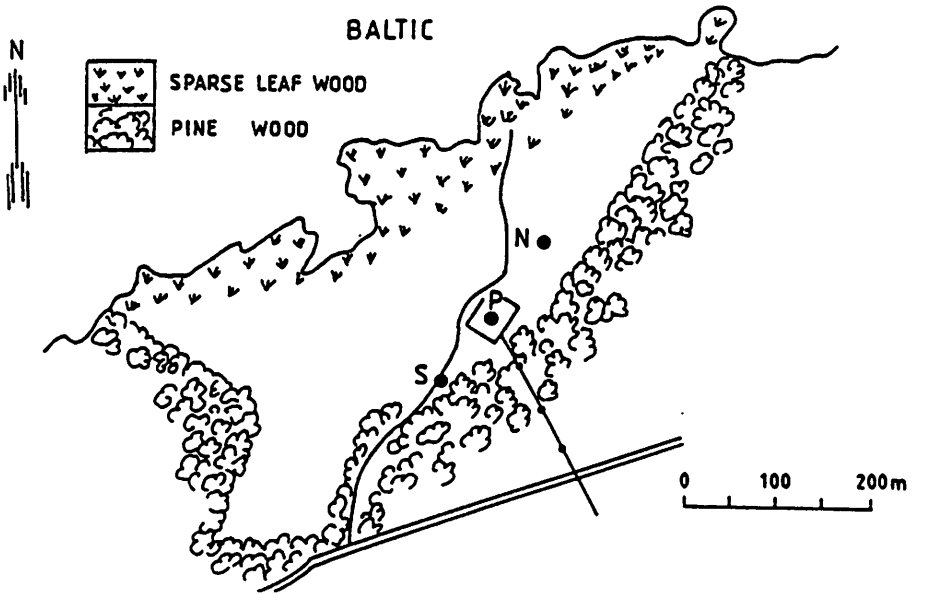


Figure 2. Map of the WECS site Kalkugnen. P is the 63 kW wind turbine. The meteorological measurements discussed in this paper have been taken in the mast at N.

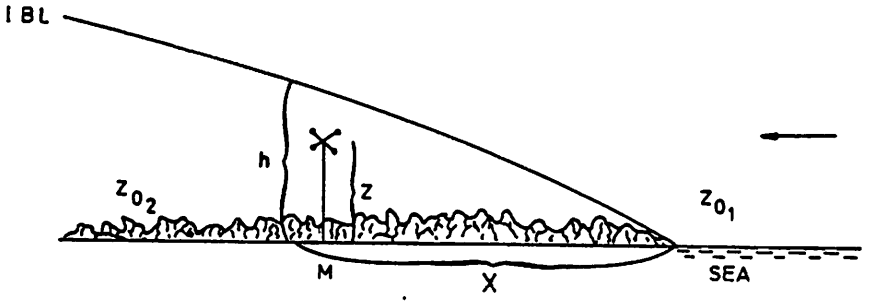


Figure 3. Sketch showing the gradual formation of an internal boundary layer as a result of a discontinuity in surface roughness.

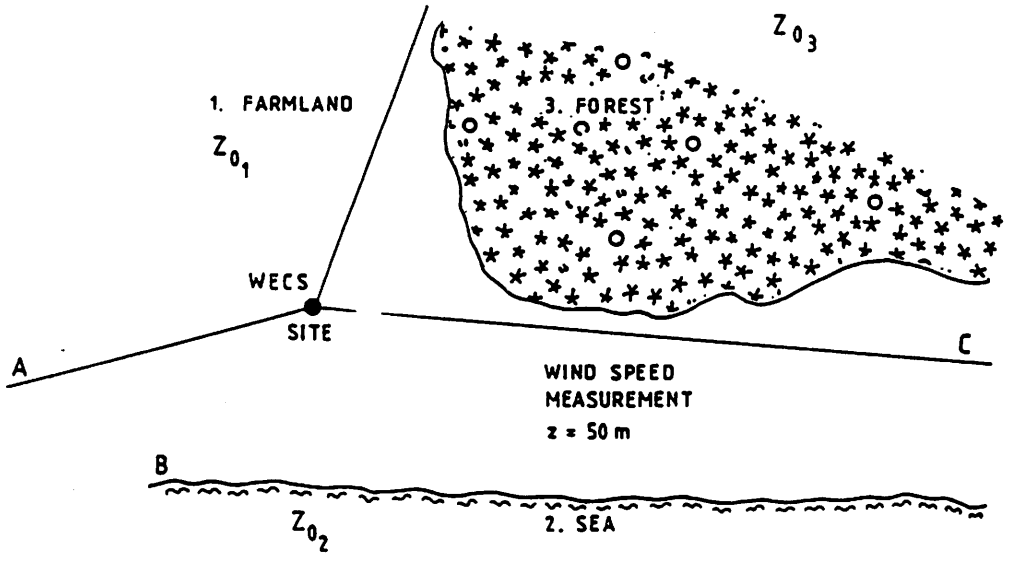


Figure 4. Schematic map illustrating a complex roughness configuration around a WECS site.

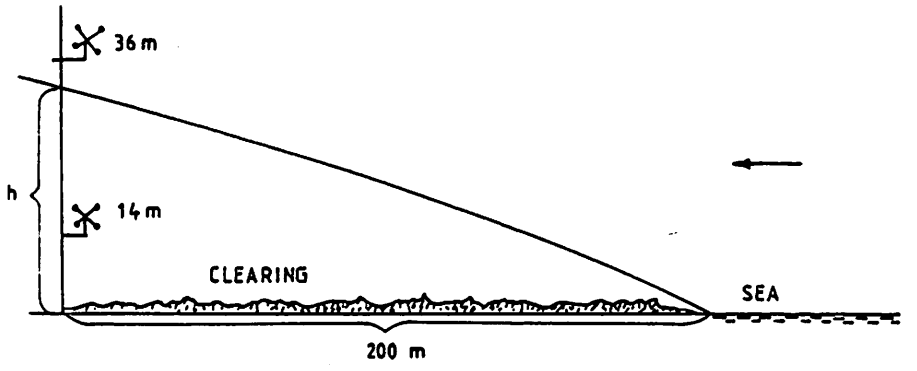


Figure 5. Schematic cross section at the Kalkugnen site (cf. Fig.2) with northerly winds. At the measuring site 'N', 170 m from the shoreline the height of the IBL has been estimated to 31 m with Eq (5). It means that the measurements at 14 m are taken well in the IBL but the measurements at 36 m represent the overlaying marine boundary layer.

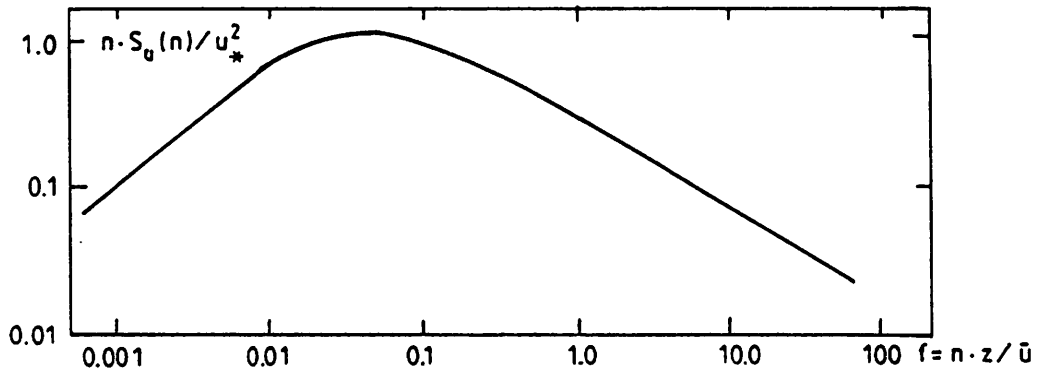


Figure 6A. The normalized longitudinal spectrum according to Eq (1).

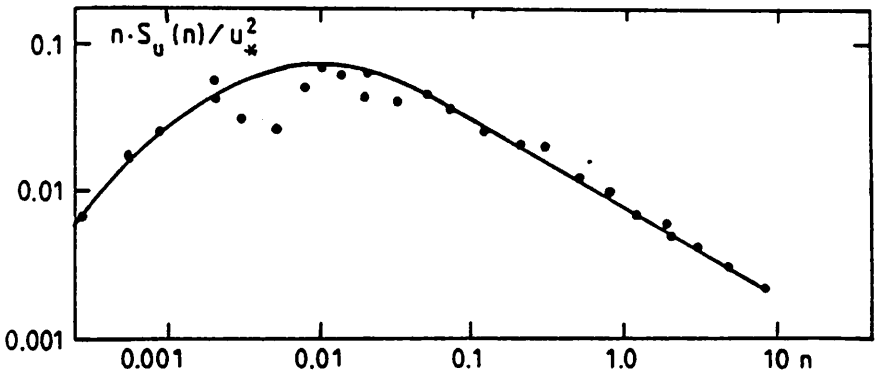


Figure 6B. The curve has been obtained from Fig. 6A by multiplication of the ordinate with the $u_*^2$-value measured at 36 m at Kalkugnen and by transforming the abscissa to ordinary frequency n. The dots are spectral measurements at 36 m.

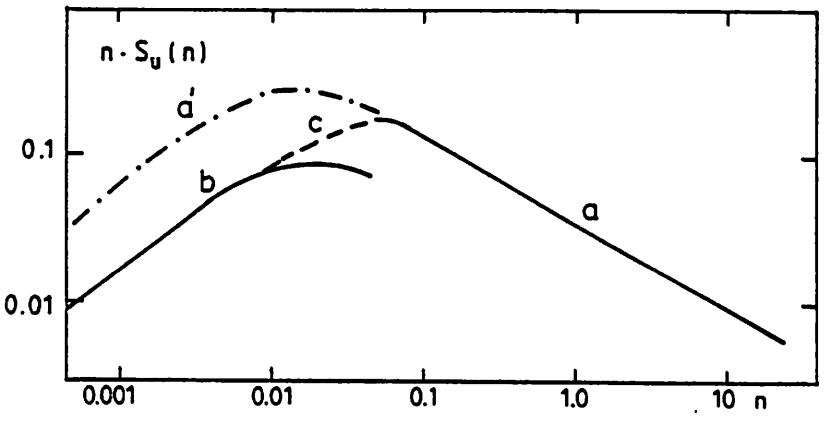


Figure 7A. Example from Kalkugnen showing application of the matching proceedure - see the text for details. Height 14 m.

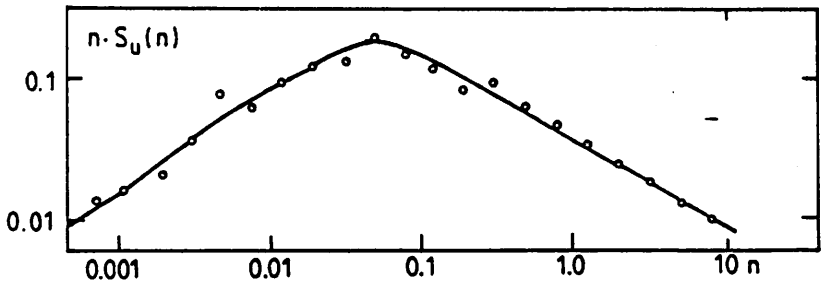


Figure 7B. The curve is the b-c-a curve of Fig. 7A. The dots are spectral measurements at 14 m at Kalkugnen.

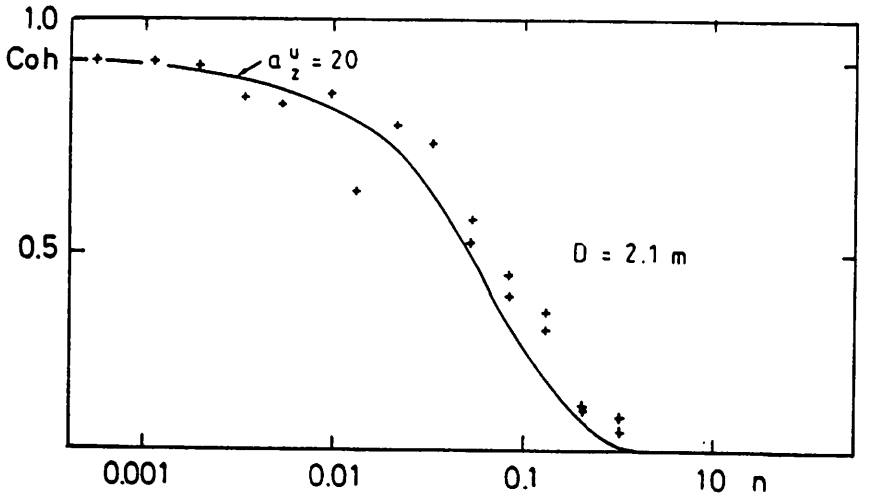


Figure 8. Vertical coherence measurements performed at Gränby, Uppsala for the u-component. D = 2.1 m

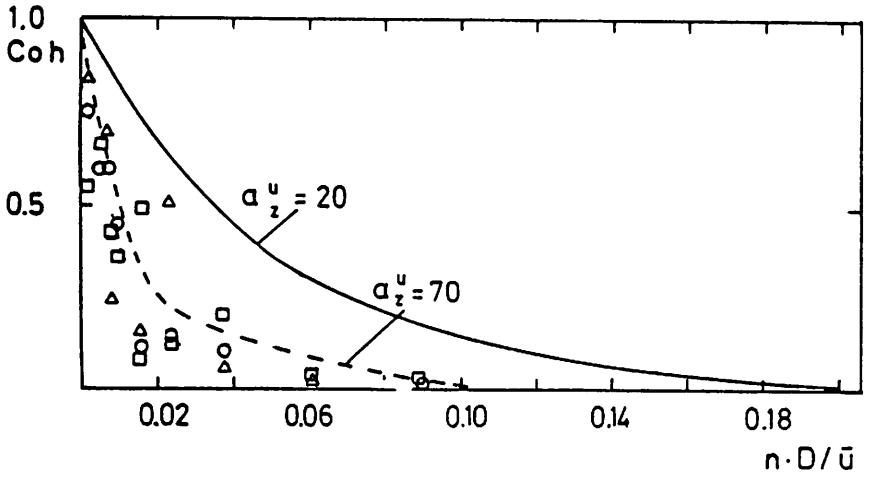


Figure 9. Vertical coherence measurements performed at Kalkugnen for the u-component. D = 22 m.

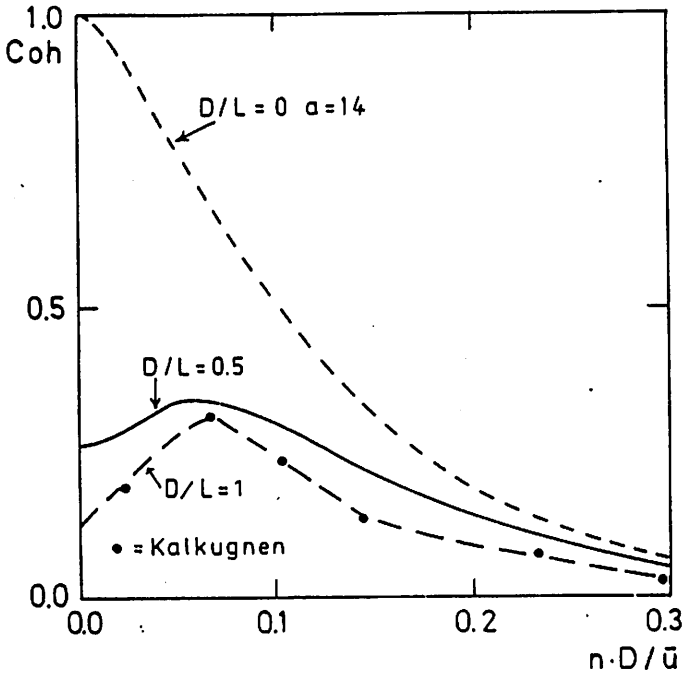


Figure 10. Calculated lateral coherence function for D/L = 0 (---) and D/L = 0.5 (—) together with a measured curve for D/L ≈ 1 (•••).

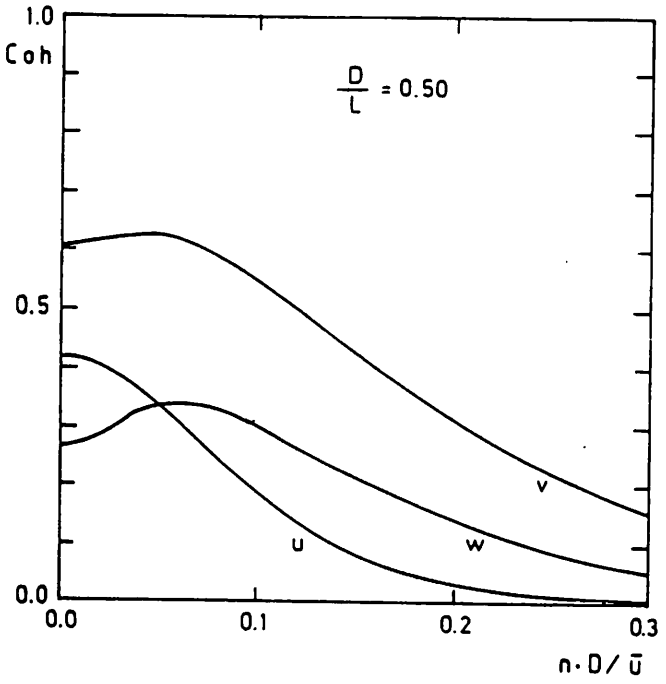


Figure 11A. Calculated coherence for vertical separation (D/L = 0.5) for the three components (u, v, w).

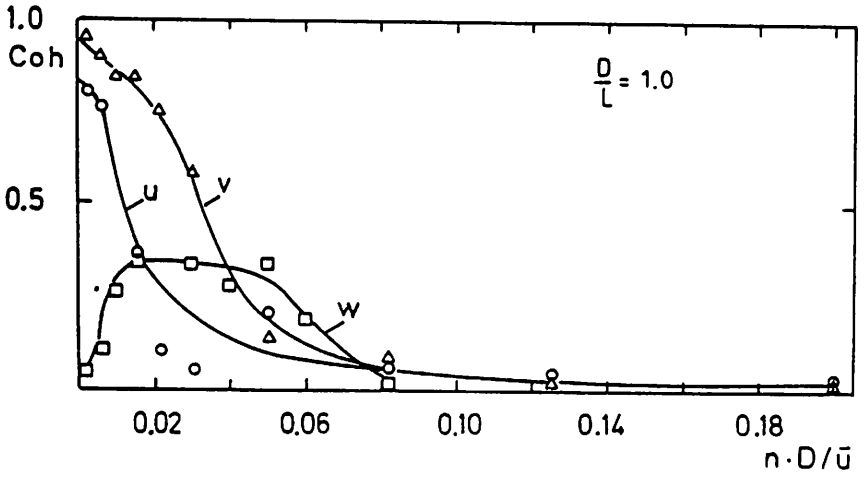


Figure 11B. Measured coherence for vertical separation (D/L ≈ 1) at Maglarp for the three components (u, v, w).

# A GENERALIZED METHOD TO DERIVE GUST STATISTICS FOR DYNAMIC-RESPONSE ANALYSIS OF SMALL WINDTURBINES

P.E.J. Vermeulen

The analysis of the dynamic behaviour of wind turbines or wind-turbine components is most often carried out through simulations in the time domain. Consequently, also a description of the wind input is needed in the time domain.
Such a description can either be deterministic, in the form of a "gust", or be a realisation of a stochastic wind speed signal.
The first way of description is most often used to determine extreme design loads while the latter is often used to analyse the stability and control behaviour of the total system.

At MT-TNO a method has been developed which can be used to derive the properties of a deterministic wind gust on a statistical sound basis.
The method comprises the following items:
- use is made of a complete model of the atmospheric turbulence;
- the lateral and vertical structure of turbulence is taken into account by integrating the cross-power spectrum over the rotor area. This results in a spectrum of the rotor averaged wind speed fluctuations;
- statistical techniques are used to derive from the spectrum the amplitude distribution of the wind speed; the zero crossing rate of the wind speed signal and the distribution of the wind speed acceleration;
- from the above mentioned parameters a time-domain description of a wind gust is constructed, using specifications for terrain roughness, wind speed and exceedance probabilities of the amplitude and acceleration of the wind speed.

The method has been used to derive "gusts" for the determination of extreme loads and fatigue loads for a number of wind turbine projects in the Netherlands.

Jorgen Hoystrup

# Measurements of Lateral Coherence at Nibe

## Outline

- How good does the description of turbulence have to be?
- Turbulence: A function of many variables!
- Lateral Coherence
- Turbulence structure of wakes

## The variability of turbulence

- Neutral conditions

  Diabatic conditions

  -- Velocity profiles
  -- Length scales
  -- Spectra

- Homogeneous terrain

  -- Roughness changes
  -- Hills
  -- Buildings, other wind turbines

- More simplifications

  Isotropy, gaussian processes
  Taylor hypothesis

# Lateral coherence

Davenport (1961) Vertical coherence:

$$Coh_3 = \exp\left(-a \frac{f D_3}{u}\right)$$

$$= \exp\left(-a \frac{D_3}{\lambda_{bar}}\right)$$

Pielke, Panofsky (1970) used same expression for streamwise and lateral separations.

$$Coh_i(D_j) = \exp\left(-a_{ij} \frac{f D_j}{u}\right)$$

Nice, simple model, just one problem: $a_{ij}$'s not constants

lateral coherence only:
(neutral conditions).
only a function of $D_2/z$
(Shiotani, Iwatani 1979,
Kristensen et al 1987,
Panofsky + Dutton 1984)

$$a_{12} = 28\left(\frac{D_2}{z}\right)^{0.45}, \text{ Iwatani}$$

$a_{12} \to 14$ for $D_2/z \ll 1$
$a_{12} \to 50$ for $D_2/z \gg 1$ } Kristen

Kristensen + Jensen:

$$f\frac{D_2}{u} \longrightarrow \left(\left(\frac{D_2}{L}\right)^2 + \left(\frac{2\pi f D_2}{u}\right)^2\right)^{1/2}$$

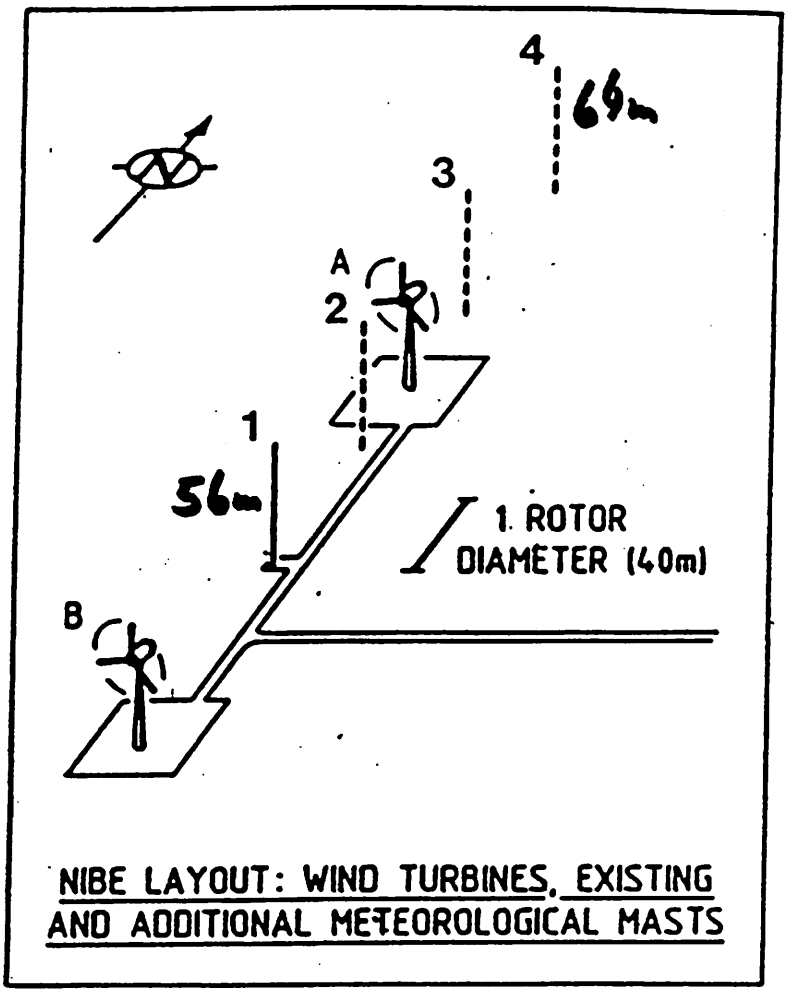


NIBE LAYOUT: WIND TURBINES, EXISTING AND ADDITIONAL METEOROLOGICAL MASTS

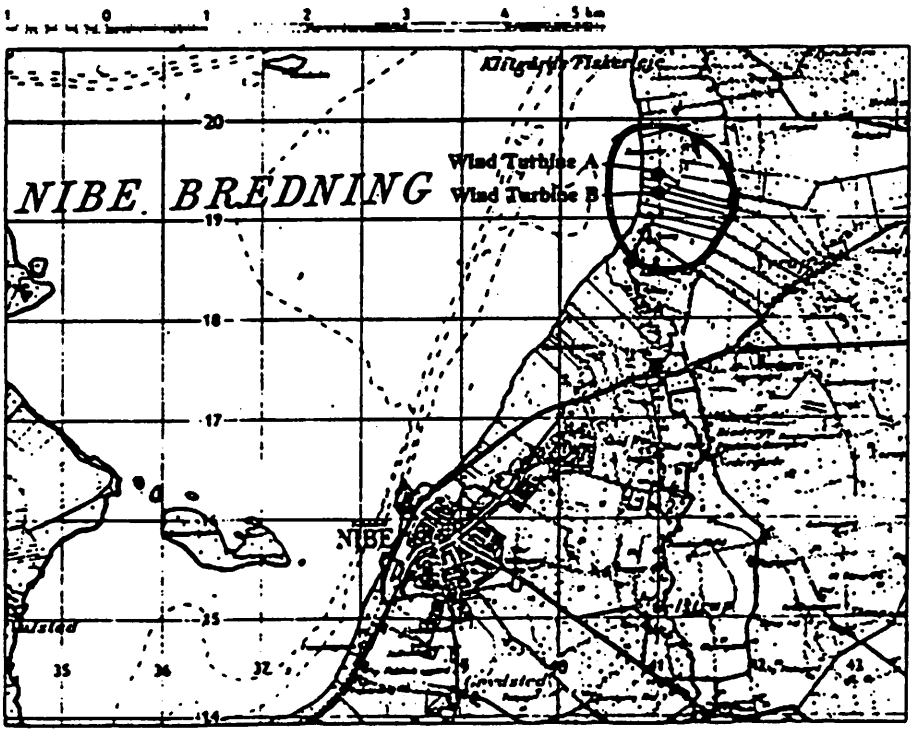

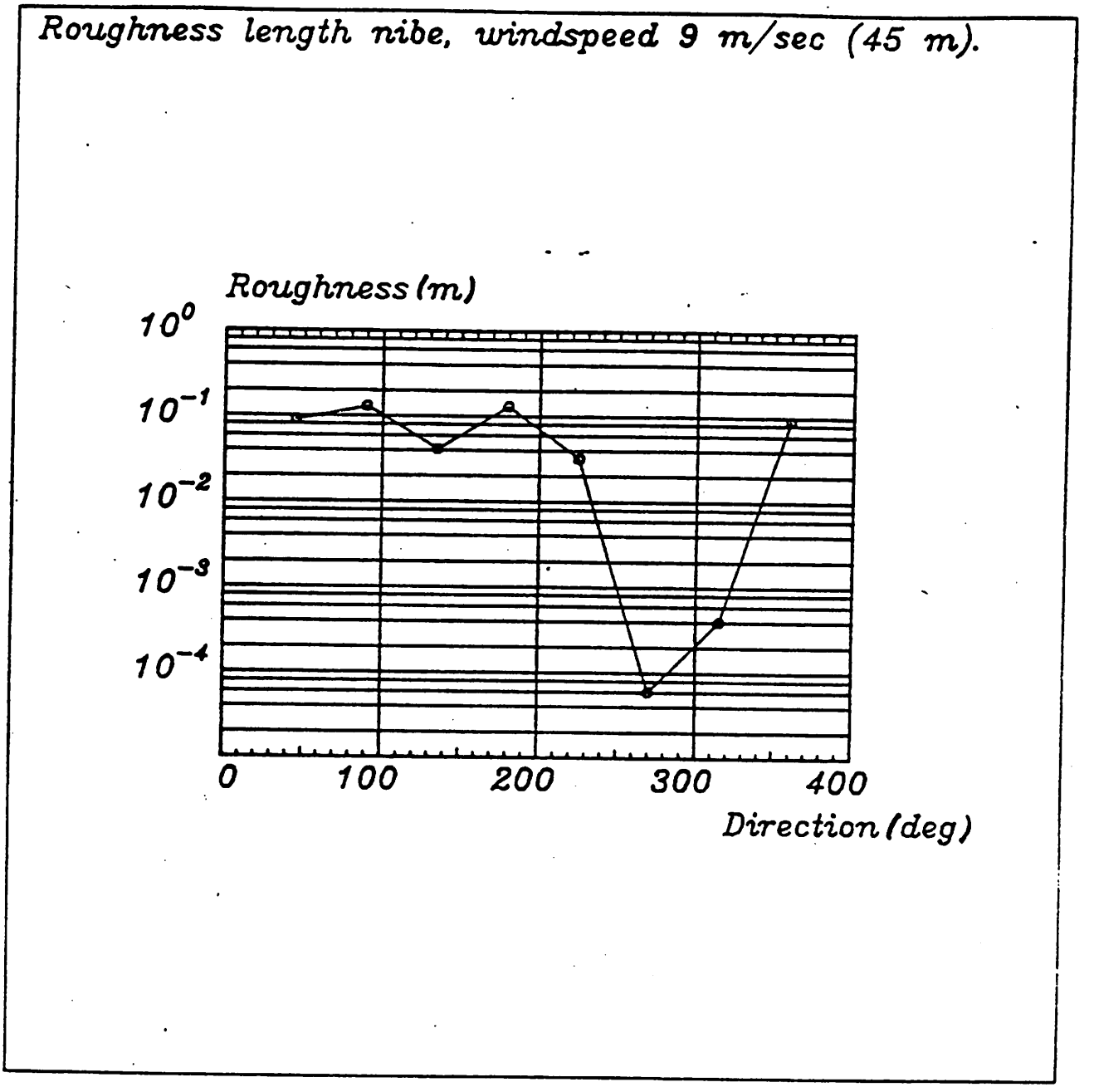


Fig. 2.
Measured roughness lengths at the Nibe site based on velocity profiles from three years of data (1981-1983). The data shown refer to situations where the wind speed at 45 m was in the range 7.5 - 10.5 m/sec. Data with the wind turbines running upstream of the anemometers have been excluded.

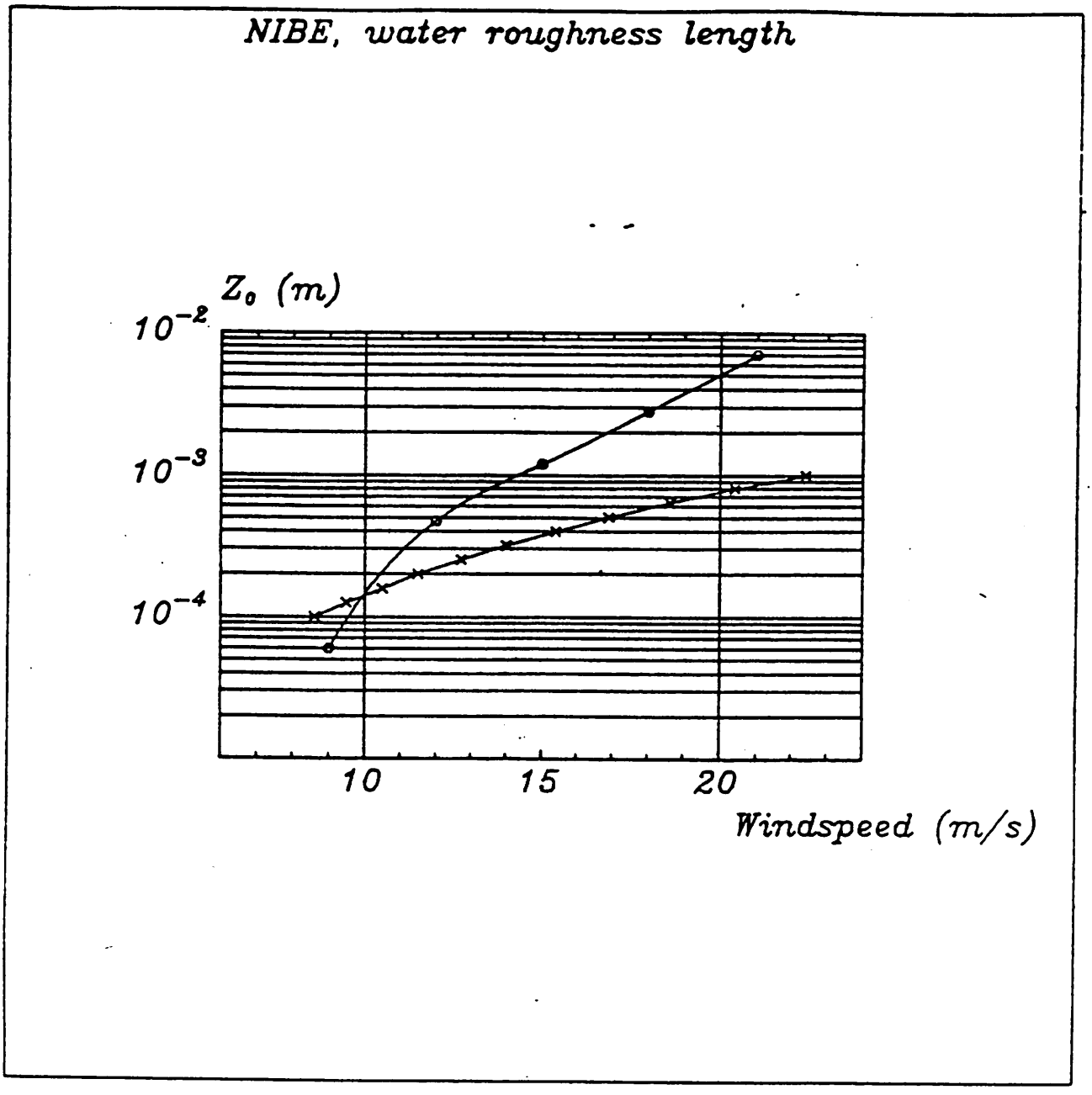


Fig. 3.
Measured roughness length as a function of wind speed for the 45 degree west sector. Measured values are denoted by "o". The curve denoted by "x" is the water roughness length as calculated using Charnocks formulation:

$$z_o = c \frac{u_*^2}{g} \quad , \quad g = \text{gravitational acceleration}$$

(Charnock 1955) with a value of a = 0.014 (Garratt 1977).

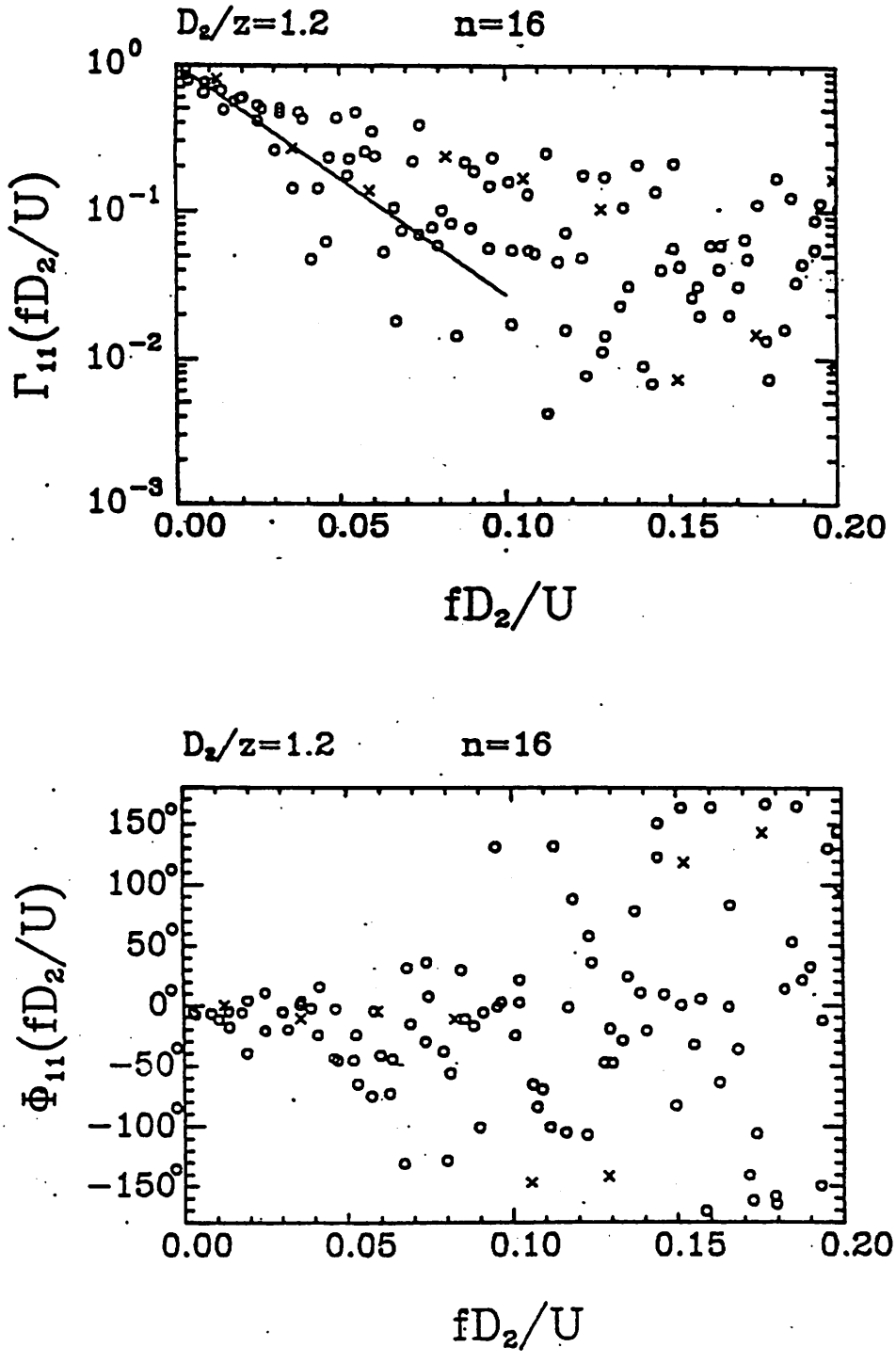


Fig. 6.
The Nibe 4 (o) and Nibe 5 (x) coherence and phase data for $D_2/z$ = 1.2. The straight line in the coherence plot is the exponential coherence model with a decay parameter of 36.

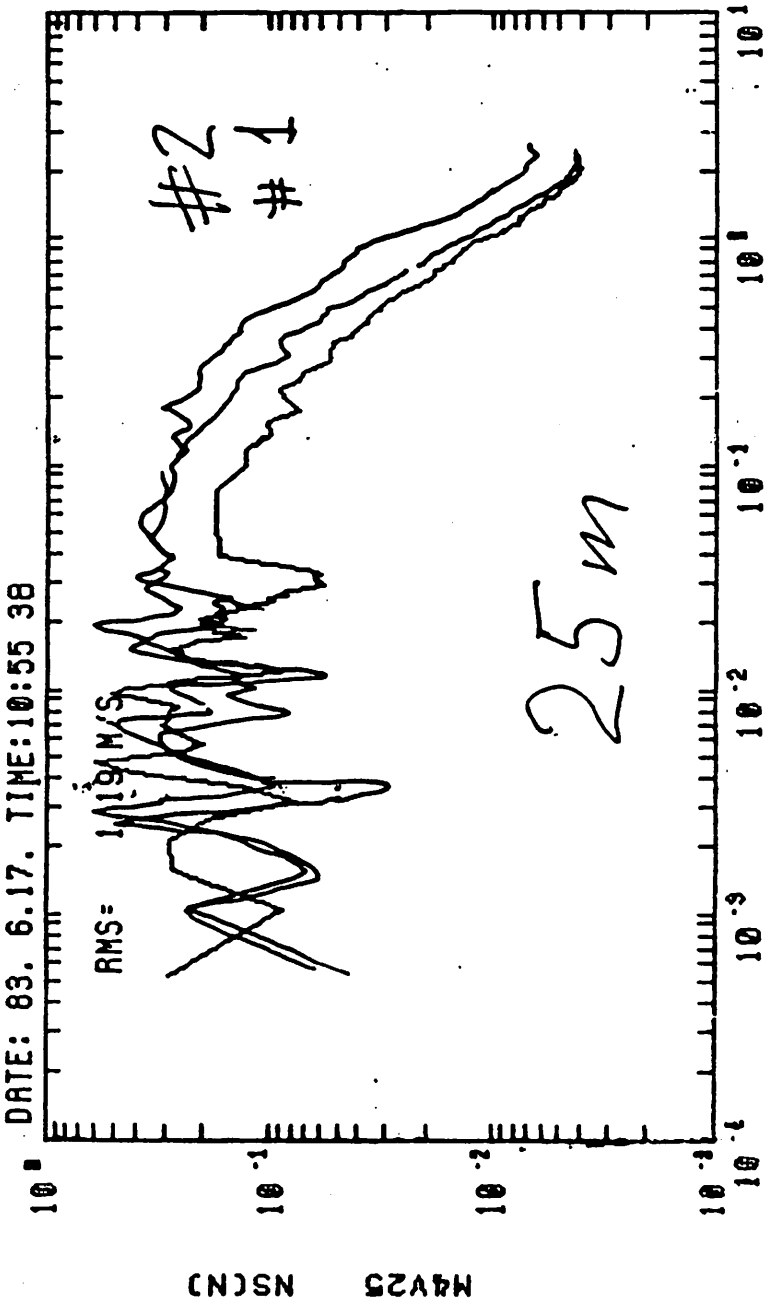
M4V25 NSCN3
DATE: 83. 6.17. TIME:10:55 38
RMS= 1.19 M/S
#2
#1
25m
FREQUENCY [HZ]

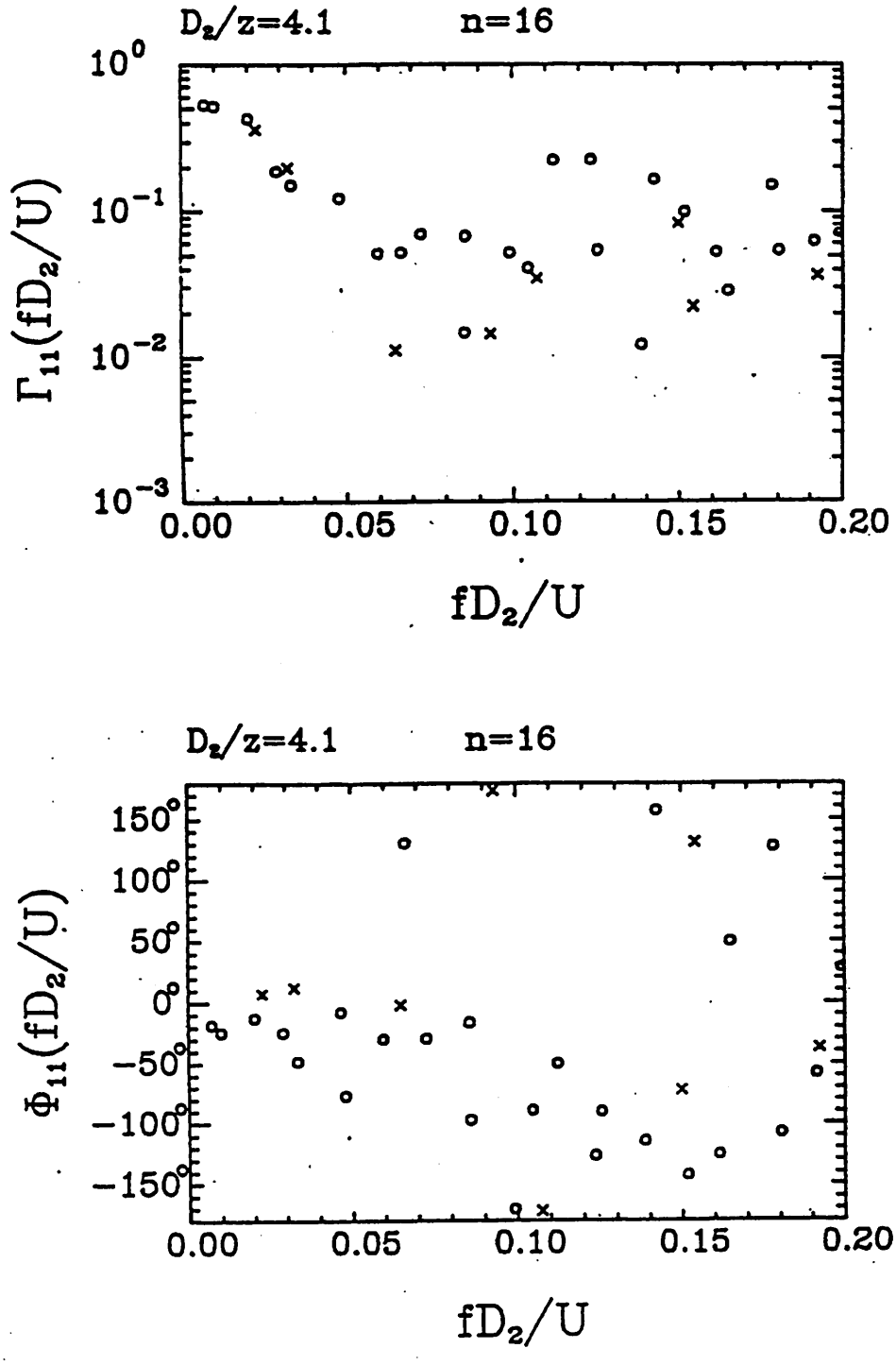


Fig. 7.
The Nibe 4 (o) and Nibe 5 (x) coherence and phase data for $D_2/z$ = 4.1.

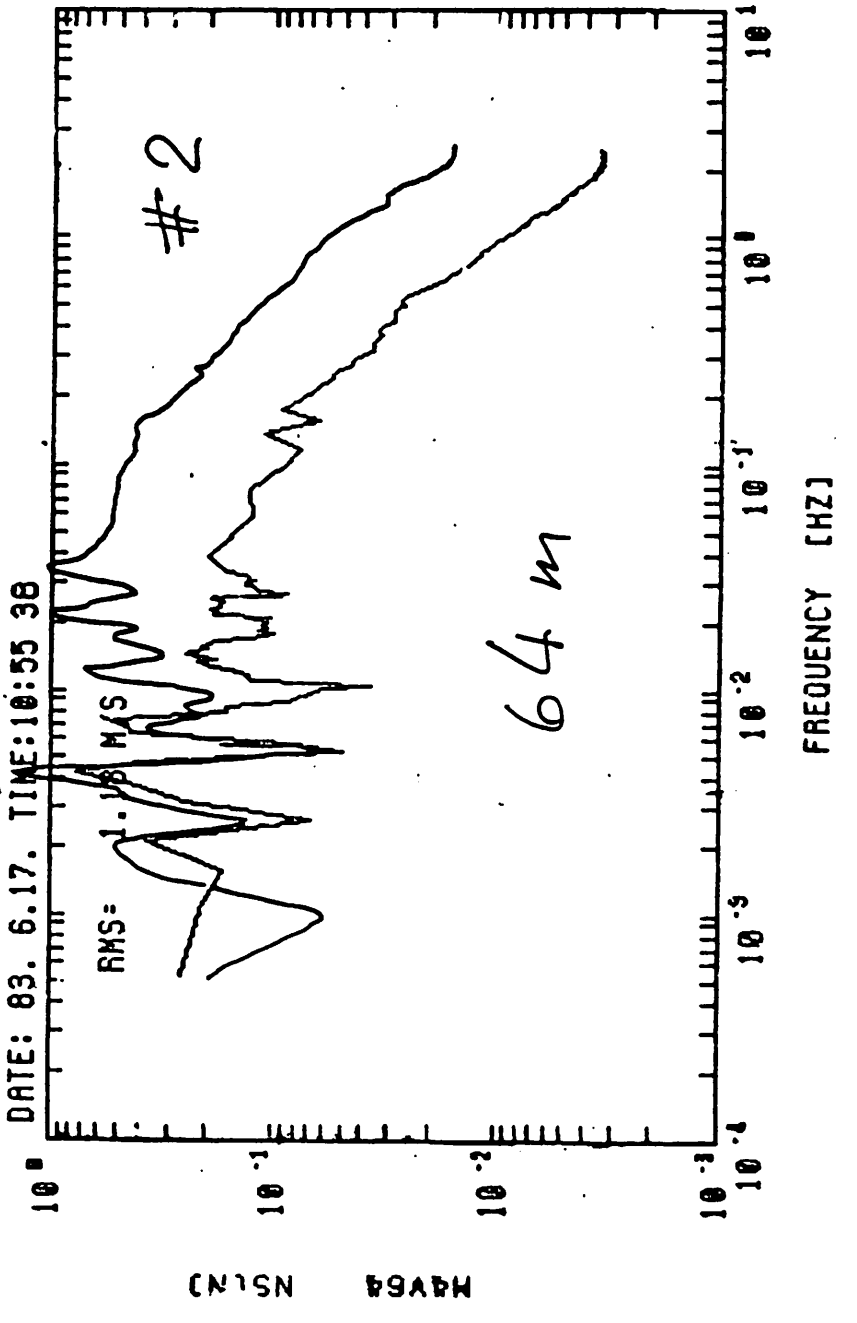
#2
64 m
DATE: 83. 6.17. TIME:10:55 38
RMS= 1.18 M/S
FREQUENCY [HZ]
M4V64 NS[N]

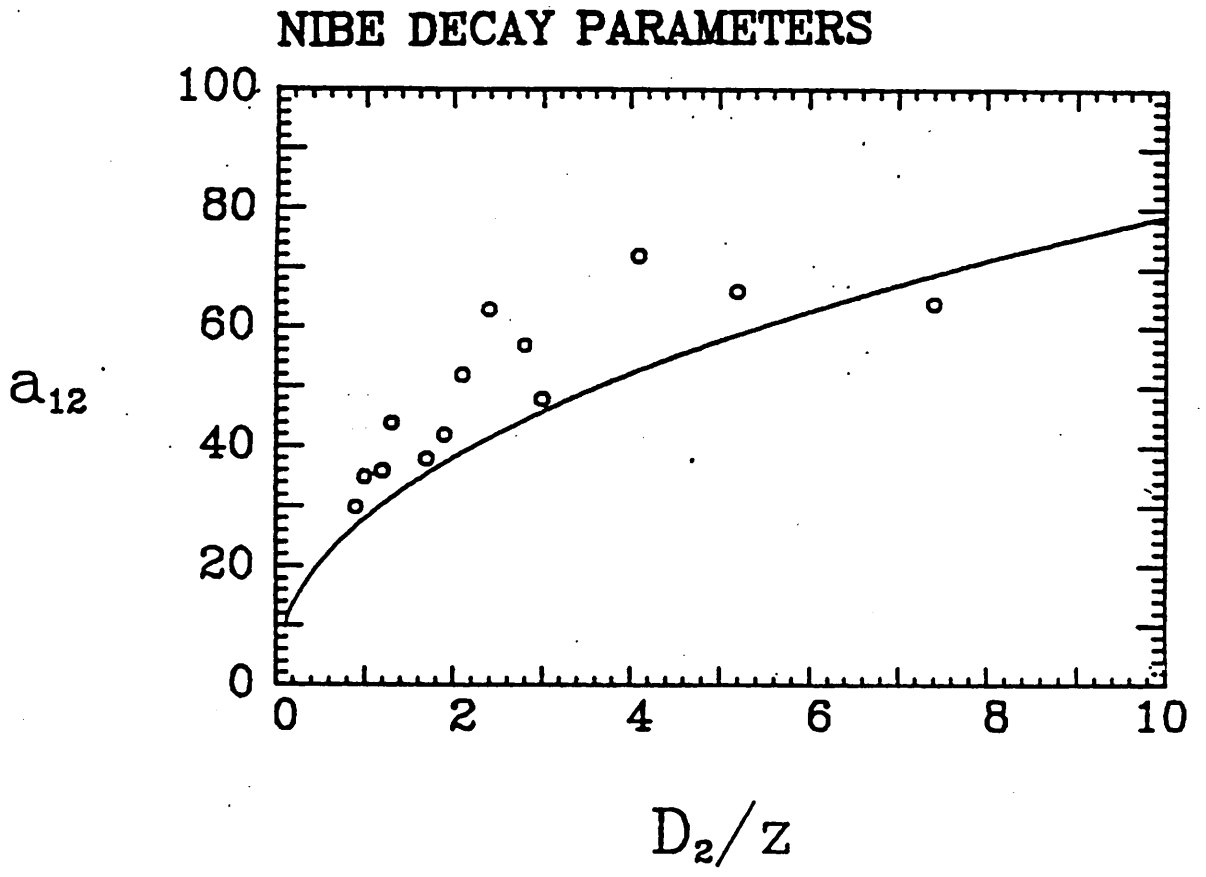


Fig. 8.
The Nibe decay parameters as a function of $D_2/z$. The curve is Iwatani's (1977) equation for $a_{12}$.

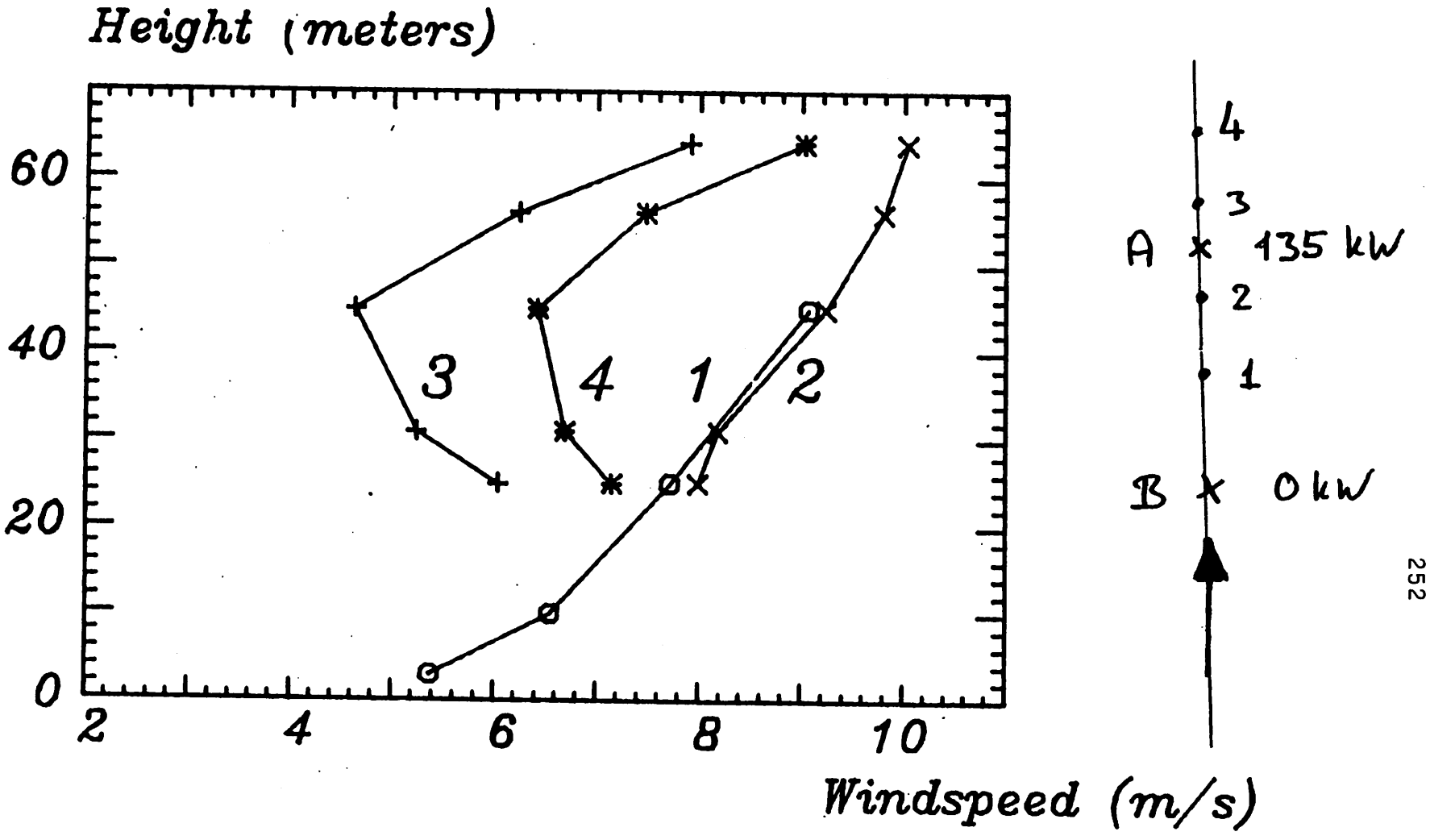


Average of 38 2 minute values
Direction 188 deg + − 5 deg, speed 6−8 m/s

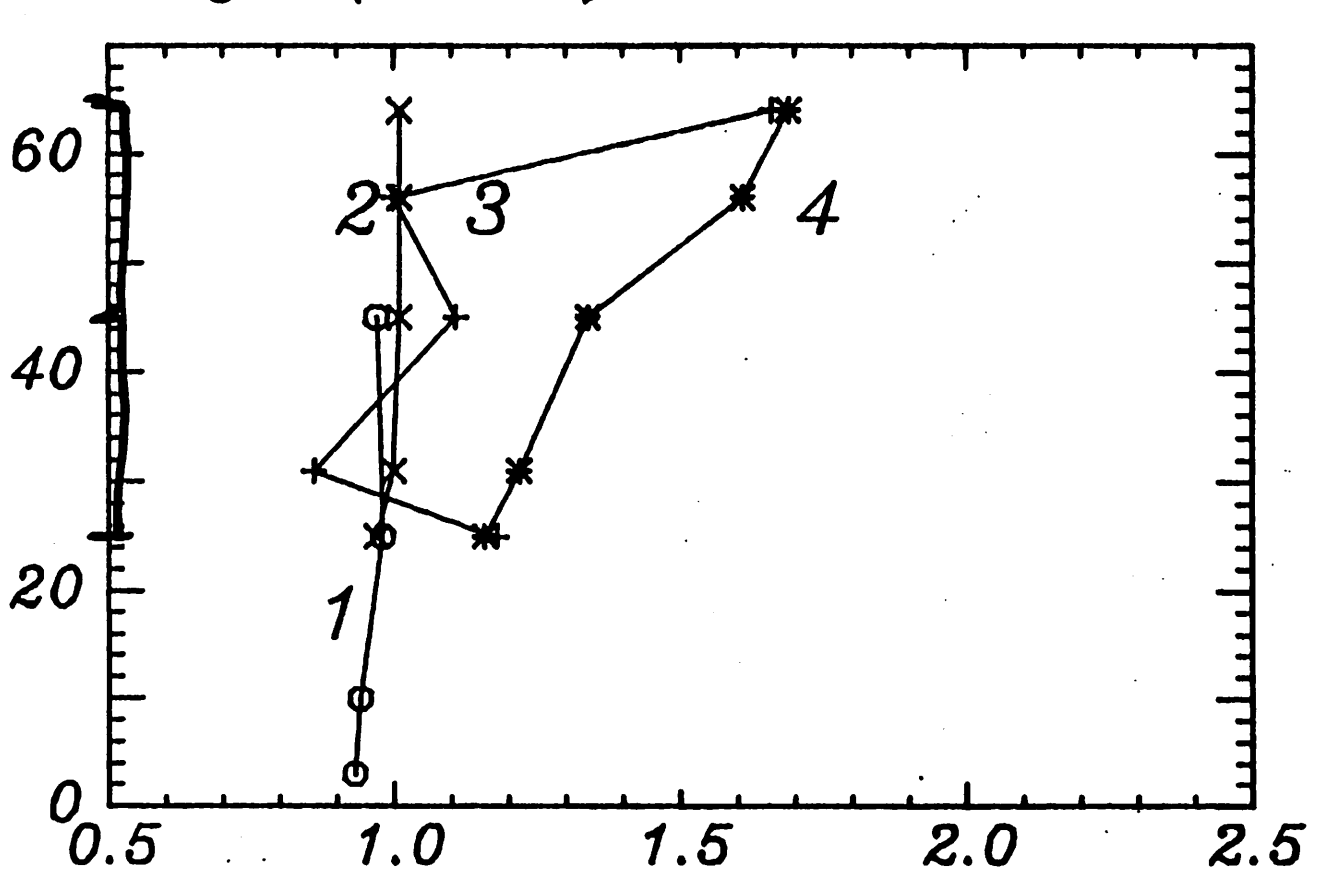


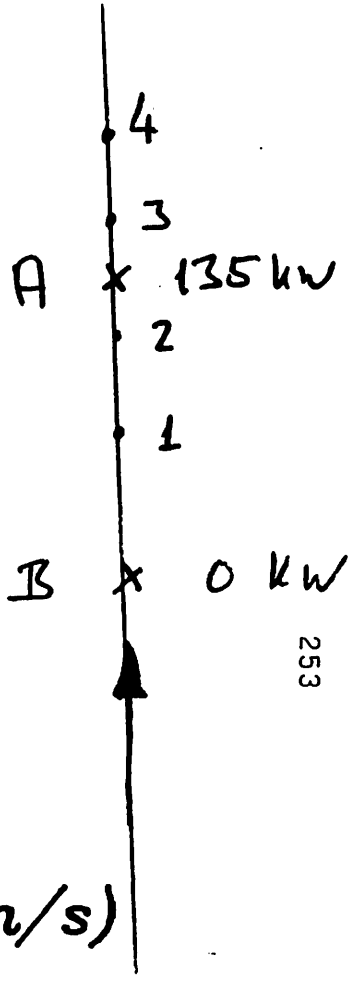


253

Average of 38 2 minute values
Direction 188 deg + − 5 deg. speed 6−8 m/s

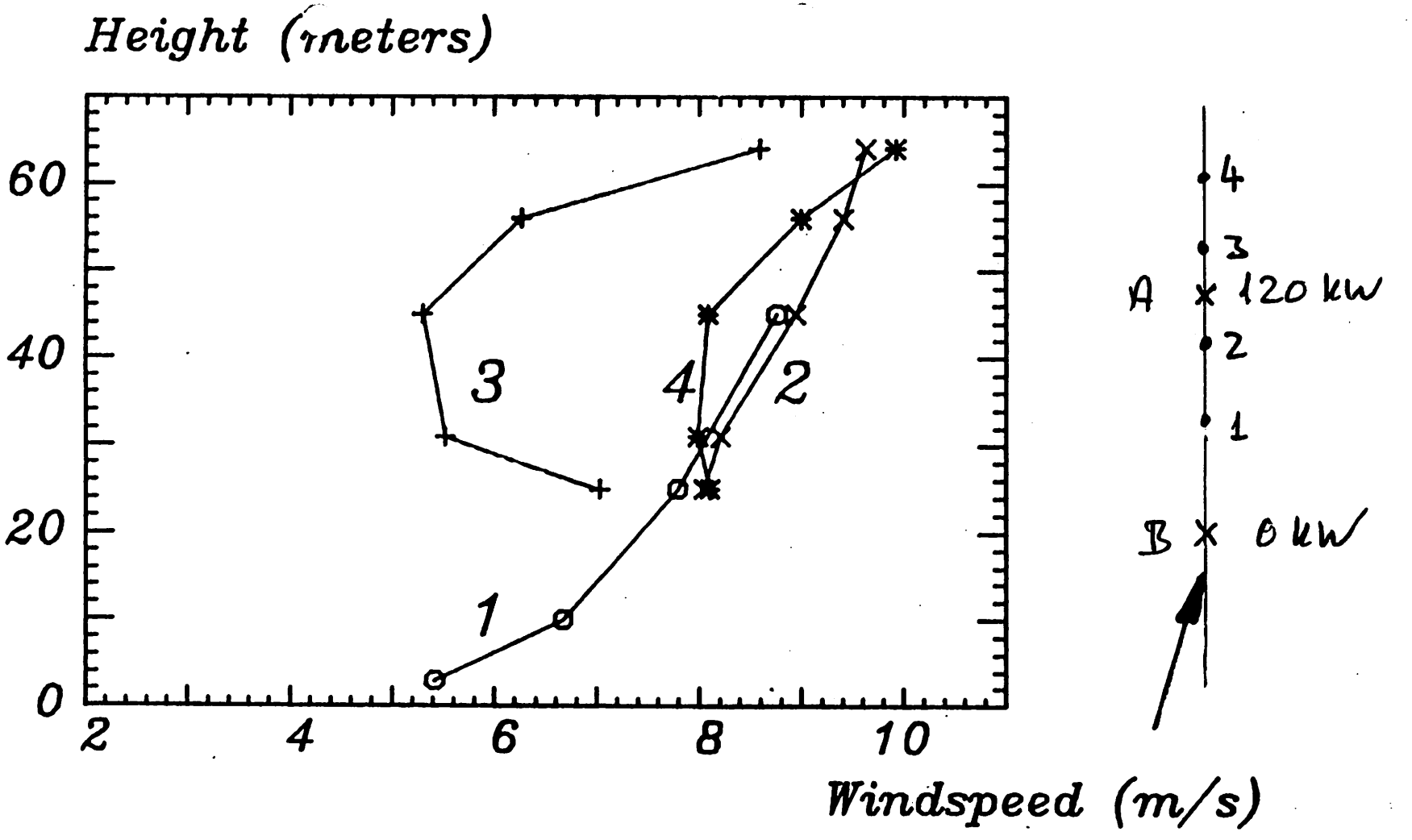


Average of 122 2 minute values
Direction 198 deg + − 5 deg, speed 6−8 m/s

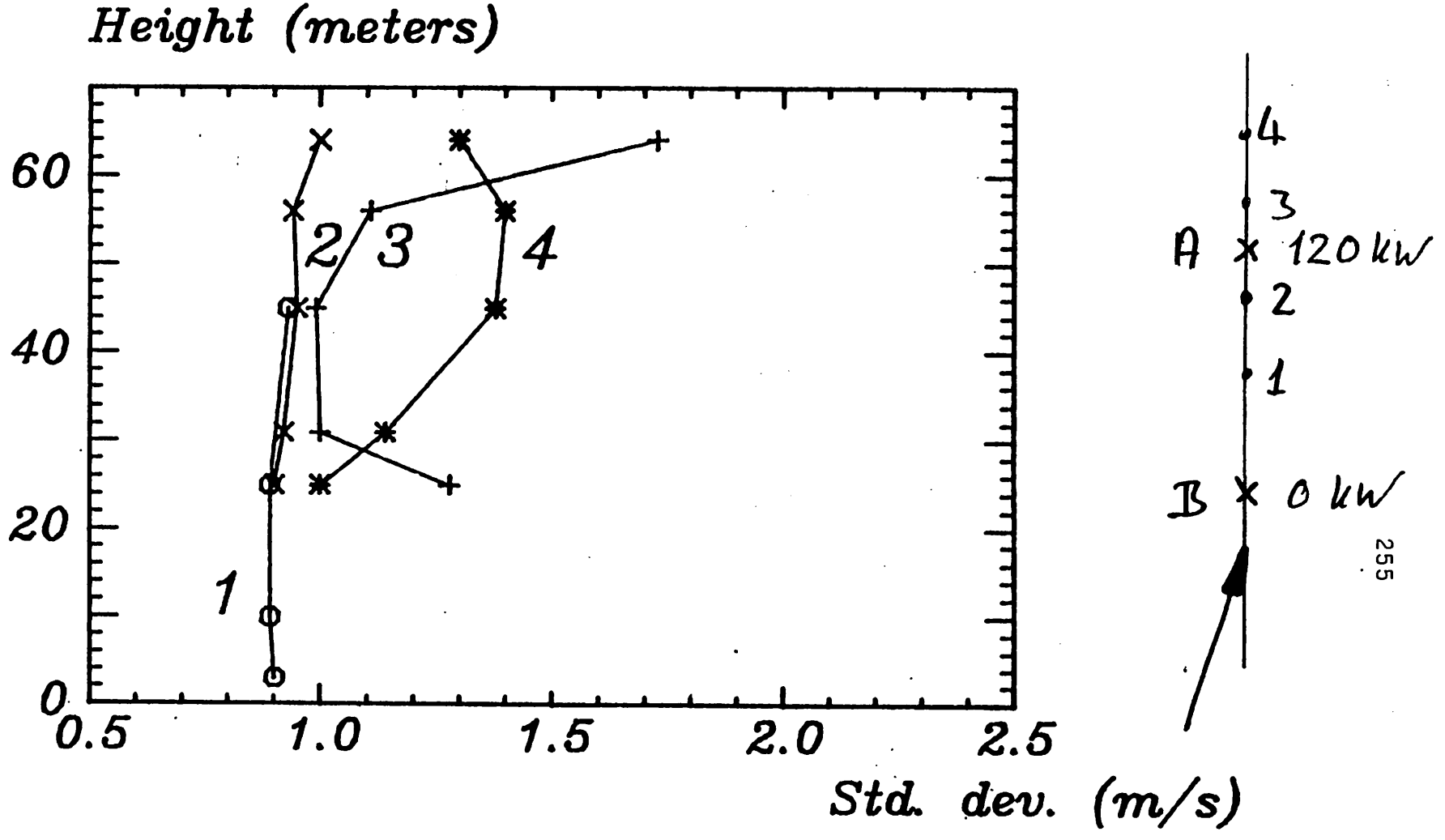


Average of 122 2 minute values

Direction 198 deg + − 5 deg. speed 6−8 m/s

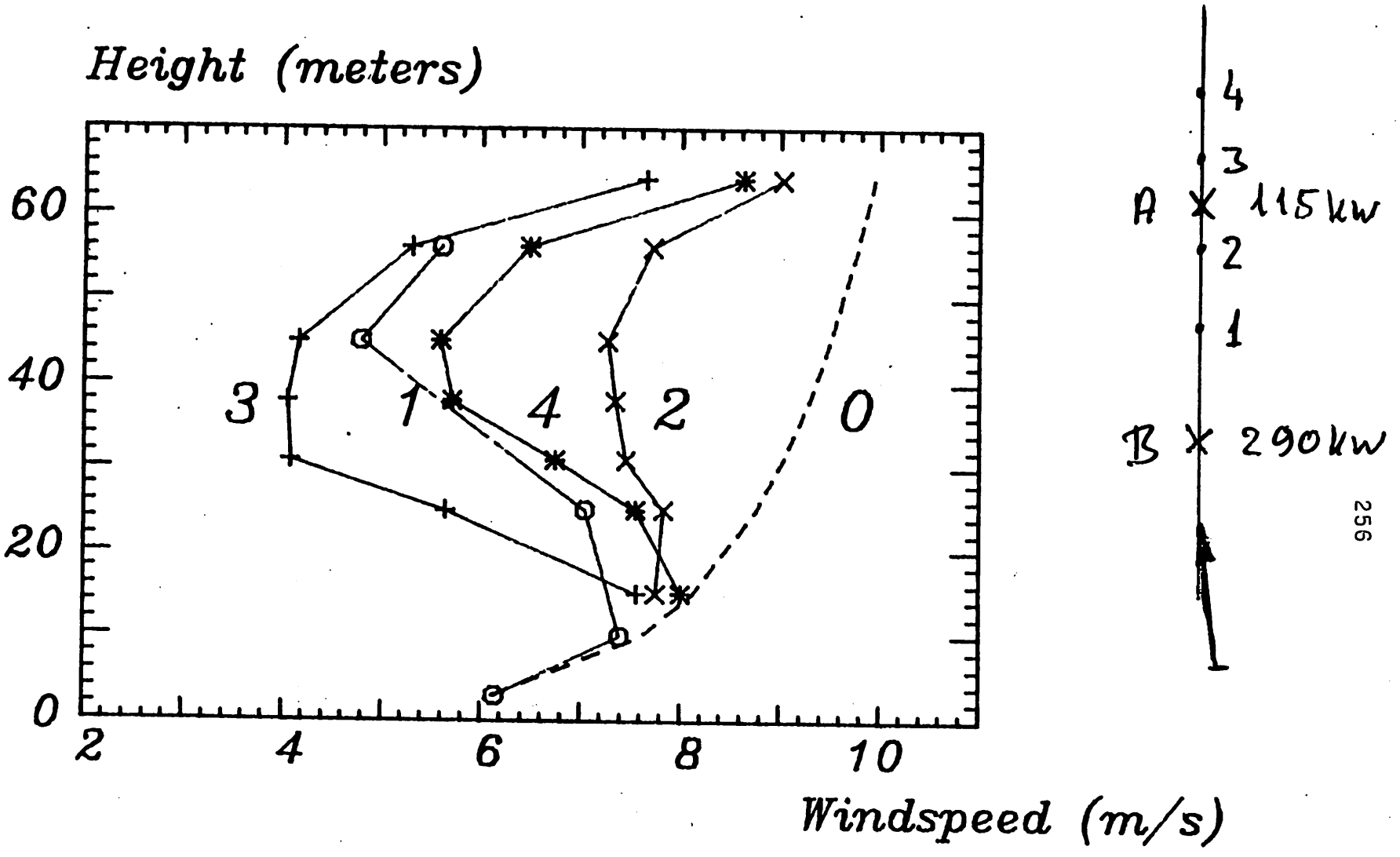


NIBE 27-nov-84
Direction 182 degrees
Power(A) 115 KW, Power(B) 290 KW

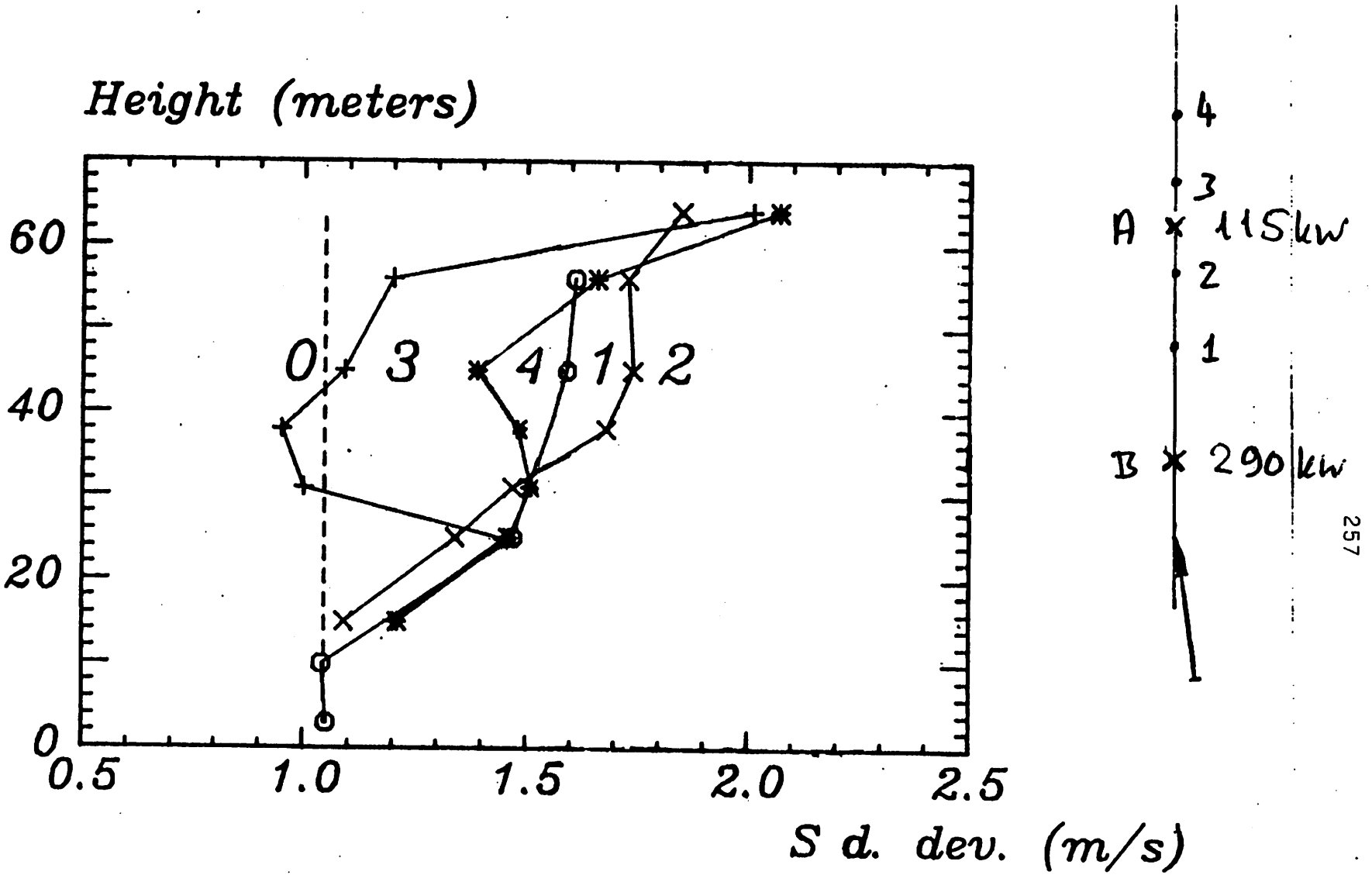


NIBE 27-nov-84
Direction 182 degrees
Power A) 115 KW Power(B) 290 KW

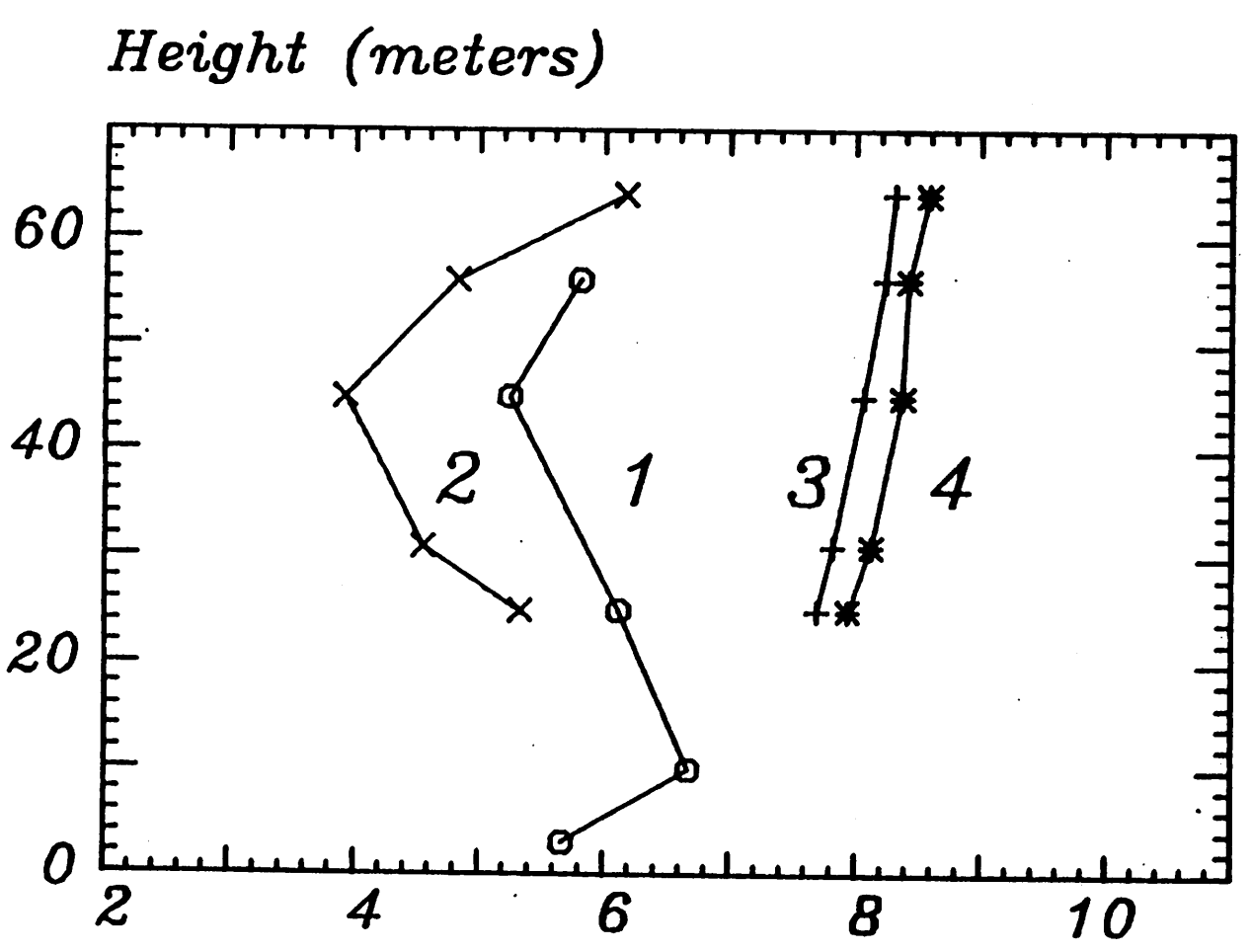


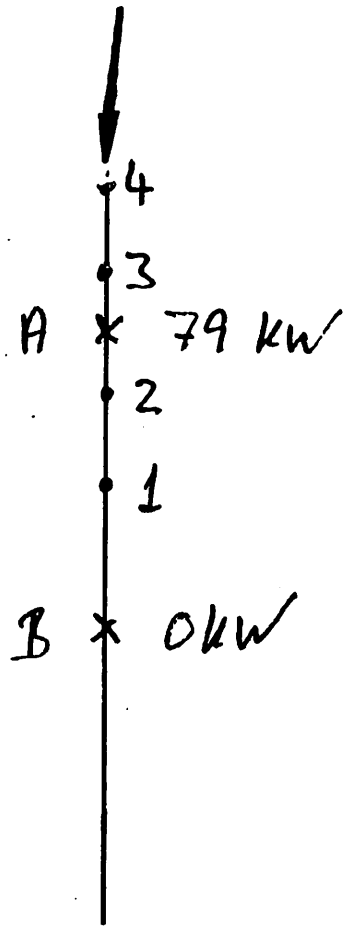


17-jun-83 1055-1127, 5hz, 9600 scans

Direction 3 degrees off mast line (11deg), POW(A) = 79 KW

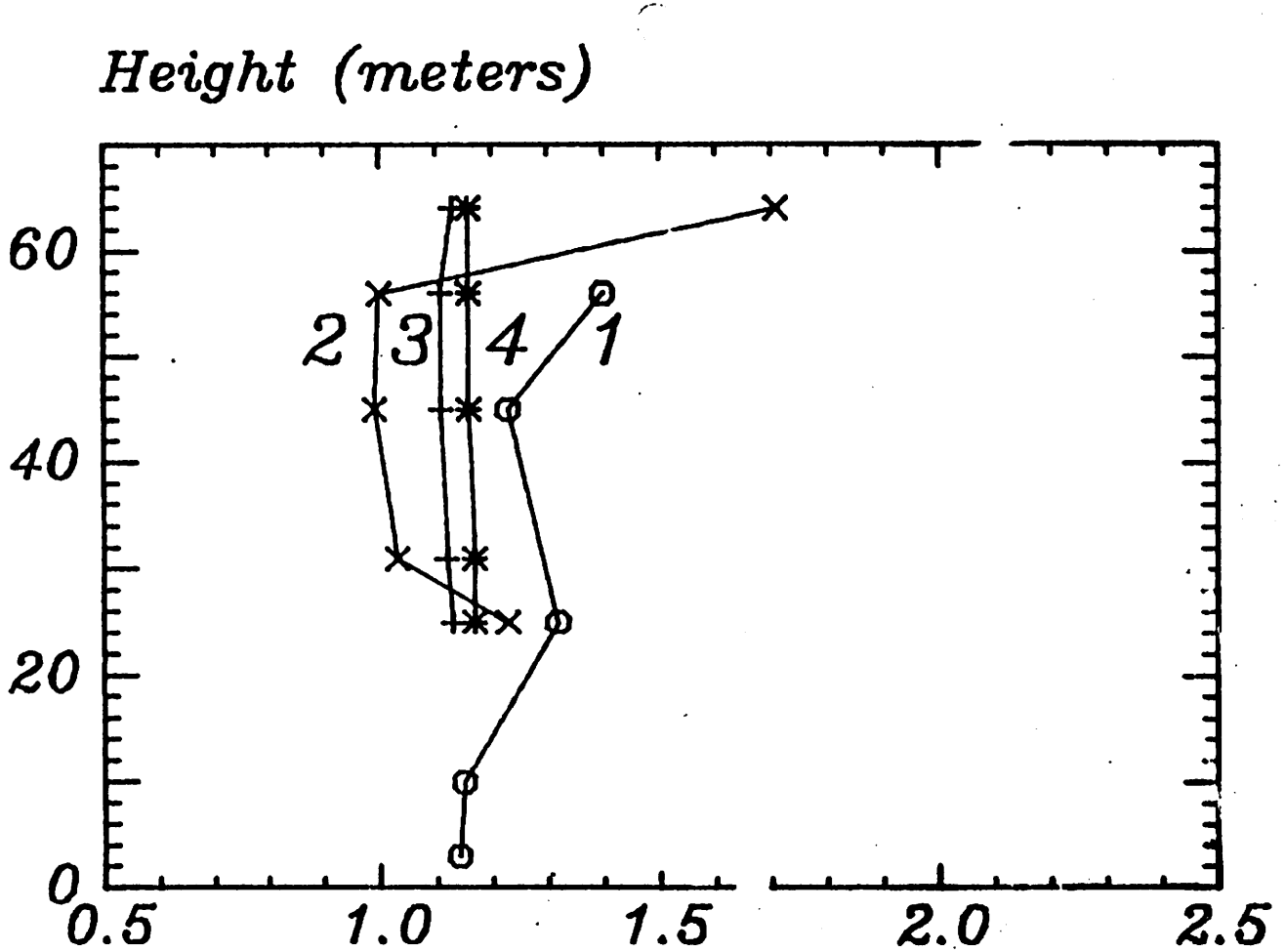


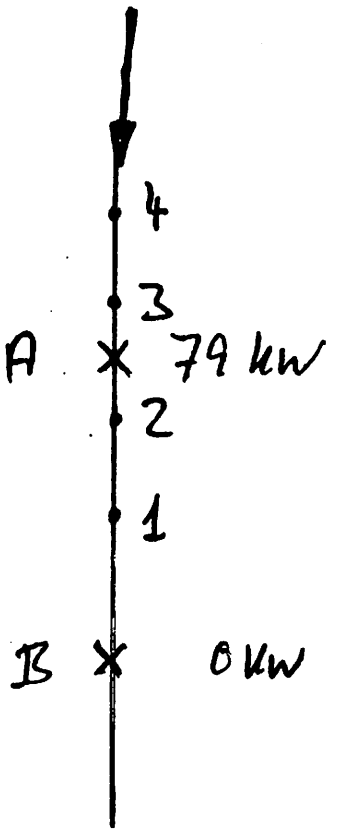


17-jun-83 1055-1127, 5hz, 9600 scans

Direction 3 degrees off mast line (11deg), POW(A) = 79 KW

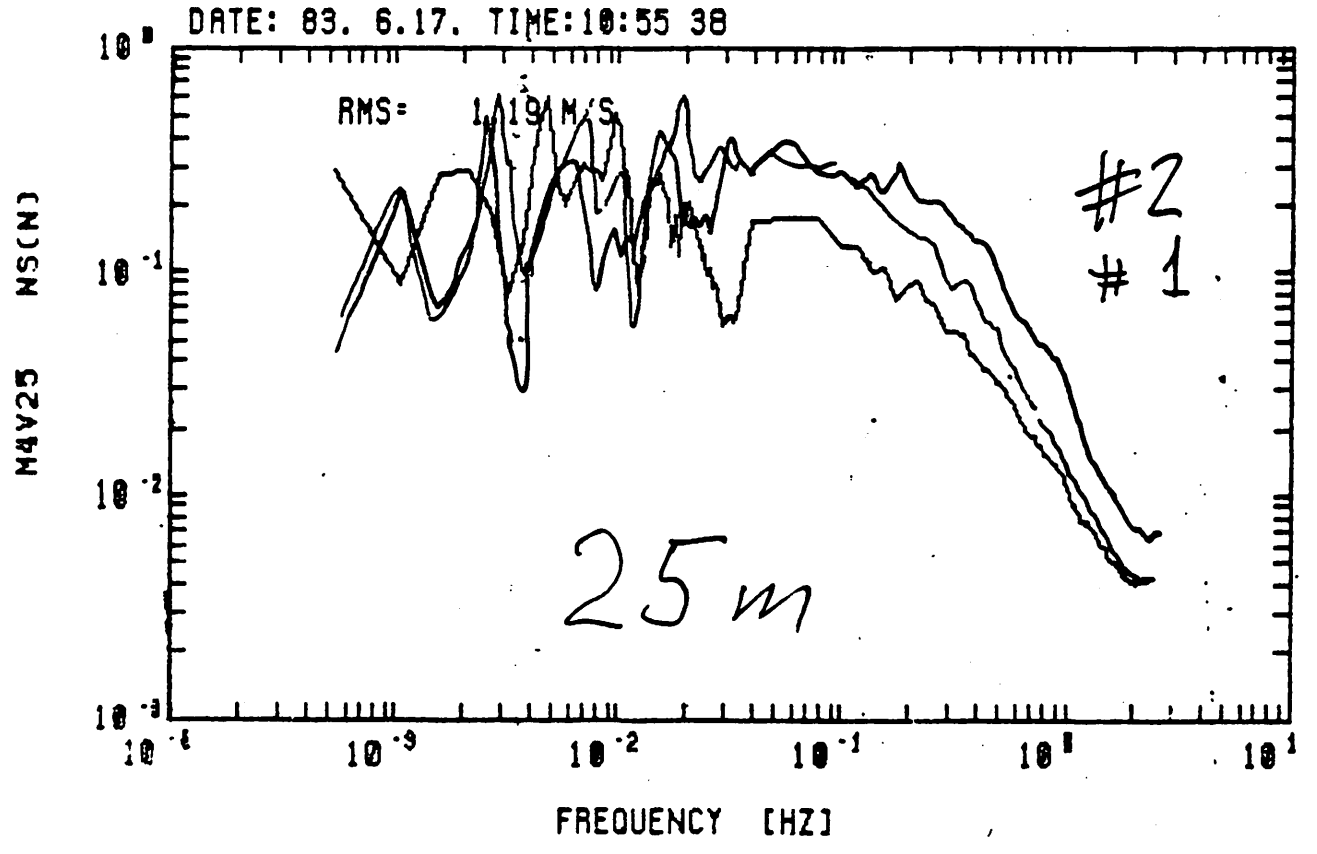
DATE: 83. 6.17. TIME:10:55 38
RMS= 1.19 M/S
#2
#1
25m
M4V25 NS(N)
FREQUENCY [HZ]

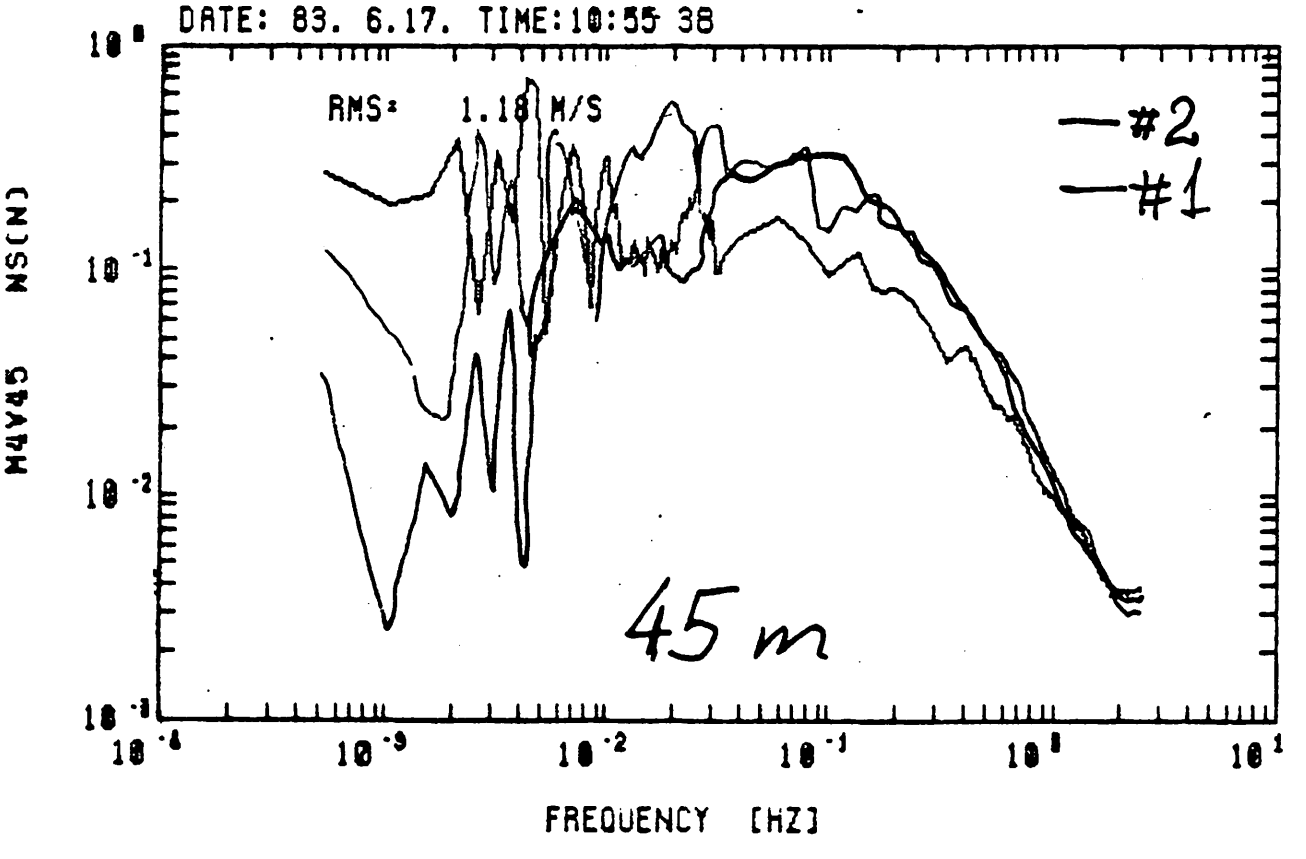
DATE: 83. 6.17. TIME:10:55 38
RMS= 1.18 M/S
#2
#1
45m
M4V45 NS(N)
FREQUENCY [HZ]

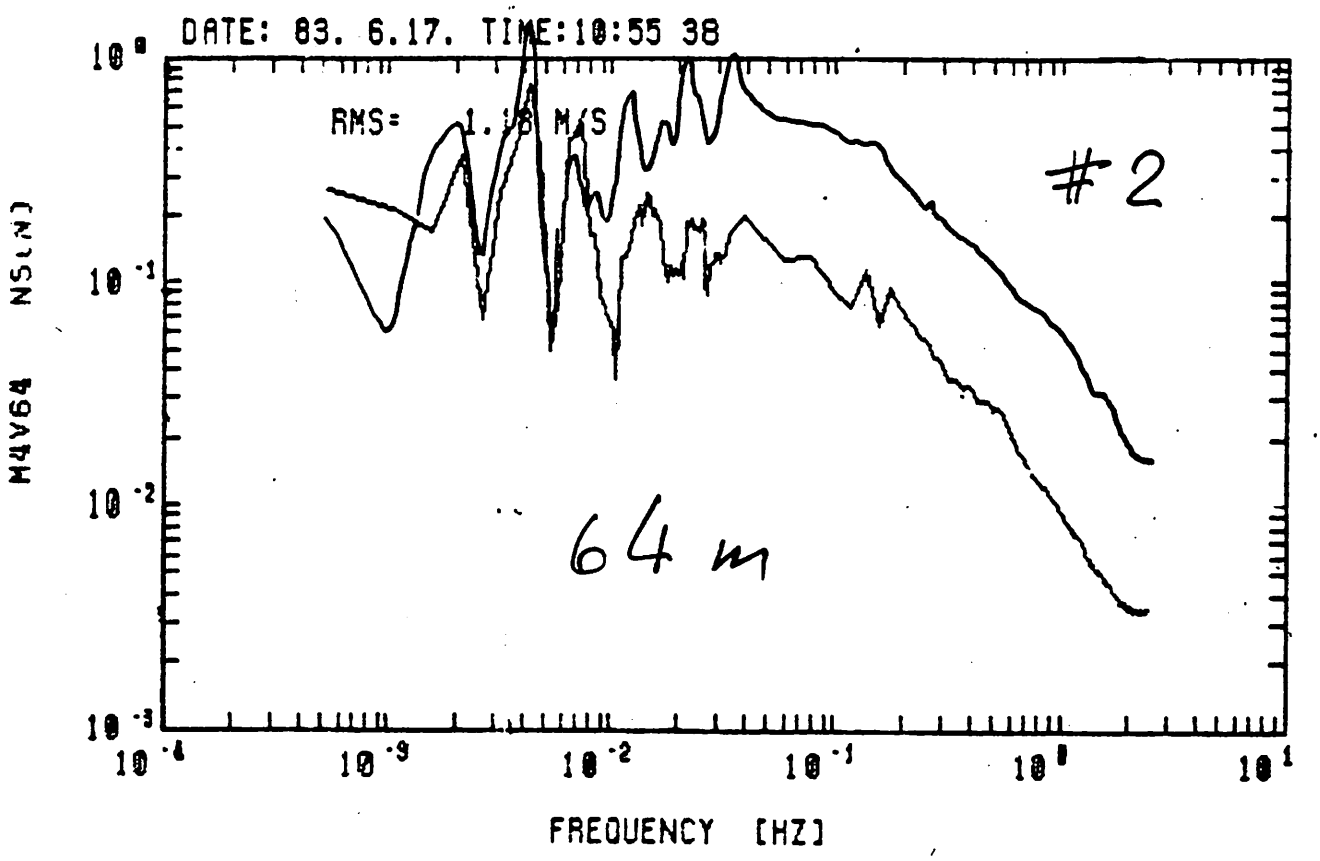
DATE: 83. 6.17. TIME:10:55 38
RMS= 1.18 M/S
#2
64 m
M4V64 NS(N)
FREQUENCY [HZ]

# MEASUREMENTS OF THE TOWER WAKE AT MAGLARP

Jan-Ake Dahlberg

Measurements of the tower wake has been carried out at the Maglarp wind turbine.

The results from theese measurements have already been presented elswhere (Hamburg Oct 1984) why only some figures are included here.

Figure 1 show the 10 meter measurement bar, tightend to the blade-inspection platform, and equipped with 8 hotwire anemometers.

Figure 2 show instantaneous (0.025 sec averaged) velocity profiles repeated every 1.2 sec corresponding to every blade passage.

Figure 3 shows the maximum velocity deficit in the wake vs downstream position. The blade will always experience this deficit when passing through the tower wake.

Figure 4 show autospectral density functions from signals measured at the middle position.
Since there are no marked peaks the flow conditions could not be considered to be periodic although released vorticies clearely could bee seen from the velocity signals.

The measurements were also completed with smoke visualization of the flow in the tower wake.

The intention of the experiment was to see how the vorticies where correlated.with height and to see if vorticies were triggered by the passage of the blade.

From the Video recording (showed at the meeting) it is clear that there is a strong vorticity correlation with height and hardly no influence from the blade to the released vorticies.

Figure 1

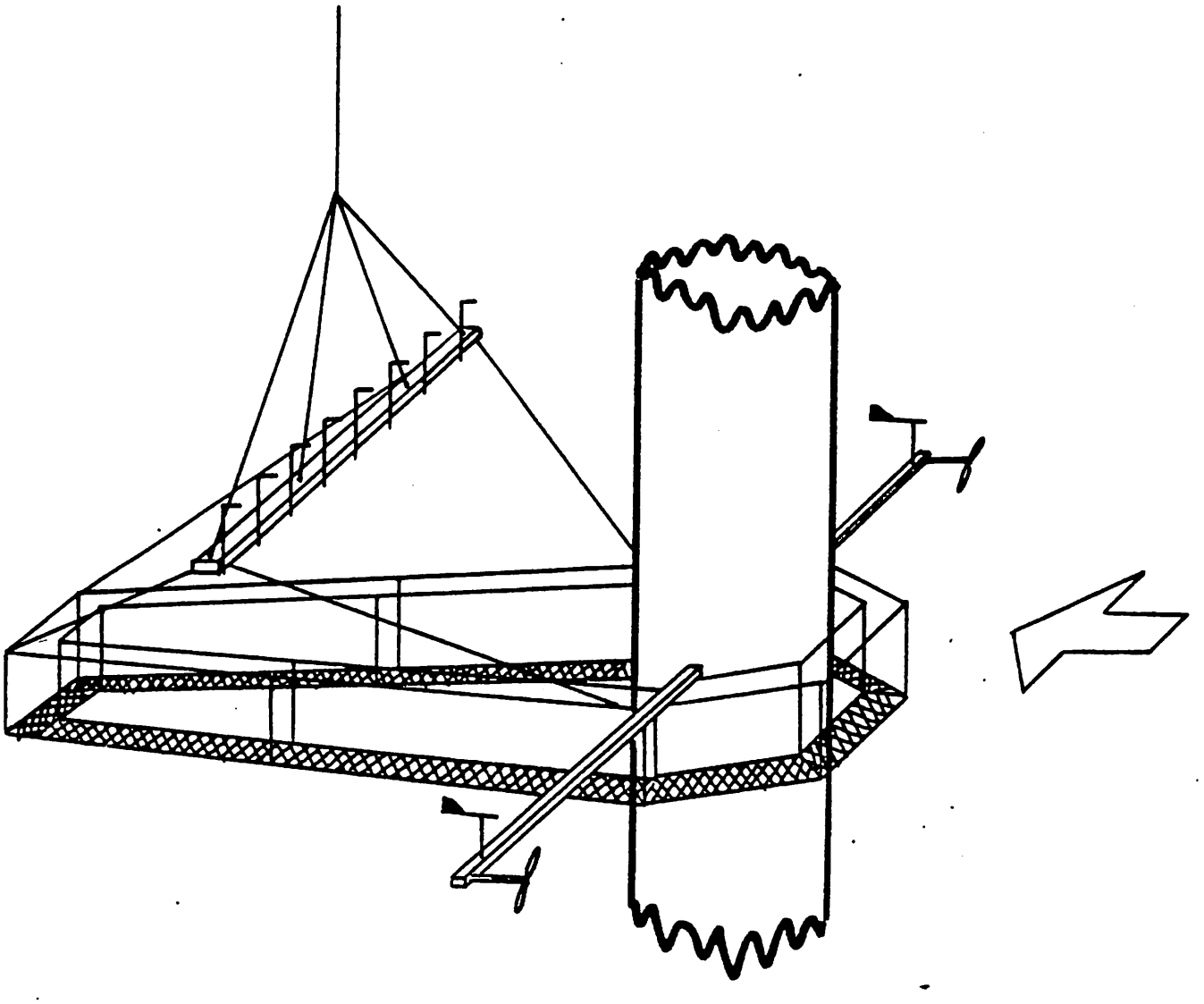

Figure 2

FFA THE AERONAUTICAL RESEARCH INSTITUTE OF SWEDEN 16-OCT-84 0836

MAGLARP TOWER WAKES AT X/D=2.3

| | |
|---|---|
| FILTER CUT OFF FREQUENCY: | 124Hz |
| EACH WAKE AVERAGED DURING: | .025s |
| NUMBER OF SAMPLES PER WAKE | 5 |
| REFERENCE MEAN WIND SPEED: Uo | 8.1m/s |
| REYNOLDS NUMBER | 2400000 |

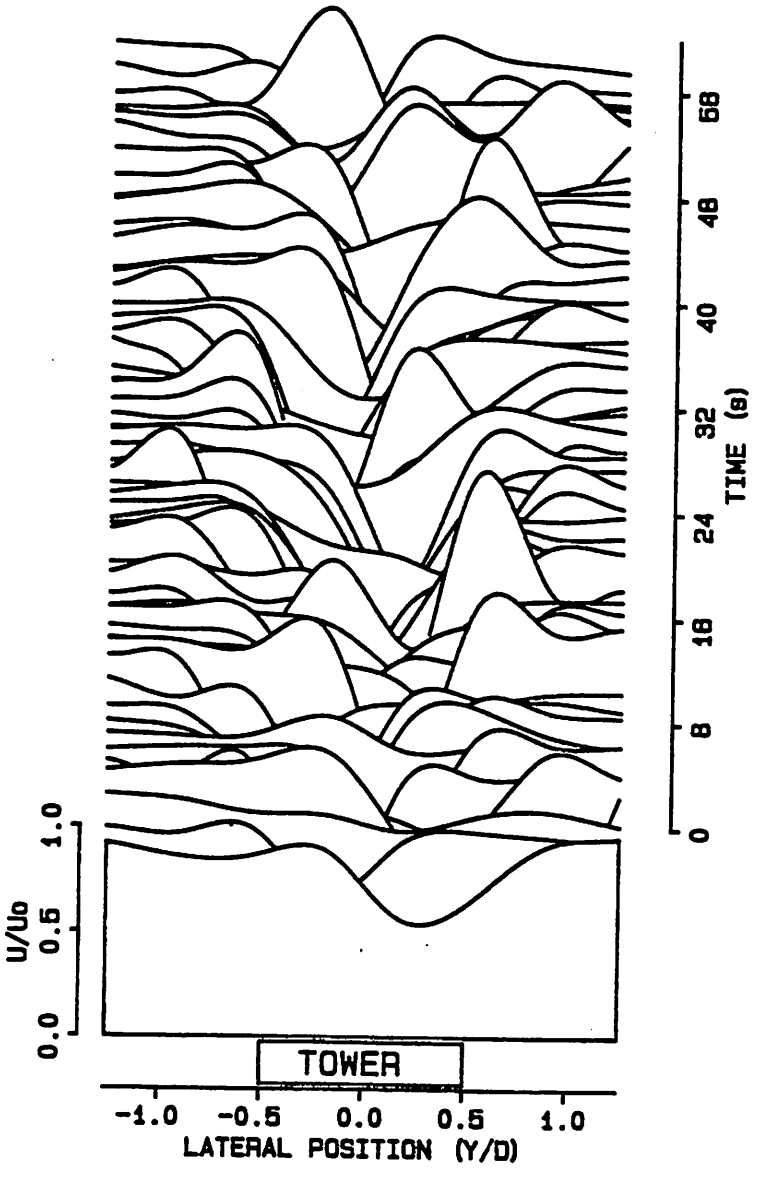

Figure 3

# Maximum velocity deficit vs downstream position

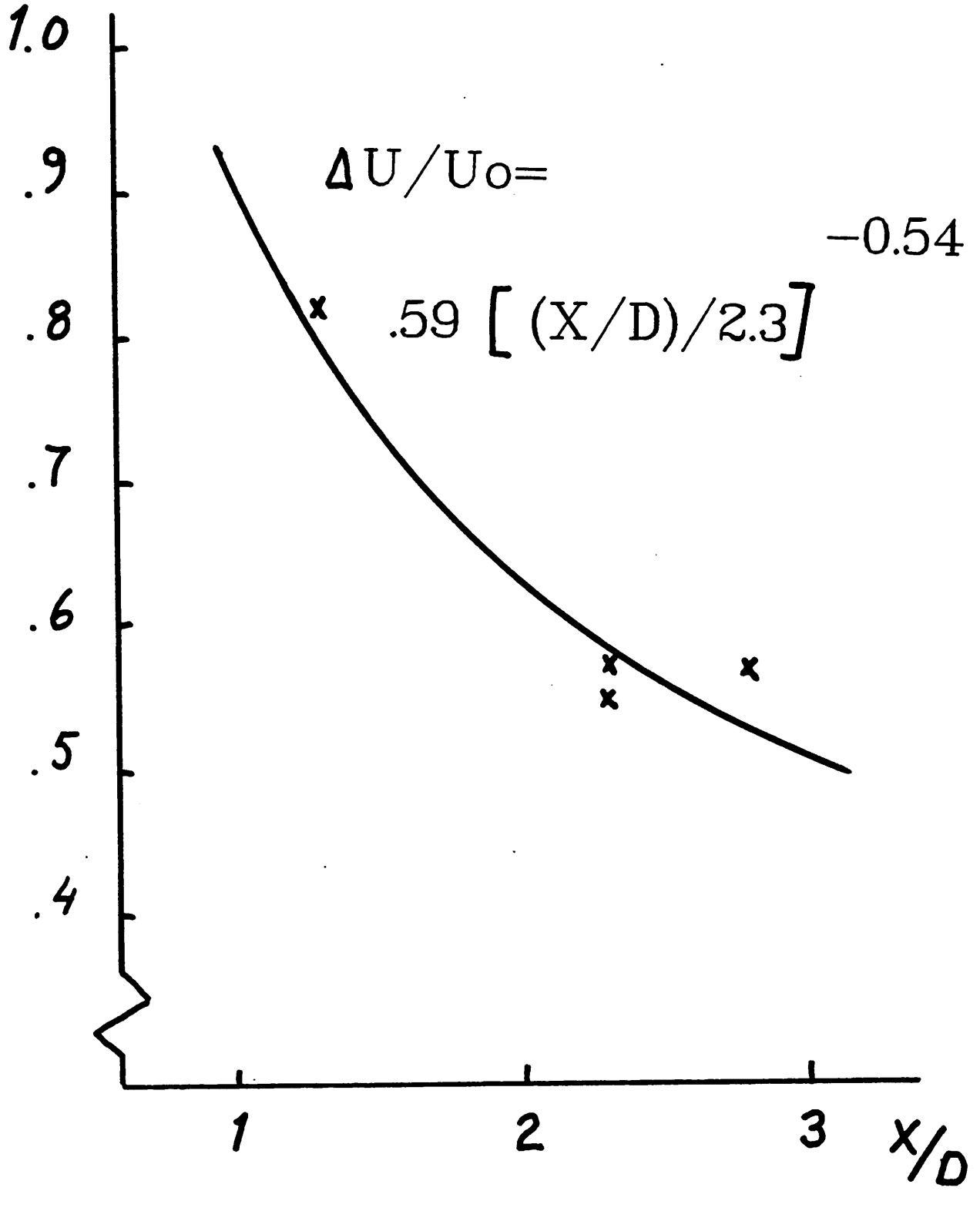

Figure 4

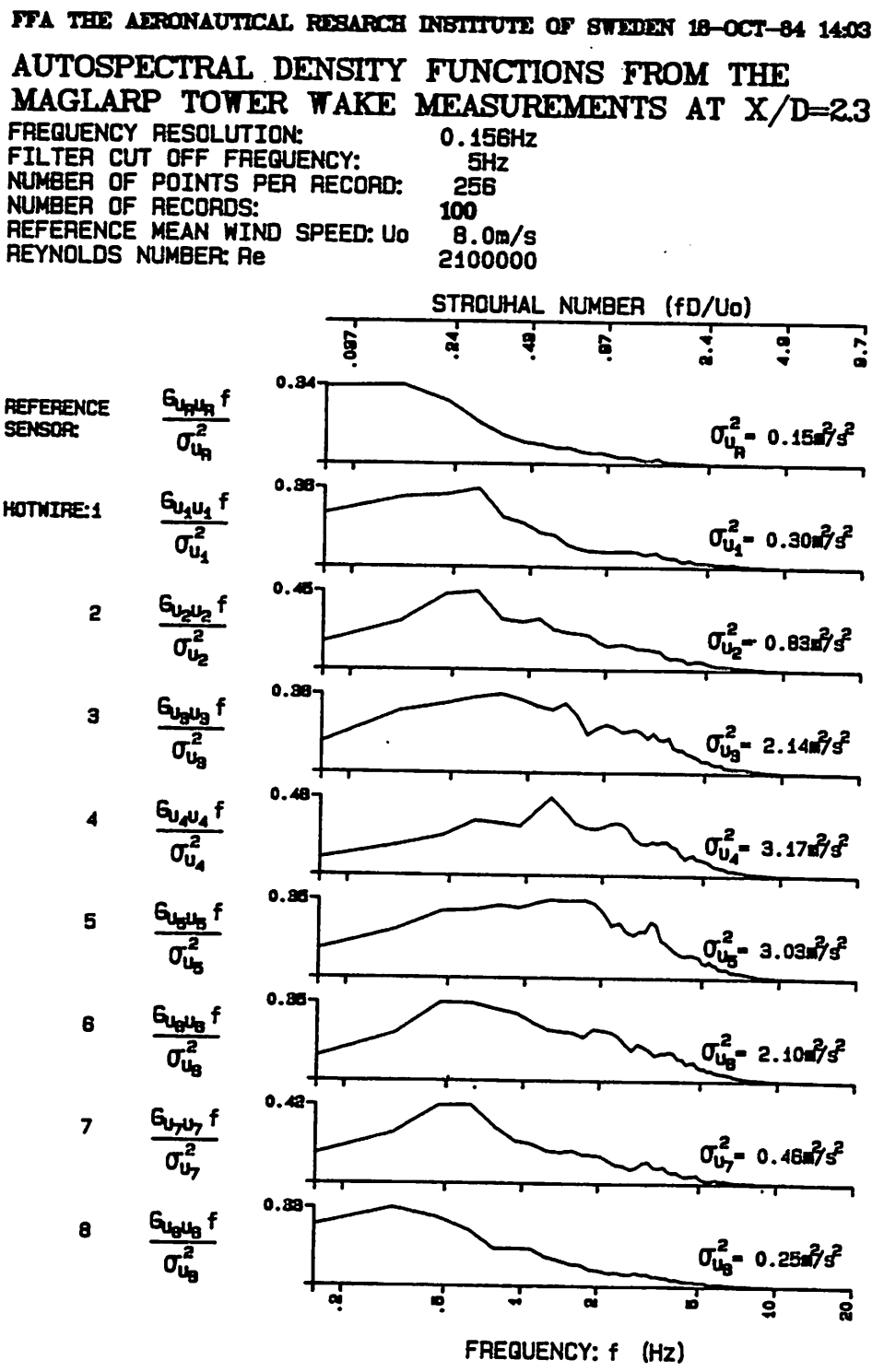
FFA THE AERONAUTICAL RESEARCH INSTITUTE OF SWEDEN 18-OCT-84 14:03
AUTOSPECTRAL DENSITY FUNCTIONS FROM THE MAGLARP TOWER WAKE MEASUREMENTS AT X/D=2.3
FREQUENCY RESOLUTION: 0.156Hz
FILTER CUT OFF FREQUENCY: 5Hz
NUMBER OF POINTS PER RECORD: 256
NUMBER OF RECORDS: 100
REFERENCE MEAN WIND SPEED: Uo 8.0m/s
REYNOLDS NUMBER: Re 2100000
STROUHAL NUMBER (fD/Uo)
.097
.24
.49
.97
2.4
4.8
9.7
REFERENCE SENSOR:
HOTWIRE:1
2
3
4
5
6
7
8
0.34
0.38
0.45
0.38
0.48
0.36
0.36
0.42
0.33
$\sigma^2_{u_R}$= 0.15m²/s²
$\sigma^2_{u_1}$= 0.30m²/s²
$\sigma^2_{u_2}$= 0.83m²/s²
$\sigma^2_{u_3}$= 2.14m²/s²
$\sigma^2_{u_4}$= 3.17m²/s²
$\sigma^2_{u_5}$= 3.03m²/s²
$\sigma^2_{u_6}$= 2.10m²/s²
$\sigma^2_{u_7}$= 0.46m²/s²
$\sigma^2_{u_8}$= 0.25m²/s²
.1
.5
1
2
5
10
20
FREQUENCY: f (Hz)

# MODELLING OF ATMOSPHERIC TURBULENCE

Edmund J. Fordham

You may be interested to know that my thesis work covered turbulence spatial structure, rotational sampling and transformation between fixed and rotating reference frames, turbulence distortion effects and transfer to aerodynamic loads in addition to a practical field programme. Some of the results have been published as BWEA conference papers (Fordham and Anderson (1982) and Fordham (1983) in particular) although not in full detail.

The Wind Engineering article represents chapter 1 only of my thesis, and was first written over New Year 1984, now nearly two years ago. (I should caution you incidentally against several mathematical misprints in the published paper). The rotational sampling analysis was done with Mike Anderson in 1981/2. (Based on data from the Battelle experiment on which Dr Connell did a similar paper).

In addition, I had many interesting discussions while at the Cavendish Lab, with Dr A A Townsend, FRS, (author of "The Structure of Turbulent Shear Flow") and with Dr J C R Hunt of the Cambridge Applied Maths Dept on dynamically rational methods of full 3-dimensional turbulence structure modelling. By this I mean a mathematical model able to predict any statistical correlation function, with any spatial separation and any time delay, for any two turbulence velocity components, and satisfying equations of continuity and (linearised) equations of motion for the turbulent flow field. Such a model is dynamically and statistically rational, says as much about the statistics as it is possible to say (for a stochastic field assumed to be jointly normal in its probability distributions, anyway) and, being based on time domain statistics, is available for immediate translation to a moving reference frame (at least at constant rotational speed).

The model discussed would be based on Townsend's 1970 analysis of the rapid distortion of an initially isotropic field by a uniform plane shear. Several adjustable parameters and an initial turbulence spectrum would be available for "tuning" the model to agree with available observational data. The model would reproduce major features of the observed anisotropy of atmospheric turbulence, in particular $Ly^{(w)}/Lx^{(w)}<0.5$ and the existence of "eddy slopes" in the vertical direction. See chapters 3 and 4 of Townsend's book (1976 edition) and the iso-correlation plots of Figure 4.5 in particular. My thesis comments on these ideas briefly in the 'suggestions for further work' category.

I coded up many of the necessary calculations early last year, but did not have time to finish the work, as I was under pressure to present my thesis. This was in itself a disappointment; most of my turbulence work (which seems to me to have been of the greater interest) had to be done almost in spare time in between my obligations in building and instrumenting two 5m turbines. I would still be interested in finishing the work; my only problem is time (and possibly computing resources).

On the topic of your meeting, I would advocate the following:

1) that more attention is paid to the sizes and variability of the gross scaling parameters of the turbulence (variances, mean velocities, and especially the various integral length scales) than to detailed functional forms for spectra or correlations. The definitions and different methods of determination of the length scales in particular need attention. See Teunissen (1980) for the best discussion I know.

2) that time domain statistics (ie: the correlation functions) be regarded as primary, rather than fixed reference-frame spectra which have no obvious application to wind turbine rotor problems. Translation to moving reference frames is only straightforward from time domain statistics.

3) that any turbulence model should be dynamically rational ie: should satisfy fluid continuity and at least approximate equations of motion.

4) that even if inherent non-linearities in the transfer between turbulence velocities and structural response force attention onto direct time-stepping dynamic simulations, linear statistical models should still be explored as a far cheaper and easier way of conducting parametric surveys (compare eg: Anderson's PhD simulation (BWEA 1982) applicable only to a few design cases, with Anderson, Garrad and Hassan, Jnl. of Wind Engineering and Ind. Aerod. 1984, which demonstrates trends in results with variation of scaling parameters).

5) that any time-stepping turbulence simulation, however dervied, should have the statistical properties of its output checked against real atmospheric turbulence statistics.

6) that so-called "discrete gust models" be confined to analysis of extreme events, and worst-case loading design, and not applied to general fatigue life problems unless it can be shown that they satisfy (5) and (3).

I note one possible confusion of terminology in your introductory notes. I think that there is a distinction to be made between "stochastic" or "analytical" models, and "time-stepping" or "direct simulation" ones, but not between "frequency domain" and "time domain". I suggest that the latter two terms are equally applicable to "stochastic" modelling of turbulence; a correlation function (time domain) is related to a spectrum function (frequency domain) by a simple Fourier transform, and both representations are in principle exactly equivalent in the information they contain about the turbulence. My point in (2) above is that the "time domain" representation is the more convenient for wind turbine analyses, because it can be immediately related to a moving reference frame, which spectra cannot, except by going through a Fourier transform to time domain statistics. It is also more useful for the anisotropic cases where a rotating reference frame description may become non-stationary (ie: not all orientations of the blades are statistically equivalent). I am not convinced that such cases are usefully described by spectra at all.

What I call "time-stepping" or "direct simulation" models seem to be referred to as "time domain" in much of the wind turbine literature, which I feel is misleading. Their important feature is that they involve abandoning an "analytical stochastic" approach, for the good reason that the aero and structural dynamic transfer between turbulence and random load may well be non-linear, and there is no good theory relating stochastic inputs and outputs for non-linear systems.

Improvement in modelling the dynamics is however likely to carry the penalties:

1) the need for a complicated simulation of random turbulence inputs- possibly very expensive computationally if a full 3-D simulation is used.

2) the difficulty of conducting parametric surveys (variation of scaling parameters) without running a long list of design cases, further multiplying computational cost.

3) the difficulty of checking the simulated inputs against observational data except in a statistical sense.

These are the reasons lying behind my advocacy of (4) above.

# P A R T I C I P A N T S

| | |
|---|---|
| Anderson, M.B. | McAlpine & Sons Ltd, Great Britain |
| Berg, D. | Sandia National Lab., USA |
| Bergström, H. | Meteorlogiska Finst, Sweden |
| Connell, J.R. | Battelle/PNL, USA |
| Dahlberg, J.-A. | FFA, Sweden |
| Dragt, J.B. | Netherlands Energy Research Foundation, Netherlands |
| Engström, St. | Statens Energieverk, Sweden |
| Fordham, E.J. | Cavendish Laboratory, Great Britain |
| Ganander, H. | Teknikgruppen AB, Sweden |
| Garrad, A.D. | Garrad Massan & Partners, Great Britain |
| Gustafsson, A. | FFA, Sweden |
| Hansen, K. | Denmarks Tekniske H., Denmark |
| Hojstrup, J. | Riso National Laboratories, Denmark |
| Linde, M. | FFA, Sweden |
| Matthies | Germanischer Lloyd, Germany |
| Molly, J.P. | DFVLR, Germany |
| Montgomerie, B. | FFA, Sweden |
| Oye, St. | Denmarks tekniske H., Denmark |
| Pazsit, I. | Studsvik Energiteknik AB, Sweden |
| Pedersen, M. | DTH, Sweden |
| Quarton, D.Ch. | Taylor Woodrow Contribution, Great Britain |
| Raab, A.D. | Garrad Massan & Partners, Denmark |
| Smedman, A.-S. | Meteorologiska Finst, Sweden |
| Vermeulen, P. | MT-TNO, Netherlands |
| Windheim, R. | KFA Jülich, Germany |

IEA - Implementing Agreement LS-WECS

Previous Expert Meetings

1. Seminar on Structural Dynamics, Munich, October 12, 1978

2. Control of LS-WECS and Adaptation of Wind Electricity to the Network, Copenhagen, April 4, 1979

3. Data Acquisition and Analysis for LS-WECS, Blowing Rock, North Carolina, Sept. 26-27, 1979

4. Rotor Blade Technology with Special Respect to Fatigue Design Problems, Stockholm, April 21-22, 1980

5. Environmental and Safety Aspects of the Present LS WECS, Munich, September 25-26, 1980

6. Reliability and Maintenance Problems of LS WECS, Aalborg, April 29-30, 1981

7. Costings for Wind Turbines, Copenhagen, November 18-19, 1981

8. Safety Assurance and Quality Control of LS WECS during Assembly, Erection and Acceptance Testing, Stockholm, May 26-27, 1982

9. Structural Design Criteria for LS WECS, Greenford, March 7-8, 1983

10. Utility and Operational Experiences and Issues from Mayor Wind Installations, Palo Alto, October 12-14, 1983

11. General Environmental Aspects, Munich, may 7-9, 1984

12. Aerodynamic Calculational Methods for WECS, Copenhagen, October 29-30, 1984

13. Economic Aspects of Wind Turbines, Petten, May 30-31, 1985
(no written report)

14. Modelling of Atmospheric Turbulence for Use in WECS Rotor Loading Calculations, Stockholm, December 4-5, 1985